

Gas Phase Chemical Physics Program

DOE Principal Investigators'
Abstracts

May, 2019

Chemical Sciences, Geosciences, and Biosciences Division
Office of Basic Energy Sciences
Office of Science
U.S. Department of Energy

The research grants and contracts described in this document are supported by the U.S. DOE Office of Science, Office of Basic Energy Sciences, Chemical Sciences, Geosciences and Biosciences Division.

Foreword

The Gas Phase Chemical Physics (GPCP) program enjoyed a significant expansion in the number of new principal investigators over the past year with awards covering a range of exciting topics impacting combustion, catalysis, and quantum information science. The GPCP program supports fundamental gas phase chemical physics research in four areas: Light-Matter Interactions, Chemical Reactivity, Chemistry-Transport Interactions, and Gas-Particle Interconversion. In addition to its traditional focus on clean and efficient combustion, the program has evolved to support fundamental research that impacts other energy-related areas with an emphasis on understanding, predicting, and ultimately controlling matter and energy at the electronic, atomic, and molecular level. The depth and breadth of this fundamental gas phase chemical physics research is reflected in this collection of abstracts and aligns well with the research objectives of the Department of Energy's Office of Basic Energy Sciences (BES).

We appreciate the privilege of serving in the management of this research program. In carrying out these tasks, we learn from the achievements and share the excitement of the research of the many sponsored scientists and students whose work is summarized in the abstracts published on the following pages. We thank all of the researchers whose dedication and innovation have advanced DOE BES research. We look forward to our assembly in 2020 for our 40th annual meeting.

Jeff Krause
Wade Sisk

Table of Contents

Table of Contents

Foreword	iii
Table of Contents	v
Abstracts	1
<u>Keynote Speaker Abstract</u>	
Michael Wasielewski, Department of Chemistry and Institute for Sustainability and Energy at Northwestern, Northwestern University – Exploiting Chemistry and Chemical Systems for Quantum Information Science.....	1
<u>Principal Investigators’ Abstracts</u>	
Musahid Ahmed, Martin Head-Gordon, Daniel M. Nuemark, David G. Prendergast and Kevin R. Wilson – Molecular Reactivity in Complex Systems.....	3
Scott L. Anderson – Nanoparticle Surface Kinetics and Dynamics by Single Nanoparticle Mass Spectrometry	7
Josette Bellan – Predictive Large-Eddy Simulation of Supercritical-Pressure Reactive Flows in the Cold Ignition Regime	11
Michael Burke – Chemical Kinetic Data of Benchmark Accuracy through Multi-Scale Informatics Strategies.....	15
David W. Chandler, Jonathan H. Frank, David L. Osborn, Leonid Sheps, and Judit Zádor – Chemical Dynamics Methods and Applications.....	19
Jacqueline H. Chen, Robert S. Barlow, and Jonathan H. Frank – Turbulence – Chemistry Interactions.....	23
Robert E. Continetti – Dynamics and Energetics of Elementary Combustion Reactions and Transient Species.....	27
Rainer N. Dahms, Reese Jones, Christopher J. Kliever, Hope A. Michelsen, and Judit Zádor – Gas Phase Interactions with Other Phases	31
H. Floyd Davis – Dynamics of Combustion Reactions.....	35
Michael J. Davis – Exploration of chemical-kinetic mechanisms, chemical reactivity, and thermochemistry using novel numerical analysis.....	39
Richard Dawes – Electronic structure methods and protocols with application to dynamics, kinetics and thermochemistry.....	43
Gary Douberly and Henry F. Schaefer III – Theoretical and Experimental Studies of Elementary Hydrocarbon Species and Their Reactions.....	47
Michael A. Duncan – Coordination and Solvation of Actinide Cations Studied with Selected-Ion Infrared Spectroscopy.....	51
Robert W. Field – Spectroscopic and Dynamical Studies of Highly Energized Small Polyatomic Molecules.....	55
C. Franklin Goldsmith – Gas Phase Chemical Kinetics Under Extreme Conditions.....	59

William H. Green – Computer-Aided Construction of Chemical Kinetic Models.....	61
Nils Hansen, David L. Osborn, and Krupa Ramasesha – Advanced Mass Spectrometry and X-Ray Diagnostics.....	65
Nils Hansen, Habib N. Najm, David L. Osborn, Craig A. Taatjes, and Judit Zádor – Chemical Kinetics for Complex Systems.....	69
Martin Head-Gordon, Eric Neuscammann, and David Prendergast – Theory of Electronic Structure and Chemical Dynamics.....	73
Ahren W. Jasper – Semiclassical Methods for Pressure Dependent Kinetics and Electronically Nonadiabatic Chemistry	77
Ahren W. Jasper, Stephen J. Klippenstein (PI), Raghu Sivaramakrishnan, Robert S. Tranter, Leonid Sheps, and Craig A. Taatjes (PI) – Argonne-Sandia Consortium on High-Pressure Combustion Chemistry.....	81
Ralf I. Kaiser – Probing the Reaction Dynamics of Hydrogen-Deficient Hydrocarbon Molecules and Radical Intermediates via Crossed Molecular Beams.....	85
Christopher J. Kliewer, David L. Osborn, Farid El Gabaly, Jonathan H. Frank, Nils Hansen, Coleman Kronawitter, and Ambarish Kulkarni – Imaging the Near-Surface Gas Phase: A New Approach to Coupled Gas-Surface Chemistry.....	89
Christopher J. Kliewer, David W. Chandler, Krupa Ramasesha, and Jonathan H. Frank – Ultrafast Physics: Nonlinear Optical Spectroscopy and Diagnostics.....	93
Stephen J. Klippenstein - Theoretical Chemical Kinetics.....	97
Nicole J. Labbe, G. Barney Ellison, and John W. Daily - A Coupled Theoretical and Experimental Approach to Elucidating the Mechanisms of Methyl Esters.....	101
Stephen R. Leone and Daniel M. Neumark– Fundamental Molecular Spectroscopy and Chemical Dynamics.....	105
Marsha I. Lester – Spectroscopy and Dynamics of Reaction Intermediates in Combustion Chemistry.....	109
Robert P. Lucht – Advanced Nonlinear Optical Methods for Quantitative Measurements in Flames.....	113
Laura R. McCunn – Thermal Decomposition of Cyclic, Oxygenated Hydrocarbons.....	117
Habib N. Najm – Estimation and Analysis of Uncertain Chemical Models.....	119
David J. Nesbitt - Spectroscopy, Kinetics and Dynamics of Combustion Radicals.....	123
Kang-Kuen Ni – State-to-State Reactions in the Ultracold Regime.....	127
William J. Pitz and Charles K. Westbrook – Chemical Kinetic Modeling of Combustion Chemistry.....	131
Stephen B. Pope and Perrine Pepiot - Investigation of Non-Premixed Turbulent Combustion.....	135
Stephen T. Pratt - Optical Probes of Atomic and Molecular Decay Processes.....	139
Kirill Prozument – Reaction Mechanisms Studied with Chirped-Pulse Rotational Spectroscopy.....	143
Krupa Ramasesha and Christopher Kliewer – Ultrafast Chemistry: Spectroscopic Probes of Non-Adiabatic Dynamics.....	147
Hanna Reisler - Photoinitiated Reactions of Radicals and Diradicals in Molecular Beams.....	151
Branko Ruscic – Active Thermochemical Tables.....	155

Trevor J. Sears – Spectroscopic Investigations of Molecular Symmetry Breakdown.....	159
Ron Shepard – Theoretical Studies of Potential Energy Surfaces and Computational Methods.....	163
Raghu Sivaramakrishnan – Mechanisms and Models for Simulating Gas Phase Chemical Reactivity.....	167
John F. Stanton – Quantum Chemistry of Radicals and Reactive Intermediates.....	171
Arthur G. Suits – Universal and State-Resolved Imaging Studies of Chemical Dynamics.....	175
Jeffrey A. Sutton – Multiscale Interaction of Turbulence, Temperature, and Soot Formation: Measurements for Critical Assessments of Chemical Kinetics and Mechanisms.....	179
Robert S. Tranter – Elementary Reactions of PAH Formation.....	183
Donald Truhlar, David R. Yarkony, and Hua Guo – Nonadiabatic Photochemistry.....	187
Lai-Sheng Wang – Probing Nonvalence Excited States of Anions Using Photodetachment and Photoelectron Spectroscopy.....	191
Margaret S. Wooldridge, Andrew B. Mansfield, and Robert S. Tranter – Fundamental Chemical Kinetics of Siloxane and Silicon Compounds.....	195
Timothy S. Zwier – Isomer-specific Spectroscopy of Aromatic Fuels and Their Radical Intermediates.....	197
Participant List	201

Keynote Speaker

Exploiting Chemistry and Chemical Systems for Quantum Information Science

Michael R. Wasielewski

Department of Chemistry and Institute for Sustainability and Energy at Northwestern
Northwestern University, Evanston, IL 60208-3113

The power of chemistry to prepare new compositions of matter has driven the quest for new chemical approaches to problems that have global societal impact, such as renewable energy, healthcare and information sciences. In the latter case, the intrinsic quantum nature of molecules offers intriguing new possibilities to advance the emerging field of Quantum Information Science (QIS). In this presentation, we will discuss how chemistry and chemical systems can impact quantum computing, communication and sensing. Hierarchical molecular design and synthesis from small molecules to supramolecular assemblies combined with new spectroscopic probes of quantum coherence, and theoretical modeling of complex systems offer a broad range of possibilities to realize practical QIS applications.

Chemically derived species differ from solid-state defect-based systems in two important ways. First, chemical synthesis allows control over the nature of the qubit itself, thus enabling the careful tuning of individual quantum states. Second, covalent and noncovalent interactions between molecules can be used to construct atomically precise arrays of qubit. This approach offers the possibility to interrogate the properties of an individual qubit in isolation and subsequently within an array through molecular design and spectroscopy, providing significant promise for discovering new insights into the quantum properties of multi-qubit arrays.

A fundamental criterion for a qubit is that it possesses at least two well-defined quantum states, making electron and/or nuclear spins in molecules natural qubit candidates. A single electron spin qubit may comprise an organic radical or paramagnetic metal center, in which the number of available spin states is defined by its spin multiplicity ($2S+1$). These spin states can be further split by hyperfine interactions, spin-orbit coupling, and zero-field splitting. The spin state population at a given temperature is dictated by Boltzmann statistics, which depends on the energy gap (ΔE) between the spin states and the available thermal energy (kT); thus if $\Delta E \gg kT$, the lowest energy spin state can be prepared as a pure quantum state. The use of chemistry to prepare molecular systems with desirable QIS properties will be illustrated by recent work on molecules having well-defined electron spin states. These states can be prepared using a variety of optical techniques including direct generation of higher multiplicity excited states, diradicals and triradicals.

*Abstracts
of
Principal Investigator
Awards*

Molecular Reactivity in Complex Systems

Musahid Ahmed, Martin Head-Gordon, Daniel M. Neumark, David G. Prendergast, Kevin R. Wilson
Lawrence Berkeley National Laboratory, 1 Cyclotron Road, Berkeley, CA-94720.
mahmed@lbl.gov, mhead-gordon@lbl.gov, dmneumark@lbl.gov, dgprendergast@lbl.gov, krwilson@lbl.gov.

Program Scope: We seek to target complex multistep and multiphase chemical transformations that extend beyond elementary unimolecular and excited state reactions. The approach is to build complexity from isolated elementary bimolecular reactions to gas surface reaction dynamics to coupled networks of elementary unimolecular and bimolecular pathways embedded at a gas/solid or liquid interface. In each of these areas, the gas phase is central for controlling reactivity. Activities in this subtask drive new theory and simulation to enrich the molecular level interpretation of experiments. Cross-cutting themes of *Chemistry at Complex Interfaces* and *Reaction Pathways in Diverse Environments* are explored, providing valuable basic insights into microscopic processes relevant to energy generation, storage and combustion.

Recent Progress:

Non-covalent Interactions and Molecular Chemistry. This research effort investigates proton and charge transfer in hydrogen bonded, π -stacked and solvated systems using synchrotron based molecular beams mass spectrometry coupled with electronic structure calculations of Head Gordon.¹ Ahmed and Head-Gordon have formulated an understanding as to how non-covalent interactions can drive chemical reactivity in small acetylene clusters upon photoionization. A dramatic dependence of product distribution on the ionization conditions is observed and interpreted by theory.² Within a polycyclic aromatic hydrocarbon (PAH) system interacting with water, there is an increase in the scope for interesting structural rearrangements to stabilize the positive charge upon ionization, as well as increased potential for reactive chemical events to occur upon ionization.³ A novel microfluidic device to probe gas phase evaporation from liquids has been incorporated into the experimental suite.⁴

Molecular Chemistry of Hydrocarbon Growth & Decomposition. The multistep reaction network of PAHs with free radicals is being examined in collaboration with Ralf Kaiser (Hawaii) and Alex Mebel (Florida International). This is achieved by simulating combustion relevant conditions (pressure, temperature, reactant molecules) in a high temperature ‘chemical reactor’. The reactions of the styrenyl and the *ortho*-vinylphenyl radicals—key transient species of the Hydrogen Abstraction Acetylene Addition (HACA) mechanism—with C_2H_2 does lead to the formation of naphthalene,⁵ and the reaction of *ortho*-biphenyl radical with C_2H_2 , also leads to the synthesis of phenanthrene,⁶ but not to anthracene. A new mechanism – hydrogen abstraction-vinylacetylene (HAVA) addition^{7,8} is needed in addition to HACA to explain formation of 4 membered rings, demonstrated recently for the 4-phenanthrenyl radical reaction with acetylene.⁹ The HAVA mechanism is also invoked to understand low temperature formation pathways for the formation of anthracene and phenanthrene in the reaction of the naphthyl radical with vinylacetylene via the formation of van der Waals complexes.¹⁰ A synthetic route to racemic helicenes via a vinylacetylene mediated gas phase chemistry involving elementary reactions with an aryl radical, 4-phenanthrenyl radical was demonstrated.¹¹

The unimolecular decomposition pathways of jet fuel (decane,¹² dodecane,¹² and *exo*-tetrahydrodicyclopentadiene¹³) decomposition and new radical pathways have been elucidated experimentally and confirmed via theoretical calculations and simulations in collaboration with Kaiser and Mebel. The functional relationships between kinetic, flow, and geometrical parameters of the micro-reactor have recently been established.¹⁴ In collaboration with Barney Ellison (Colorado), the thermal decomposition of the benzyl radical,¹⁵ the simplest carbohydrate, glycolaldehyde, and glyoxal,¹⁶ and lignin model compounds: Salicylaldehyde and Catechol, were completed.¹⁷

Multiphase Reaction Networks: Substantial effort has been dedicated to understanding how gas phase mechanisms of peroxy radicals (RO_2) and Criegee intermediates (CI) are modified by the presence of an organic interface. Recently, we reported a new multiphase reaction mechanism¹⁸ by which Criegee intermediates (CIs), formed by ozone attack at an alkene surface, oxidize SO_2 to SO_3 to produce sulfuric acid.

Using our previously validated kinetic model¹⁹ developed in collaboration with Frances Houle (LBNL), we were able to quantitatively predict the reaction rates and product formation pathways as well as the observed facile chemical erosion of the interface. This model also predicted the rapid nucleation of H₂SO₄ particles from the heterogeneous production of SO₃ by CI. This system is a nice example of how interfacial reactions involving CI can activate gas phase molecules that participate in further reactive chemistry.

Reaction-Diffusion in Heterogeneous Reactions: In collaboration with Frances Houle (LBNL) we have completed a simulation study²⁰ of how the kinetics of a gas-surface reactions depend upon diffusion times of molecules two and from an interface. We found for a given reaction network involving standard OH initiated peroxy radical chemistry, that the diffusive properties of the interface (e.g. glass or semisolid vs. liquid) activate different branches of a reaction network during a heterogeneous reaction.²¹ This originates from competition between the relative reaction and diffusion timescales. For example, for the same reaction network ketone reaction products are favored when diffusively limited to an interface, compared with mixtures of alcohols and ketone when the transformation is only reaction limited. When the OH collision and organic diffusion rates are comparable, the overall heterogeneous reactivity is highly sensitive to the details of both OH concentration and internal mixing dynamics.

Particle formation Pathways: In an ongoing collaboration with Hope Michelsen (Sandia)²²⁻²⁵ we examined soot formation chemistry using flame sampling aerosol mass spectrometry. In recent work²⁴ led by Michelsen with theory from Martin Head-Gordon, a new mechanism for incipient particle formation was proposed. Central to this mechanism is the rapid molecular clustering–reactions by radicals with extended conjugation, which form covalently bound complexes that promote further molecular weight growth by regenerating resonance-stabilized radicals.

Future Plans:

Bimolecular gas phase chemistry - Ahmed in collaboration with Ralf Kaiser plan to understand how larger ring (4 and higher) formation leads to the mass-growth processes from simple PAHs to soot particles utilizing the heated reactor coupled to synchrotron based mass spectrometry. This will be achieved, by preparing the brominated precursor molecules (synthesized by Felix Fischer, LBNL) which can undergo bromine-carbon bond ruptures by pyrolysis leading to radical intermediates that react subsequently with acetylene or vinylacetylene to form coronene, fluoranthene, and/or corannulene. The elucidation of the formation routes of these three key PAHs has the potential to revolutionize the understanding of the underlying mass growth processes from simple precursors via complex PAHs. Alex Mebel has been instrumental in computing reaction mechanisms based upon our observations, and also predicting certain pathways and we will be guided by him in this enterprise. These theoretical and experimental details will be necessary to design and interpret the reaction mechanisms that will no doubt arise as we move towards understanding the 2D and 3 D structures of these carbon growth processes. A new direction is to probe gas phase hydrocarbon reactions in confined spaces such as in zeolites by introducing these species into the heated reactor. We anticipate that our scaled down reactor with chemistry being arrested after microsecond reaction times (typical residence times in our reactor are 20-50 microseconds) will allow for reactive intermediates to be captured in the supersonic expansion of a molecular beam. A key here is that the gas phase chemistry will have been directly probed using the same reactor, to allow a comparison with heterogeneity in the dynamics with an introduction of a surface.

Non-covalent Interactions: Reactions Dynamics in Clusters. We will continue our program on the application of VUV photoionization and theoretical calculations to decipher kinetics, dynamics and photo-induced reactivity in molecular clusters, especially hydrogen-bonded and van der Waals clusters.²⁶ We will examine glycerol/water as a model for hydrophilic interactions to compare and contrast ongoing work with PAH/water as a model for hydrophobic interactions. Glycerol contains three hydroxyl groups and is miscible with water; we believe that such rich dynamics based upon hydrogen bonding between water and glycerol can become accessible with a judicious combination of experiments and theory.

Gas liquid interface scattering dynamics: Increasing in complexity beyond bimolecular reactive events in clusters, Neumark leads a new direction in gas surface reactions, by the scattering of atoms and free radicals from the liquid interfaces of flat jets, with particular focus on water jets. The role of solvent and the surface should affect the dynamics substantially when compared to the analogous dynamics observed in binary gas phase collisions. This approach, which focuses on the "gas side" of the gas-liquid interface, connects to work on multiphase reactions pathways at organic nanoparticles surfaces, examined by Wilson. The incorporation of flat jet technology into Neumark's existing molecular beam scattering instrument will bring a new capability to this program. The planned experiments will provide unprecedented insights into how the well-understood binary interactions that govern gas phase collision dynamics are modified when one of the scattering partners is a liquid. Initial experiments will focus on elastic and inelastic scattering of rare gas atoms from a flat water jets through measurement of angular and translational energy distribution of the scattered atoms. This will be followed by scattering water soluble molecules such as CH₃OH and NH₃ in order to determine the relative contributions of direct scattering from the surface vs. uptake into the solution followed by thermal desorption. Ultimately the goal of this work will be to study reactive scattering from liquid water jets.

Multiphase Reaction Mechanisms: Future work will focus on addressing heterogeneous reaction mechanisms in the OH + alkene system. Preliminary evidence shows OH prefers to add to the C=C at an alkene interface. After subsequent O₂ addition we find evidence for the facile conversion of the hydroxy peroxy radical into a CI. Efforts are currently underway to examine the subsequent fate of the CI in the condensed phase, but preliminary experiments show evidence for autooxidation driven by the decomposition of the CI producing an OH radical. Working with Martin Head-Gordon we are examining mechanisms for the interconversion of hydroxyl peroxy radicals and CI in an effort to build a predictive multiphase kinetic model of OH addition reaction at organic interfaces.

Heterogeneous reactions of Criegee Intermediates: We will examine the heterogeneous reactivity of small CI at organic interfaces. Using the CI precursors, developed by Taatjes, Osborn and coworkers at Sandia, we will measure the reaction probability of the C₁ CI at nanoparticle surfaces comprised of carboxylic acids and alcohols. Here the objective is to use growing knowledge base of gas phase reaction rates and mechanisms of CI to understand how these elementary pathways are modified at an organic surface.

X-ray Probes of Heterogeneous Reactions: Working with Ahmed we will continue^{27, 28} our development of photoemission probes of gas-surface reactions. We will use nanoparticle X-ray photoelectron spectroscopy and X-ray Absorption Spectroscopy in conjunction with mass spectrometry to examine the reactions outlined above under diffusively confined conditions in which the reaction is expected to be localized within a few nanometers of the interface. Instrumentation development will consist of efforts of increasing solid nanoparticle transmission efficiency through the aerodynamic lens interface.

Work supported by BES-GPCP program (2016-present)

1. B. Bandyopadhyay, T. Stein, Y. Fang, O. Kostko, A. White, M. Head-Gordon and M. Ahmed, *J. Phys. Chem. A* **120**, 5053–5064 (2016).
2. T. Stein, B. Bandyopadhyay, T. P. Troy, Y. Fang, O. Kostko, M. Ahmed and M. Head-Gordon, *Proc. Natl. Acad. Sci. U.S.A.* **114** (21), E4125-E4133 (2017).
3. B. Xu, T. Stein, U. Ablikim, L. Jiang, J. Hendrix, M. Head-Gordon and M. Ahmed, *Faraday Discussions* (2019). DOI: 10.1039/c8fd00229k
4. R. Komorek, B. Xu, J. Yao, U. Ablikim, T. P. Troy, O. Kostko, M. Ahmed and X. Y. Yu, *Rev Sci Instrum* **89** (11), 115105 (2018).
5. T. Yang, T. P. Troy, B. Xu, O. Kostko, M. Ahmed, A. M. Mebel and R. I. Kaiser, *Angew Chem Int Edit* **55** (48), 14983-14987 (2016).
6. T. Yang, R. I. Kaiser, T. P. Troy, B. Xu, O. Kostko, M. Ahmed, A. M. Mebel, M. V. Zagidullin and V. N. Azyazov, *Angew Chem Int Edit* **56** (16), 4515-4519 (2017).

7. L. Zhao, R. I. Kaiser, B. Xu, U. Ablikim, M. Ahmed, M. V. Zagidullin, V. N. Azyazov, A. H. Howlader, S. F. Wnuk and A. M. Mebel, *J Phys Chem Lett* **9** (10), 2620-2626 (2018).
8. L. Zhao, B. Xu, U. Ablikim, W. Lu, M. Ahmed, M. M. Evseev, E. K. Bashkirov, V. N. Azyazov, A. H. Howlader, S. F. Wnuk, A. M. Mebel and R. I. Kaiser, *ChemPhysChem* **20**, 791, (2019).
9. L. Zhao, R. I. Kaiser, B. Xu, U. Ablikim, M. Ahmed, D. Joshi, G. Veber, F. R. Fischer and A. M. Mebel, *Nature Astronomy*, doi:10.1038/s41550-41018-40399-y (2018).
10. L. Zhao, R. I. Kaiser, B. Xu, U. Ablikim, M. Ahmed, M. M. Evseev, E. K. Bashkirov, V. N. Azyazov and A. M. Mebel, *Nature Astronomy* **2** (12), 973-979 (2018).
11. L. Zhao, R. I. Kaiser, B. Xu, U. Ablikim, W. Lu, M. Ahmed, M. M. Evseev, E. K. Bashkirov, V. N. Azyazov, M. V. Zagidullin, A. N. Morozov, A. Hasan-Howlader, S. F. Wnuk, A. M. Mebel, D. Joshi, G. Veber and F. R. Fischer, *Nature Communications* **10**, 1-8 (2019).
12. L. Zhao, T. Yang, R. I. Kaiser, T. P. Troy, B. Xu, M. Ahmed, J. Alarcon, D. Belisario-Lara, A. M. Mebel, Y. Zhang, C. C. Cao and J. B. Zoue, *Phys Chem Chem Phys* **19** (24), 15780-15807 (2017).
13. L. Zhao, T. Yang, R. I. Kaiser, T. P. Troy, M. Ahmed, J. M. Ribeiro, D. Belisario-Lara and A. M. Mebel, *J. Phys. Chem. A* **121** (6), 1281-1297 (2017).
14. M. V. Zagidullin, R. I. Kaiser, D. P. Porfiriev, I. P. Zavershinskiy, M. Ahmed, V. N. Azyazov and A. M. Mebel, *J Phys Chem A* **122** (45), 8819-8827 (2018).
15. G. T. Buckingham, J. P. Porterfield, O. Kostko, T. P. Troy, M. Ahmed, D. J. Robichaud, M. R. Nimlos, J. W. Daily and G. B. Ellison, *J. Chem. Phys.* **145** (1), 014305 (2016).
16. J. P. Porterfield, J. H. Baraban, T. P. Troy, M. Ahmed, M. C. McCarthy, K. M. Morgan, J. W. Daily, T. L. Nguyen, J. F. Stanton and G. B. Ellison, *J. Phys. Chem. A* **120** (14), 2161-2172 (2016).
17. T. K. Ormond, J. H. Baraban, J. P. Porterfield, A. M. Scheer, P. Hemberger, T. P. Troy, M. Ahmed, M. R. Nimlos, D. J. Robichaud, J. W. Daily and G. B. Ellison, *J Phys Chem A* **122** (28), 5911-5924 (2018).
18. N. Heine, C. Arata, A. H. Goldstein, F. A. Houle and K. R. Wilson, *The Journal of Physical Chemistry Letters* **9** (12), 3504-3510 (2018).
19. N. Heine, F. A. Houle and K. R. Wilson, *Environ. Sci. Technol.* **51** (23), 13740-13748 (2017).
20. F. A. Houle, A. A. Wiegel and K. R. Wilson, *Environmental Science & Technology* **52** (23), 13774-13781 (2018).
21. A. Wiegel, M. Liu, W. D. Hinsberg, K. R. Wilson and F. A. Houle, *Phys Chem Chem Phys* (2017).
22. K. O. Johansson, T. Dillstrom, P. Elvati, M. F. Campbell, P. E. Schrader, D. M. Popolan-Vaida, N. K. Richards-Henderson, K. R. Wilson, A. Violi and H. A. Michelsen, *Proceedings of the Combustion Institute* **36** (1), 799-806 (2017).
23. K. O. Johansson, T. Dillstrom, M. Monti, F. El Gabaly, M. F. Campbell, P. E. Schrader, D. M. Popolan-Vaida, N. K. Richards-Henderson, K. R. Wilson, A. Violi and H. A. Michelsen, *Proceedings of the National Academy of Sciences* **113** (30), 8374-8379 (2016).
24. K. O. Johansson, M. P. Head-Gordon, P. E. Schrader, K. R. Wilson and H. A. Michelsen, *Science* **361** (6406), 997-1000 (2018).
25. K. O. Johansson, J. Zádor, P. Elvati, M. F. Campbell, P. E. Schrader, N. K. Richards-Henderson, K. R. Wilson, A. Violi and H. A. Michelsen, *The Journal of Physical Chemistry A* **121** (23), 4475-4485 (2017).
26. O. Kostko, B. Bandyopadhyay and M. Ahmed, *Annu. Rev. Phys. Chem.* **67** (1), 19-40 (2016).
27. M. I. Jacobs, O. Kostko, M. Ahmed and K. R. Wilson, *Physical Chemistry Chemical Physics* **19** (20), 13372-13378 (2017).
28. M. I. Jacobs, B. Xu, O. Kostko, N. Heine, M. Ahmed and K. R. Wilson, *J Phys Chem A* **120** (43), 8645-8656 (2016).

Nanoparticle Surface Kinetics and Dynamics by Single Nanoparticle Mass Spectrometry

Scott L. Anderson,

Chemistry Department, University of Utah

315 S. 1400 E.

Salt Lake City, UT 84112

anderson@chem.utah.edu

Program Scope

This project is focused on developing and using single nanoparticle mass spectrometry (NPMS) – a new method – to measure reaction kinetics and emission spectroscopy for individual laser-heated carbon nanoparticles (NPs) trapped in controlled atmospheres. The focus is on sublimation and oxidation of carbon NPs, but NPMS is broadly applicable to nano-structured refractory materials. The main questions we seek to address relate to the effects of heterogeneity on NP kinetics and spectroscopy. There are two types of heterogeneity of interest: 1. NPs are inherently heterogeneous, with significant NP-to-NP variation in size, shape, and structure, all of which can affect reaction kinetics, and possibly spectroscopy. In particular, carbon NPs of interest for energy applications (e.g. soot, chars) are extremely heterogeneous materials. 2. *Individual NPs* also have significant distributions of surface sites, and the site distributions and resulting surface reaction kinetics vary significantly as the NP evolves during reaction. In addition to fundamental interest in

understanding heterogeneity effects, this kind of information is essential to understanding and modeling carbon NP chemistry on a molecular level.

Methodology

The NPMS trap and optical system is shown in Fig. 1. A single NP is confined in the split ring-electrode quadrupole trap (SRET),¹ by the effects of an rf voltage with amplitude (V_0) and frequency (F_0). The trapped NP motion can be described as slow “secular” motion, with superimposed micro-

motion at frequency F_0 .² The secular motion is harmonic, with frequencies f_z and f_r , for axial and radial motion, proportional to Q/M . For example, $f_z = \frac{|Q|}{M} \left(\frac{V_0 \sqrt{2}}{F_0 z_0^2 4\pi^2} \right)$, where z_0 is a trap geometric parameter (2.97 mm). As shown by the inset in Fig. 2, the NP is detected optically, f_z is measured by a resonance method, and Q is determined exactly by observing steps in f_z from $\pm e$

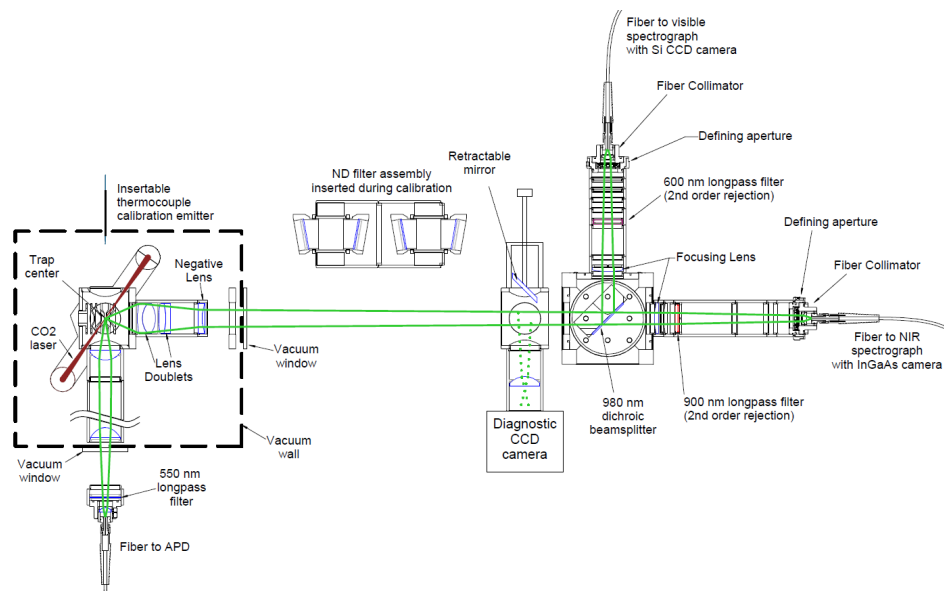


Fig. 1. SRET with new optical system

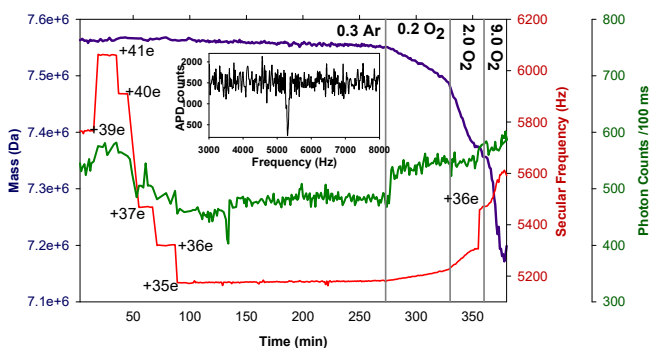


Fig. 2. f_z , APD signal, and M vs. time for a graphite NP pumped at 532 nm. Q is indicated at each charge step.

changes in Q (main part, Fig. 2), induced by a VUV lamp. M , thus, can be measured over time by repeated f_z measurements.

Kinetics for sublimation, addition reactions, and etching reactions like oxidation, can be followed by tracking M vs. time, as the NP is laser-heated and exposed to either inert or reactive atmospheres. (Some gas is needed to damp NP motion). NPMS allows the NP-to-NP heterogeneity of particles of different types to be directly measured. In addition, the number of reactive defect and edge sites on each individual NP can be measured using a site titration process. For example, acetylene selectively adds to graphitic defect and edge sites, allowing kinetics to be correlated with the number of reactive sites.

Typical Results

To illustrate the method, and the dynamic nature of the kinetics we are observing, Figs. 3 and 4 show typical results for sublimation and oxidation of individual graphite and carbon black NPs. The graphite NP in Fig. 3 had initial mass of ~ 35.13 MDa, which would be ~ 37 nm diameter, if the particle were spherical. The ~ 10 K random fluctuations in NP temperature (T_{NP}) an artifact of the fitting process used to extract T_{NP} , and provide a measure of the T_{NP} uncertainty. Note that T_{NP} decreases by ~ 25 K (1.3%) in the hour-long experiment, despite the measured laser intensity having been held constant using a PID controller. The implication is that the absorption cross section for the 532 nm heating laser changed as the particle evolved.

Two types of kinetics are illustrated. For the first ~ 1200 sec, the NP was trapped in Ar, sublimating at a steady rate of ~ 8 carbon atoms/sec. If the particle were spherical, this would correspond to loss of $\sim 10^{-4}$ monolayers/sec. At 1200 sec, 0.05 mTorr of O_2 was added to the argon, and the mass loss rate increased to ~ 115 carbon atoms/sec, due to oxidation. One interesting point is that the oxidation rate slows substantially with time, even though T_{NP} is stable to better than 1%. We frequently see this kind of behavior during oxidation or sublimation at faster rates, and attribute it to evolution of the particle surface site distribution.

Both sublimation and oxidation occur primarily at low coordination edge or defect sites, rather than the more stable basal plane sites. The number of these low coordination sites evolves as the NP reacts/sublimes, due to a combination of preferential reaction at those sites, and annealing of the surface that tends to remove such sites. In the example in Fig. 3, reactive site loss dominated. Note that when the O_2 was removed, the final sublimation rate was also slower, for the same reason.

Fig. 4 shows a similar experiment for a carbon black NP (~ 61.5 nm, assuming 1.7 g/cc density), in which both the laser intensity and the gas composition were varied. In the initial period, T_{NP} was stepped down from 1670 K to 1572 K (temperatures averaged for each segment), resulting in sublimation rate dropping from 50 to 20 carbon atoms/sec. T_{NP} was then lowered to ~ 1400 K, and $\sim 6\%$ O_2 added to the Ar buffer gas. Oxidative mass loss occurred at rates ranging from 1022 C atoms/sec, generally slowing with time to ~ 304 C atoms/sec.

This figure shows two additional complexities, which we frequently see during oxidation. The addition of O_2 takes less than a second, i.e., much less than the time between mass points. Note, however, that when O_2 was first introduced, the oxidation rate slowly increased for the first few minutes. As noted, the rate then gradually slowed with time (with some evidence of inflections), but then over the last ~ 1000 seconds, began to increase again. As discussed above, decreasing oxidation rates are taken as evidence that the number of low-coordination reactive sites decreased during the oxidation or sublimation of the

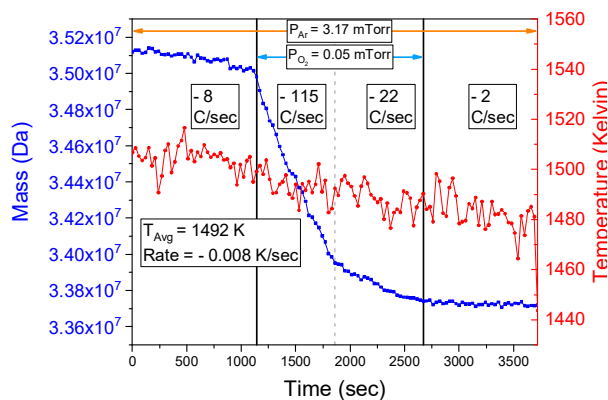


Fig. 3. M and T_{NP} vs. time for a graphite NP in inert and oxidizing atmospheres.

NP. Increasing rates are typically seen at higher temperatures or faster oxidation rates, and we tentatively attribute them to the competition between annealing, which tends to remove reactive sites, and etching which can add reactive sites by, for example, etching pits into basal plane surfaces.

Recent Progress

A major activity since the project started has been development of an optical system (Fig. 1) that has sufficient sensitivity to measure single NP spectra quickly, but that also has accurately calibrated sensitivity vs. wavelength.

This includes a Si avalanche photodiode (APD) for f_z measurements, and a pair of spectrographs that use deep-cooled Si CCD and InGaAs photodiode arrays to record spectra over the 400 nm to 1650 nm range, with high sensitivity. In addition, the system includes a pair of inexpensive CCD cameras, one of which is shown, used to align the emitter used in calibration of the optical sensitivity. Achieving accurate sensitivity calibration over such a wide wavelength (λ) range turns out to be the most difficult aspect of the problem. An initial version of the optical system, and details of the calibration method, were published in early 2019,³ however, we since have improved the system, which is briefly described here.

In principle, the approach is simple. A CO₂-laser-heated thermocouple (TC) fabricated from 78 micron dia. type C (W-Re) wire is used as the calibration emitter. Emissivity of W and Re are well known, thus the TC provides variable spectra with well-known intensity vs. λ . The procedure is as follows. A single NP is trapped and imaged on the two Si CCD alignment cameras, thus marking the trap center to within a few microns. A precision XYZ vacuum manipulator, in conjunction with the alignment cameras, is then used to position the hot TC, which has a flatten bead with ~ 280 μm diameter, such that its front face is centered at the trap center. This gives us a well-defined emitter at the same source position as the NPs. Spectra are recorded for the TC emitter at several temperatures, and then the detection sensitivity vs. λ is determined as the ratio of the experimental spectra to the emissivity-corrected Planck's law spectra. This sensitivity function can then be used to correct measured NP spectra.

There are several complications in implementing this approach, however. First, the TC emission spectra are $\sim 10^8$ times more intense than the NP spectra, and clearly it is not reasonable to assume that the detector arrays are linear over such a wide range. Therefore, we constructed an attenuator with 4 OD 2 neutral density filters, which is inserted in the optical path when the TC is being measured. The difficulty, of course, is that neutral density filters are not very "neutral", and the manufacturer transmission data are not accurate enough for our purposes. Therefore, we measured the filter transmission using our spectrograph system, finding that the net transmission varies non-monotonically between 3.65 and 5.70×10^{-8} over our λ range.

The more difficult problem is assuring that the system has identical chromatic aberrations for the TC and NP spectra, so that they cancel, and the issue is that the TC emitter size (~ 280 μm) is substantially larger than the NP emitter size, which is effectively the volume that the NP explores in its oscillations in the trap (~ 100 μm). The published optical system used an aspheric achromat to collect and image light onto a pair of apertures that only allowed detection of light from the central region of the TC. That worked, but was found to be extremely sensitive to misalignment of the optics. Therefore, ray-tracing was used to develop the more elaborate 5-element light collection system shown in Fig. 1, and the optics coupling light into the fibers were also changed. The new system is substantially more achromatic, and the spectra are found to be tolerant to substantial misalignment. That means that the apertures, focusing

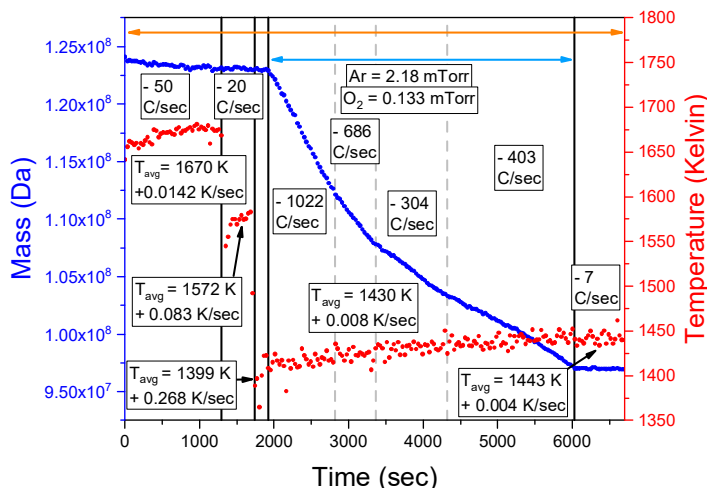


Fig. 4. M and T_{NP} vs. time for a carbon black NP in inert and oxidizing atmospheres.

lenses, and fiber collimators can all be misaligned at least ± 1 mm radially, and ± 6 mm axially, with no change in the spectral shape, the TC-corrected NP spectra, or the extracted NP temperature. In addition, the new optical system is more efficient – the signal/noise of the NP spectra was improved by a factor of ~ 5 . Example spectra, acquired during the kinetics experiments of Figs. 3 and 4, are shown in Fig. 5, along with fits used for T_{NP} determination. It can be seen that the signal/noise is excellent. Note also that there are significant differences in the curvature of the spectra for graphite and carbon black, suggesting that we may need a more sophisticated function to represent the effects of materials properties, i.e., $n(\lambda)$, on the spectra.

Future plans

We have made substantial progress in automating the entire experiment over the past year. T_{NP} is now determined during the kinetics measurements, rather than by post-experiment spectral fitting, and the mass-determination algorithm is now able to handle the large jumps in f_z that accompany charge steps or NP fragmentation, which tend to occur at higher T_{NP} . We are currently working on automatic charge stepping for Q determination, and NP injection from an ensemble of NPs stored a linear quadrupole just before the trap. Once that is completed, automated 24/7 operation will be possible.

So that activities like automation development, or testing new NP sources (e.g., aerosol/flame sampling), can be done without impeding the kinetics and spectroscopy experiments, we have completed construction of a 2nd instrument. This was possible because I had spare chambers and duplicates of the NP source, trap and other ion optics, and an undergraduate interested in instrumentation. This 2nd “test” instrument is functionally identical to the main instrument, with the exception that it does not have the spectrographs. It does, however, have all the parts needed to test NP injection, charge stepping, new sources, and initial kinetics work as function of laser power, rather than T_{NP} .

On the main instrument, experiments are proceeding on two fronts. We are currently doing a series of experiments measuring emission spectra for different carbon (graphite, graphene, carbon black, carbon dots) and non-carbon (silicon, silica, tungsten) NPs, with the goal of understanding how the spectra depend on the composition, T_{NP} , atmosphere. These results should be quite interesting to other groups interested in understanding NP thermal emission, and using NPs as temperature probes. These spectra are being acquired in the course of kinetics experiments on these particles, and we intend to publish the spectral results first, as they require much less analysis, but then the kinetics results, as they are analyzed to obtain insight into the effects of NP structure and T_{NP} on reaction rates.

References

1. Gerlich, D.; Decker, S., Trapping Ions at High Temperatures: Thermal Decay of C_{60}^+ . *Appl. Phys. B: Lasers Opt.* **2014**, *114*, 257-266.
2. Schlemmer, S.; Illelmann, J.; Wellert, S.; Gerlich, D., Nondestructive High-Resolution And Absolute Mass Determination Of Single Charged Particles In A Three-Dimensional Quadrupole Trap. *J. Appl. Phys.* **2001**, *90* (10), 5410-5418.
3. Long, B. A.; Rodriguez, D. J.; Lau, C. Y.; Anderson, S. L., Thermal emission spectroscopy for single nanoparticle temperature measurement: optical system design and calibration. *Appl. Opt.* **2019**, *58* (3), 642-649.

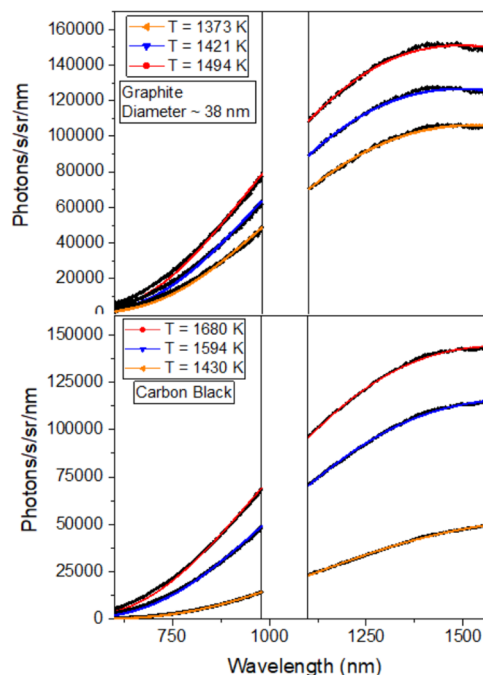


Fig. 5. Emission spectra measured for T_{NP} determination during kinetics.

Predictive Large-Eddy Simulation of Supercritical-Pressure Reactive Flows in the Cold Ignition Regime

Josette Bellan

Mechanical and Civil Engineering Department, California Institute of Technology
Pasadena, CA 91125

Josette.Bellan@jpl.nasa.gov

DOE Award Number: **02_GR-ER16107-14-00**

STRIPES award number: **SC0002679/0009**

I. Program Scope

This study addresses issues highlighted in the Basic Energy Needs for Clean and Efficient Combustion of 21st Century Transportation Fuels (DOE BES, 2006) under the topic of Combustion under Extreme Pressure. It is there noted that “the most basic concepts of thermal autoignition” are “based on experience and theory at near atmospheric pressures” and that “as pressure increases significantly..., many of these conceptual pictures begin to change or disappear”. It is also stated “A better description of the coupling and interaction of high pressure flow and molecular transport processes with chemistry is also necessary”, particularly because “Ignition and flame propagation of alternative and renewable fuels, as well as of the changing feed stocks of conventional fossil-based fuels, are very likely to be much different at very high pressures than under the more familiar, lower pressure conditions of current engines.” Recognizing that “Under such (*increasing pressure*) conditions distinctions between gas and liquid phases become moot, new equations of state must be used...”, it is immediately apparent that there must be “a re-examination of the basic assumptions that govern the physics and chemistry related to combustion; and the need for this type of re-examination increases as the combustion pressure increases.” This recognition is also stated under the topic of Multiscale Modeling since due to the new equations of state “The combination of unexplored thermodynamic environments and new physical and chemical fuel properties results in complex interactions among multiphase (*according to the above, the multiphase distinction becomes moot with increasing pressure*) fluid dynamics, thermodynamic properties, heat transfer, and chemical kinetics that are not understood even at a fundamental level.” From the theoretical viewpoint for “systems at high pressure, fluid dynamic time scales can be comparable to chemical time scales.” and therefore “completely diffusion-controlled reactions ... can become important”.

Thus, the objective of this study is the investigation of the coupling among thermodynamics, transport properties, intrinsic kinetics and turbulence under the high-pressure and the relatively (with respect to combustion) low-temperature conditions typical of the auto-ignition regime, with particular emphasis on the manifestation of this coupling on the effective kinetic rate. We have initiated a collaboration with Dr. Branko Ruscic of Argonne National Laboratory on the topics of thermodynamics and transport properties.

II. Recent Progress

This report contains results obtained during the previous year of funding. The focus of the research during that year was on obtaining an accurate model of the turbulent reaction rate under high-pressure (high-p) conditions and on examining the influence of the simplified representation of a mixture composition as far as the behavior of each species. To this effect we (1) used our Direct Numerical Simulations (DNS) high-p reactive flow database [i] to evaluate the concept behind the Double-Conditioned Source-term Estimation (DCSE) method

[ii] for modeling the turbulent reaction rate, and (2) analyzed the DNS database of increasingly complex mixtures, to determine whether the large density gradients ($O(10^6)$ kg/m^4) populating the flow field necessitate revision of the Navier-Stokes equations to account for potential material interfaces.

(1) The DNS database considered is of a temporal three-dimensional mixing layer having coordinates (x_1, x_2, x_3) and the analysis is performed at the time station of the domain-integrated peak pressure (t_{pp}^*). In DCSE, the complexity of the spatial distribution of the turbulent reaction rate is addressed by judiciously

selecting variables such that, when conditioning the turbulent reaction rate (TRR) on these variables, the variation of the conditioned reaction rate decreases with respect to the known variation of the conditioning variable. To understand the target to be achieved in DCSE, we first computed the TRR p.d.f. at t_{pp}^* . This p.d.f. is shown in Fig. 1 for one of the realizations of the DNS database; to mimic

a LES database, i.e. the template, the DNS database has been filtered (top-hat filter; filter width Δ). The success in reproducing the TRR with DCSE with the mixture fraction as a first conditioning variable is shown in Fig 2 for two Δ values. In Figs 2a and 2c, the 45 degrees line signifies a perfect model. Of note are the excellent results in Figs. 2b and 2d obtained for a non-dimensional reaction rate larger than 0.4, even for an enlargement by a factor of $O(10^5)$ in the computational volume, i.e. $\Delta/\Delta_{\text{DNS}} = 48$.

(2) We have extended Korteweg's second-gradient theory, made it valid for a mixture of an indefinite number of species, and made it consistent with the Harstad and Bellan [iv] form of the fluxes thereby extending the Korteweg theory to the formulation of Masi et al. [v]; this is a major fundamental development. In so doing, we have found that not only is the contribution to the pressure-tensor more complex than in the previously existing theory, but also that there are contributions to the species and energy conservation equations in the form

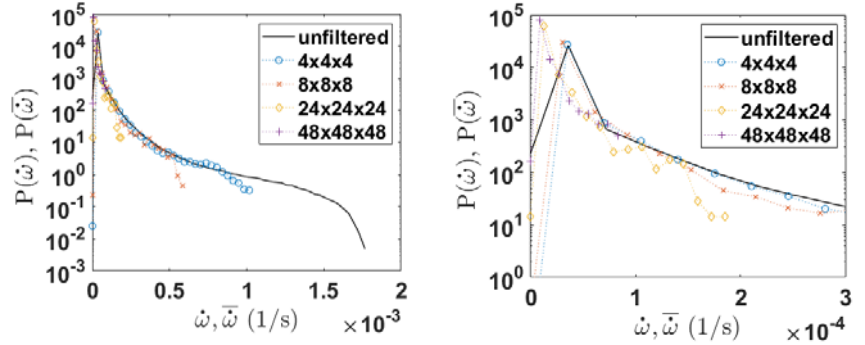


Figure 1. Probability density function of the turbulent reaction rate, and of the filtered turbulent reaction rate at different values of $\Delta/\Delta_{\text{DNS}}$ (left) the entire p.d.f.s and (right) enlargement of the smaller reaction-rate regime.

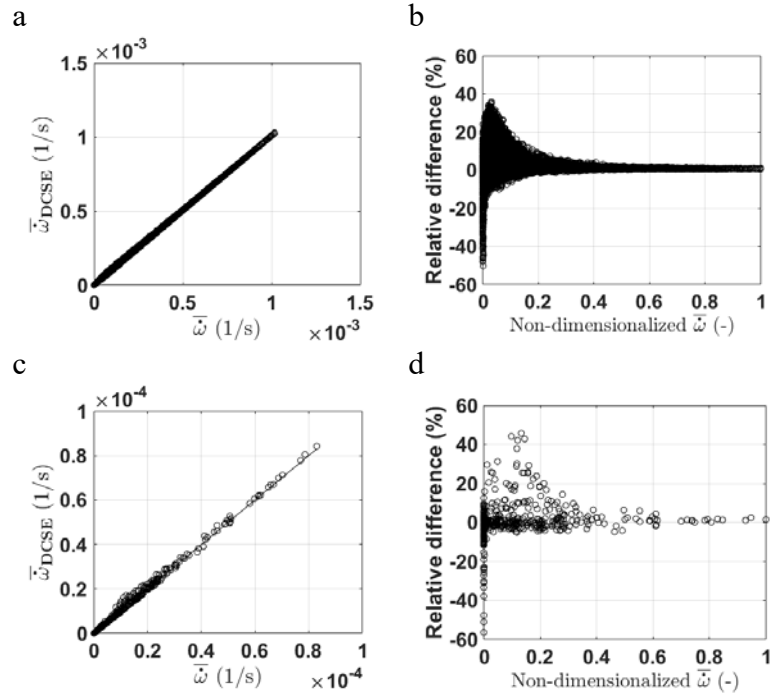


Figure 2. DCSE predictions using a normalized Y_{CO_2} as the second conditioning variable. (a,b) $\Delta/\Delta_{\text{DNS}} = 4$; (c,d) $\Delta/\Delta_{\text{DNS}} = 48$.

of additional fluxes; the detailed derivations appear in [7] and are extensive. We have assessed the importance of the multi-species-extended Korteweg tensor [iii] in the momentum equation.

By comparing the magnitudes of the gradient of the capillarity terms and the pressure gradient, we performed an order-of-

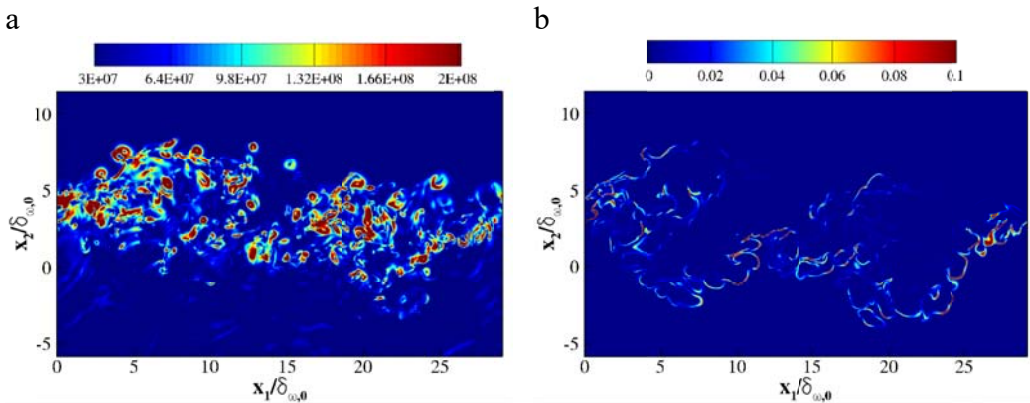


Figure 3. Values at t^*_{tr} of (a) $|\nabla p|$ and (b) $|\kappa \nabla [(\nabla \rho)^2]|$ for the case with the largest $|\nabla p|$ values. Units are $\text{kg}/(\text{ms})^2$. From [7].

magnitude analysis in order to estimate the influence of the Korteweg stresses in the momentum equation. The results illustrated in Fig. 3 are at the transitional time t^*_{tr} for the $Re_0 = 3500$ case, for which density gradients reach values as high as $|\nabla \rho| \approx 8 \times 10^5 \text{ kg m}^{-4}$, show that the gradient term is almost nine orders of magnitude smaller than the pressure gradient, yielding thus a negligible contribution to the generalized pressure tensor. Even in the regions of the largest Korteweg tensor $|\kappa \nabla [(\nabla \rho)^2]|$ values, Fig. 3 shows that the value of $|\nabla p|$ at those locations is orders of magnitude larger than the values of $|\kappa \nabla [(\nabla \rho)^2]|$. A grid convergence analysis showed that when the grid is refined by a factor of 50% in each direction, the quantitative results obtained with the coarser grid are recovered. The conclusion is that the modification to the actual thermodynamic pressure is also negligible, and thus that the present DNS database is appropriate for the purpose of this study, which enabled us to pursue the examination of specific features bringing a deeper understanding of uphill diffusion and its consequences.

The PI has interacted when warranted with researchers at Argonne National Laboratory on the topics of thermodynamics and transport properties.

III. Future Plans

The following activities are planned:

- Examine the influence of the interaction coefficients in the real-gas equation of state on the evolution of the flow and its characteristics at transition.
- Develop a DNS database for complex fuels composed of several hydrocarbon species mixing with air and products of final combustion at high pressure.

IV. References

- i. Bellan, J., *Combust. Flame.*, **2017** 176 245
- ii. Dovizio, D., Labahn, J.W., Devaud, C.B., *Combust. Flame.*, **2015** 162(5) 1976
- iii. Korteweg, D. J., *Archives Néerlandaises des sciences exactes et naturelles*, **1901** 6 1
- iv. Harstad, K. and Bellan, J., *Journal of Chemical Physics*, **2004** 120(12) 5664
- v. Masi, E., Bellan, J., Harstad, K. and Okong'o N., *J. Fluid Mech.*, **2013** 721 578

V. Publications, presentations, submitted articles supported by this project 2015- 2018

- [1] Borghesi, G.; Bellan, J., Irreversible entropy production rate in high-pressure turbulent reactive flows, *Proc. of the Comb. Inst.*, 35, 1537-1547, 2015

- [2] Borghesi, G.; Bellan, J., *A priori and a posteriori* analysis for developing Large Eddy simulations of multi-species turbulent mixing under high-pressure conditions, *Phys. Fluids.*, 27, 035117 (35 pages), 2015
- [3] Bellan, J., Direct Numerical Simulation of a high-pressure turbulent reacting mixing layer, *Combust. Flame*, 176, 245-262, 2017
- [4] Gnanaskandan, A.; Bellan, J., Numerical Simulation of jet injection and species mixing under high-pressure conditions, in print *Journal of Physics*, Institute of Physics Conference Series: Materials Science and Engineering, 821, 012020, 2017
- [5] Bellan, J., Evaluation of mixture-fraction-based turbulent-reaction-rate model assumptions for high-pressure reactive flows, *Combust. Flame*, 179, 253-266, 2017
- [6] Gnanaskandan, A.; Bellan, J., Side-jet effects in high-pressure turbulent flows: Direct Numerical Simulation of nitrogen injected into carbon dioxide, *J. Supercritical Fluids*, 140, 165-181, 2018
- [7] Sciacovelli, L.; Bellan, J., The influence of the chemical composition representation according to the number of species during mixing in high-pressure turbulent flows, *Journal of Fluid Mechanics*, 863, 293-340, 2019
- [8] Devaud, C.; Bushe, W.K; and J. Bellan, J., The modeling of the turbulent reaction rate under high-pressure conditions: *a priori* evaluation of the Conditional Source-term Estimate concept, in (minor) revision for *Combustion and Flame*
- [9] Gnanaskandan, A.; Bellan, J., Large Eddy Simulations of high pressure jets : Effect of subgrid scale modeling, accepted in the *AIAA Progress Series* book titled *High Pressure Flows for Propulsion Applications* (Ed. J. Bellan), to appear 2019
- [10] Bellan, J., Modeling and numerical simulations of multi-species high-pressure reactive flows, **Invited Plenary Lecture**, Summer Program of the SFBTRR40, Institute of Aerodynamics and Fluid Mechanics Technische Universität München, Garching, Germany, August 3, 2015
- [11] Bellan, J., Modeling and numerical simulations of multi-species high-pressure reactive flows, **Invited Seminar**, Purdue University, West Lafayette, IN., October 22, 2015
- [12] Bellan, J., Reduced models for the simulation of multi-scale problems in physics and chemistry, **Invited Seminar**, Cornell University, Ithaca, NY., November 17, 2015
- [13] Bellan, J., Modeling and Numerical Simulations of Multi-Species High-Pressure Turbulent Mixing and Combustion, **Invited Seminar**, SpaceX, Hawthorne, CA., 12/14/2016
- [14] Borghesi, G.; Bellan, J., Models for the LES equations to describe multi-species mixing occurring at supercritical pressure, paper 2014-0823 presented at the 52nd Aerospace Sciences Meeting, New Harbor, MD, January 13-17, 2014 Borghesi, G. and Bellan, J., Irreversible entropy production rate in high-pressure turbulent reactive flows, *Proc. of the Comb. Inst.*, 35, 1537-1547, 2015
- [15] Borghesi, G.; Bellan, J., *A priori and a posteriori* analyses of multi-species turbulent mixing layers at supercritical-*p* conditions, paper 2015-0162 presented at the 53rd Aerospace Sciences Meeting, Kissimmee, FL., January 5-9, 2015; also presented at the 9th US National Combustion Meeting, Cincinnati, OH., May 17-20, 2015
- [16] Bellan, J., The mixture fraction for high-pressure turbulent reactive flows, paper 2016-1686 presented at the 54th Aerospace Sciences Meeting, San Diego, CA, January 4-8, 2016
- [17] Gnanaskandan, A.; Bellan, J., Large Eddy Simulations of high pressure jets: Effect of subgrid scale modeling, paper 2017-1105 presented at the 55th Aerospace Sciences Meeting, Grapevine, TX, January 9-13, 2017
- [18] Sciacovelli, L.; Bellan, J., Mixing in high pressure flows: the influence of the number of species, paper 2018-1189, presented at the 56th Aerospace Sciences Meeting, Kissimmee, FL., January 8-12, 2018
- [19] Devaud, C.; Bushe, W.K; and J. Bellan, J., Assessment of Conditional Source-term Estimation for High-Pressure Turbulent Combustion Modeling, presented at SciTech 2019, January 7-11, 2019, San Diego, FL; also presented at the 11th US. National Meeting of the Combustion Institute, March 24-27, 2019, Pasadena, CA.
- [20] Banuti, D.; Bellan, J., Influence of the real-gas equation-of-state binary interaction coefficients on the turbulent mixing of many species at diesel-engine high-pressure conditions, presented at the 11th US. National Meeting of the Combustion Institute, March 24-27, 2019, Pasadena, CA

Chemical Kinetic Data of Benchmark Accuracy through Multi-Scale Informatics Strategies

Michael P. Burke

*Department of Mechanical Engineering, Department of Chemical Engineering, & Data Science Institute
Columbia University, New York, NY 10027
mpburke@columbia.edu*

Program Scope

The reliability of predictive simulations for advanced energy conversion devices depends on the availability of accurate data for thermochemistry, chemical kinetics, and transport. In that regard, accurate data are critically important for both their direct use in predictive simulations and for benchmarking improved theoretical methodologies that can similarly produce accurate data for predictive simulations. The use of informatics-based strategies for the determination of accurate thermochemical data with well-defined uncertainties, i.e. the Active Thermochemical Tables (ATcT),¹ has revolutionized the field of thermochemistry – ATcT provides thermochemical data of unprecedented accuracy for direct use in predictive simulation and has served as a key enabler of *ab initio* electronic structure methodologies of equally impressive accuracy. The goal of this program, which started a few months ago, is to develop an active database for chemical kinetics, akin to that for thermochemistry, to establish high-accuracy kinetic data for predictive simulation and to evaluate emerging *ab initio*-based theoretical kinetics methods, using our multi-scale informatics approach. We are particularly interested in reaction systems where non-thermal kinetic sequences arise and/or where combining theoretical and experimental data is necessary to unravel complex reaction data into chemical information.

Recent Progress

There are a number of significant challenges in deriving high-accuracy kinetic data of relevance to the complex reactions encountered in combustion, planetary atmospheres, and interstellar environments. First, even the most “direct” experimental rate constant determinations are often influenced by uncertainties in secondary reactions – leading to a complex web of interdependences among kinetic parameters for many reactions (and an opportunity to gain more information than has been attained previously, since uncertainties are seldom at the noise floor of the measurements). Second, there is rarely enough experimental data to constrain the full temperature, pressure, and composition ($T/P/X$) dependence of rate constants for many reactions – rendering usual rate-parameter-based uncertainty quantification approaches ineffective. Third, many of the reaction systems of interest to various application domains and gas-phase theoretical chemistry involve non-thermal kinetic sequences¹⁻⁶ – posing an additional problem for rate-parameter-based approaches.

During the past several years, we have been developing a multi-scale uncertainty quantification approach, multiscale informatics,⁷⁻¹⁰ to address the challenges involved in 1) unraveling the complex web of interdependences among reactions in complex systems data, 2) sufficiently constraining the $T/P/X$ dependence of rate constants, and 3) analyzing data from reaction systems involving non-thermal kinetic sequences. Our multi-scale informatics (MSI) approach identifies optimized values and constrained uncertainties for a set of theoretical kinetics parameters, rate constant parameters, and physical model parameters as informed by data across a range of scales from a variety of sources. These data include *ab initio* electronic structure calculations of molecular-level properties, experimental thermal rate constant determinations, and macroscopic observables from multi-reaction systems. Physics-based models relay

information across the scales within the framework. Theoretical kinetics models (e.g. TST or RRKM-master equation) relate theoretical kinetics parameters to rate constants for thermal species. Physical models (e.g. 0-D adiabatic reactors) relate rate constants to macroscopic observables (e.g. time-dependent OH concentrations). Active theoretical parameters can include barrier heights, well depths, vibrational frequencies, imaginary frequencies, hindered rotor potentials, scaling factors for VRC-TST calculations, and average energies transferred per collision (among others) to represent uncertainties related to energetics, partition function, tunneling, and collisional energy transfer models in the theoretical model. Similarly, active physical model parameters can include initial temperatures, pressures, and mixture compositions (including impurities) used in the physical model for the experiments and absorption cross-sections used in interpreting measured observables.

For this program, we have mapped out a tour through various reaction systems that serve to both anchor the database and grow the database in way that leverages its anchored foundations. With regard to the latter, we have recently leveraged our previous MSI analysis of the H_2O_2 decomposition system^{7,10} to analyze data for the $\text{CH}_3 + \text{HO}_2$ reaction (R6 and R7 in Table 1), for which many experimental determinations of the rate constant and branching ratio are relatively indirect. In this recent analysis, we incorporated the theoretical treatment of $\text{CH}_3 + \text{HO}_2$ from Jasper and co-workers¹¹ and analyzed raw experimental measurements from shock-heated $\text{CH}_4/\text{H}_2\text{O}_2/\text{H}_2\text{O}/\text{O}_2/\text{Ar}$ mixtures¹² and $\text{CH}_4/\text{O}_2/\text{Kr}$ mixtures¹³ originally used to derive rate constants for R6 and R7. The general conclusion from this analysis was that, once constraints from theoretical data were imposed, the experiments provided minimal additional information about these rate constants. For example, the MSI rate constants and uncertainties are essentially identical to those of the theoretical data only (the “prior” model) in Fig. 1.

This result can be rationalized on the basis of uncertainty-weighted sensitivity analysis, which identifies the parameters whose uncertainties influence prediction uncertainties and, likewise, the parameters which could be informed by experimental data for those observables. For

Table 1. Relevant reactions

- (R1) $\text{H}_2\text{O}_2 (+\text{M}) = \text{OH} + \text{OH} (+\text{M})$
- (R2) $\text{H}_2\text{O}_2 + \text{OH} = \text{HO}_2 + \text{H}_2\text{O}$
- (R3) $\text{HO}_2 + \text{HO}_2 = \text{H}_2\text{O}_2 + \text{O}_2$
- (R4) $\text{HO}_2 + \text{OH} = \text{H}_2\text{O} + \text{O}_2$
- (R5) $\text{OH} + \text{OH} = \text{O} + \text{HO}_2$
- (R6) $\text{CH}_3 + \text{HO}_2 = \text{CH}_4 + \text{O}_2$
- (R7) $\text{CH}_3 + \text{HO}_2 = \text{CH}_3\text{O} + \text{OH}$
- (R8) $\text{CH}_4 + \text{OH} = \text{CH}_3 + \text{H}_2\text{O}$

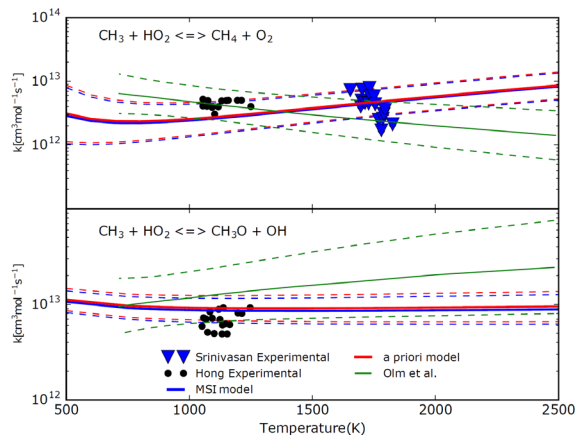


Figure 1. Selected rate constants for R6 and R7. Symbols designate experimental determinations.¹²⁻¹³ Solid lines and dashed lines show model predictions and uncertainties for the prior and MSI models.

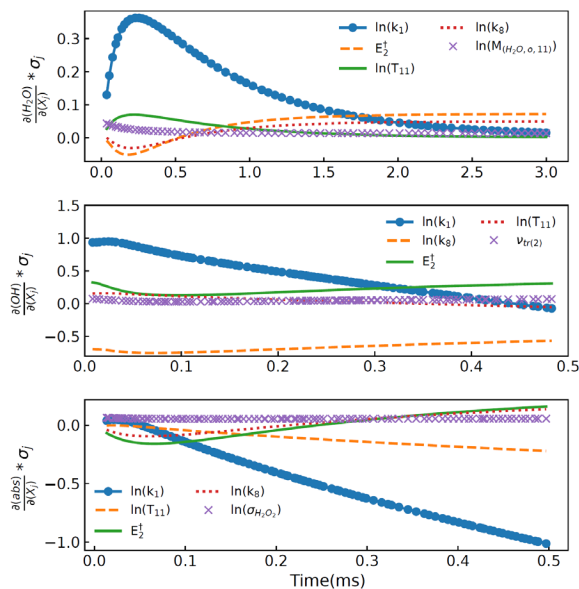


Figure 2. Uncertainty-weighted sensitivity analysis for OH, H_2O , and absorbance at 227 nm in shock-heated $\text{CH}_4/\text{H}_2\text{O}_2/\text{H}_2\text{O}/\text{O}_2/\text{Ar}$ mixtures.

example, as shown in Fig. 2, predictions of all three experimental observables from shock-heated $\text{CH}_4/\text{H}_2\text{O}_2/\text{H}_2\text{O}/\text{O}_2/\text{Ar}$ mixtures¹² are predominantly influenced by uncertainties in parameters related to k_1, k_2 (the barrier height, E_2^\ddagger , and a scaling factor for vibrational frequencies of the transition state, $\nu_{tr(2)}^\ddagger$), k_8 , and physical model parameters (temperature, T , initial water mole fraction $M_{\text{H}_2\text{O}}$, and the absorption coefficient of hydrogen peroxide at 227 nm, $\sigma_{\text{H}_2\text{O}_2}$) rather than any parameters related to k_6 or k_7 . (Similar results are obtained for $\text{CH}_4/\text{O}_2/\text{Kr}$ mixtures.¹³)

Predicted time profiles for the same three observables are shown in Fig. 3 along with the experimental measurements of Hong et al.¹² While the prior model yields higher OH mole fractions and lower absorbance signals than observed experimentally, the MSI model yields predictions for all three profiles consistent with experimental measurements within associated uncertainties. In fact, as one might anticipate based on the discussion in the preceding paragraph, inclusion of only H_2O_2 decomposition experimental targets¹⁴⁻¹⁷ (without any CH_4 containing experiments as targets) yielded MSI predictions that are remarkably close to the those obtained when including all target data.¹²⁻¹⁷ Inclusion of the shock-heated $\text{CH}_4/\text{H}_2\text{O}_2/\text{H}_2\text{O}/\text{O}_2/\text{Ar}$ experiments as targets did yield modest improvements in the peak OH and peak absorbance (of roughly 10%). However, optimized active parameters describing R1-R5 reach nearly identical values when the optimization is performed with and without these shock-heated $\text{CH}_4/\text{H}_2\text{O}_2/\text{H}_2\text{O}/\text{O}_2/\text{Ar}$ experiments. Some minor adjustments in parameters describing R6-R8 are observed when CH_4 experimental targets are included, though as per the above, predictions with these parameters at their nominal values (but R1-R5 parameters optimized to H_2O_2 experimental targets) already yield reasonable predictions.

These results highlight the utility of interpreting the raw experimental data in a manner that can effectively leverage information from other sources and quantify the information content of the data accurately. They similarly also indicate the challenges in constraining rate constants across wide $T/P/X$ ranges and achieving the levels of data redundancy necessary to identifying “optimistic” uncertainty assignments – motivating the use of MSI and our planned methodological developments to allow a greater variety of data types to be used to constrain kinetic parameters.

With regard to methodological improvements, we have nearly finished an initial rewrite of our MSI code in Python with an emphasis on making the code more modular and, therefore, more amenable to future additions of new data types. The new code also allows for use of both Variflex¹⁸ and MESS¹⁹ for *ab initio* TST-ME calculations and Cantera²⁰ for kinetic model calculations. The ability of our new code to run MESS¹⁹ should help enable planned methodological improvements focused largely on incorporating non-thermal kinetic sequences directly within the MSI framework.

Future Plans

In the coming months, we plan to venture into reaction subsystems that have been possible to study relatively directly and are commensurately relatively well known, yet still reducing or quantifying their remaining uncertainties is nearly always important and combines data across a broad array of data sources. These initial, relatively well known subsystems should allow further anchoring of the database and allow

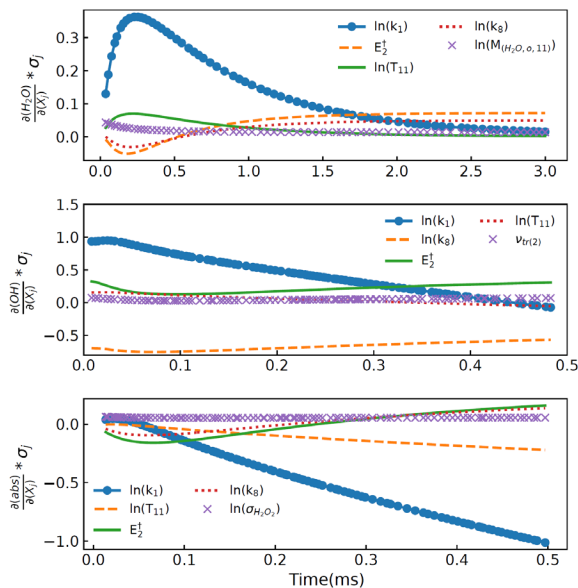


Figure 3. Model predictions and experimental measurements¹² of OH, H_2O , and absorbance at 227 nm in shock-heated $\text{CH}_4/\text{H}_2\text{O}_2/\text{H}_2\text{O}/\text{O}_2/\text{Ar}$ mixtures.

more experience to be gathered about the capabilities and limitations of the framework. These planned reactions of interest include $\text{H} + \text{O}_2 = \text{OH} + \text{O}$, $\text{OH} + \text{H}_2 = \text{H} + \text{H}_2\text{O}$, $\text{O} + \text{H}_2 = \text{H} + \text{OH}$, $\text{H} + \text{O}_2 (+\text{M}) = \text{HO}_2 (+\text{M})$, $\text{NO}_2 + \text{H} = \text{NO} + \text{OH}$, $\text{H} + \text{HO}_2 = \text{H}_2 + \text{O}_2$, $\text{H} + \text{HO}_2 = \text{OH} + \text{OH}$, and $\text{H} + \text{HO}_2 = \text{H}_2\text{O} + \text{O}$. Most experimental determinations of rate constants for these eight reactions usually involve at least one of the others, such that a full analysis of them together should allow the experimental information to be unraveled onto kinetic parameters for each reaction. For $\text{H} + \text{O}_2 (+\text{M}) = \text{HO}_2 (+\text{M})$, we anticipate that 2D-ME results (from Jasper, Klippenstein, and co-workers) and consideration of mixture rule uncertainties²¹⁻²² in experimental interpretations will be especially useful. We also plan to take advantage of high-level theoretical calculations now available for many of those reactions. Similarly, motivated by some recent high-level theoretical calculations from Klippenstein and co-workers on $\text{HO}_2 + \text{HO}_2$ which identified new product pathways,²³ we plan to revisit our previous analysis of the H_2O_2 decomposition system using an updated theoretical treatment for this reaction to assess any differences in predictions and experimental interpretations from those of our original study.

Afterwards, we plan to explore less characterized and difficult-to-isolate subsystems, such as those involving CH_3 , HO_2 , and CH_2OH , where the anchored database can be leveraged for the analysis, and then non-equilibrium kinetic sequences. Along the way, we are also planning a number of methodological improvements to the MSI approach that allow data for collisional energy transfer kernels, product energy distributions, microcanonical rate constants, and photolysis quantum yields, among others, to be included as targets. We anticipate that these data types will allow a greater degree of data redundancy and allow more rigorous evaluations of theoretical methodologies for calculating non-equilibrium kinetic sequences.

References

1. B. Ruscic, R. Pinzon, M. L. Morton, G. Laszevski, S. Bittner, S. G. Nijssure, K. A. Amin, M. Minkoff, A. F. Wagner. *J Phys Chem A* 108 (2004) 9979–9997.
2. M.P. Burke, S.J. Klippenstein. *Nature Chemistry* 9 (2017) 1078-1082.
3. D.R. Glowacki, J. Lockhart, M.A. Blitz, S.J. Klippenstein, M.J. Pilling, S.H. Robertson, P.W. Seakins, *Science* 337 (2012) 1066.
4. M.C. Barbet, K. McCullough, M.P. Burke. *Proc Combust Inst* 37 (2019) 347-354.
5. M.P. Burke, C.F. Goldsmith, Y. Georgievskii, S.J. Klippenstein. *Proc Combust Inst* 35 (2015) 205–213.
6. C.F. Goldsmith, M.P. Burke, Y. Georgievskii, S.J. Klippenstein. *Proc Combust Inst* 35 (2015) 283-290.
7. M.P. Burke, S.J. Klippenstein, and L.B. Harding. *Proc Combust Inst* 34 (2013) 547–555.
8. M.P. Burke, C.F. Goldsmith, S.J. Klippenstein. *J Phys Chem A* 119 (2015) 7095–7115.
9. O. Welz, M.P. Burke, I.O. Antonov, C.F. Goldsmith, J.D. Savee, D.L. Osborn, C.A. Taatjes, S.J. Klippenstein, L. Sheps. *J Phys Chem A* 119 (2015) 7116–7129.
10. M.P. Burke. *International Journal of Chemical Kinetics* 48 (2016) 212–235.
11. A.W. Jasper, S.J. Klippenstein, L.B. Harding. *Proc Combust Inst* 32 I (2009) 279–286.
12. Z. Hong, D.F. Davidson, K.-Y. Lam, R.K. Hanson. *Combustion and Flame* 159 (2012) 3007–3013.
13. N.K. Srinivasan, J.V. Michael, L.B. Harding, S.J. Klippenstein. *Combustion and Flame* 149 (2007) 104–111.
14. C. Kappel, K. Luther, J. Troe. *Phys Chem Chem Phys* 4 (2002) 4392–4398.
15. Z. Hong, A. Farooq, E. A. Barbour, D. F. Davidson, R. K. Hanson. *J Phys Chem A* 113 (2009) 12919–12925.
16. Z. Hong, K.-Y. Lam, R. Sur, S. Wang, D.F. Davidson, R.K. Hanson. *Proc Combust Inst* 34 (2013) 565–571.
17. Z. Hong, S.S. Vasu, D.F. Davidson, R.K. Hanson. *J Phys Chem A* 114 (2010) 5520–5525.
18. S.J. Klippenstein, A.F. Wagner, R.C. Dunbar, D.M. Wardlaw, S.H. Robertson, J.A. Miller, VARIFLEX, version 1.14m; 2005.
19. Y. Georgievskii, J.A. Miller, M.P. Burke, S.J. Klippenstein. *J Phys Chem A* 117 (2013) 12146-12154.
20. D.G. Goodwin, H.K. Moffat, R.L. Speth, Cantera: An Object-Oriented Software Toolkit for Chemical Kinetics, Thermodynamics, and Transport Processes, doi:10.5281/zenodo.170284.
21. M.P. Burke, L. Lei. The role of mixture rules in experimental interpretations of third-body efficiencies. 11th U.S. National Combustion Meeting (2019).
22. M.P. Burke, R. Song. *Proc Combust Inst* 36 (2017) 245-253.
23. S.J. Klippenstein, R. Sivaramakrishnan, U. Burke, K.P. Somers, H.J. Curran, L. Cai, H. Pitsch, M. Pelucchi, T. Faravelli, P. Glarborg. $\text{H}\dot{\text{O}}_2 + \text{H}\dot{\text{O}}_2$: High level theory and the role of singlet channels. 11th U.S. National Combustion Meeting (2019).

BES-supported products (9/2018-present)

C.E. LaGrotta, M.C. Barbet, L. Lei, M.P. Burke. Towards a High-Accuracy Kinetic Database Informed by Theoretical and Experimental Data. 11th U.S. National Combustion Meeting, March 2019, Pasadena, CA.

CHEMICAL DYNAMICS METHODS AND APPLICATIONS

David W. Chandler, Jonathan H. Frank, David L. Osborn, Leonid Sheps, Judit Zádor
Sandia National Laboratories, MS 9051, Livermore, CA 94551-0969

chand@sandia.gov, jhfrank@sandia.gov, dlosbor@sandia.gov, lsheps@sandia.gov, jzador@sandia.gov

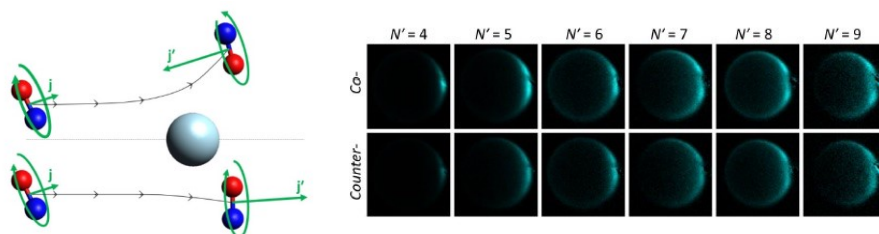
PROGRAM SCOPE

This program focuses on the chemical dynamics of gas phase molecular species, the detailed study of the motion of molecules and atoms on inter- or intra- molecular potential energy surfaces to learn about the details of the surface as well as the dynamics of their interactions. This task studies processes, typically at a single-collision or quantum state-resolved level, that underlie the more complex reactions and processes studied in the “Chemical Kinetics for Complex Systems” task; ignition and non-equilibrium chemistry that may arise in plasmas and combustion, energy flow that determines high-pressure kinetics. Our program includes detailed investigations into energy transfer processes in photodissociation, inelastic and reactive molecular scattering, electron scattering and dissociative electron attachment, ionization, and molecular alignment by light-matter interactions. We use a suite of multiplexed spectroscopy and mass spectrometry techniques in combination with molecular dynamics simulations to provide fundamental insights into reaction dynamics, often relying on advanced methods developed in the “Ultrafast Physics: Nonlinear Optical Spectroscopy and Diagnostics” or “Advanced Mass Spectrometry and X-Ray Diagnostics” tasks. Velocity mapped imaging (VMI) of ions and electrons is used in single and crossed molecular beam configurations to provide time-resolved velocity measurements of products. Time-resolved multiplexed photoionization mass spectrometry (MPIMS) provides a universal method to sensitively and selectively probe chemical reactions and reaction intermediates. The Sandia-designed MPIMS instrument utilizes tunable vacuum ultraviolet light from the Advanced Light Source (ALS) synchrotron at Lawrence Berkeley National Laboratory (LBNL) for sensitive, isomer specific ionization of reactant and product molecules sampled from chemical reactions. We also use continuous scanning and step-scan Fourier transform spectroscopy (FTS) to probe multiple species in chemical reactions. Advances in photoelectron photoion coincidence spectroscopy (PEPICO) provide a powerful tool for time-resolved probing of gas phase chemical reactions with superior performance in many areas compared to MPIMS.

RECENT PROGRESS

Non-intuitive rotational reorientation in collisions of NO($A^2\Sigma^+$) with Ne from direct measurement of a four-vector correlation

Non-intuitive rotational reorientation in collisions of NO($A^2\Sigma^+$) with Ne from direct measurement of a four-vector correlation has been observed. A molecular beam of NO molecules seeded in Ne is intersected at right angles with a beam of pure Ne. Circularly polarized light at 226 nm is used to state-selectively prepare NO($A^2\Sigma^+$; $v=0$; $N=2$, $j=1.5$) molecules with a distribution of \mathbf{j} that is *oriented*. This means that there is a preferred sense of rotation of the molecules, or, equivalently, a preference for a given sign of the m_j quantum number when defined relative to \mathbf{k} . The propagation direction of the preparation laser is close to being parallel to \mathbf{k} such that the angular momentum distribution before and after the collision is cylindrically symmetric about this axis. After 370 ns, the NO($A^2\Sigma^+$; $v=0$; N') products are state-selectively



Left: Illustration of two types of collisions, ones that conserve the direction of rotation and ones that flip the direction of rotation. Right: Data for co- and counter-rotating inelastic scattering of NO(A) initially in $N=2$ rotational state. For low N , co-rotating images are much more intense.

ionized using $[1 + 1']$ REMPI via the $E^2\Sigma^+$ state, employing circularly polarized 600 nm light, counter-propagating relative to the preparation laser beam, to effect the $E \leftarrow A$ transition in order to give sensitivity to the

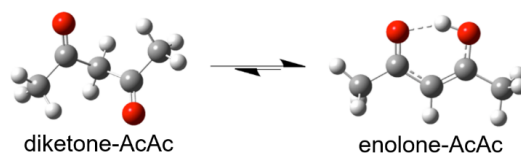
orientation of the products. We find that there is only one angle ($80^\circ \pm 20^\circ$) for one quantum state ($N=5$) where counter-rotating is the preferential product.

Two-color alignment and dissociation of molecular hydrogen excited to the E,F electronic state under intense laser fields to determine the ease of aligning the excited state molecule

Velocity mapped imaging is used to image H atoms formed in the $N=3$ quantum state after dissociation of H_2 excited to the E,F electronic state under varying laser intensity conditions. H^+ photofragment images were generated by 2-photon dissociation of H_2 (E,F $v=0, J=0$) forming $H(N=0) + H(N=3)$ followed by 2-photon ionization of the $H(N=3)$ using a weakly focused 532-nm beam of photons in the presence of varying intensities of 1064-nm laser light. The velocity (angle and speed) distribution of the H^+ atoms are recorded and analyzed. The 1064-nm laser beam is overlapped in time and space with the weak 532-nm beam, and its intensity is increased while the H^+ angular distribution is monitored. In this manner, angular distribution of the H^+ is measured as a function of 1064-nm laser intensity, and this is expected to mirror the alignment of the H_2 parent molecule as the dissociation is from excitation to a repulsive state of H_2 . We model this alignment behavior with a simple two state model involving stark mixing of the initially prepared $J=0$ with $J=2$ rotational state. This model is able to explain all of the observed angular distribution and permits us to extract from the fit the polarizability anisotropy, $\delta\alpha$, of H_2 (E,F) electronic state (the difference in polarizability parallel and perpendicular to the bond axis). We determine this value to be $\delta\alpha = 5301 \pm 714$ A.U., which is extremely large as one would expect $\delta\alpha \sim 2$ from the pure H_2 (E,F) electronic state.

Photochemistry of acetylacetone: a panoply of new channels and thermodynamic insights

Acetylacetone (AcAc, pentane-2,4-dione) is the smallest β -diketone, but in the gas phase at 300 K, it exists predominantly in its enolone form, as shown to the right, which is stabilized by conjugation and an internal hydrogen bond. The photochemistry of this molecule contains structural elements of carbonyls (the C=O bond), alkenes (C=C bond), conjugated polyenes (O=C-C=C π molecular orbitals), and enols (C=C-OH group). The photochemistry of these first three groups are well studied, and we wished to learn which aspects of AcAc's electronic and molecular structure determine its photochemistry. Previous work on dynamics following excitation of the strong, structureless $\pi\pi^*(S_2 \leftarrow S_0)$ transition has concluded that OH loss by simple bond cleavage from the enolone isomer is the only product channel. These investigations determined the C-OH bond strength experimentally and theoretically to be ~ 90 kcal \cdot mol $^{-1}$.



We utilized three complementary time-resolved methods to study this system following 266 and 248 nm excitation: 1) multiplexed VUV photoionization mass spectrometry, 2) VUV PEPICO spectroscopy, and 3) infrared absorption spectroscopy of OH $X(^2\Pi)$. Results reveal a much richer photochemistry than previously appreciated. We observed 15 unique products representing 6 one-photon product channels, and several two-photon product channels. PEPICO spectroscopy provides the best spectral fingerprints for isomer-specific assignments of these product channels. Fluence dependence reveals that OH production requires at least two photons, a result consistent with our calculated C-OH bond strength of 121.7 kcal \cdot mol $^{-1}$, far greater than previous determinations. Phototautomerization, producing the diketone form, is also a major process, with strong evidence that the diketone form serves as an intermediate to several product channels that arise from ground electronic state dissociation. However, our results also imply that some of the product channels are born on excited state potential energy surfaces. Although the strong oscillator strength of the $S_2 \leftarrow S_0$ transition results from the ($\pi\pi^*$) excitation of the C=C-C=O backbone, similar to conjugated polyenes, the participation of triplets in the dissociation pathways of acetylacetone appears to have more in common with ketone photochemistry.

Finally, photoionization spectroscopy shows that distinct daughter ions arise from each of the two neutral isomers via dissociative ionization. From the temperature dependence of these daughter ion signals, we are able to measure the equilibrium constant of this keto-enol tautomerization on S_0 from 320 to 600 K and extract $\Delta H = 4.1 \pm 0.3$ kcal \cdot mol $^{-1}$, and $\Delta S = 6.8 \pm 0.5$ cal \cdot mol $^{-1}\cdot$ K $^{-1}$ using a van't Hoff analysis.

Measuring thermochemistry of QOOH, with roaming dynamics

Methyl hydroperoxide (MHP) is the simplest alkylhydroperoxide, which may decompose via roaming dynamics. Another interesting aspect of MHP is that it can form the smallest so-called QOOH radical, CH_2OOH , when one of its methyl hydrogens is abstracted. QOOH radicals are extremely unstable, decomposing rapidly to form $\text{OH} + \text{product}$ or $\text{HO}_2 + \text{product}$ bimolecular pairs. As a result, they eluded most direct experimental investigations despite their importance. To date there are only two direct studies on QOOH radicals both from Sandia, and only in our second work were we able to directly detect an example of this ephemeral species.

Accurate thermodynamic parameters are also absent in the literature for QOOH radicals. Establishing firm values for the heats of formation of MHP and its unimolecular dissociation products is required for strong anchor values. Moreover, future studies involving more complex organic hydroperoxides will benefit from studying the smallest homologue. The goal of this project was to establish the heat of formation values for the smallest QOOH, CH_2OOH . Threshold photoelectron photoion coincidence (TPEPICO) experiments in collaboration with Prof. Bálint Sztaray (U Pacific) provided direct measurements of the ionization energy and fragmentation kinetics of the MHP cation. These observations, combined with theory, yielded not only accurate thermodynamic parameters for neutral CH_2OOH , but some interesting dynamical processes. RRKM modeling of the complex web of possible rearrangement-dissociation processes was used to model the higher-energy fragmentation. Supported by Born–Oppenheimer molecular dynamics simulations, we found that the HCO^+ fragment ion is produced through a roaming transition state followed by a low barrier. H_3O^+ is formed in a consecutive process from the CH_2OOH^+ fragment ion, while direct C–O fission of the molecular ion leads to the methyl cation.

FUTURE WORK

Photodissociation of pyruvic acid: signatures of a carbene?

In collaboration with Prof. Hanna Reisler (USC), we are investigating the 351 and 193 nm photodissociation of pyruvic acid ($\text{CH}_3\text{C}(\text{O})\text{COOH}$) using MPIMS. This approach complements the less universal but more dynamically rich data Prof. Reisler obtains in her lab using VMI. In preliminary experiments at the Advanced Light Source, we observed production of two isomers with mass=44 amu: acetaldehyde (CH_3CHO) and ethenol ($\text{H}_2\text{C}=\text{CHOH}$). Because we also observe direct production of CO_2 , we hypothesized that the co-product of CO_2 might be a third isomer at mass=44, namely $\text{CH}_3\text{-C-OH}$ (methyl hydroxyl carbene). It has the lowest ionization energy of all the mass 44 isomers, and we have some indication that we have observed this species. Our goal is to use the MPIMS approach to provide a global view of all photodissociation processes. Partial deuteration of pyruvic acid is also planned to assist in the assignment of dissociation pathways. This work will complement the work in Prof. Reisler’s lab, where the translational energy release and angular distributions of this photodissociation can be studied under collisionless conditions. That information will provide clues to the initial electronic states excited at the two UV excitation wavelengths, and the initial branching leading to the multiple product channels observed using MPIMS. This project provides fundamental understanding of complex photodissociation pathways mediated by multiple electronic states and affected by large-amplitude nuclear motion during dissociation.

Photodissociation of a super-rotor: how does parent angular momentum affect the outcome?

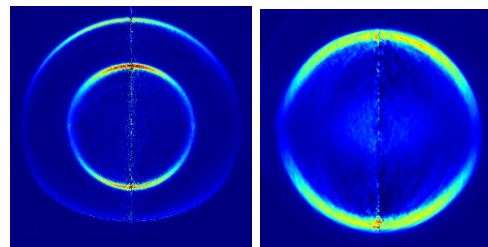
Inspired by work of Prof. Amy Mullin (University of Maryland), we are constructing an apparatus to study the photodissociation dynamics of molecules with very large rotational excitation, also known as super-rotors. The experiment consists of three parts. First, a pair of oppositely chirped, circularly polarized picosecond laser pulses will excite N_2O to very high rotational states (e.g. $J = 150\text{--}200$). This excitation process leads to N_2O spinning in a plane in the lab frame. Next, we will dissociate N_2O at ~ 203 nm, and observe the $\text{O}(^1\text{D})$ and/or the N_2 fragments via velocity map ion imaging. Prior work on the photodissociation of N_2O by Neyer & Chandler shows that the N_2 photoproduct is born with very high rotational excitation ($J = 55\text{--}85$), due to excitation from the linear ground state to a dissociative electronic state that induces strong bending motion during dissociation. When the initial N_2O molecule is placed in $J = 150$ via the chirped pulse excitation, its rotational angular momentum vector is oriented in the lab frame. We therefore ask, when highly rotationally excited and oriented N_2O is promoted to a dissociative excited

state, how does the angular momentum of the parent molecule affect the angular momentum imparted to the N_2 and $O(^1D)$ fragments? In the extreme rotational state of a super-rotor N_2O , will the molecular frame bending induced via UV excitation still be equally probable when the N_2 rotational angular momentum is either parallel or antiparallel to the parent angular momentum vector? These are questions we'll seek to answer about this light-matter interaction.

High-energy resolution electron scattering measured by velocity mapped electron imaging.

We are developing a new capability for time-resolved electron scattering with very high energy resolution (~ 0.1 meV) by modifying a single beam velocity mapped imaging spectrometer. A molecular beam containing the target molecule for electron scattering is co-expanded with Kr atoms. A two-step process generates electrons with tunable energies and a narrow energy distribution using multiphoton ionization of the Kr atoms. First, a 214.7-nm laser beam excites Kr to the $5p[3/2]_{\frac{1}{2}}$ state. The $5p[3/2]_{\frac{1}{2}}$ state efficiently fluoresces to the metastable $5s[3/2]_{\frac{1}{2}}$ state at an energy 79971.74 cm^{-1} above the ground state. Laser ionization from the long-lived metastable state is then performed with a tunable UV laser generating electrons with the resolution of the laser beam. All voltages are turned off before the tunable UV light ionizes the Kr atoms, providing a “zero” field environment for electron scattering. After a 3 ns period of the electrons travelling through the molecular beam and encountering some of the target molecules, a -3 kV pulse with a 1.7 ns duration is applied to the repeller plate to project the electrons through an electrostatic lens and onto the imaging detector. An example image of the un-scattered electrons using 246-nm light is shown below. At this wavelength, one sees two velocities of electrons since there are two possible spin orbit states of the Kr that can be formed. The energies of these electrons are 0.96 eV and 0.32 eV.

Our first demonstration of this apparatus was to co-expand C_2H_2 with the Kr and to image the C_2H^- anions formed by dissociative electron attachment of 3.3 eV electrons, as shown in the image on the right. From this image, we can determine the velocity distribution of the C_2H^- product of the DEA process. Our next target is to measure the width of the low energy scattering resonances of O_2 . At an energy of approximately 0.69 eV, there is a resonance that corresponds to transiently exciting a vibrational level of O_2^- and then having the electron detach leaving vibrationally excited oxygen molecules in $v=1$ or $v=2$. This energy loss should be observable with the velocity resolution in this apparatus. By scanning the frequency of the photoionization laser, we will measure the width and therefore the lifetime of these transient states.



Inverse Abel transform of velocity mapped images. Left: Electrons generated by photoionization of Kr in the metastable $5s$ state. Right: C_2H^- anions produced by dissociative electron attachment to C_2H_2 .

BES-sponsored publications, 2017 – present

- 1) Alignment, Dissociation and Ionization of H_2 Molecule in Intense Laser Fields using Velocity Mapped Imaging, G. V. Lopez, M. Fournier, J. Jankunas, A. K. Spiliotis, T. P. Rakitzis, D. W. Chandler, *J. Chem. Phys.* **147**, 13948 (2017).
- 2) Perspective: Advanced Particle Imaging, D. W. Chandler, D. H. Parker and P. H. Houston, *J. Chem. Phys.* **147**, 013601 (2017).
- 3) Infrared spectra of gas-phase 1- and 2-propenol isomers, M. F. Shaw, D. L. Osborn, M. J. T. Jordan, and S. H. Kable, *J. Phys. Chem. A* **121**, 3679 (2017).
- 4) Non-intuitive rotational reorientation in collisions of $NO(A^2\Sigma^+)$ with Ne from direct measurement of a four-vector correlation, T. R. Sharples, J. G. Leng, T. F. Luxford, K. G. McKendrick, P. G. Jambrina, F. J. Aoiz, D. W. Chandler, M. L. Costen, *Nat. Chem.*, **10**, 1148-1153 (2018).
- 5) Vacuum ultraviolet photoionization cross section of the hydroxyl radical, L. G. Dodson, J. D. Savee, S. Gozem, L. Shen, A. I. Krylov, C. A. Taatjes, D. L. Osborn, and M. Okumura, *J. Chem. Phys.* **148**, 184302 (2018).
- 6) Photo-tautomerization of acetaldehyde as a photochemical source of formic acid in the troposphere, M. F. Shaw, B. Sztaray, L. K. Whalley, D. E. Heard, D. B. Millet, M. J. T. Jordan, D. L. Osborn, and S. H. Kable, *Nat. Comm.* **9**, 2584 (2018).
- 7) Photoionization of methyl hydroperoxide: Thermochemistry of the smallest QOOH radical and the detection of a roaming fragmentation channel, K. Covert, K. Voronova, K. G. Torma, A. Bodi, J. Zador, B. Sztaray, *Phys. Chem. Chem. Phys.*, **20**, 21085-21094 (2018).

TURBULENCE-CHEMISTRY INTERACTIONS

Jacqueline H. Chen, Robert S. Barlow, and Jonathan H. Frank
Sandia National Laboratories, MS 9051, Livermore, California 94551-0969
jhchen@sandia.gov, barlow@sandia.gov, jhfrank@sandia.gov

Program Scope

In this research program we have developed a detailed understanding, through petascale direct numerical simulation (DNS) and experiments utilizing cutting-edge diagnostic approaches, of how transport processes couple with gas-phase chemistry to influence the rates and importance of different reaction steps in complex reacting mixtures and, in some cases, to even influence the reaction pathways that occur. The primary focus has been on turbulent combustions flows, as these are practically important and are characterized by extreme gradients in composition and temperature that pose a considerable challenge to accurately measure and predict, particularly in highly turbulent flows wherein there exists a large dynamic range of scales that are nonlinearly coupled. Active research in this research area largely ceased at the end of FY19, specifically in the area of turbulent flame studies.

Recent Progress

In the last year, we have investigated the role of molecular and turbulent transport coupled with combustion chemistry on: 1) development of new methods to determine heat release rate and chemical mode from single-shot Raman/Rayleigh/OH data, 2) measurement of turbulent flame scalar data on unique multi-regime turbulent burners, 3) development of a 4-D (spatio-temporal) LIF imaging capability, 4) coupling between flame heat release, vorticity, and strain rate in turbulent flames, 5) identification of premixed propagation modes, including deflagration and spontaneous autoignition, and 6) determination of the regimes of premixed turbulent spontaneous ignition and deflagration under gas-turbine reheat combustion conditions.

Method to Determine Heat Release Rate and Chemical Mode from Raman/Rayleigh/OH Data

We have used DNS results from two flame configurations (Wang et al. *Proc. Combust. Inst.* 2017; Sankaran et al. *Combust. Flame* 2015) to further evaluate methods for deriving heat release rate and chemical explosive mode from experimental data for temperature, major species, and the OH radical. The approximation method was applied along 1D slices from the DNS, using the simulated T, CH₄, O₂, N₂, CO₂, H₂O, H₂, CO, and OH values as input to a constrained homogeneous reactor. This reactor allows minor species and intermediates to build up to steady state, creating an approximation of the full thermochemical state of the sample. Heat release rate and chemical mode derived from this approximate state were within a few percent, on average, of results based on the full DNS.

Multi-Regime Flame Experiments in the Turbulent Combustion Laboratory

We hosted four visiting experiments during the latter half of FY2018. In parallel with the DNS analysis described above, a system for quantitative line imaging of OH LIF was implemented in the Turbulent Combustion Laboratory in combination with the Raman/Rayleigh/CO-LIF line-imaging system, and experiments were conducted on laminar and turbulent methane and methane/hydrogen flames in collaboration with visiting scientists Dirk Geyer (TU Darmstadt, Germany) and Matthew Dunn (Sydney University). Preliminary results on a new Multi-Regime Burner (MRB), brought by visiting PhD student, David Butz (TU Darmstadt, Germany) and the University of Michigan HiPilot Burner, brought by Dr. Tim Wabel (University of Toronto), were presented at the TNF14 Workshop. Scalar measurements from the HiPilot Burner revealed that the highest Ka number cases (i.e. the cases with slowest chemical rates relative to turbulent mixing) with this burner have back-supported stratified reaction zones, rather than uniformly premixed reaction zones. The [TNF14 Workshop](#) was held at Trinity College Dublin, Ireland (July 27-28, 2018) with 98 participants from 16 countries.

Technique for 3-D Imaging of the Temporal Evolution of Species in Chemically Reacting Flows

Many chemically reacting flows involve 3-D distributions of species that evolve in time, which presents a significant diagnostics challenge. We recently developed a diagnostic capability for 4-D (spatio-temporal) LIF imaging of species such as formaldehyde using a Sandia-built 100-kHz burst-mode laser to enable studies of the evolution of species distributions in chemically reacting systems. The laser delivers 500 laser pulses with 10 μ s separation, each formatted into a sheet that is rapidly rastered normal to the sheet using an acousto-optic deflector and synchronized with a high-speed CMOS camera. Results reveal the temporal evolution of the 3-D formaldehyde distribution. This capability is particularly valuable for studying the topology of chemically reacting regions as well as the abrupt appearance or disappearance of species, as occurs in ignition and extinction. Future plans will extend this capability for detection of species important to the coupling between gas-phase and surface reactions, as part of Sandia's new project within this program.

Coupling between Heat Release, Strain Rate, and Vorticity in Turbulent Premixed Flames

We have used simultaneous OH-LIF imaging and tomographic PIV measurements to investigate the coupling between flame heat release, fluid dynamic strain rate, and vorticity. This coupling is a function of the magnitude of the strain rate tensor eigenvectors, the vorticity vector, and their alignment relative to the flame-front normal direction. Fluctuations in the fluid dynamic strain rate affect the progress of chemical reactions due to finite-rate chemistry effects, which leads to variations in heat release rates. The heat release in turn introduces changes in density, viscosity, and diffusivity that can have important effects on the turbulence, thus creating feedback between chemical reactions and transport. We investigated these interactions in turbulent premixed counterflow flames, which are subject to large compressive strain. Dilatation due to the heat release introduces regions of strong extensive strain that partially counteract the main compressive strain, resulting in weaker compressive strain rates near the flame front. The heat release also locally modifies the probability of alignment between vorticity, strain, and the flame-front normal. Results address some inconsistencies that have been reported in the literature and impact the development of turbulent combustion models.

Identification of Premixed Flame Propagation Modes Using Chemical Explosive Mode Analysis

A criterion based on chemical explosive mode analysis (CEMA) is proposed to identify different local combustion modes, such as auto-ignition, diffusion-assisted ignition, and local extinction in laminar and turbulent premixed flames. The criterion is employed to distinguish between two different propagation modes of one-dimensional (1-D) freely propagating premixed flames, that is the canonical deflagration wave controlled by heat and species back-diffusion, which features a unique flame speed, and the auto-ignition controlled reaction front propagation, which may feature an arbitrary propagation speed. In the CEMA-based diagnostic, the local chemistry and diffusion source terms are projected to the chemical explosive mode (CEM), such that the roles of diffusion and chemistry in the CEM can be quantified and compared for identification of the flame propagation mode. The new criterion is further applied to analyze two-dimensional (2-D) DNS datasets of homogeneous charge compression ignition (HCCI) combustion of *n*-heptane/air with different levels of thermal stratification. Both flame propagation modes are observed and contribute significantly to the overall flame burning in the case with a high level of thermal stratification, while the flame propagation is found dominated by the auto-ignition mode in the case with a low level of thermal stratification, which agrees with the finding in previous studies.

Regimes of premixed turbulent spontaneous ignition and deflagration under gas-turbine reheat combustion conditions

We address the problem of turbulent spontaneous ignition vs. deflagration propagating against a mean residence time gradient, particularly relevant to the stabilization of quasi-steady diesel jet flames and gas-turbine reheat combustion, by performing a large series of statistically one-dimensional premixed turbulent DNS. An autoignitive mixture of hydrogen-vitiated air representative of gas-turbine reheat combustion is considered. First, we demonstrate that turbulence can trigger the transition from spontaneous ignition to a deflagration. We then construct a spontaneous ignition vs. deflagration regime diagram based on velocity,

turbulent velocity fluctuations and integral length scale and identify the mechanism that governs the transition from one propagation mode to the other. Finally, we propose a theoretical model that accurately captures this transition and assess the validity of a proxy based on chemical explosive mode analysis to determine the local propagation mode in complex configurations.

BES Publications (2017-2019)

1. Cutcher, H.C.; Magnotti, G.; Barlow, R.S.; Masri, A.R., Turbulent Flames with Compositionally Inhomogeneous Inlets: Resolved Measurements of Scalar Dissipation Rates, *Proc. Combust. Inst.* 36 (2017) 1737–1745.
2. Stahler, T.; Geyer, D.; Magnotti, G.; Trunk, P.; Dunn, M.J.; Barlow, R.S.; Dreizler, A., Multiple conditioned analysis of the Turbulent Stratified Flame A, *Proc. Combust. Inst.* 36 (2017) 1947–1955.
3. Magnotti, G.; Barlow, R.S., Dual-Resolution Raman Spectroscopy for Measurements of Temperature and Twelve Species in Hydrocarbon-Air Flames, *Proc. Combust. Inst.* 36 (2017) 4477–4485.
4. Barlow, R.S.; Magnotti, G.; Cutcher, H.C.; Masri, A.R., On defining progress variable for Raman/Rayleigh experiments in partially-premixed methane flames, *Combust. Flame* 179 (2017) 117–129.
5. B. Coriton, J.H. Frank, Impact of heat release on strain rate field in turbulent premixed Bunsen flames, *Proc. Combust. Inst.* 36 (2017) 1885-1892.
6. B. Coriton, S.-K. Im, M. Gamba, J.H. Frank, Flow field and scalar measurements in a series of turbulent partially-premixed dimethyl ether/air jet flames, *Combust. Flame* 180 (2017) 40-52.
7. M. Kamal, B. Coriton, R. Zhou, J.H. Frank, S. Hochgreb, Scalar dissipation rate and scales in swirling turbulent premixed flames, *Proc. Combust. Inst.* 36 (2017) 1957-1965.
8. F. Salehi, M. Talei, E. Hawkes, A. Bhagatwala, J.H. Chen, S. Kook, Doubly conditional moment closure modeling for HCCI with temperature inhomogeneities, *Proc. Combust. Inst.* 36 (2017) 3677-3685.
9. A. Krisman, E. R. Hawkes, M. Talei A. Bhagatwala, J.H. Chen, A DNS of a cool-flame affected autoignition in diesel engine-relevant conditions, *Proc. Combust. Inst.* 36 (2017) 3567-3575.
10. H. Wang, E.R. Hawkes, B. Zhou, J.H. Chen, Z. Li, M. Alden, A comparison between DNS and experiment of the turbulent burning velocity-related statistics in a turbulent methane-air premixed jet flame at high Karlovitz number, *Proc. Combust. Inst.* 36 (2017) 2045-2053.
11. S. Karami, M. Talei, E.R. Hawkes, J.H. Chen, Local extinction and reignition mechanism in a turbulent lifted flame: a DNS study, *Proc. Combust. Inst.* 36 (2017) 1685-1692.
12. E.S. Richardson and J.H. Chen, Analysis of turbulent flame propagation in equivalence ratio-stratified flow, *Proc. Combust. Inst.* 36 (2017) 1729-1736.
13. H. Wang, E.R. Hawkes, B. Zhou, J.H. Chen, Z. Li, M. Alden, Petascale direct numerical simulations of a high Ka laboratory premixed jet flame, *J. Fluid Mech.* 815 (2017) 511-536.
14. M. Kuron, Z. Ren, H. Zhou, E. Hawkes, J. Tang, J.H. Chen, and T. Lu, Performance of transported PDF mixing models in a turbulent premixed flame, *Proc. Combust. Inst.* 36 (2017) 1987-1995.
15. M. Kuron, Z. Ren, E.R. Hawkes, H. Zhou, H. Kolla, J.H. Chen, T. Lu, A mixing timescale model for TPDF simulations of turbulent premixed flames, *Combust. Flame* 177 (2017) 171-183.
16. A. Krisman, E.R. Hawkes, and J.H. Chen, Autoignition and edge flames in a turbulent jet at diesel engine relevant thermochemical conditions, *J. Fluid Mech.* 824 (2017) 5-41.
17. C. Han, D.O. Lignell, E.R. Hawkes, J.H. Chen, H. Wang, Examination of differential molecular diffusion in DNS of turbulent non-premixed flames, *Intl. J. Hydrogen Energy* 42 (2017) 11879-11892.
18. S. Chaudhuri, D. Simanshu, H. Kolla, H. Dave, E.R. Hawkes, J.H. Chen, C.K. Law, Flame thickness and conditional scalar dissipation rate in a premixed temporal turbulent reacting jet, *Combust. Flame* 184 (2017) 273-285.
19. H. Wang, E.R. Hawkes, J.H. Chen, A direct numerical simulation study of flame structure and stabilisation of an experimental high Ka CH₄/air premixed jet flame, *Combust. Flame* 180 (2017) 110-123.

20. H. Pouransari, H. Kolla, J. H. Chen, A. Mani, Spectral analysis of energy transfer in turbulent flows laden with heated particles, *J. Fluid Mech.* 813 (2017) 1156-1175.
21. Fuest, F.; Barlow, R.S.; Magnotti, G.; Sutton, J.A., Scalar dissipation rates in a turbulent partially-premixed dimethyl ether/air jet flame, *Combust. Flame* 188 (2018) 41–65.
22. Hartl, S.; Geyer, D.; Dreizler, A.; Magnotti, G., Barlow, R.S.; Hasse, C., Reaction zone detection and characterization from Raman/Rayleigh line measurements in partially premixed flames, *Combust. Flame* 189 (2018) 126–141.
23. Straub, C.; Kronenburg, A.; Stein, O.T.; Kuenne, Guido; Janicka, J.; Barlow, R.S.; Geyer, D., Multiple mapping conditioning coupled with an artificially thickened flame model for turbulent premixed combustion, *Combust. Flame* 196 (2018) 325–336.
24. Z. Ren, M. Kuron, X. Zhou, T. Lu, H.N. Kolla, and J.H. Chen, Micromixing models for PDF simulations of premixed flames, in press *Combustion Science and Technology*.
25. A. Krisman, E. Hawkes, and J.H. Chen, The structure and propagation of laminar flames under autoignitive conditions, *Combust. Flame* 188 (2018) 399-411.
26. G. Borghesi, A. Krisman, T. Lu and J.H. Chen, A DNS investigation of turbulent n-dodecane / air mixing layer autoignition, *Combust. Flame* 195 (2018) 183-202.
27. H. Wang, E.R. Hawkes, B. Savard, and J.H. Chen, Direct numerical simulation of a high Ka CH₄/air stratified premixed jet flame, *Combust. Flame* 193 (2018) 229-245.
28. C. Xu, M. Muhsin, S. Som, J. H. Chen, Z. Ren and T. Lu, “Dynamic adaptive combustion modeling of spray flames based on chemical explosive mode analysis,” *Combust. Flame* (2018) 195:30-39.
29. Hartl, S.; Van Winkle, R.; Geyer, D.; Dreizler, A.; Magnotti, G.; Hasse, C.; Barlow, R.S., Assessing the relative importance of flame regimes in Raman/Rayleigh line measurements of turbulent lifted flames, *Proc. Combust. Inst.* 37 (2019) 2297–2305.
30. Scheider, S.; Geyer, D.; Magnotti, G.; Dunn, M.J.; Barlow, R.S.; Dreizler, A., Structure of a stratified CH₄ flame with H₂ addition, *Proc. Combust. Inst.* 37 (2019) 2307–2315.
31. Straub, C.; Kronenburg, A.; Stein, O.; Barlow, R.S.; Geyer, D., Modelling stratified flames with and without shear using multiple mapping conditioning, *Proc. Combust. Inst.* 37 (2019) 2317–2324.
32. J.W. Labahn, H. Wu, B. Coriton, J.H. Frank, M. Ihme, Data assimilation using high-speed measurements and LES to examine local extinction events in turbulent flames, *Proc. Combust. Inst.* 37 (2019) 2259-2266.
33. B. Zhou, J.H. Frank, Effects of heat release and imposed bulk strain on alignment of strain rate eigenvectors in turbulent premixed flames, *Combust. Flame* 201 (2019) 290-300.
34. K. Aditya, A. Gruber, C. Xu, T. Lu, A. Krisman, M. Bothien, J.H. Chen, Direct numerical simulation of flame stabilization assisted by autoignition in a reheat gas turbine combustor, *Proc. Comb. Inst.* 37 (2019) 2635-2642.
35. A. Krisman, C. Mounaim-Rousselle, R. Savaramakrishnan, J.A. Miller, and J.H. Chen, Reference natural gas flames at nominally autoignitive engine relevant conditions, *Proc. Comb. Inst.* 37 (2019) 1631-1638.
36. D.H. Shin, E.S. Richardson, V. Aparace-Scutariu, Y. Minamoto, and J.H. Chen, Residence time-based analysis of a lifted turbulent dimethyl ether jet flame, *Proc. Comb. Inst.* 37 (2019) 2215-2222.
37. A. Krisman, E.R. Hawkes, and J.H. Chen, A parametric study of ignition dynamics at ECN Spray A thermochemical conditions using 2D DNS, *Proc. Comb. Inst.* 37 (2019) 4787-4795.
38. W. Han, H. Wang, G. Kuenne, E.R. Hawkes, J.H. Chen, J. Janicka, and C. Hasse, Large-eddy simulation/dynamic thickened flame modeling of a high Karlovitz number turbulent premixed jet flame, *Proc. Comb. Inst.* 37 (2019) 2555-2563.
39. F. Galeazzo, B. Savard, H. Wang, E. Hawkes, J.H. Chen, G. Filho, Performance assessment of flamelet models in flame-resolved LES of a high Karlovitz methane/air stratified premixed jet flame, *Proc. Comb. Inst.* 37 (2019) 2545-2553.

Dynamics and Energetics of Elementary Combustion Reactions and Transient Species

Grant DE-FG03-98ER14879

Robert E. Continetti (rcontinetti@ucsd.edu)

Department of Chemistry and Biochemistry, University of California San Diego
9500 Gilman Drive, La Jolla, CA 92093-0340

I. Program Scope

This research program obtains experimental results that benchmark fundamental advances in the theoretical understanding of chemical reactions, including the development of accurate potential energy surfaces (PESs) and computational studies of the dynamics of chemical reactions. The primary focus has been on the bimolecular reactions of the hydroxyl radical, but during this project period the focus has shifted to oxygenated carbon radicals and pump-probe studies of dissociative photodetachment processes, with implications for understanding the photochemistry of negative ions, transient anion resonances, and using these resonances to promote unique chemical pathways. The studies involve the development and application of advanced experimental techniques using photodetachment and dissociative photodetachment of anionic precursors to prepare energized radicals and collision complexes. Laser photodetachment, coupled with the detection of photoelectrons, stable photoneutrals, and photofragments in coincidence has allowed us to establish the technique of photoelectron-photofragment coincidence (PPC) spectroscopy, providing kinematically complete measurements of energy partitioning in reaction dynamics. During the last year, we published a characterization of cold and hot anions in the laboratory, building upon the examination of the photochemistry of O_3^- which demonstrated a dramatic suppression of an $O + O_2^-(v)$ channel with the quenching of parent anion vibration through buffer gas cooling (DOE pub. 1).¹ The O_3 system was used to quantify the control over anion temperatures due to the sensitivity of precursor anions to the relative intensities of the dissociative and autodetachment channels (DOE pub. 6). We continued our ongoing collaboration with Jun Li and Hua Guo in an examination of the dynamics of $OH/OD + CH_4/CD_4 \rightarrow H_2O + CH_3/CD_3$ initiated by photodetachment of the OH^- -hydrocarbon complexes. Interpretation of the experimental results were aided by quasiclassical trajectory calculations which showed general agreement between experiment and theory (DOE pub. 7). Finally, building upon our study with John Stanton that reassigned the low-lying electronic states of ethylenedione, C_2O_2 , to the oxyallyl diradical²⁻⁴ (DOE pub. 4), we published below threshold measurements of the oxyallyl diradical, in which the observation of excitation to a dipole bound state resulted in either a delayed photoemission process or dissociative photodetachment via a two photon process (DOE pub. 5).⁵ Further studies on the oxyallyl diradical are also underway, with the implementation of ultrafast pump-probe excitation to the previously observed dipole bound state. Dissociative photodetachment above threshold of the oxyallyl diradical via the oxyallyl anion has also been observed, and the results are currently being analyzed. Ongoing efforts also include characterization of the photodissociation of nitrogen oxide species such as $N_2O_2^-$ and a high-energy isomer of NO_3^- studying the complex dissociation/autodetachment dynamics exhibited by these systems in the near-UV. In the following sections, recent progress will be discussed in more detail, followed by a brief review of future work on OH-complexes, as well as returning to the IR excitation experiments^{6,7} (DOE pub. 2) to study the excitation and isomerization of the HOCO system.

II. Recent Progress

A. Control of O_3^- Internal Energy Demonstrated by Photodissociation Dynamics using a Cryogenic Octopole Accumulation Trap

The first PPC study using a radio frequency (RF) cryogenic octopole accumulation trap (COAT) to collisionally cool precursor anions with buffer gas was reported in a study of the photodissociation of O_3^- .¹ This study showed the production of two ionic dissociation pathways, (1) $O_2(^1\Delta_g) + O^-(^2P)$ and (2) $O_2(^2\Pi_g) + O(^3P)$, as well as photodetachment, (3) $O_3 + e^-$ at a photon energy of 3.20 eV. The coldest anions were produced at 17 K COAT temperature with 80 ms trapping using a He/H₂ buffer gas mix. A significant decrease in the 1_1^0 hot bands from photodetachment channel (3) and suppression of the sequential autodetachment of $O_2^-(v'' < 4)$ produced by channel (2) was observed and have been published (DOE pub. 1). The capabilities of COAT were further explored by ranging experiments between room temperature and $T < 17$ K, varying trap timings, and varying COAT electrode voltages. The coldest spectra were obtained with longer trap timings (80 ms) which allowed the thermalization of

internal energy of precursor ions with the He/H₂ buffer gas. This resulted in the suppression of O₂⁻(*v*" < 4) autodetachment and reduction of photodetachment of O⁻ produced in channel (1) via a two-photon process. The production of hotter ions was achieved by varying ion injection voltages into COAT, using neat He buffer gas, and shorter trapping times (500 μs). Autodetachment peaks O₂⁻ (*v*" = 4, 5, and 6) and the enhancement of the O⁻ two-photon process were observed under hot conditions. Franck-Condon simulations showed good agreement with the coldest spectrum assuming 0 K ion temperature for all modes. The hottest spectrum was reproduced assuming *v*₁ = 2,000 K and *v*₂ = 1,500 K. These results have recently been published (DOE pub. 6) and demonstrate the ability to cool or heat ions through enhanced control over internal energy of precursor anions, demonstrated by studying the dissociation dynamics of O₃⁻.

B. Hydroxyl Radical Reactions: OH/OD + CH₄/CD₄ → H₂O + CH₃/CD₃

The elementary reaction OH + CH₄ → H₂O + CH₃ reaction is involved in the oxidation of methane in combustion and atmospheric chemistry, so we have endeavored to study this and other hydroxyl radical reactions using clusters with OH⁻. In a recent publication (DOE pub. 7), PPC measurements were carried out on OH⁻(CH₄) at a photon energy of 3.20 eV which yielded stable, OH-

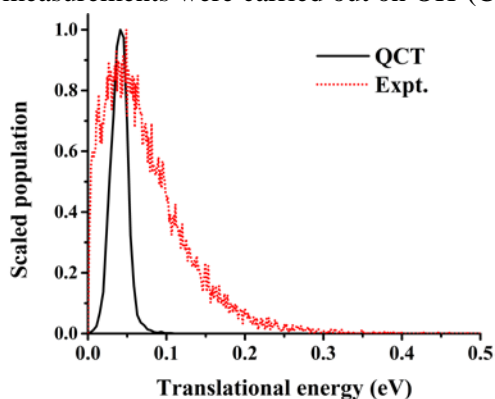


Figure 1. Experimentally measured and theoretically calculated KER distribution in the OH + CH₄ channel.

CH₄ + e⁻, and dissociative, OH + CH₄ (*v*₁ or *v*₃, *v* = 0, 1) + e⁻, channels. The main channel was dissociation with a low kinetic energy release (KER) peaking at 0.04 eV. In collaboration with Jun Li and Hua Guo, an anion potential energy surface was constructed at a level of CCSD(T)-F12a/AVTZ and a previously calculated neutral potential energy surface was used.⁸ Owing to the dimensionality of the problem, the photodetachment dynamics were simulated using a quasiclassical trajectory method using initial conditions sampled from the Wigner distribution for the anion. A total of 4,000 trajectories were carried out with most yielding slowly recoiling OH + CH₄ fragments. The measured and calculated KER distribution in the OH + CH₄ channel, seen in Figure 1, demonstrates overall agreement. This supports the conclusion that upon photodetachment, the initial wave packet is placed on the entrance channel of

the neutral PES and has weak repulsion between OH-CH₄ leading to a low KER. Some of the CH₄ fragments were also found to have some excitation in the symmetric and asymmetric stretching modes in agreement with experimental results. The combined experimental and theoretical results validated the accuracy of the anion and neutral PESs and helped shed new insights into the dissociation dynamics of this important reaction. This seven-atom system is a measure of the limit of full-dimensionality quantum dynamics calculations at this point that will hopefully be surmounted in the future.

C. Oxyallyl Diradical: Dissociation Dynamics Above and Below Threshold

The oxyallyl diradical is a transient species that is known to have two nearly degenerate electronic states, as well as one low-lying excited state. Multiple studies have been conducted on the oxyallyl system. The nearly degenerate ³B₂ and ¹A₁ states have been observed through anion photoelectron spectroscopy,⁹ which determined that the Franck-Condon region is not a true minimum on the singlet surface, but rather a transition state with ~170 fs lifetime. This has been supported by theoretical studies on this system,¹⁰ which predict the singlet state will undergo ring closure to reach the energetically stable cyclopropanone. When the oxyallyl anion is photodetached at 3.20 eV, the resulting neutral products are predominately stable with a minor dissociation pathway. The photoelectron spectrum measured in coincidence with a single stable product was used to justify the reassignment of the photoelectron spectrum of ethylenedione^{3,4} (OCCO) to the oxyallyl diradical (C₃H₄O) in the literature, as reported last year in DOE pub. 4.² The minor dissociation has been determined to result from all three of the electronic states accessible at 3.20 eV, with the singlet undergoing dissociative photodetachment to produce vibrationally excited CO + C₂H₄. Both the triplet ground and excited states undergo intersystem crossing to the singlet surface in order reach the same spin allowed dissociation. This is the first observation of the dissociation dynamics of the oxyallyl diradical system.

Measurements were also carried below the photodetachment threshold of the oxyallyl anion at 775 nm (1.6 eV), to examine potential multiphoton photodetachment processes. These measurements revealed both significantly different dissociation dynamics (DOE pub. 5) as well as the existence of a delayed ionization pathway unexpected in such a small anion.⁵ This was attributed to excitation to a dipole bound state (DBS) prior to autodetachment or dissociative photodetachment. The singlet state of the oxyallyl diradical is known to be a transition state, and owing to a significant zwitterionic character, it has a large dipole (4.2 D) that can support a DBS well below the detachment threshold. The behavior of DBSs are characterized by their neutral cores, in this case cyclization of the singlet state. However, the cyclopropanone anion is unstable with respect to its neutral counterpart, resulting in a delayed autodetachment when the neutral core can no longer support the DBS, as seen in

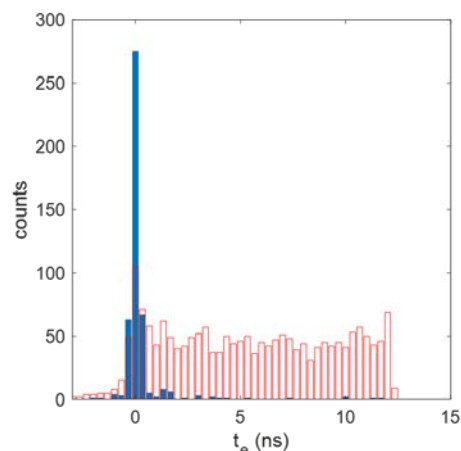


Figure 2. Electron time-of-arrival events in coincidence with stable neutral (red bars) or dissociative neutral fragments (blue bars).

Figure 2. During this cyclization, a second photon can also interact with the system, leading to dissociative photodetachment to vibrationally excited CO + C₂H₄. This is the first report of a small, cold anion exhibiting a delayed photoemission process, as well as the first observation of a dipole bound state for the oxyallyl system. The observation of the two-photon dissociative photodetachment process in this case shows that the timescale of this dissociation process is less than 1.2 ps given the laser pulsewidth.

Recently, our Ti:Sapphire regenerative amplifier (Clark MXR CPA-2000) was converted into a femtosecond laser with 280 fs pulse width. This has allowed the opportunity to study lifetimes and dynamics that may occur on a smaller timescale that was previously unresolved at a 1.2 ps laser pulse width. Pump-probe experiments using 775 nm output have been designed to better quantify the two-photon process leading to dissociation of the oxyallyl diradical DBS into the neutral products CO + C₂H₄. Preliminary results suggest that at a 300 fs delay, more dissociation is observed than at t = 0 or t = 600 fs. This effectively demonstrates that dissociation is enhanced 300 fs after accessing the DBS. These experiments demonstrate a new capability by our PPC spectrometer for ultrafast time-resolved pump-probe experiments which allows for studying the dynamics of photoexcited long-lived anion resonances.

D. Photodissociation and autodetachment of N₂O₂⁻/NO₃⁻

The N₂O₂ and NO₃ systems are important intermediates in atmospheric and combustion chemistry, and known for their various dissociation pathways.¹¹⁻¹⁴ These pathways are dependent on both the photon energy used to study these systems, as well as the precursor anion state accessed. Using PPC spectroscopy, photodissociation of both N₂O₂⁻ and NO₃⁻ anions was observed. For N₂O₂⁻, the reaction pathways were disentangled to obtain distinct spectra based on different neutral product fragmentation. Three channels were observed through ionic photodissociation followed by anion product photodetachment or autodetachment at 3.20 eV. These channels are assigned to N₂O₂⁻ + hν → N₂O + O⁻ + hν → N₂O + O + e⁻, via a two photon process, N₂O₂⁻ + hν → NO + NO⁻(v=0) + hν → NO + NO + e⁻, and N₂O₂⁻ + hν → NO + NO⁻(v>0) → NO + NO + e⁻, with NO⁻(v>0) undergoing autodetachment due to the low electron affinity of NO. These coincidence measurements provide the first state-resolved data on the autodetachment of the highly vibrationally and rotationally excited NO anion products. For the NO₃ system, ionic photodissociation followed by anion product photodetachment or autodetachment was also observed at 3.20 eV. These channels are assigned to NO₃⁻ + hν → NO + O₂⁻ + hν → NO + O₂ + e⁻, via a two photon process and NO₃⁻ + hν → O₂ + NO⁻(v>0) → NO + NO + e⁻ in a similar autodetachment process as N₂O₂⁻. In collaboration with John Stanton, who provided the relative anion energetics, it was determined that the cis and trans isomers of the peroxyxynitrite anion are being accessed. The peroxyxynitrite anion isomers are over 2 eV higher in energy than the ground state NO₃⁻. These measurements were carried out with COAT to internally cool the precursor anions to their ground vibrational states, allowing excited anions to be stabilized in local minima. The results from these two

systems are currently in preparation for publications, and will provide new information on photochemistry of N_2O_2^- as well as the first detailed report of photodissociation of the high energy NO_3^- isomers.

E. Future Work

In the coming months, we will finish pump-probe studies on the oxyallyl system. When these experiments are completed, the new pump-probe capability of the PPC spectrometer can be applied to other simple diradicals in order to study the dynamics of photoexcited long-lived anion resonances. Building upon the $\text{OH}^-(\text{CH}_4)$ study, we will work with the negative ion sources to synthesize new precursors including studies of other relevant hydroxyl radical systems through association reactions in the RF trap including $\text{OH}^-(\text{C}_2\text{H}_4)$, $\text{OH}^-(\text{C}_2\text{H}_2)$, $\text{OH}^-(\text{NO})$ and $\text{OH}^-(\text{NH}_3)$. We can then return to IR excitation studies which vibrationally excite anions for control of product branching ratios. Using selective IR excitation, we will vibrationally induce the *cis*- $\text{HOCO}^-/\text{trans}$ - HOCO^- and $\text{HCO}_2^-/\text{HOCO}^-$ isomerizations (DOE pub. 2), and then study the mode-specific dissociation dynamics of HOCO using the dissociative photodetachment technique.^{15, 16} These efforts will pave the way for future studies of transient species with controlled internal excitation, providing benchmark data for fundamental understanding of chemical phenomena.

F. DOE-supported publications by this project 2017-2019

1. B. Shen, Y. Benitez, K. G. Lunny, R. E. Continetti, *Internal energy dependence of the photodissociation dynamics of O_3^- using cryogenic photoelectron-photofragment coincidence spectroscopy*, J. Chem. Phys., **147**, 094307 (2017).
2. A. W. Ray, J. Ma, R. Otto, J. Li, H. Guo, R. E. Continetti, *Effects of vibrational excitation on the $\text{F} + \text{H}_2\text{O} \rightarrow \text{HF} + \text{OH}$ reaction: dissociative photodetachment of overtone-excited $[\text{F}-\text{H}-\text{OH}]^-$* , Chemical Science, **8**, 7821-7833 (2017).
3. R.E. Continetti and H. Guo, *Dynamics of transient species via anion photodetachment*, Chem. Soc. Rev. **46**, 7650-7667 (2017).
4. K. G. Lunny, Y. Benitez, Y. Albeck, D. Strasser, J. F. Stanton, R. E. Continetti, *Spectroscopy of Ethylenedione and Ethynediolide: A Reinvestigation*, Angew. Chemie. Int. Ed. **57**, (19), 5394-5397 (2018). <https://doi.org/10.1002/anie.201801848>
5. Y. Albeck, K. G. Lunny, Y. Benitez, A. J. Shin, D. Strasser and R. E. Continetti, *Resonance-Mediated Below-Threshold Delayed Photoemission and Non-Franck-Condon Photodissociation of Cold Oxyallyl Anions* Angew. Chem. Int. Ed. **58** (16), 5312-5315 (2019). <https://doi.org/10.1002/anie.201900386>
6. B. Shen, K. G. Lunny, Y. Benitez, R. E. Continetti, *Photoelectron-Photofragment Coincidence Spectroscopy with Ions Prepared in a Cryogenic Octopole Accumulation Trap: Collisional Excitation and Buffer Gas Cooling*, Frontiers in Chemistry, In Press (2019).
7. Y. Benitez, D. Lu, K. G. Lunny, J. Li, H. Guo, R. E. Continetti, *Photoelectron-Photofragment Coincidence Studies on the Dissociation Dynamics of the $\text{OH}-\text{CH}_4$ Complex*, J. Phys. Chem. A., In Press (2019).

References

1. B. Shen, Y. Benitez, K. G. Lunny and R. E. Continetti, J. Chem. Phys. **147**, 094307 (2017).
2. K. G. Lunny, Y. Benitez, Y. Albeck, D. Strasser, J. F. Stanton and R.E. Continetti, Angew. Chem. Int. Ed. **57** (18), 5394-5397 (2018).
3. A. Dixon, T. Xue and A. Sanov, Angew. Chem. Int. Ed. **54** (127), 8764-8767 (2015).
4. A. Dixon, T. Xue and A. Sanov, J. Chem. Phys. **144** (2016).
5. Y. Albeck, K. G. Lunny, Y. Benitez, A. J. Shin, D. Strasser and R. E. Continetti, Angew. Chem. Int. Ed. **58** (16), 5312-5315 (2019).
6. R. Otto, A. W. Ray, J. S. Daluz and R. E. Continetti, EPJ Techniques and Instrumentation **1** (1), 3 (2014).
7. A. W. Ray, J. Ma, R. Otto, J. Li, H. Guo and R. E. Continetti, Chemical Science **8** (11), 7821-7833 (2017).
8. J. Li and H. Guo, J. Chem. Phys. **143** (22), 221103 (2015).
9. T. Ichino, S. Villano, A. Gianola, D. Goebbert, L. Velarde, A. Sanov, S. Blanksby, X. Zhou, D. Hrovat, W. T. Borden and W. C. Lineberger, J. Phys. Chem. A **115**, 1634 (2011).
10. V. Mozhayskiy, D. Goebbert, L. Velarde, A. Sanov and A. Krylov, J. Phys. Chem. A **114** (2010).
11. D. W. Arnold and D. M. Neumark, J. Chem. Phys. **102**, 7035 (1995).
12. D. L. Osborn, D. J. Leahy, D. R. Cyr and D. M. Neumark, J. Chem. Phys. **104**, 5026 (1995).
13. L. A. Posey and M. A. Johnson, J. Chem. Phys. **88**, 5383 (1988).
14. R. A. Relph, J. C. Bopp, M. A. Johnson and A. A. Viggiano, J. Chem. Phys. **129**, 064305 (2008).
15. C. J. Johnson, R. Otto and R. E. Continetti, Phys. Chem. Chem. Phys. **16**, 19091 (2014).
16. A. W. Ray, B. B. Shen, B. Poad, L. J. and R. E. Continetti, Chem. Phys. Lett. **592**, 30-35 (2014).

GAS PHASE INTERACTIONS WITH OTHER PHASES

Rainer N. Dahms, Reese Jones, Christopher J. Kliewer, Hope A. Michelsen, and Judit Zádor
Combustion Research Facility, Sandia National Labs, Livermore, CA 94550
rjones@sandia.gov, cjkliew@sandia.gov, hamiche@sandia.gov, jzador@sandia.gov

I. Program Scope

This research program impacts the synergistic research themes of *Chemistry at Complex Interfaces* and *Reaction Pathways in Diverse Environments*; it encompasses experimental and computational investigations of a wide range of multiphase phenomena, probing the gas-phase side of interfaces and the physical and chemical interactions between the phases. Understanding reactions that lead to particle formation draws on work in the “Chemical Kinetics for Complex Systems” task, and experiments employ innovations from the “Ultrafast Physics: Nonlinear Optical Spectroscopy and Diagnostics” and “Advanced Mass Spectrometry and X-Ray Diagnostics” tasks. Our recent work predominantly focuses on two main areas: chemically controlled gas-to-particle conversion at high temperatures and non-equilibrium interfacial phenomena at gas-liquid interfaces. Experimental work focuses on the development and use of diagnostics for carbonaceous particles in high-temperature, atmospheric, and other environments and the use of these diagnostics to study particle inception, growth, chemical and physical evolution, oxidation, and other chemical processing. Studies are targeted at developing an understanding at a fundamental level of particle-light interactions. Computational studies involve quantum chemical calculations to complement experimental particle characterization and provide insight into carbonaceous-particle chemistry. Computational investigations also involve simulations of gas-liquid multi-component interfaces under thermodynamic conditions far from equilibrium.

II. Recent Progress

Gas-to-Particle Conversion of Hydrocarbons at High Temperature

The formation of solid carbonaceous particles at high temperatures is important in numerous natural environments, energy production and use technologies, and commercial applications. Such particles are formed in hot carbon plasmas, by spray pyrolysis, and during the detonation of explosives. They are produced commercially for pigments, adsorbents, and composite materials. They are generated in the outflow of carbon-rich stars and are one of the main components of interstellar dust.¹ The most ubiquitous and notorious of carbon particles formed under high-temperature conditions is soot, a product of incomplete combustion of hydrocarbon fuels. Despite its ubiquity and its enormous negative impact on human health and the environment,²⁻³ the chemical pathways for soot formation are unknown, and its surface chemistry following formation is poorly understood.⁴

There is a large body of evidence linking polycyclic aromatic hydrocarbon (PAH) species to soot

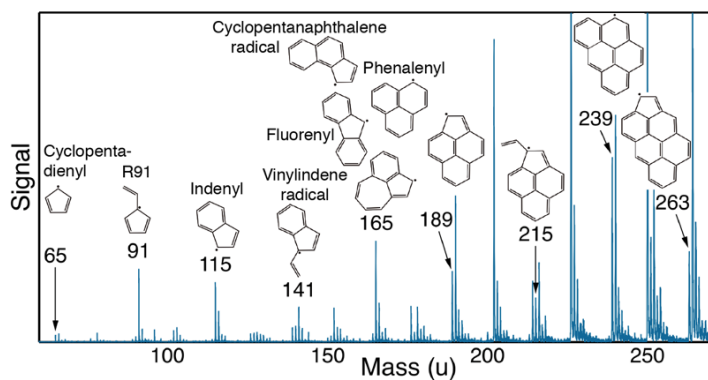


Figure 1. VUV-AMS spectrum for a sample extracted from a premixed ethylene-oxygen flame, recorded at a photon energy of 9.4 eV at the ALS. Predicted molecular structures are shown for highlighted masses. From Ref. 6.

formation,⁵ but the mechanisms driving the transition of these gas-phase precursors to condensed-phase particles (i.e., particle inception) are not known. Another gap in the understanding of soot formation involves the rapid growth of these incipient particles or hydrocarbon clusters by hydrocarbon addition. At temperatures where soot inception occurs (≥ 1200 K), the PAHs typically present in appreciable quantity are in the range of two to five aromatic rings and are far too small and volatile to form stable clusters bound by dispersive or van der Waals forces.⁵ A long history of research indicates a need for a chemical mechanism that rapidly bonds hydrocarbon precursors

covalently at these temperatures. Current proposed chemical mechanisms for cluster formation are simply too slow to explain particle formation. Most PAH-radical reactions require activation of highly stable PAHs through H abstraction via significant barriers. In addition, reactions between radicals quickly consume the radical pool and yield very stable species that again require activation via appreciable barriers.

We have collaborated with Dr. Kevin R. Wilson (LBNL) and Prof. Martin P. Head-Gordon (LBNL, Univ. of California Berkeley) to investigate a new mechanism for soot inception involving radical-chain reactions driven by resonance-stabilized radicals.⁶ Figure 1 shows a mass spectrum of vaporized particles extracted from an atmospheric-pressure laminar premixed ethylene-oxygen flame measured using vacuum ultraviolet aerosol mass spectrometry (VUV-AMS) at a photon energy of 9.4 eV provided by the Advanced Light Source. This mass spectrum demonstrates a sequence of masses attributable to resonance-stabilized radicals (highlighted). These species are seen frequently in mass spectra from vaporized particle samples extracted from flames but are seldom

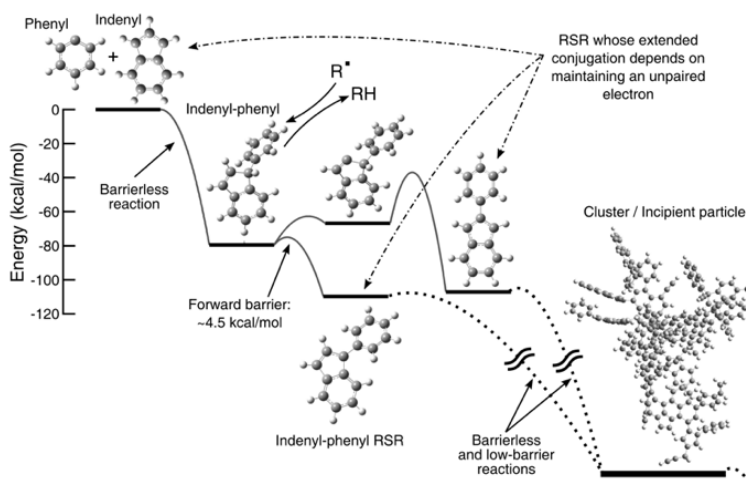


Figure 2. Example mechanism for hydrocarbon clustering. The potential energy diagram shows formation of an adduct of an RSR (indenyl) and another radical species (phenyl). Subsequent H abstraction stabilizes the bond and regenerates an RSR whose extended conjugation requires an unpaired electron. Repeated similar reactions lead to hydrocarbon clustering and incipient soot formation. From Ref. 6.

observed in gas-phase samples. Calculations employing density functional theory demonstrate that this sequence of resonance-stabilized radicals (RSRs) can be readily produced at flame temperatures. Additional calculations suggest that these RSRs can drive a radical-chain-reaction mechanism for covalent clustering of hydrocarbon species and soot inception at high temperatures.

An example of this mechanism is shown in Fig. 2. The mechanism is initiated by a resonantly stabilized π radical whose extended conjugation depends on maintaining an unpaired π electron (i.e., indenyl in Fig. 2). This RSR loses conjugation when it reacts to form a σ bond. The reaction of indenyl with phenyl in Fig. 2 is barrierless, but indenyl loses conjugation during the reaction. The barrier to H abstraction from the site of phenyl attachment is low because it restores conjugation and regenerates an RSR to propagate the mechanism and further clustering. The low barriers to reaction and significant exothermicity minimize reversibility. These RSRs can also react with unsaturated aliphatic and nonradical aromatic species. This mechanism could be critical to soot formation during combustion and relevant to the formation of stardust in the outflow from carbon-rich stars in interstellar space.⁶

Characteristics of Gas-Liquid Interfaces at Conditions Far from Equilibrium

The simplest gas-liquid interface is found in single-component two-phase systems. For classical subcritical conditions, the width of a two-phase interface is on the order of a nanometer and is characterized by a step-change in density between phases. Under these conditions, the transition between the gas and liquid phases is classified as a first-order transition. In contrast, second-order phase transitions are characterized by a gradual change in density and are associated with supercritical conditions for which two-phase interfaces are not sustainable. Sharp density transitions in gas-liquid interfaces can only exist along the co-existence curve when gas and liquid are in thermodynamic equilibrium (i.e., at the same pressure and temperature). The co-existence curve eventually ends at the critical point where the densities of both phases become equal, and the surface tension and gas-liquid interface disappear. In multi-component mixtures, the same physical arguments apply with respect to density differences across classical phase

transitions. However, the corresponding envelope of first-order and second-order phase transitions changes because of the added complexity of chemical composition differences between vapor and liquid phases. First-order phase transitions appear over a much wider range of conditions because the different constituents of the vapor and liquid have different densities at the same pressure and temperature.

This classical view of phase transitions is valid when both phases are in thermodynamic equilibrium. However, extreme thermodynamic gradients can drive the interfacial structure out of equilibrium and broaden the gas-liquid interface. Under these conditions, classical two-phase theory and conventional gas-liquid interface dynamics are no longer applicable. The conditions for which classical theory breaks down can be roughly estimated using Non-Linear Gradient Theory with non-ideal, real-fluid, multi-component thermodynamics and transport.⁷ These conditions can be expressed in terms of the relative magnitudes of the interface thickness (L_{VLE}) and the thermal collision length scale (L_{th}) as shown in Fig. 3 for a ternary n-dodecane/ CO_2/N_2 mixture. Figure 3 shows that, at ambient conditions, L_{th} is significantly larger than L_{VLE} . Because of the disparity in length scales of L_{th} and L_{VLE} , there is no appreciable temperature gradient within the interface. This remains true at high-pressure, low-temperature conditions, although L_{th} can become comparable to the interface thickness.⁸ However, for certain combinations of chemical constituents at subcritical high temperature and pressure, L_{th} is significantly smaller than the interface thickness, as illustrated in Fig. 3, and thermal gradients can exist within the gas-liquid interfacial structure. Then, the interface can no longer be viewed as an isolated system in equilibrium. Instead, the interfacial dynamics become fully coupled to the large thermodynamic gradients imposed by the bordering regions in the gas and liquid phases. The full extent of this regime cannot be determined using equilibrium assumptions. Recent calculations by R. Dahms, based on non-equilibrium assumptions, suggest that such non-equilibrium interfacial structures can significantly broaden to thicknesses on the order of 80 nm, as shown in Fig. 3 for n-dodecane injected into a CO_2/N_2 mixture at an interface temperature of 580 K at 60 bar. In addition, a recent molecular dynamics simulation of a similar system⁹ predicted the interfacial thickness to be in the range of 50-60 nm, consistent with the theoretical predictions of Dahms. These non-equilibrium interface dynamics are not a classical subcritical-to-supercritical transition but rather a transformation caused by imposing large thermodynamic gradients on a multi-component, subcritical interface.

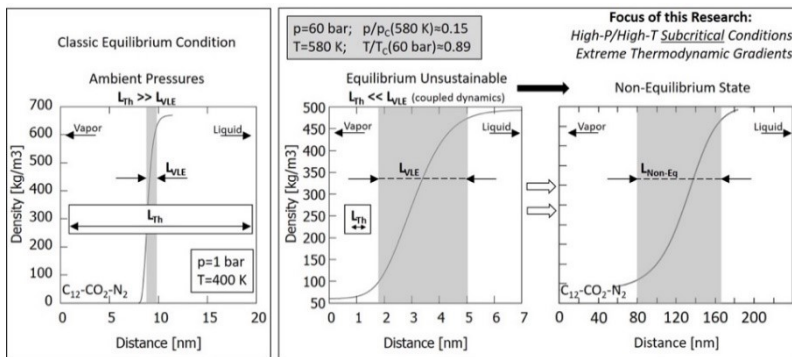


Figure 3. Gas-liquid interface mean-field density profiles, thicknesses (L_{VLE}) (shaded area) and vapor phase thermal collision length scales (L_{Th}) for n-dodecane injected into a CO_2/N_2 mixture at (left) ambient conditions, (middle) subcritical high-p, high-T conditions where thermodynamic equilibrium becomes unsustainable under extreme thermodynamic gradients and (right) resultant significant interfacial

These predictions of interfacial thickness provide general guidelines, but questions remain about the validity of the thermodynamic analysis for these far-from-equilibrium conditions and the underlying chemical physics of this regime. It is of fundamental interest to understand how the molecular interactions influence the chemical physical properties of this unexplored gas-liquid interface and how the average orientation in the interface changes as the interface transitions from sharp to diffuse. Knowledge of the intermolecular forces, molecular ordering, and speciation in the interface are

needed to guide advances in the theory. Current predictions have significant uncertainties arising from a lack of experiments and uncertain thermodynamic and transport properties for these conditions. While thermodynamic properties of pure chemical constituents are usually known with high accuracy, large uncertainties exist for gas-liquid interface structures since they comprise unstable and metastable regimes of fluid densities where experimental data is usually not available and modeling approaches are questionable. Transport properties within the interface are even more uncertain as they build upon already uncertain thermodynamic data and are not directly applicable to confined regions within interfaces. Furthermore, data for multi-component interfaces obtained from thermodynamic mixing-rules are semi-

empirical and not fully suitable for confined interface regions. The mean-field density-gradient theory also does not account for effects of variations in molecular orientation and symmetry within far-from-equilibrium interfaces.

To answer these questions, R. Jones has been conducting molecular dynamics simulations. Molecular dynamics is the most appropriate simulator since the feature sizes are on the order of 100 nm, they form rapidly and do not involve reactive chemistry. Starting with simpler systems (2 component Lennard-Jones fluids in thermal equilibrium) and building to more complex systems (multicomponent fluids with molecular structure with steady heat fluxes) he has been investigating what combination of material properties and external conditions (composition, temperature, and temperature gradient) lead to broadened interfaces using optimization and sampling methods. Investigation is on-going and includes: (a) the design of custom order parameters to detect interface thickening and its relation to molecular orientation and the like, and (b) theory to explain how fluid structures on the order of 100 nm can be stabilized by intermolecular forces and how this connects to classical theory like Cahn-Hilliard.

III. Proposed work

The program will continue to use experiments, theory, and data science methods to investigate gas-phase molecular weight growth reactions and the nature of the interactions that lead to particulate formation, e.g., the radical-product channels of recombination reactions of resonance-stabilized radicals that drive the radical chain-reaction mechanism for soot inception. We will experimentally investigate the response of liquid interfaces under high gas pressures to laser-induced temperature gradients. We plan investigations of reactive interactions of the gas-phase with solid carbonaceous and liquid organic surfaces (complementing catalytic surface investigations in "Imaging the Near-Surface Gas Phase") and eventually extend such studies to the gas phase near electrochemical three-phase boundaries.

References

- (1) Allamandola, L. J.; Tielens, A. G. G. M.; Barker, J. R. Polycyclic Aromatic Hydrocarbons and the Unidentified Infrared Emission Bands-Auto Exhaust Along the Milky Way. *Astrophys. J.* **1985**, *290*, L25-L28.
- (2) Bond, T. C. et al., Bounding the Role of Black Carbon in the Climate System: A Scientific Assessment. *J. Geophys. Res.* **2013**, *118*, 5380-5552.
- (3) WHO 7 Million Premature Deaths Annually Linked to Air Pollution. <http://www.who.int/mediacentre/news/releases/2014/air-pollution/en/>.
- (4) Michelsen, H. A. Probing Soot Formation, Chemical and Physical Evolution, and Oxidation: A Review of *in Situ* Diagnostic Techniques and Needs. *Proc. Combust. Inst.* **2017**, *36*, 717-735.
- (5) Wang, H. Formation of Nascent Soot and Other Condensed-Phase Materials in Flames. *Proc. Combust. Inst.* **2011**, *33*, 41-67.
- (6) Johansson, K. O.; Head-Gordon, M. P.; Schrader, P. E.; Wilson, K. R.; Michelsen, H. A. Resonance-Stabilized Hydrocarbon-Radical Chain Reactions May Explain Soot Inception and Growth. *Science*. **2018**, *36*, 997-1000.
- (7) Dahms, R. N. Understanding the Breakdown of Classic Two-Phase Theory and Spray Atomization at Engine-Relevant Conditions. *Phys. Fluids*. **2016**, *28*, 042108.
- (8) Dahms, R. N.; Oefelein, J. C. Liquid Jet Breakup Regimes at Supercritical Pressures. *Combust. Flame*. **2015**, *162*, 3648-3657.
- (9) Xiao, G.; Luo, K. H.; Ma, X.; Shuai, S. Liquid-Fuel Evaporation Under Supercritical Conditions. *Commun. Comput. Phys.* **2018**, *23*, 1241-1262.

IV. Published journal articles supported by this project 2017-2019

1. Q. Wang, P. Elvati, D. Kim, K. O. Johansson, P. E. Schrader, H. A. Michelsen, and A. Violi, "Spatial dependence of polycyclic aromatic compound growth in counterflow flames", *Carbon*, in press (2019).
2. K. O. Johansson, M. P. Head-Gordon, P. E. Schrader, K. R. Wilson, and H. A. Michelsen, "Resonance-stabilized hydrocarbon-radical chain reactions may explain soot inception and growth", *Science* **361**, 997-1000 (2018).
3. M. F. Campbell, P. E. Schrader, A. L. Catalano, K. O. Johansson, G. A. Bohlin, N. K. Richards-Henderson, C. J. Kliewer, and H. A. Michelsen, "A small porous-plug burner for studies of combustion chemistry and soot formation", *Rev. Sci. Instrum.* **88**, 125106 (2017).
4. K. O. Johansson, F. El Gabaly, P. E. Schrader, M. F. Campbell, and H. A. Michelsen, "Evolution of maturity levels of particle surface and bulk during soot growth and oxidation in a flame", *Aerosol Sci. Technol.* **51**, 1333-1344 (2017).
5. K. O. Johansson, M. F. Campbell, P. Elvati, P. E. Schrader, J. Zádor, N. K. Richards-Henderson, K. R. Wilson, A. Violi, and H. A. Michelsen, "Photoionization efficiencies of five polycyclic aromatic hydrocarbons", *J. Phys. Chem. A* **121**, 4447-4454 (2017).
6. K. O. Johansson, J. Zádor, P. Elvati, M. F. Campbell, P. E. Schrader, N. K. Richards-Henderson, K. R. Wilson, A. Violi, and H. A. Michelsen, "Critical assessment of photoionization efficiency measurements for characterization of soot-precursor species", *J. Phys. Chem. A* **121**, 4475-4485 (2017).
7. H. A. Michelsen, "Probing soot formation, chemical and physical evolution, and oxidation: A review of *in situ* diagnostic techniques and needs", *Proc. Combust. Inst.* **36**, 717-735 (2017).
8. K. O. Johansson, T. Dillstrom, P. Elvati, M. F. Campbell, P. E. Schrader, D. M. Popolan-Vaida, N. K. Richards-Henderson, K. R. Wilson, A. Violi, and H. A. Michelsen, "Radical-radical reactions, pyrene nucleation, and incipient soot formation in combustion", *Proc. Combust. Inst.* **36**, 799-806 (2017).
9. R. N. Dahms, G. A. Paczko, S. A. Skeen, and L. M. Pickett, "Understanding the ignition mechanisms of high-pressure spray flames", *Proc. Combust. Inst.* **36**, 2615-2623 (2017).

Dynamics of Combustion Reactions

H. Floyd Davis
Department of Chemistry and Chemical Biology
Cornell University, Ithaca, NY 14853-1301
hfd1@cornell.edu

I. Program Scope:

Bimolecular and unimolecular reactions of gas-phase polyatomic free radicals often involve multiple reaction intermediates and transition states, leading to competing product channels. We are carrying out experimental studies of these reactions using a crossed molecular beams apparatus. Experiments involve measuring product branching ratios as well as the product kinetic energy and angular distributions. The major goal of these experimental studies is to gain insight into the topography of the relevant ground and excited electronic state reactive potential energy surfaces controlling reactions. Unimolecular studies are focusing on electronic and C-H vibrational overtone excitation of hydrocarbon free radicals. Bimolecular studies include oxidation reactions of hydrocarbon free radicals with O₂, and reactions of OH with alkenes.

II. Recent Progress:

Our DOE-supported research employs a rotatable source crossed molecular beams apparatus that originally utilized synchrotron radiation at LBNL for product photoionization detection. This apparatus has been combined with a windowless VUV beamline in the 8.8-11.9 eV range at Cornell employing tabletop pulsed lasers.^{1,2} High intensity pulsed tabletop VUV light sources provide several advantages^{1,2} over quasi-continuous synchrotron radiation in experiments using pulsed radical beams.

Most of the development and testing of our VUV light source, and the development and characterization of pulsed hydrocarbon free radical sources, have involved studies of the UV photodissociation dynamics of alkyl halide molecules⁴ including 1-iodopropane, 2-iodopropane, t-butyl iodide, and more recently, several other molecules as described below. We found that HI elimination plays an important role in secondary and tertiary iodoalkane photochemistry.⁴ Also, a sharp increase in the degree of nonadiabatic behavior, as evidenced by the I(²P_{3/2}) : I(²P_{1/2}) branching ratios, was observed with increasing hydrocarbon branching.

While VUV photoionization detection has many merits, the determination of product branching ratios can be difficult because photoionization cross sections are often not well-known for product species, especially radicals. Electron impact ionization, while less sensitive than photoionization, provides a valuable complementary detection method because electron impact ionization cross sections (absolute or relative) are either known, measurable, or can be calculated empirically. We have recently devoted considerable effort to optimizing the detection efficiency and sensitivity using electron impact ionization employing electrons at energies much lower than the 200 eV used historically in crossed beams machines of this type. For example, ionization at 20 eV and 30 eV allows for considerable reduction in background levels, primarily due to reduction of dissociative ionization. This makes it possible to obtain TOF spectra from photodissociation experiments with much higher signal to noise ratios than has been possible in the past. Our ability to obtain product TOF spectra using two independent “universal” detection methods, photoionization and electron impact ionization, both with very high signal to noise ratios, is of critical importance to successfully carrying out studies of the

unimolecular and bimolecular reactions of polyatomic free radicals, which typically produce small signal levels subject to significant interference from multiple sources.

We have carried out a careful analysis and comparison of large sets of data pertaining to the photodissociation of stable molecules, using both electron impact and photoionization detection in back to back experiments.⁴ In most cases, both counterfragments for each channel were detected. These data revealed a number of subtle differences for the complementary detection methods. In some cases, these provided new insight into the dependence of polyatomic radical photoionization cross sections on the level of vibrational excitation. In other cases, our analysis led to a better knowledge of the apparatus function and even the inherent velocity distributions of our pulsed molecular beams. For example, analysis of TOF spectra recorded using different pulsed valve to laser delays revealed that due to the presence of a significant velocity “chirp”, the instantaneous speed ratios of helium-seeded molecular beams ($\approx v/\Delta v$) are significantly higher than is derived from conventional analysis using a slotted chopper wheel. These efforts are important so we can properly analyze angular and velocity distributions for less well-defined systems, including the bimolecular and unimolecular reactions described below.

Flash pyrolysis of azo compounds ($R-N=N-R$, where $R = CH_3, C_2H_5, 1-C_3H_7$ and $2-C_3H_7$) using a short (~ 1 cm) heated SiC tube ($1000-1300^\circ C$) attached to a pulsed valve nozzle provides intense beams of alkyl radicals. Using this alkyl radical source, we have carried out studies of the UV photodissociation of 1- and 2-propyl radicals (C_3H_7).⁵ Previous studies by others showed that H atom elimination forming propene plays an important role in the UV photodissociation dynamics. Fission of a C-H bond can occur from either C_3H_7 isomer via a small barrier in excess of the bond dissociation energy on the ground electronic surface. However, C-C bond fission producing $CH_3 + C_2H_4$ is actually the thermodynamically more favorable channel, but has not been detected in previous experiments. These C-C fission channels also possess barriers along the reaction pathways, even in the case of 1- C_3H_7 , where C-C bond fission can produce methyl radicals + ethylene. Production of CH_3 directly from C-C bond fission in the 2-propyl radical produces the high-energy singlet ethylidene isomer, ($CHCH_3$) lying ~ 70 kcal/mol above ground state singlet ethylene.

We have observed both C-H and C-C bond fission from 248 nm photolysis of both 1- and 2- propyl radicals. Similarities that we observe in the dynamics of both isomers *could* be taken as evidence that isomerization of the 1-propyl radical to the 2-propyl form occurs after excitation and prior to C-C bond fission. However, an alternative possibility is that isomerization of the 1-propyl radical to the more stable 2-propyl form occurs *in our pyrolysis source*, prior to supersonic expansion of radicals from the nozzle. To clarify this issue, we are carrying out studies of the photoionization of the two isomers near their photoionization thresholds (7.4 eV and 8.1 eV for 2-propyl and 1-propyl, respectively). In addition, parallel studies of the photodissociation of 1- and 2- propyl radicals produced by *photolytic* (rather than *pyrolytic*) sources are desirable, since there is reason to expect that photolytic sources of alkyl radicals will not involve significant isomerization. However, the primary photochemistries of most photolytic precursors have not been fully elucidated to date. Therefore, we have carried out additional photodissociation experiments in order to characterize the production of hydrocarbon free radicals using a number of precursors at various wavelengths (denoted in brackets). These include iodoalkanes (266 nm), nitroalkanes (213 nm), bromoalkanes (213 nm), alkyl nitrites (266 nm), and azoalkanes (355 nm). We have found that while iodoalkane photodissociation leads to the most intense beams of hydrocarbon radicals, due to the relatively large absorption cross section for alkyl iodides at 248 nm, undissociated parent molecules lead to large

background signals that interfere with the analysis. Nitroalkanes have been used by several groups as photolytic sources of alkyl radicals. However, we have found that UV photolysis of nitroalkanes leads to a number of competing processes, with HONO + alkene channels playing an important role in some cases. We expect these studies will form the basis for a paper focusing on nitroalkane UV photodissociation, which has been studied previously but remains poorly understood. Bromoalkanes absorb strongly only at wavelengths below 220 nm. While undissociated parent molecules will not produce interfering signals at 248 nm, in the past 193 nm excimer lasers have been required for efficient radical generation because no other pulsed light sources have been able to provide intense (>10 mJ/pulse) pulsed radiation at wavelengths shorter than 220 nm. However, the recent availability of a new and highly efficient nonlinear crystal, CLBO, opens up the opportunity for production of intense 213 nm light via 5th harmonic generation (266 + 1064 nm) of the Nd:YAG laser. This provides two advantages. First, solid state Nd:YAG lasers are far more stable, and have much lower operating costs as compared to excimer lasers. More importantly, our apparatus employs a rotatable source configuration, with the photolysis laser used to produce free radical beams propagated into a movable source chamber. This is most easily accomplished by propagating the laser along the axis of rotation of the source and then periscoping into the source region using a pair of mirrors. This is easily achieved using a Nd:YAG laser, which has a circular laser beam and high beam spatial quality. On the other hand, excimer laser beams, which have a rectangular shape and poor spatial beam quality, are not easily propagated into a non-stationary source.

III. Future Plans:

a) Oxidation Reactions of Hydrocarbon Radicals:

The reactions of alkyl radicals with molecular oxygen are important in combustion chemistry. The $C_2H_5 + O_2$ system is the simplest prototype, for C_2H_5 is the smallest saturated hydrocarbon radical in which formation of HO_2 and OH are both thermodynamically accessible elementary channels. The $C_3H_7 + O_2$ system is the simplest case in which the reactivity of two different hydrocarbon isomers can be compared directly. The propyl radicals have been produced primarily by 266 nm photodissociation of 1- and 2- propyl iodide or by pyrolysis of the appropriate azoalkanes synthesized via a 3-step procedure. One issue that was encountered is the presence of aldehyde or ketone impurities in the azoalkane samples, which interfere with the observation of the primary product channel leading to OH production. We have therefore developed methods for purification of the azoalkane samples using chromatography.

b) Reactions of OH Radicals with Alkenes

The reactions of hydroxyl radicals (OH) with alkenes are of considerable interest in combustion chemistry. In addition to the H atom elimination channels forming enols (compounds having adjacent $C=C$ and OH moieties), rearrangement of the initially-formed intermediates can lead to production of several competing product channels. Because of its large absorption cross section, 193 nm photolysis of nitric acid was used for OH production in all of our previous reactive scattering studies. However, the HONO + O channel is actually dominant, with ground (3P_1) and singlet (1D_2) excited oxygen atom production, leading to possible interfering reactions. Although 248 nm photolysis of HNO_3 yields exclusively $OH + NO_2$, the absorption cross section is too small ($2 \times 10^{-20} \text{ cm}^2$) to make this a viable radical source. However, since the HNO_3 absorption is significant ($\sigma = 7 \times 10^{-19} \text{ cm}^2$) at 213 nm, the 5th harmonic of the Nd:YAG laser can be used to photolyze nitric acid to produce OH . Since HNO_3

photodissociation at 213 nm has not been characterized previously we are now undertaking studies of its primary photochemistry at this wavelength.

c) Unimolecular reactions of hydrocarbon radicals on their ground electronic state surfaces:

We plan to study the unimolecular decomposition of vibrationally-excited ground electronic state hydrocarbon radicals induced by C-H vibrational overtone excitation. Our first experiments will focus on the 1- and 2- propyl radicals. We have considerable experience generating these species and both C-H and C-C bond fission is expected to occur at low energies on the ground electronic state surfaces. Our first experiments will involve pumping the fourth overtone ($v = 5$) of the C-H stretching region near 750 nm. Since H atoms are produced by C-H bond fission, after mapping out the dynamics by monitoring the heavy C_3H_6 fragment (as well as studying C-C bond fission producing $CH_3 + C_2H_4$), we can move our existing Rydberg tagging TOF detector to our universal crossed beams machine to do Rydberg tagging TOF measurements on the H (or D atom) channels.

Publications Since 2013 Citing DOE Support:

1. D.R. Albert and H.F. Davis “Experimental Studies of Bimolecular Reaction Dynamics Using Pulsed Tabletop VUV Photoionization Detection”, invited perspective article, *Phys. Chem. Chem. Phys.* 15, 14566-14580 (2013).
2. D.R. Albert, D.L. Proctor, and H.F. Davis, “High-Intensity Coherent Vacuum Ultraviolet Source Using Unfocussed Commercial Dye Lasers”, *Rev. Sci. Instrum.* 84, 063104 (2013).
3. M.A. Todt, D.R. Albert, H.F. Davis, “High Intensity VUV and XUV production by noncollinear mixing in laser vaporized Media”, *Rev. Sci. Instrum.* 87, 063106 (2016).
4. M. A. Todt, S. Datta, A. Rose, K. Leung, and H. F. Davis, “HI Elimination in the 266 nm Photodissociation of Primary, Secondary and Tertiary Alkyl Iodides”, *J. Phys. Chem. Lett.*, submitted.
5. S. Datta, M.A. Todt and H.F. Davis, “Photodissociation Dynamics of 1- and 2- propyl (C_3H_7) Radicals at 248 nm: the $CH_3 + C_2H_4$ channels”, in preparation.

Exploration of chemical-kinetic mechanisms, chemical reactivity, and thermochemistry using novel numerical analysis

Michael J. Davis

Chemical Sciences and Engineering Division
Argonne National Laboratory
Lemont, IL 60439
Email: davis@tcg.anl.gov

The work explores chemically reactive systems using novel numerical analyses. One focus of the work is exploration and theoretical validation of chemical-kinetic mechanisms, using global sensitivity analysis. An important aspect of this part of the work is the use of state of the art methods in numerical analysis, statistics, and signal processing for making global sensitivity analysis (GSA) efficient for large-scale chemical mechanisms. An effort on reaction pathway analysis has been underway. The global sensitivity and reaction pathway analyses are used to pinpoint chemical reactions that need to be studied accurately to improve the accuracy of chemical mechanisms. The expertise developed in that work has led to the implementation of these techniques for studying problems in chemical reactivity, including isolated chemical kinetics and dynamics. Key features of this focus are regression analysis, optimal sampling, power transformations, and subset selection. There is a major effort underway for using these techniques for fitting potential energy surfaces, where it is difficult to scale existing methods to larger molecular systems. Another effort underway is the application of computational optimal transport to molecular spectroscopy and dynamics.

Recent Progress

Progress has continued in three areas in the past year, and a fourth was added. The first is the application of sparse regression to select the most sensitive reactions in engine simulations, a collaboration between our group (Davis, Sivaramakrishnan *et al*) and the Engines and Emission group at Argonne (Magnotti, Som, *et al*), that led to a paper published last year. The second has been the application of a new version of reaction pathway analysis to the low-temperature ignition of propane in collaboration with Colorado (Bai and Skodje) and our group (Sivaramakrishnan and Davis), which led to a publication in 2019. The third and main focus of the progress in the last year is the development of optimal sampling strategies for fitting potential energy surfaces with basis functions, a collaboration with Jasper in our group, which just led to a published paper. A fourth area is the application of optimal transport to molecular spectroscopy.

The engine simulations modeled the ignition of an n-heptane/methylbutanoate mixture using a chemical model with 914 reactions. A sparse version of GSA was used to determine the 13 reactions for which ignition was most sensitive. In the last year we finished the analysis of the algorithm and studied in more detail the chemistry that occurs in the engine cylinder guided by the results of the global sensitivity analysis in the engine cylinder .

The sparse version of sensitivity analysis is based on linear regression with a penalty

$$\text{term: } E(\mathbf{c}) = \frac{1}{2} \sum_{k=1}^M \left(t_k - \sum_{i=1}^L c_i g_j(\mathbf{u}_k) \right)^2 + \lambda \sum_{j=1}^L |c_j| \quad (1)$$

The first term in this expression is the ordinary least squares (OLS) error and the second term is a penalty term. In Eq. (1), M is the number of points used in the fit and for OLS, M must be greater than the number of terms in the expansion (L), which is generally several thousand, as there are 914 reactions and the basis functions, g_j , in Eq (1), are polynomials. For global sensitivity analysis M is equal to the number of engine simulations, each of which generally takes several processor weeks to complete, and without the penalty term would require several thousand simulations. However, with the penalty term, minimizing Eq. (1) requires many less simulations, as the penalty term zeros out most of the potential coefficients. The 13 reactions that were

identified by GSA required 800 simulations rather than an estimate of more than 10,000 without the penalty term. The table below indicates the number of terms that were used in the rightmost column out of a potential of several thousand in the second column. The order of the polynomial is listed in the first column. In all calculations we used the diagonal terms in the expansion and 4422 cross-terms. So, for example, the $k = 2$ case includes 914 linear terms, 914 diagonal quadratic terms, and 4422 cross-terms ($6250 = 914+914+4422$). It is clear from the table that the sparse regression severely reduces the number of terms in the expansion, reducing the number of engine simulations necessary for accurate sensitivity results.

Sparsity Values for Engine Sparse GSA

k	Maximum Terms	Terms
2	6250	234
3	16,008	295
4	30,188	331

The global sensitivity analysis identified the 13 reactions for which ignition in the engine cylinder was most sensitive. By comparing the results in the engine cylinder with constant pressure simulations we were able to determine under which conditions the most sensitive reactions occurred in the engine cylinder. This led to a study of the chemistry as it occurred in the engine simulation. Figure 1 summarizes results for the most sensitive reaction, $2\text{-C}_7\text{H}_{15}\text{O}_2 (\text{RO}_2) = \text{C}_7\text{H}_{14}\text{OOH}2\text{-4} (\text{QOOH})$. The two curves in each panel show the equivalence ratio, ϕ , vs. temperature with the curves color-coded for the mass fraction of the QOOH species (see color bar on the side). The curves describe the chemistry as the distance from the center of the spray is increase in 0.35 mm increments and the headings of the two panels indicate the distance from the fuel spray injector. The two curves in each plot are labeled with a time to ignition and the symbols on the plot have the following meaning: the large square is the initial point taken at 0.35 mm from the center of

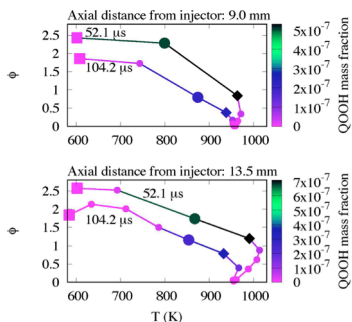


Fig. 1. See the text.

of the fuel spray, the large dot indicates the location of the maximum of the RO_2 species and the large diamond the location of the maximum of the QOOH species. Note that the RO_2 species always peaks before the QOOH. The most likely reason for this behavior is that the RO_2 and QOOH are in quasi-equilibrium or are part of a quasi-equilibrium among several species in the RO_2/QOOH cycle. The new reaction pathway approach allows for the enumeration and the calculation of the relative weight of all pathways that contribute to the formation of a species, through a pathway summation. For ignition, a key species is OH and Fig. 2 shows how the formation of OH can be broken down into a series of pathways for the low-temperature ignition of propane. The primary cycle for formation of OH is the typical RO_2/QOOH cycle. The top panel in Fig. 2 shows with a solid red line the fraction of OH generated via the primary cycle as a function of time on the way to final ignition which occurs at $t = 0.77$ s (note that this is a two-stage ignition process, as indicated by the inflection points at $t = 0.55$ s). The dashed line in the top panel shows the fraction of OH formed by all other cycles, labeled there as “secondary”. The top panel of Fig. 2 indicates that even before the first ignition time the secondary cycles account for more of the formation of OH than does the primary cycle. The bottom panel shows the effect of most of the secondary cycles, which are listed in the legend on the left half of the panel.

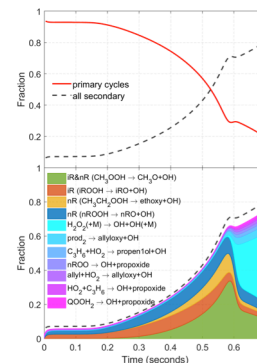


Fig. 2. The top panel compares the role of the primary cycle and the secondary cycles. The bottom panel enumerates the secondary cycles

We use a multi-objective approach to fitting potential energy surfaces. The fitting is a trade-off among these three conflicting objectives: 1) the accuracy of the fit, 2) the computational cost of making the fit, and 3) the cost of the evaluation of single points from the fit. The first paper on fitting of potential energy surfaces just appeared online. Among the key conclusions of that paper was the importance of good sampling strategies for fitting the potential surfaces efficiently. As with most functional forms of potential surfaces used in trajectory calculations, these surfaces were fit with coordinates defined by internuclear distances. However, as is commonly done, the points at which quantum chemistry calculations were performed and from which the fit is generated, were chosen based on the sampling in physical coordinates, specifically polar coordinates in the published paper. As noted in that paper such sampling gives poor coverage in the space of internuclear distances and as noted in our subsequent work described here, is even less likely to provide good coverage for the basis functions used in the fitting, which are products of exponentials. Several successful steps were undertaken to overcome this difficulty in the published manuscript, but these steps tend to be less effective under the more complex systems studied in that paper, such as the intermolecular energy transfer properties of H₂O with CH₃OH.

The basis set expansion of a potential surface uses linear regression:

$$\hat{y} = Hy, \quad H = X(X^T X)^{-1} X^T, \quad y_i - \hat{y}_i^{(-i)} = \frac{y_i - \hat{y}_i}{1 - h_{ii}}, \quad \langle h_{ii} \rangle = \frac{p}{n} \quad (2a)$$

The first expression in Eq. (2a) describes how the fitted value of the potential, \hat{y} , is related to the calculated value of the function, y , through the matrix H , commonly called the hat matrix, defined in the second term. The matrix X is defined by the basis functions:

$$X_{jk} = \phi_k(\mathbf{r}_j), \quad \hat{y} = \sum_{k=1}^n c_k \phi_k(\mathbf{r}_j), \quad \phi(\mathbf{r}_j) = e^{-m_1 r_1} e^{-m_2 r_2} e^{-m_3 r_3} \dots \quad (2b)$$

The H matrix does not depend on y and is set by the basis functions and the sampling. The final two expressions in Eq. (2a) demonstrate how the basis functions and sampling can affect the efficiency of the expansion. The first of these expressions describes the relationship between the predictive error (left hand side) and the fitting error (the numerator of the right hand side). The term $\hat{y}_i^{(-i)}$ describes the prediction of y_i from a fit that included all points except for the i th. Because of their importance, the diagonal elements of H , h_{kk} , are referred to as “leverages”. Elements of the Hat matrix are between 0.0 and 1.0, with all columns and rows summing to 1.0. The predictive expression in Eq. (2a) demonstrates that values of H that are nearly 1.0 should be avoided as they can lead to large prediction errors and thus can lead to overfitting. In fact, it is generally desirable to have values of h_{kk} that are never larger than approximately twice the average, shown in the last expression in Eq. (2a), where p is the number of terms in the expansion and n is the number of fitting points. Also, note that Eq. (2b) demonstrates that the elements of X depend on the basis set, which is chosen by us to be a direct product, so that difficulties of sampling coverage is an interplay between the sampling plan and the basis set.

Typical sampling starts in physical space and then converts to distances which are inserted into the basis functions in Eq. (2b), and generally have too many high leverages. We developed a straightforward algorithm that samples nearly uniformly in the one coordinate basis functions that make up the direct product functions in Eq. (2b), e^{-r_j} , etc. However, the basis set includes direct product of terms with higher powers (e.g. $e^{-2r_1} e^{-r_2} \dots$), so the “basis sampling” may still lack good coverage for small to medium sized samples, that will help to achieve the first two objectives noted above, accuracy and cost of fit. To overcome these difficulties, we implemented a two-stage approach to sampling, with the first stage being the basis sampling and the second

stage which chooses subsamples (the “optimal design”) that minimize one of these two criteria or

$$\text{the product of the two: } f_V = \frac{1}{n} \text{tr}[\mathbf{X}(\mathbf{X}_D^T \mathbf{X}_D)^{-1} \mathbf{X}^T], f_G = \max \text{diag} [\mathbf{X}(\mathbf{X}_D^T \mathbf{X}_D)^{-1} \mathbf{X}^T] \quad (3)$$

The matrix \mathbf{X}_D , the design space, describes the subsample and is calculated to minimize one of the criteria or the product of the two. The first criterion in Eq. (3) chooses \mathbf{X}_D to minimize the average of the predictive variance for the full space, \mathbf{X} the basis sampling, and the second

criterion chooses a design \mathbf{X}_D that minimizes the maximum predictive variance in the full space.

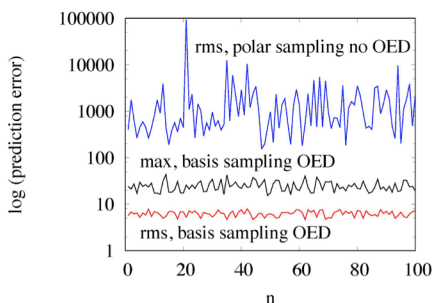


Fig. 3. The results of ordinary polar sampling are compared to basis set sampling with and without OED.

Figure 3 shows how two-stage sampling decreases the prediction error. The results in this figure are for He + HO₂, with HO₂ fixed at its equilibrium. The basis set is shown in Eq. (2b), with the sum of the m’s taken to be 3 or less, giving 20 basis functions. Ground truth is a previously made nonlinear fit. Only 30 points were used for the fit, based on minimizing the product of the two criteria in Eq. (3). The full basis sampling used 1500 points. This means that the fitting was done with 30 points and predictions were made with 1470 points.

Figure 3 shows 100 test cases and shows that the basis set sampling followed by OED is effective. The error for polar sampling is much higher than the maximum errors and rms errors for basis/OED sampling.

Future Plans

The new sampling procedures will be applied to several of the five potentials studied in the recently published paper. Subset selection will be used to prune the large basis sets necessary for fitting larger systems. Further studies of propane will be done with the pathway analysis and we plan on studying reaction pathways for catalysis. We will investigate several tools in computational optimal transport that should be useful in studies of chemical reactivity and quantum chemistry, for example, displacement interpolation and Wasserstein barycenters, which can be used for mixing quantum densities. We began a project on comparing molecular spectra using optimal transport. Two spectra are compared using the optimal transport distance (OTD), which uses information about line positions and intensities to compare spectra. Because optimal transport of spectra implicitly weights uncertainties in line positions and intensities, we will investigate how typical uncertainties in these quantities affect the OTD.

Publications

1. B. Narayanan, A. Kinaci, F. G. Sen, M. J. Davis, S. K. Gray, M. K. Y. Chan, and S. K. R. S. Sankaranarayanan, “Describing the Diverse Geometries of Gold from Nanoclusters to Bulk—A First-Principles-Based Hybrid Bond-Order Potential”, *J. Phys. Chem. C* **120**, 13787-13800 (2016).
2. B. Narayanan, K. Sasikumar, Z.-G. Mei, A. Kinaci, F. G. Sen, M. J. Davis, S. K. Gray, M. Chan, and S. K. Gray, M. K. Y. Chan, and S. K. R. S. Sankaranarayanan, “Development of a Modified Embedded Atom Force Field for Zirconium Nitride Using Multi-Objective Evolutionary Optimization”, *J. Phys. Chem. C* **120**, 17475–17483 (2016).
3. A. Kinaci, B. Narayanan, F. G. Sen, M. J. Davis, S. K. Gray, M. Chan, and S. K. Gray, M. K. Y. Chan, and S. K. R. S. Sankaranarayanan, “Unraveling the Planar-Globular Transition in Gold Nanoclusters through Evolutionary Search”, *Scientific Reports* **6**, online in November, 2016.
4. M. J. Davis, W. Liu, and R. Sivaramakrishnan, “Global Sensitivity Analysis with Small Sample Sizes: Ordinary Least Squares Approach”, *J. Phys. Chem. A* **121**, 553-570 (2017).
5. G. M. Magnotti, Z. Wang, W. Liu, R. Sivaramakrishnan, S. Som, and M. J. Davis, “Sparsity Facilitates Chemical Reaction Selection for Engine Simulations”, *J. Phys. Chem. A* **122**, 7227-7237 (2018).
6. S. Bai, R. Sivaramakrishnan, M. J. Davis, and R. T. Skodje, “A Chemical Pathway Perspective on the Kinetics of Low-Temperature Ignition of Propane”, *Combustion and Flame* **202**, 154-178 (2019).
7. A. W. Jasper and M. J. Davis, “Parameterization Strategies for Intermolecular Potentials for Trajectory-Based Collision Parameters”, *J. Phys. Chem. A*, in press.

Electronic structure methods and protocols with application to dynamics, kinetics and thermochemistry

Richard Dawes, dawesr@mst.edu

Missouri University of Science and Technology
400 W. 11th street, Rolla, MO 65409

I. Program Scope:

(NOTE – this project is supported jointly through the CTC and GPCP programs and this report will be submitted to both programs)

Hydrocarbon combustion involves the reaction dynamics of a tremendous number of species beginning with many-component fuel mixtures and proceeding via a complex system of intermediates to form primary and secondary products. Combustion conditions corresponding to new advanced engines and/or alternative fuels rely increasingly on autoignition and low-temperature-combustion chemistry. In these regimes various transient radical species such as HO₂, ROO·, ·QOOH, HCO, NO₂, HOCO, and Criegee intermediates play important roles in determining the detailed as well as more general dynamics. A clear understanding and accurate representation of these processes is needed for effective modeling. Given the difficulties associated with making reliable experimental measurements of these systems, computation can play an important role in developing these energy technologies.

Accurate calculations have their own challenges since even within the simplest dynamical approximations such as transition state theory, the rates depend exponentially on critical barrier heights and these may be sensitive to the level of quantum chemistry. Moreover, it is well-known that in many cases it is necessary to go beyond statistical theories and consider the dynamics. Quantum tunneling, resonances, radiative transitions, and non-adiabatic effects governed by spin-orbit or derivative coupling can be determining factors in those dynamics.

Building upon progress made during a period of prior support through the *DOE Early Career Program*, this project combines developments in the areas of potential energy surface (PES) fitting and multistate multireference quantum chemistry to allow spectroscopically and dynamically/kinetically accurate investigations of key molecular systems (such as those mentioned above), many of which are radicals with strong multireference character and have the possibility of multiple electronic states contributing to the observed dynamics. Figure 1 illustrates the predictive level of insight that is achievable via these approaches.¹

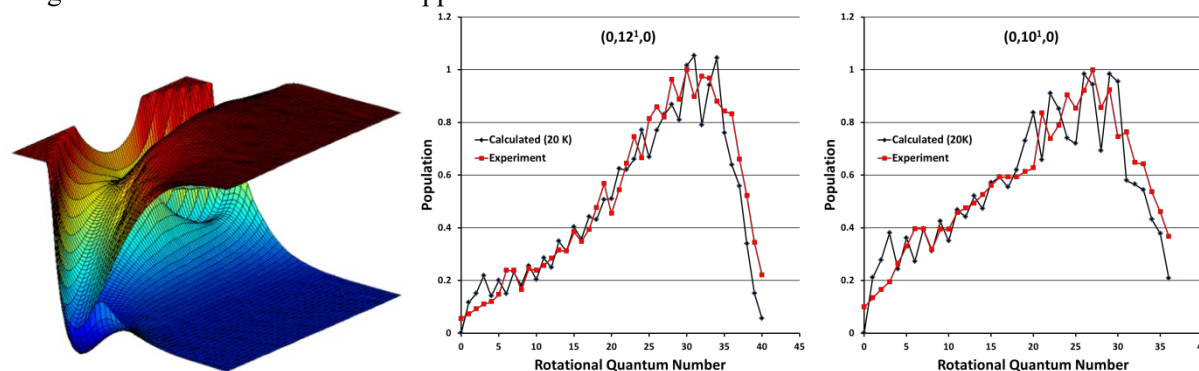


Figure 1: (left) Surface plot of the fitted adiabatic *X* and *A* state PESs for HCO in Jacobi coordinates as a function of $R_{\text{H-CO}}$ and theta. (middle) Calculated and recorded rotational distributions of CO product, with thermal averaging over initial rotational states based on the estimated 20 K beam temperature. (right) same as middle panel, but with different excitation.

An ongoing area of investigation is to develop general strategies for robustly convergent electronic structure theory for global multichannel reactive surfaces including diabaticization of energy and other relevant surfaces such as dipole transition. Combining advances in *ab initio* methods with automated interpolative PES fitting allows the construction of high-quality PESs (incorporating thousands of high level data) to be done rapidly through parallel

processing on high-performance computing (HPC) clusters.

In addition, new methods and approaches to electronic structure theory will be developed and tested through applications. This project will explore limitations in traditional multireference calculations (*e.g.*, MRCI) such as those imposed by internal contraction, lack of high-order correlation treatment and poor scaling. Methods such as DMRG-based extended active-space CASSCF and various Quantum Monte Carlo (QMC) methods will be applied (including VMC/DMC and FCIQMC). Insight into the relative significance of different orbital spaces and the robustness of application of these approaches on leadership class computing architectures will be gained. A computational thermochemistry project recently conducted through support by the DOE SCGSR student fellowship program and collaboration with Branko Ruscic (Argonne National Labs) will be extended. A workflow framework that allows community driven expansion of the ATcT thermochemical database will be further developed. Synergy with other components of this research program such as automated PES fitting and multireference quantum chemistry will be used to address challenges encountered by the standard approaches to computational thermochemistry (those being single-reference quantum chemistry and perturbative treatments of the anharmonic vibrational energy, which break down for some cases of electronic structure or floppy strongly coupled vibrational modes).

II. Recent Progress (NOTE – the start date for this project was March 1, 2019, so only preliminary results have been obtained at the time of writing this report (April 2019)).

Perhaps the most significant progress in the first 6 weeks of this project has been the implementation of automated thermochemical scripts whose development began last summer in collaboration with Branko Ruscic (ANL) and David Bross (ANL).

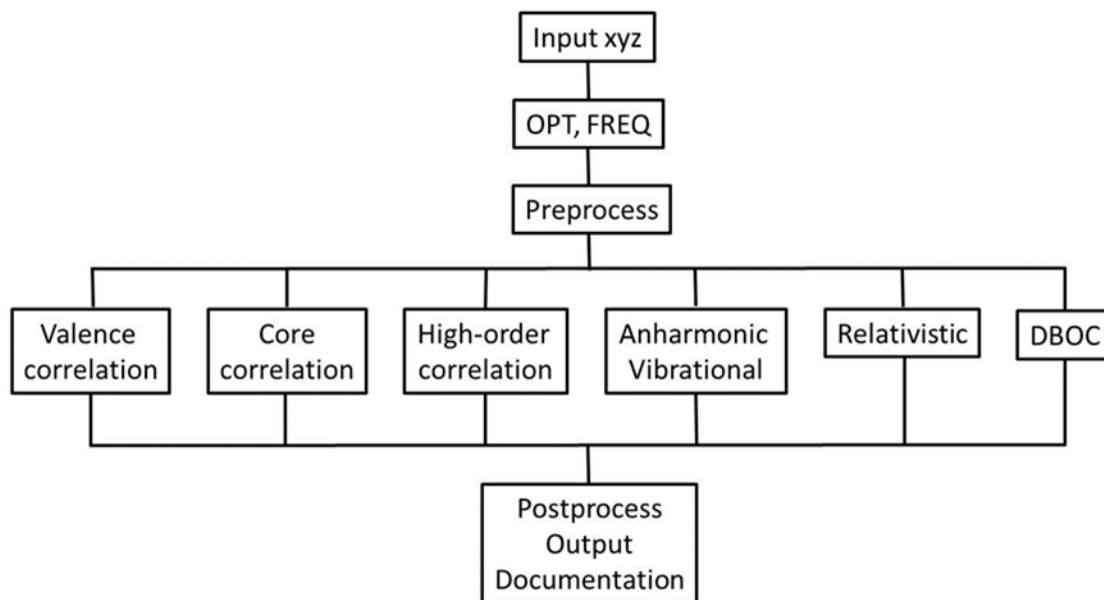


Figure 2: Flowchart of the automated thermochemical protocol.

The Python scripting to distribute and execute a series of high-level quantum chemistry calculations across multiple resources has now been extensively tested on roughly two hundred small to medium sized molecular systems by multiple users (including undergraduate students) and is proving to be very robust, reliable and efficient. Two related publications in preparation are already close to submission. Graduate student Bradley Welch supported on this project will defend his thesis in May 2019. Bradley will continue related work as a postdoc with Angela Wilson (MSU).

Grant Numbers and Grant Titles

Grant No. DE-SC0019740; Electronic structure methods and protocols with application to dynamics, kinetics and thermochemistry

Grant No. DE-SC0010616; Multiple coupled potential energy surfaces with application to combustion

Postdoc(s): Steve A. Ndengué; Ernesto Quintas Sánchez

Student(s): Bradley K. Welch; Sangeeta Sur

Up to Ten Publications Acknowledging these Grants in the last 3-4 years

¹ Shanyu Han, Xianfeng Zheng, Steve Ndengué, Yu Song, Richard Dawes, Daiqian Xie, Jingsong Zhang, and Hua Guo. "Dynamical interference in the vibronic bond breaking reaction of HCO." *Science advances* **5**, no. 1 (2019): eaau0582.

² R. Dawes and E. Quintas-Sánchez, The Construction Of Ab Initio-Based Potential Energy Surfaces, *Rev. Comput. Chem* **31**, 199-264 (2018).

³ S. Ndengué, R. Dawes, F. Gatti, H. Guo, The influence of Renner-Teller coupling between electronic states on inelastic scattering, *J. Phys. Chem. A*, **122**, 6381 (2018).

⁴ Silver Nyambo, Brandon Uhler, Lloyd Muzangwa, Maxim Ivanov, Bradley K. Welch, Richard Dawes, Scott A Reid, Reactive Pathways in the bromobenzene-ammonia dimer cation radical: evidence for a roaming halogen radical, *J. Mol. Struct.*, 1172, **113** (2018).

⁵ Andrew Powell, N.S. Dattani, RFK Spada, FBC Machado, H. Lischka, R. Dawes, Investigation of the ozone formation pathway: Comparisons of FCIQMC and fixed node DMC with icMRCI and ucMRCI. *J. Chem. Phys.* **147**, 094306 (2017).

⁶ Moumita Majumder, Steve Ndengue, Richard Dawes, new view (with author profile): automated construction of potential energy surfaces, *Molecular Physics* **114**, 1 (2016).

⁷ Richard Dawes and Steve Ndengué, Single- and multireference electronic structure calculations for constructing potential energy surfaces, *Int. Rev. Phys. Chem.* **35**, 441, (2016).

⁸ Phalgun Lolur, Richard Dawes, Michael Heaven, Theoretical study of vibronic perturbations in Magnesium Carbide, *Molecular Physics* **114**, 162 (2016).

⁹ Andrew D. Powell and Richard Dawes, Calculating potential energy curves with fixed-node diffusion Monte Carlo: CO and N₂, *J. Chem. Phys.* **145**, 224308 (2016).

¹⁰ Steve Ndengué, Richard Dawes and Hua Guo, A new set of potential energy surfaces for HCO: Influence of Renner-Teller coupling on the bound and resonance vibrational states. *J. Chem. Phys.* **144**, 244301 (2016).

Theoretical and Experimental Studies of Elementary Hydrocarbon Species and Their Reactions (DE-SC0018412)

Gary E. Douberly and Henry F. Schaefer III

University of Georgia, Center for Computational Quantum Chemistry and Department of Chemistry, 1004 Cedar St., Athens, GA 30602-1546

douberly@uga.edu

Program Scope

The objective of this research is to isolate and stabilize transient intermediates and products of prototype combustion reactions. This will be accomplished by Helium nanodroplet isolation (HENDI) spectroscopy, a novel technique where liquid helium nanodroplets freeze out high energy metastable configurations of a reacting system, permitting infrared spectroscopic characterizations of products and intermediates that result from hydrocarbon radical reactions with molecular oxygen and other small molecules relevant to combustion environments. A major aim of this work is to directly observe the elusive hydroperoxyalkyl radical (QOOH) and its oxygen adducts (O₂QOOH), which are important in low temperature hydrocarbon oxidation chemistry.

Recent Projects

Ethyl + O₂ in Helium Nanodroplets: Infrared Spectroscopy of the Ethylperoxy Radical

Helium-solvated ethylperoxy radicals (CH₃CH₂OO•) are formed *via* the *in situ* reaction between ²A' ethyl radical and ³Σ_g⁻ dioxygen. The reactants are captured sequentially through the droplet pick-up technique. Helium droplets are doped with ethyl radical *via* pyrolysis of di-*tert*-amyl peroxide or *n*-propyl nitrite in an effusive, low-pressure source. An infrared spectrum of ethylperoxy, in the CH stretching region, is recorded with species-selective droplet beam depletion spectroscopy. Spectral assignments are made *via* comparisons to second-order vibrational perturbation theory with resonances (VPT2+K) based on coupled-cluster full quartic force fields. Cubic and quartic force constants, evaluated using a small basis set, are transformed into the normal coordinate system of the higher level quadratic force constants. This transformation procedure eliminates the mismatch between normal modes, which is a source of error whenever normal coordinate force constants from different levels of theory are combined. The spectrum shows signatures of both the *C*₁ *gauche* and *C*_s *trans* rotamers in an approximate 2:1 ratio; this is despite the prediction that the *gauche* rotamer lies 44 cm⁻¹ lower on the zero-Kelvin enthalpic potential surface for torsional interconversion. Helium droplets are 0.4 K at equilibrium; therefore, *in situ* ethylperoxy production is highly non-thermal.

Infrared Spectrum of Fulvenallene and Fulvenallenyl in Helium Droplets

Fulvenallene is the global minimum on the C₇H₆ potential energy surface. Rearrangement of fulvenallene to other C₇H₆ species and dissociation to produce fulvenallenyl radical (C₇H₅) is carried out in a continuous-wave SiC pyrolysis furnace at 1500 K. Prompt pick-up and solvation by helium droplets allows for the acquisition of vibrational spectra of these species in the CH stretching region. Anharmonic frequencies for fulvenallene, fulvenallenyl, and three isomers of ethynylcyclopentadiene are computed *ab initio*; VPT2+K spectral simulations are based on hybrid CCSD(T) force fields with quadratic (cubic and quartic) force constants computed using the ANO1 (ANO0) basis set. The acetylenic CH stretch of the fulvenallenyl radical is a sensitive marker of the extent by which the unpaired electron is delocalized

throughout the conjugated propargyl and cyclopentadienyl subunits. The nature of this electron delocalization is explored with spin density calculations at the ROHF-CCSD(T)/ANO1 level of theory. Atomic partitioning of the spin density allows for a description of the fulvenallenyl radical in terms of two resonance structures: fulvenallenyl is approximately 24% allenic and 76% acetylenic.

tert-Butyl Peroxy Radical: Ground and First Excited State Energetics and Fundamental Frequencies

Alkylperoxy radicals (RO₂) are key intermediates in combustion and atmospheric oxidation processes. As such, reliable detection and monitoring of these radicals can provide a wealth of information about the underlying chemistry. The tert-butyl peroxy radical is the archetypal tertiary peroxy radical, yet its vibrational spectroscopy is largely unexplored. To aid in future experimental investigations, we have performed a high-level theoretical study of the fundamental vibrational frequencies of the ground- and first excited states. A conformer search on both electronic surfaces reveals single minimum-energy structures. We predict an A ²A' ← X ²A'' adiabatic excitation energy of 7738 cm⁻¹ via focal point analysis, approximating the CCSDT(Q)/CBS level of theory. This excitation energy agrees to within 17 cm⁻¹ of the most precise experimental measurement. We compute CCSD(T) fundamental vibrational frequencies via second-order vibrational perturbation theory (VPT2), using a hybrid force field in which the quadratic (cubic/quartic) force constants are evaluated with the ANO1 (ANO0) basis set. Anharmonic resonance polyads are treated with the VPT2+K effective Hamiltonian approach. Among the predicted fundamental frequencies, the ground state O-O stretch, excited state O-O stretch, and excited state C-O-O bend fundamentals are predicted at 1138, 959, and 490 cm⁻¹, respectively. Basis set sensitivity is found to be particularly great for the O-O stretches, similar to what has already been noted in smaller, unbranched peroxy radicals. Exempting these O-O stretches, agreement with the available experimental fundamentals is generally good (± 10 cm⁻¹).

Ongoing Work and Future Plans

Sequential Capture of O(³P) and Alkenes by Helium Nanodroplets: Infrared Spectroscopy and Ab Initio Computations of the Triplet Biradical Intermediates

According to Smith *et al.* [Smith, I. W. M.; Sage, A. M.; Donahue, N. M.; Herbst, E.; Quan, D. *Faraday Discuss.* **2006**, 133, 137.], for molecule + radical reactions, the energetic difference between the molecule's ionization energy (IE) and the radical's electron affinity (EA) can provide insight into the nature of the reaction barrier, either *above* or *below* the reactant asymptote. They propose that a difference (IE – EA) greater than 8.75 eV indicates a real barrier above the asymptotic limit, whereas a value below 8.75 eV indicates a submerged barrier. Indeed, this difference for the O(³P) + HCN system is 12.2 eV. Accordingly, the barrier to oxygen insertion into the CN π system is ~10 kcal/mol above the reactant asymptote, and a van der Waals complex is observed when these species are brought together in a 0.4 K helium nanodroplet. However, O(³P) reactions with *alkenes* are predicted to cross the postulated 8.75 eV threshold as the alkene substitution pattern evolves from ethene (no substitution) to propene (methyl group substitution) to butene (dimethyl substitution, of which there are four different isomers), and this trend was tested by Sabbah *et al.* [Sabbah, H.; Biennier, L.; Sims, I.R.; Georgievskii, Y.; Klippenstein, S.J.; Smith, I. W. *Science* **2007**, 317, 102.]. Their findings corroborated the behavior predicted by Smith *et al.* The HCN + O(³P) results presented here demonstrate the feasibility for analogous alkene + O(³P) spectroscopic studies, in which O(³P) and alkenes of varying substitution are combined in helium droplets *via* the sequential capture scheme. As the *real* reaction barrier (*i.e.* for the ethene and propene reactions) evolves to being *submerged* below the asymptotic limit (*i.e.* for the butene reactions), one might expect that strongly bound reaction intermediates, such as triplet biradicals, will be observed in helium droplets, rather than van der Waals complexes. Given the fact that a 10,000 atom helium droplet can dissipate 140 kcal/mol, it should be possible to quench the internal energy of these reaction intermediates and probe them for the first time spectroscopically.

Infrared Spectroscopy of Alkyl and Alkyl Peroxy Radicals in Solid para-Hydrogen

We have initiated a collaboration with Yuan-Pern Lee's group at the National Chiao Tung University in Taiwan. One of the Douberly group's graduate students, Gregory T. Pullen, visited Professor Lee's group, and he measured spectra of alkyl radicals and alkyl peroxy radicals isolated in solid *para*-H₂. We are now analyzing the spectra, and we have recently submitted a paper to the *Journal of Molecular Spectroscopy* that reports the comprehensive assignment of the mid-IR spectra of *n*- and *i*-propyl radicals. Papers on propyl peroxy and butyl radicals are forthcoming. In these studies, we are employing both normal mode and local mode effective Hamiltonian models to help assign spectra. We are studying the transferability of local mode Hamiltonian coupling parameters over a range of alkyl radical systems.

Gregory T. Pullen, Peter R. Franke, Karolina A. Haupa, Yuan-Pern Lee, Gary E. Douberly, "Infrared Spectroscopy of *n*-Propyl and *i*-Propyl Radicals in Solid *para*-Hydrogen" *Journal of Molecular Spectroscopy*, (2019). Submitted: April 2019.

Publications acknowledging DOE support (2013-2019):

1. Paul L. Raston, Tao, Liang and Gary E. Douberly, "Infrared Spectroscopy and Tunneling Dynamics of the Vinyl Radical in ⁴He Nanodroplets" *Journal of Chemical Physics*, **138**, 174302 (2013). Published: May 7, 2013.
2. Paul L. Raston, Jay Agarwal, Justin M. Turney, Henry F. Schaefer III and Gary E. Douberly, "The Ethyl Radical in Superfluid Helium Nanodroplets: Rovibrational Spectroscopy and Ab Initio Computations" *Journal of Chemical Physics*, **138**, 194303 (2013). Published: May 21, 2013.
3. Alexander M. Morrison, Paul L. Raston and Gary E. Douberly, "Rotational Dynamics of the Methyl Radical in Superfluid ⁴He nanodroplets" *Journal of Physical Chemistry A* **117**, 11640-11647 (2013). Published: November 21, 2013.
4. Christopher P. Moradi, Alexander M. Morrison, Stephen J. Klippenstein, C. Franklin Goldsmith and Gary E. Douberly, "Propargyl + O₂ Reaction in Helium Droplets: Entrance Channel Barrier or Not?" *Journal of Physical Chemistry A* **117**, 13626-13635 (2013). Published: December 19, 2013.
5. Christopher M. Leavitt, Christopher P. Moradi, Bradley W. Acrey and Gary E. Douberly, "Infrared Laser Spectroscopy of the Helium-Solvated Allyl and Allyl Peroxy Radicals" *Journal of Chemical Physics* **139**, 234301 (2013). Published: December 21, 2013.
6. Christopher M. Leavitt, Christopher P. Moradi, John F. Stanton and Gary E. Douberly "Communication: Helium Nanodroplet Isolation and Rovibrational Spectroscopy of Hydroxymethylene" *Journal of Chemical Physics* **140**, 171102 (2014). Published: May 5, 2014.
7. Bernadette M. Broderick, Laura McCaslin, Christopher P. Moradi, John F. Stanton and Gary E. Douberly "Reactive Intermediates in ⁴He Nanodroplets: Infrared Laser Stark Spectroscopy of Dihydroxycarbene" *Journal of Chemical Physics* **142**, 144309 (2015). Published: April 14, 2015.
8. Christopher P. Moradi and Gary E. Douberly "On the Stark Effect in Open Shell Complexes Exhibiting Partially Quenched Electronic Angular Momentum: Infrared Laser Stark Spectroscopy of OH-C₂H₂, OH-C₂H₄, and OH-H₂O" *Journal of Molecular Spectroscopy* **314**, 54-62 (2015). Published: June 22, 2015.

9. Bernadette M. Broderick, Christopher P. Moradi and Gary E. Douberly "Infrared Laser Stark Spectroscopy of Hydroxymethoxycarbene in ^4He Nanodroplets" *Chemical Physics Letters* **639**, 99-104 (2015). Published: September 7, 2015.
10. Christopher P. Moradi, Changjian Xie, Matin Kaufmann, Hua Guo and Gary E. Douberly "Two-center Three-electron Bonding in ClNH_3 Revealed via Helium Droplet Infrared Laser Stark Spectroscopy: Entrance Channel Complex along the $\text{Cl} + \text{NH}_3 \rightarrow \text{ClNH}_2 + \text{H}$ Reaction" *Journal of Chemical Physics*, **144**, 164301 (2016). Published: April 2016.
11. Matin Kaufmann, Daniel Leicht, Martina Havenith, Bernadette M. Broderick, Gary E. Douberly "Infrared Spectroscopy of the Tropylium Radical in Helium Droplets" *Journal of Physical Chemistry A*, **120**, 6768-6773 (2016). Published: August 16, 2016.
12. Joseph T. Brice, Tao Liang, Paul L. Raston, Anne B. McCoy, Gary E. Douberly "Infrared Stark and Zeeman spectroscopy of OH-CO: The Entrance Channel Complex along the $\text{OH} + \text{CO} \rightarrow \text{trans-HOCO}$ Reaction Pathway" *Journal of Chemical Physics*, **145**, 124310 (2016). Published: September 2016.
13. Peter R. Franke, Daniel Tabor, Christopher P. Moradi, Gary E. Douberly, Jay Agarwal, Henry F. Schaefer, Edwin L. Sibert "Infrared Laser Spectroscopy of the *n*-propyl and *i*-propyl Radicals: Stretch-Bend Fermi Coupling in the Alkyl CH Stretch Region" *Journal of Chemical Physics*, **145**, 224304 (2016). Published: December 2016.
14. Paul L. Raston, Emmanuel I. Obi, Gary E. Douberly "Infrared Spectroscopy of the Entrance Channel Complex Formed Between the Hydroxyl Radical and Methane in Helium Nanodroplets" *Journal of Physical Chemistry A*, **121**, 7597-7602 (2017). Published: September 2017.
15. Alaina R. Brown, Peter R. Franke, Gary E. Douberly "Helium Nanodroplet Isolation of the Cyclobutyl, 1-Methylallyl and Allylcarbinyl Radicals: Infrared Spectroscopy and Ab Initio Computations" *Journal of Physical Chemistry A*, **121**, 7576-7587 (2017). Published: September 2017.
16. Joseph T. Brice, Peter R. Franke, Gary E. Douberly "Sequential Capture of $\text{O}(^3\text{P})$ and HCN by Helium Nanodroplets: Infrared Spectroscopy and Ab Initio Computations of the $^3\Sigma\text{O-HCN}$ Complex" *Journal of Physical Chemistry A*, **121**, 9466-9473 (2017). Published: November 2017.
17. Peter R. Franke, Joseph T. Brice, Christopher P. Moradi, Henry F. Schaefer, Gary E. Douberly, "Ethyl + O_2 in Helium Nanodroplets: Infrared Spectroscopy of the Ethylperoxy Radical" *Journal of Physical Chemistry A*, **123**, 3558-3568 (2019). Published: April 2019.
18. Alain R. Brown, Joseph T. Brice, Peter R. Franke, Gary E. Douberly, "Infrared Spectrum of Fulvenallene and Fulvenallenyl in Helium Droplets" *Journal of Physical Chemistry A*, (2019), DOI: 10.1021/acs.jpca.9b01661. Published: April 2019.
19. Peter R. Franke, Kevin B. Moore, Henry F. Schaefer, Gary E. Douberly, "tert-Butyl Peroxy Radical: Ground and First Excited State Energetics and Fundamental Frequencies" *Physical Chemistry Chemical Physics*, (2019), DOI: 10.1039/C9CP01476D. Published: April 2019.
20. Michael C. Bowman, Gary E. Douberly, Henry F. Schaefer, "Convergent Energies and Anharmonic Vibrational Spectra of Ca_2H_2 and Ca_2H_4 Constitutional Isomers" *Physical Chemistry Chemical Physics*, (2019). Accepted: April 2019.

Coordination and Solvation of Actinide Cations Studied with Selected-Ion Infrared Spectroscopy
DOE Award No. DE-SC0018835

Michael A. Duncan
Department of Chemistry, University of Georgia, Athens, Georgia 30602

maduncan@uga.edu

Program Scope

Actinide metal and metal oxide cation-molecular complexes are studied in the gas phase to investigate their bonding, ligand coordination and solvation. Cation-molecular complexes of the form $M^{n+}(L)_y$, where $M = U$ or Th in singly- or doubly-charged states, and $L =$ small molecules such as H_2O , CO , N_2 , CO_2 , O_2 , or CH_3CN , are produced in a molecular beam by pulsed laser vaporization of solid metal targets. Similar methods are used to produce metal oxide complexes. Complexes containing a metal or oxide core ion with a specific number of ligand or solvent molecules are cooled by a supersonic expansion, size-selected in a time-of-flight mass spectrometer, and studied with infrared laser photodissociation spectroscopy. The resulting vibrational spectra reveal the shifts that occur for ligand/solvent vibrations upon binding to these metals and how these vary with the charge state, the number of ligands or solvent molecules present, the geometric and electronic structures of complexes, and the possible occurrence of ligand reactions mediated by the metal center. Additional experiments employ photofragment imaging technology to further investigate cation-molecular bond energies, and photodissociation experiments on larger metal oxide clusters. The experimental work is complemented by computational chemistry, with careful attention to relativistic and spin-orbit effects. The goal of these studies is an increased understanding of the fundamental interactions and electronic structure involved in actinide bonding, coordination and solvation.

Recent Progress

In the first few months of this new grant we have focused on exploring the kinds of metal ion-molecular complexes and metal oxide clusters that can be produced from laser ablation of uranium in the form of metal rod samples. We have secured metal rod samples of thorium, but have not yet include it in experiments. We have produced complexes of the form $U^+(L)_x$ and $U^{2+}(L)_x$ for the ligand/solvent molecules $L =$ water, CO_2 , CO , acetylene and benzene. Figures 1 and 2 show examples of the mass spectra produced for CO_2 and acetylene. In each case, both singly-charged and doubly-charge ion-molecule complexes are produced. Oxides are produced from the CO_2 , presumably via a metal oxidation reaction.

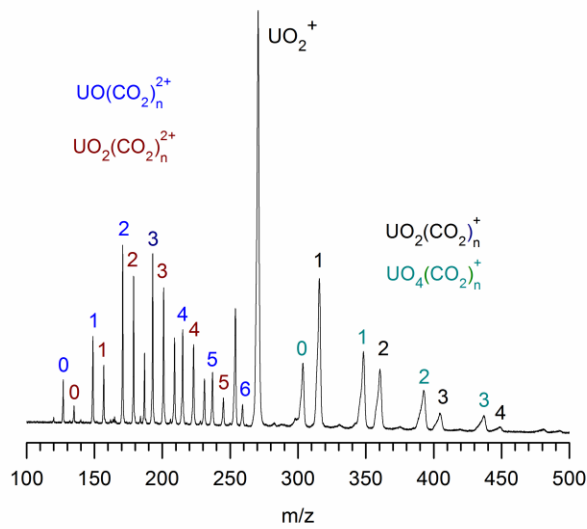


Figure 1. The mass spectrum resulting from laser ablation of uranium metal with a CO_2 expansion gas.

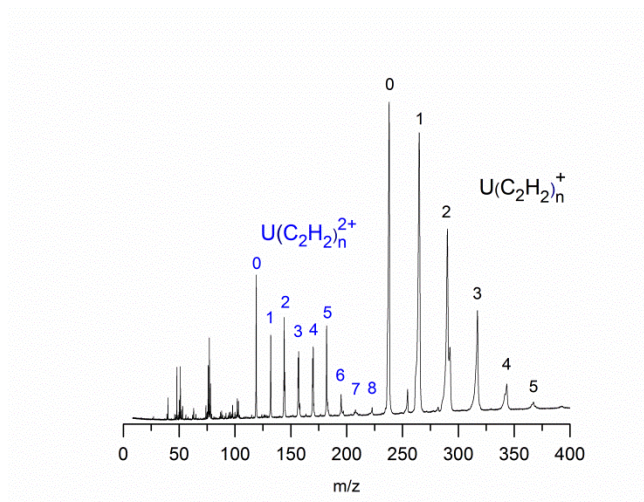


Figure 2. The mass spectrum resulting from laser ablation of uranium metal with acetylene seeded into the expansion gas.

Uranium oxide clusters have been produced via laser ablation, with a few percent of oxygen added to a helium expansion. The mass spectrum resulting from this is shown in Figure 3. Based on previous experience with other metal oxide clusters, we understand that the masses produced here are determined by both the stability of oxide clusters and the kinetics of oxidation reactions. To separate these effects, we use multiphoton dissociation of size-selected clusters, with the understanding that stable clusters will appear repeatedly from many dissociation events, either as abundant cations produced or as inferred neutrals eliminated. Figure 4 shows an example of such a photodissociation experiment. The cations U_2O_5^+ and U_3O_8^+ are produced repeatedly from the decomposition of larger clusters, suggesting that these species have

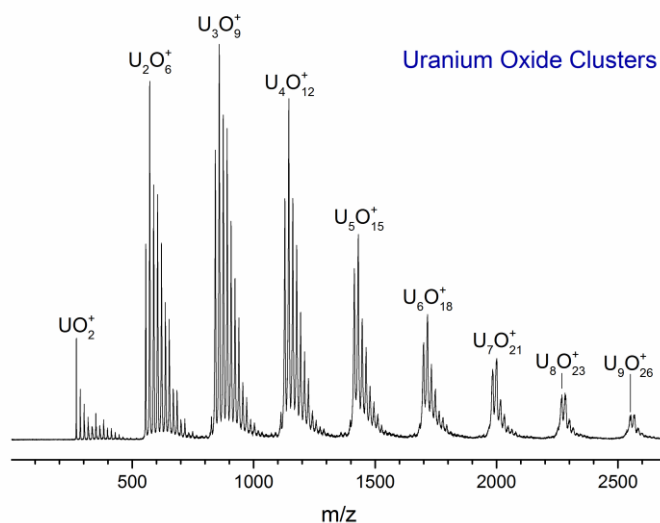


Figure 3. Mass spectrum of uranium oxide cluster cations produced by laser ablation.

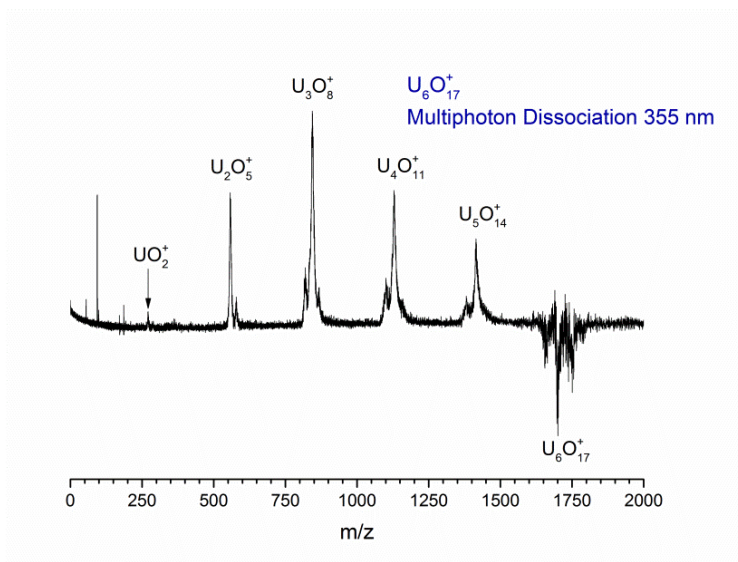


Figure 4. Multiphoton dissociation of the $U_6O_{17}^+$ cluster ion at 355 nm. The negative signal represent the amount of parent ion dissociation and the positive signal represents the photofragment cations produced.

enhanced stability. In a new collaboration with Prof. David Dixon (University of Alabama), we are investigating the structures of these species. Figure 5 shows the structure found to be most stable for $U_3O_8^+$.

We have continued our studies on the infrared spectroscopy of $U^+(L)_x$ and $UO_n(L)_x^+$ complexes. In the past, we examined the carbonyl complexes of uranium and uranium oxide cations. In more recent work, we have extended these studies to complexes with $L = CO_2$.

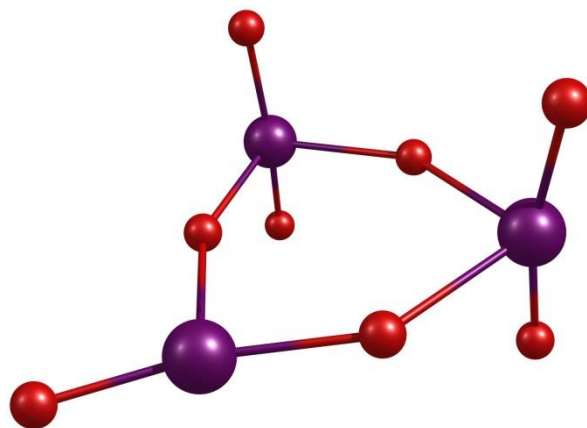


Figure 5. The structure predicted by theory for $U_3O_8^+$.

Future Plans

In plans for future research, we will investigate the small oxide clusters of thorium using photodissociation experiments like those shown in Figure 4. We will also initiate computational studies on the species indicated to be stable. We will continue the infrared spectroscopy experiments by examining uranium-acetylene and uranium-benzene complexes. Uranium cations have been suggested previously to catalyze the cyclo-trimerization reaction to form benzene, but there is no spectroscopic evidence to confirm this.

BES Supported Publications (2016 – present; from previous funding in the CPIMS Program)

1. T. B. Ward, P. D. Carnegie, M. A. Duncan, "Infrared Spectroscopy of the $Ti(H_2O)Ar^+$ Ion-Molecule Complex: Electronic State Switching Induced by Argon," *Chem. Phys. Lett.* **654**, 1–5 (2016). DOI: 10.1016/j.cplett.2016.04.065.
2. T. B. Ward, E. Miliordos, P. D. Carnegie, S. S. Xantheas, M. A. Duncan, "Ortho-Para Interconversion in Cation-Water Complexes: The Case of $V^+(H_2O)$ and $Nb^+(H_2O)$ Clusters," *J. Chem. Phys.* **146**, 224305 (2017). DOI: 10.1063/1.4984826.

Spectroscopic and Dynamical Studies of Highly Energized Small Polyatomic Molecules

Robert W. Field
Massachusetts Institute of Technology
Cambridge, MA 02139
rwfield@mit.edu

I. Introduction

The aim of this research program is to develop models for qualitative and quantitative understanding of complex processes, such as vibronic coupling, predissociation, photodissociation, and isomerization. Simple models capture physical insight and lead to intuition which can be applied to a broad array of problems. The beauty of the underlying quantum mechanisms is not uncovered by a more short-sighted approach based on finding the best numerical fit to a problem. Naturally, good fits have their place, and are utilized by this program, but the primary goal of this program is to foster understanding of broadly applicable principles via the study of prototypical systems. The systems currently under investigation include atmospherically relevant sulfur-containing compounds, various processes of electronically excited acetylene, and rovibrational dynamics of formaldehyde.

II. Recent Progress

A. PFAS Detected Hot- and Cold-Band Spectroscopy of Acetylene

We have recently developed a new method for studying the first excited singlet state of acetylene. In this new method, the UV excitation laser is focused on a molecular beam of acetylene. Multi-photon dissociation occurs, resulting in electronically excited C_2 and C_2H . Fluorescence from these excited species, which spans the visible portion of the spectrum, is then collected. This new method, called Photofragment Fluorescence Action Spectroscopy (PFAS), offers considerable advantages for certain classes of S_1 acetylene states. First, it offers experimental ease. Our current iteration of PFAS requires only one focused laser, as all excitation photons can be of the same wavelength. Second, the multi-photon dissociation occurs rapidly, meaning that PFAS is relatively unaffected by the short lifetimes of S_1 vibrational states that lie above the predissociation threshold. Third, the fluorescence photons that are detected are far in frequency from that of the excitation laser, meaning that the intense excitation pulse can be efficiently blocked, allowing for detection against a very small background signal.

We are currently pursuing two objectives with this experimental technique, with one goal in common. The aim is to gain a full understanding of *cis-trans* isomerization in the S_1 state of acetylene. A complete description of the transition state(s), isomerization dynamics, and the key indicators of isomerization is a rich field of study, and such a description will contain insights that will contribute to understanding of other systems, both other isomerizations and other chemically important large-amplitude reaction coordinates.

The first type of experiment is cold-band spectroscopy of S_1 acetylene. In order to achieve a more complete description of the relevant motions, vibrational levels that lie far above the predissociation barrier must be systematically observed. Unfortunately, these states have sufficiently short lifetimes that disentangling their Laser Induced Fluorescence (LIF) signal from excitation laser scatter has proven to be difficult. PFAS, however, offers the tools required to observe such states. Experiments in this area are ongoing.

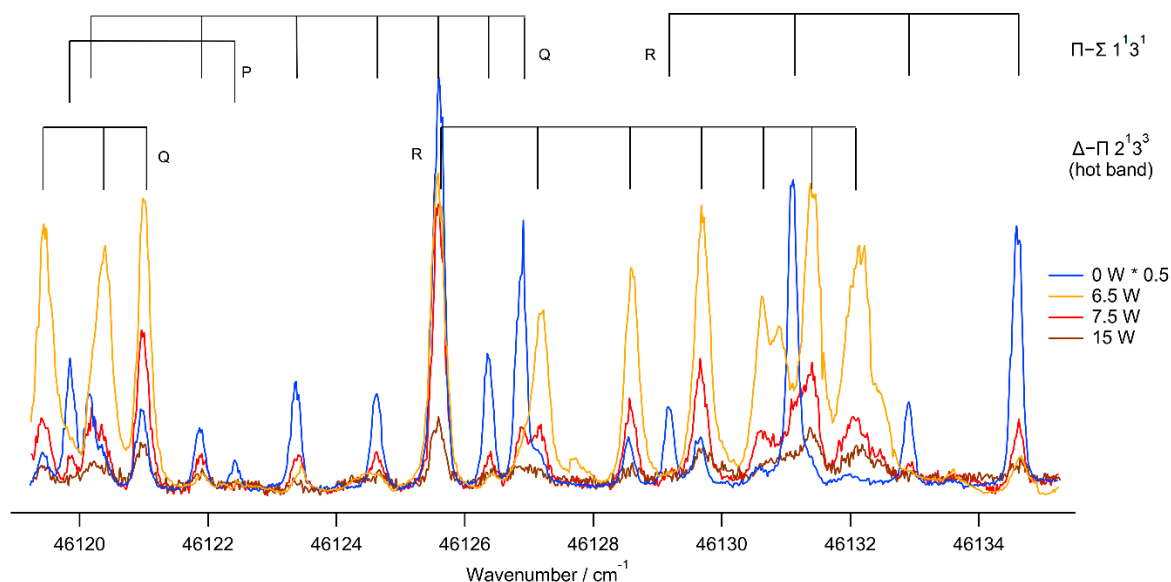


Figure 1: Changes to a portion of the spectrum of acetylene due to a change in temperature of the heated nozzle (expressed as power dissipated). In particular, the hot band lines are strongly enhanced while the intensities of the cold band lines are reduced when the heater is turned on. The total intensity decreases as the temperature of the nozzle increases, but the large intensity increases in the hot bands offsets this decrease.

The second type of experiment is hot-band spectroscopy of S_1 acetylene. Acetylene has a center of inversion so its states have g/u symmetry. Vibrational states of both symmetries must be studied in order to completely describe the system. Hot band spectroscopy accomplishes this goal, and also allows access to bands of different rotational K values from cold-band spectroscopy (essential for quantifying Coriolis interactions). The hot-band spectroscopy is accomplished by expanding the acetylene gas from a specially designed heated tube. The subsequent collisions in the supersonic expansion are very efficient at cooling rotation, but much less so at cooling vibration. The interrogated molecules, then, have enhanced hot-band signal without sacrificing the clarity of rotational assignments.

B. Dynamics of Vibrational Cooling in Supersonic Expansions

A detailed understanding of the dynamics by which molecular vibrations are cooled in supersonic expansions is essential to the interpretation of results of experiments in which hot molecules are generated and/or detected in a jet-cooled environment. Detecting changes in a vibrational population distribution (VPD) as a function of multiple parameters, such as nozzle design, probe-nozzle distance, probe-nozzle timing, or carrier gas, requires that many vibrationally excited levels can be non-negligibly populated. We use laser induced fluorescence as a method for simultaneously populating many highly vibrationally excited levels on the electronic ground state and chirped-pulse millimeter wave (CPmmW) spectroscopy to subsequently measure the VPD. Formaldehyde has been chosen as the prototype molecule for these studies for many reasons: the rotational and electronic spectroscopy of this molecule is exceptionally well understood, it is a small enough molecule that individual quantum state selectivity is possible in the electronic excitation, yet it exhibits many characteristics of larger polyatomics, intramolecular Coriolis coupling between modes 4 (out of plane bend) and 6 (CH_2

rock) affects vibrational energy transfer rates in interesting and unexpected ways, and vibronic selection rules limit the extreme dilution of population per quantum state upon fluorescence.

VPDs are conveniently encoded in rotational spectra. Rotational transitions out of vibrationally excited molecules can be observed as satellites on the ground state rotational transition, clustered within a few GHz. For H_2CO , the B and C rotational constants change by 0.3-0.4% per quantum of vibrational excitation, and transitions with up to seven quanta of vibrational excitation can be observed within a < 5 GHz bandwidth. The current CPmmW spectrometer can be chirped over 144-148.8 GHz and 148.8-156 GHz, providing access to both the $2_{02}-1_{01}$ and $2_{11}-1_{10}$ a-type pure rotational transitions of formaldehyde. In this way, a complete VPD can be sampled in a single chirped pulse.

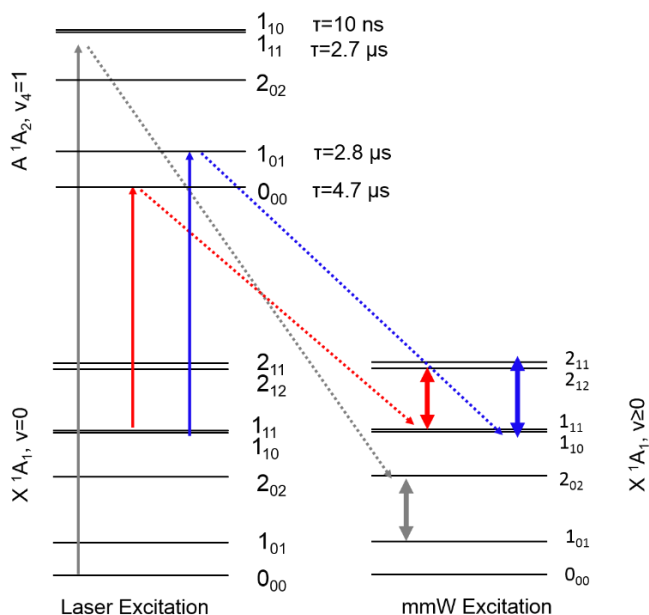


Figure 2: The proposed excitation scheme to investigate VPDs in formaldehyde. A laser pulse excites population from the ground electronic, ground vibrational state up to the $v_4=1$ vibrational band of the A electronic state. The formaldehyde molecules relax by electronic fluorescence to a distribution of vibrational states (the right side of the figure represents this distribution). Particular rotational transitions with several vibrational satellites that lie within the frequency range of our instrument are probed to determine the VPD of X-state formaldehyde.

Based on dispersed fluorescence experiments, following electronic excitation to a single rovibronic level in the A state, we predict tens of vibrationally excited levels to be populated in the ground state, and the population in any one vibrationally excited state will be highly diluted. However, the b-type vibronic selection rule ($\Delta v_4=\text{odd}$, $\Delta(v_5 + v_6)=\text{even}$) is strong. 95% of radiative transitions follow this selection rule and most of these transitions result in population in levels with excitation in combinations of modes 2 (CO stretch) and 4 (out of plane bend). Assuming $\sim 1\%$ of the H_2CO molecules in our jet are electronically excited by our laser, and that the population transferred to a particular vibrationally excited state is $\sim 1\%$ of the total number of molecules excited, the signal to noise ratio will be decreased relative to that of a pure microwave jet experiment by a factor of about 10,000. We have achieved a signal to noise ratio of 9.5 in a single shot for a $1 \text{ GHz } \mu\text{s}^{-1}$ chirp rate, indicating that substantial signal averaging ($\sim 10^6$ shots) will be required for detection of vibrationally excited levels. Although 10^6 averages can be acquired in ~ 14 hours, we are working to improve the signal to noise of the new 144-156 GHz CPmmW spectrometer. Another alternative to a broad chirped pulse experiment is to implement a sequence of multiple narrow bandwidth (~ 10 MHz) chirped pulses centered around the expected frequencies of known vibrationally excited rotational transition frequencies,

sidestepping the inverse square root relationship between the polarization of the sample by the Chirped Pulse and the linear frequency sweep rate. This possibility is also being explored.

III. Future work

We are investigating several problems in small-molecule dynamics and energetics using a Discrete Variable Representation (DVR) eigenstate analysis. The first of these projects is an expansion of our previously published analysis of \tilde{C} state SO_2 . The former analysis involved a partial diagonalization of the Hamiltonian prior to full diagonalization into eigenstates. The first step transforms the normal mode matrix into a Kellman mode matrix, or harmonic oscillator basis functions coupled by the small number of most important resonance mechanisms. We believe that additional insight will be gained by, instead of effectively setting some resonance interactions between normal modes of the molecule to zero for the pre-diagonalization, setting some resonances between internal coordinates to zero, such as turning off coupling between θ , the central angle of the molecule, and the bond lengths, r_1 and r_2 .

The second project we are pursuing in this area involves *cis-trans* isomerization of the S_1 state of acetylene. Using a reduced-dimension DVR, we will utilize the inverse participation number to look for classes of eigenstates that resemble eigenstates of the *trans* and *cis* potential wells, and states localized near the *cis-trans* transition saddle-point. Inverse participation number is a simple metric that defines how appropriate a particular basis set is for describing a state. Namely, if one basis state contributes to an eigenstate, the inverse participation number will be one, and if n states contribute equally, the inverse participation number will be n . Comparing trends in participation number of eigenstates between various basis sets will lead to insights in the patterns that can be expected in isomerization processes, and even in a general reaction coordinate.

IV. Publications supported by this project 2016-2019

1. J. Jiang, A. Muthike, T. Erickson, and R. W. Field, "One-color (212-220nm) Resonantly-Enhanced (S_1 - S_0) Multi-photon Dissociation of Acetylene" (in review).
2. J. Jiang, C. Saladrigas, T. Erickson, C. Keenan and R. W. Field, "Probing the Predissociated Levels of the S_1 State of Acetylene via H-atom Fluorescence and Photofragment Fluorescence Action Spectroscopy" *J. Chem. Phys.* **149** 174309 (2018).
3. W. Transue, A. Velian, M. Nava, M.-A. Martin-Drumel, C. Wommack, J. Jiang, G.-L. Hou, X.-B. Wang, M. McCarthy, R. W. Field, and C. Cummins, "A Molecular Precursor to Phosphoacetylene and its Application in Synthesis of the Aromatic 1,2,3,4-Phosphatriazolate Anion" *J.A.C.S.* **138**, 6731 (2016).
4. G. B. Park and R. W. Field, "Perspective: The First Ten Years of Broadband Chirped Pulse Fourier Transform Microwave Spectroscopy" *J. Chem. Phys.* **144**, 200901 (2016).
5. G. B. Park, J. Jiang, and R. W. Field, "The origin of unequal bond lengths in the \tilde{C} B_2 of SO_2 : Signatures of high-lying potential energy surface crossings in the low-lying vibrational structure" *J. Chem. Phys.* **144**, 144313 (2016).
6. J. Jiang, G. B. Park, and R. W. Field, "The Rotation-vibration Structure of the SO_2 \tilde{C} B_2 State Explained by a New Internal Coordinate Force Field" *J. Chem. Phys.* **144**, 144312 (2016).
7. G. B. Park, J. Jiang, C. A. Saladrigas, and R. W. Field, "Observation of b_2 Symmetry Vibrational Levels of the SO_2 \tilde{C} B_2 State: Vibrational Level Staggering, Coriolis Interactions, and Rotation-vibration Constants" *J. Chem. Phys.* **144**, 144311 (2016).

GAS-PHASE CHEMICAL KINETICS UNDER EXTREME CONDITIONS

C. Franklin Goldsmith, PI

Brown University

One of the grand challenges for the Department of Energy is the ability to simulate the complex interactions between fluid mechanics and chemical kinetics for gases at high pressures (e.g. 100 bar). Under these conditions, the ideal gas equation of state is not valid. Although considerable advances have been made regarding real-gas equations of state for thermodynamic properties, the same cannot be said of chemical kinetics under extreme pressures. The standard approach in computational kinetics assumes that reactions occur under isolated conditions. Real-gas behavior can have a profound effect on the chemical source terms in reactive flow simulations. These many-body interactions can change both the rate constants and the product branching fractions.

In this proposal, we will set forth a methodology to quantify many-body effects on transition states and thence high-pressure effects on rate constants. The specific aims are: (i) develop chemically accurate surrogate potential energy surfaces for computational kinetics with explicit solvent molecules, and use this surrogate model within molecular dynamics simulations; (ii) quantify the effects of high pressures on the rate constants for H-abstraction and retro-Diels-Alder; (iii) determine the pressure at which solvent cage effects will cause the branching fractions in bond-fission reactions to favor molecular elimination products; and (iv) analyze the results for possible trends that can be applied heuristically.

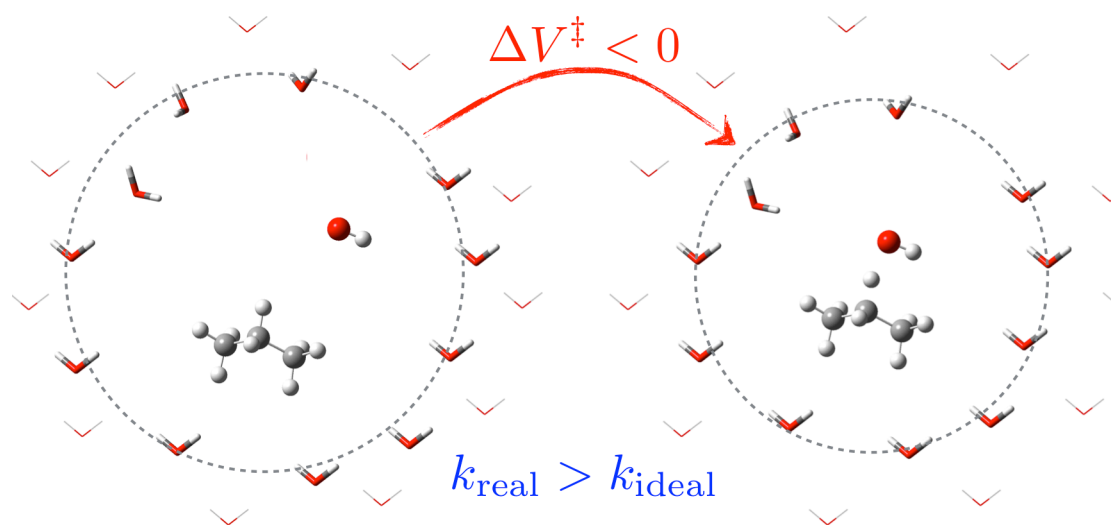


Figure 1: simple cartoon illustrating the effect of a change in the volume of activation for an H-abstraction reaction.

$$k = \frac{k_B T}{h} e^{-\Delta G^\ddagger / k_B T}$$

$$\left(\frac{\partial \ln k}{\partial P} \right)_T = - \frac{\Delta V^\ddagger}{k_B T}$$

$$k_{real} = k_{ideal} e^{-\left(\int_{P_{ref}}^{P_{high}} \Delta V^\ddagger dP \right) / k_B T}$$

$$k_{ideal} \frac{\gamma_R}{\gamma_{TS}}$$

The initial approach will build off the concept of volume of activation, depicted above in Figure 1. The idea will be to use molecular dynamics to compute the change in volume of the high-pressure gas surrounding the reactant(s) as the traverse the reaction coordinate through the transition state. From this change in volume, we can determine a “correction” to the ideal-gas rate constant.

Computer-Aided Construction of Chemical Kinetic Models

William H. Green
Department of Chemical Engineering
Massachusetts Institute of Technology
Cambridge, MA 02139
whgreen@mit.edu

I. Program Scope

The combustion chemistry of even simple fuels can be extremely complex, involving hundreds or thousands of kinetically significant species. The most reasonable way to deal with this complexity is to use a computer not only to numerically solve the kinetic model, but also to construct the kinetic model in the first place. Because these large models contain so many numerical parameters (e.g. rate coefficients, thermochemistry) one never has sufficient data to uniquely determine them all experimentally. Instead one must work in “predictive” mode, using theoretical values for many of the numbers in the model, and as appropriate refining the most sensitive numbers through experiments. Predictive chemical kinetics is exactly what is needed for computer-aided design of combustion systems based on proposed alternative fuels, particularly for early assessment of the value and viability of proposed new fuels. It is also very helpful in other fuel chemistry problems, and in understanding emissions and environmental chemistry.

Our research effort is aimed at making accurate predictive chemical kinetics practical; this is a challenging goal which necessarily includes a range of science advances. Our research spans a wide range from quantum chemical calculations on individual molecules and elementary-step reactions, through the development of improved rate/thermo calculation procedures, the creation of algorithms and software for constructing and solving kinetic simulations, the invention of methods for model-reduction while maintaining error control, and finally comparisons with experiment. Many of the parameters in the models are derived from quantum chemistry, and the models are compared with experimental data measured in our lab or in collaboration with others.

II. Recent Results

A. Predicting Nitrogen and Sulfur Chemistry

We recently developed a computer method for rapidly predicting thermal (mostly free-radical) chemistry for nitrogen-containing and sulfur-containing molecules, and distributed it open-source as part of the Reaction Mechanism Generator (RMG) software suite. This was considerably more complicated than C,H,O chemistry because both nitrogen and sulfur have several different valencies, allowing a variety of different resonance forms and quite a rich set of possible functional groups and feasible types of chemical reactions. Some of these functional groups and reaction types have been well-studied in the literature, but many have not. We filled in the gaps with quantum chemistry calculations. We made the limited experimental data, our computed values, and group-contribution based estimates for rate coefficients and thermochemical parameters based on those values publicly available through the rmg.mit.edu website.

In 2018 we used the software to develop a detailed kinetic model for high temperature pyrolysis and oxidation of ethylamine [6], which was consistent with experimental data measured by Hanson’s group at Stanford. We also used the software to predict the complicated effects of NO_x on partial oxidation of alkanes, and compared with data measured in Ju’s group at Princeton.[Zhao et al. *Energy* (2018)] Very recently we have been using our new capability to develop a model for hydrazine (N₂H₄) chemistry, starting with its exothermic decomposition, which is important both for satellite thruster design and for safety analysis. We discovered that molecular weight growth chemistry occurs in hydrazine systems

simultaneously with the decomposition chemistry, similar to how hydrocarbon pyrolysis leads to a mix of small molecules and large molecules such as polycyclic aromatics. In collaboration with Ahren Jasper we characterized the key reactions involving N_3H_x and N_4H_x molecules in a recent manuscript [12]. We are now preparing a manuscript comparing the predictions of our complete hydrazine chemistry model with experimental measurements on flame speeds and product distributions.

We also have computed a large number of sulfur-containing molecules and their reaction rates using quantum chemistry, and from them developed group contribution methods to estimate rate coefficients and thermochemical parameters for a wide variety of organosulfur compounds. We have recently published a paper demonstrating our ability to predict the pyrolysis chemistry of organic sulfides [Class et al., *Phys Chem Chem Phys* 2019 (accepted)] including the formation of thiophene rings, comparing to our own experimental data, and we are now preparing a manuscript comparing our automatically-generated detailed kinetic model for the photochemically-driven oxidation of dimethylsulfide at conditions relevant to the troposphere to experimental data in the literature.

B. Tracking isotopes, correcting symmetry factors

We have recently added the capability to track isotopic enrichment and specific isotopomers to the RMG software suite. RMG can now very reliably predicted “filiation”, e.g. given a certain mixture of ^{13}C isotopomers in the feed predict the relative yields of isotopomers in the products, and vice-versa.[Goldman et al. *Chemical Geology* (2019)] This is very helpful in certain types of isotope analysis because it avoids the need to synthesize authentic standards of isotopomers.

When predicting isotopomers we noticed that the predictions for systems where symmetrical $X + X$ reactions are important were much less accurate than for other systems. Investigation revealed that there was a factor of 2 error in the transition state theory formula for $X+X$ reactions presented in an influential 1978 paper, which propagated into many errors in reported k 's and TST software over the last 4 decades. In many cases a factor of 2 in a small number of rate coefficients is not significant compared to other errors in a simulation. but a factor of 2 is often very large compared to the small differences in reactivity of different isotopomers, so for isotope analysis it is critical to get this right. We have corrected the error and carefully explained the whole issue in a recent paper.[11]

C. Improved understanding of Fused-Ring Formation Chemistry

We have recently improved the treatment of fused cyclics and aromaticity in RMG, and then used this to develop a fuel-rich natural gas mechanism [Chu et al., *Phys Chem Chem Phys* 21, 813 (2019)] incorporating recent high-accuracy quantum chemistry calculations, many by Mebel and co-workers. Extensive experimental data from Oßwald's group at DLR confirm our model is accurate in detail all the way from methane up to formation of the three-ring compound acenaphthalene ($C_{12}H_8$).

D. Improvements to the Overall Mechanism Construction Process

We have developed an improved overall workflow, where we iterate between adding additional reactions to the mechanism (e.g. using RMG) and improving the values of uncertain rate and thermo parameters in the existing model (e.g. by automatically spawning quantum chemistry calculations [3,9]). The first step reduces the mechanism truncation error [10], i.e. it improves the structure of the model, while the second step reduces the error in the model parameters. The process works best when the new data from quantum chemistry calculations are used to improve the estimators used by RMG to select which reactions need to be added to the model. We are exploring how to use machine learning to make better estimators.[Li et al.

J Phys Chem A 123, 2142 (2019)] We are collaborating with Stephen Klippenstein and Judit Zador on the automated rate calculations, and on automating the whole process.

III. Future Plans

We have recently been measuring the reactions of radicals with acetylene and ethene, which are sometimes followed by intramolecular H-atom transfers, H-atom loss, and/or cyclization reactions, using our unique flash photolysis laser-absorption/photoionization mass spec experimental apparatus [8] supplemented by kinetic models, quantum chemistry, and master equation calculations. These reactions are key steps in HACA processes leading to PAH formation originally proposed by Frenklach and by Bittner & Howard. We are currently writing up manuscripts reporting our studies of vinyl + acetylene (forming C₄H₅, C₄H₄, and C₆H₆), phenyl + ethene (to C₈H₉ and styrene), phenyl + acetylene (C₈H₇, phenyl acetylene, and naphthalene), and naphthalenyl + C₂H₂ (to acenaphthalene, phenanthrene, anthracene, and several isomeric C₁₂H₉ radicals). We made some preliminary reports at the US Combustion meeting in March 2019. [papers by Mica Smith and by Te-Chun Chu] The overall results are largely consistent with what would have been expected based on existing theoretical models, but that prior work omitted some significant side reactions which we have now included. This study is for the first time providing firm experimental values for several of the key reactions leading towards soot/particulate formation.

We have started several projects to improve our ability to generate mechanisms for complicated systems through improved algorithms for reaction selection, parallelization, high throughput computation, and the use of learning to provide more accurate estimates. Since we usually have only a small number of high accuracy rate or thermochemical data, we are focusing on machine learning methods which work well even with sparse datasets, such as decision trees and transfer learning.

IV. Publications and submitted journal articles supported by DOE BES 2017-2019

1. Alon Grinberg Dana, Soumya Gudiyella, William H. Green, Santosh J. Shanbhogue, Dan Michaels, Nadim W. Chakroun, and Ahmed Ghoniem. “Automated Generation of Chemical Mechanisms for Predicting Extinction Strain Rates with Applications in Flame Stabilization and Combustion Instabilities”, 55th AIAA Aerospace Sciences Meeting, AIAA SciTech Forum, (AIAA 2017-0835) <http://dx.doi.org/10.2514/6.2017-0835>
2. Kehang Han, William H. Green, and Richard H. West, “On-the-Fly Pruning for Rate-Based Reaction Mechanism Generation”, *Computers and Chemical Engineering* **100**, 1-8 (2017). <http://dx.doi.org/10.1016/j.compchemeng.2017.01.003>
3. Colin M. Grambow, Adeel Jamal, Yi-Pei Li, William H. Green, Judit Zador, Yury V. Suleimanov, “Unexpected Unimolecular Reaction Pathways of a γ -Ketohydroperoxide from Combined Application of Automated Reaction Discovery Methods”, *Journal of the American Chemical Society* **140**, 1035-1048 (2018). <http://dx.doi.org/10.1021/jacs.7b11009>
4. Kehang Han, Adeel Jamal, Colin M. Grambow, Zachary J. Buras, “An Extended Group Additivity Method for Polycyclic Thermochemistry Estimation”, *International Journal of Chemical Kinetics* **50**, 294-303 (2018). <https://doi.org/10.1002/kin.21158>
5. Alan E. Long, Shamel S. Merchant, Aäron G. Vandeputte, Hans-Heinrich Carstensen, Alexander J. Vervust, Guy B. Marin, Kevin M. Van Geem, and William H. Green, “Pressure dependent kinetic analysis of pathways to naphthalene from cyclopentadienyl recombination”, *Combustion & Flame* **187**, 247-256 (2018). <https://doi.org/10.1016/j.combustflame.2017.09.008>

6. Alon G. Dana, Beat Buesser, Shamel S. Merchant, and William H. Green, “Automated Reaction Mechanism Generation Including Heteroatoms: Nitrogen”, *International Journal of Chemical Kinetics* **50**, 223-258 (2018). <http://dx.doi.org/10.1002/kin.21154>
7. Alexander J. Vervust, Marko R. Djokic, Shamel S. Merchant, Hans-Heinrich Carstensen, Alan E. Long, Guy B. Marin, William H. Green, and Kevin M. Van Geem, “Detailed experimental and modeling study of cyclopentadiene pyrolysis in the presence of ethene”, *Energy & Fuels* **32**, 3290-3934 (2018). <https://pubs.acs.org/doi/abs/10.1021/acs.energyfuels.7b03560>
8. Joshua E. Middaugh, Zachary J. Buras, Mickael Matrat, Te-Chun Chu, Young-Seok Kim, Ionut M. Alecu, AnGayle K. Vasiliou, C. Franklin Goldsmith, and William H. Green “A combined photoionization time-of-flight mass spectrometry and laser absorption spectrometry flash photolysis apparatus for simultaneous determination of reaction rates and product branching”, *Review of Scientific Instruments* **89**, 074102 (2018). <https://doi.org/10.1063/1.5024399>
9. Murat Keceli, Sarah Elliott, Yi-Pei Li, Matthew S. Johnson, Carlo Cavallotti, Yuri Georgievskii, William H. Green, Matteo Pelucchi, Justin M. Wozniak, Ahren W. Jasper, and Stephen J. Klippenstein, “Automated Computational Thermochemistry for Butane Oxidation: A Prelude to Predictive Automated Combustion Kinetics”, *Proc. Combust. Inst.* **37**, 363-371 (2019). <https://doi.org/10.1016/j.proci.2018.07.113>
10. William H. Green, “Automatic Generation of Reaction Mechanisms” in *Mathematical Modeling of Complex Reaction Systems*, ed. by Tiziano Faravelli, Flavio Manenti, and Eliseo Ranzi (2019, in press).
11. Mark J. Goldman, Shuhei Ono, and William H. Green, “Accepted method for computing X+X rates is incorrect, causes large errors in isotope analysis”, *J. Phys. Chem. A* **123**, 2320–2324 (2019). <https://doi.org/10.1021/acs.jpca.8b09024>
12. Alon Grinberg Dana, Kevin Moore, Ahren W. Jasper, and William H. Green, “Large Intermediates in Hydrazine Decomposition: A Theoretical Study of the N₃H₅ and N₄H₆ Potential Energy Surfaces”, *Journal of Physical Chemistry A* (submitted).

ADVANCED MASS SPECTROMETRY AND X-RAY DIAGNOSTICS

Nils Hansen, David L. Osborn, Krupa Ramasesha

Combustion Research Facility, Sandia National Laboratories, MS 9055, Livermore, CA 94551-0969
nhansen@sandia.gov, dlosbor@sandia.gov, kramase@sandia.gov

PROGRAM SCOPE

This task explores fundamental interactions of high-energy photons with molecules and their application to chemically specific diagnostics. The goal is developing advanced mass spectrometry and X-ray spectroscopy tools for studying fundamental gas-phase chemical physics. These diagnostics are exploited extensively in the “Chemical Kinetics for Complex Systems,” “Gas Phase Interactions with Other Phases,” and “Chemical Dynamics Methods and Applications” tasks. New initiatives in high-harmonic generation will impact dynamics studies proposed for “Ultrafast Chemistry: Spectroscopic Probes of Non-Adiabatic Dynamics” task. Mass spectrometry, especially in combination with synchrotron-based vacuum-ultraviolet (VUV) single-photon ionization, has impacted the DOE’s “Gas-Phase Physical Chemistry” program tremendously as it has been an instrumental tool for sensitive and isomer-specific detection of reactant and product molecules sampled from chemical reactions. This section describes our new push to establish photoelectron photoion coincidence (PEPICO) and tandem mass spectrometry as tools for probing of gas-phase chemical reactions with superior performance in many areas compared to the commonly applied photoionization mass spectrometers.

Beyond these mass spectrometric efforts, Sandia’s program has a long-standing interest to develop additional spectroscopic and scattering approaches using x-rays to probe core-level electrons and for Raman and other scattering spectroscopies. This section describes recent results and proposed work to push forward the frontiers of chemical physics using radiation in the x-ray regimes, both at DOE light sources and in laboratory experiments.

RECENT PROGRESS

Investigation of Sampling-Probe Distorted Temperature Fields in Flames with X-Ray Fluorescence Spectroscopy:

We have used x-ray diagnostics to study the temperature field in extreme environments to obtain a better understanding of how to accurately interpret information from common experimental devices. For example, flame-sampling experiments, especially in conjunction with laminar low-pressure premixed flames, are routinely used in combustion chemistry studies to unravel the identities and quantities of key intermediates and their pathways. In many instances, however, an unambiguous interpretation of the experimental and modeling results is hampered by the uncertainties about the probe-induced, perturbed temperature profile. To overcome this limitation, two-dimensional perturbations of the temperature field caused by sampling probes with different geometries have been investigated using synchrotron-based X-ray fluorescence spectroscopy. In these experiments which were performed at the 7-BM beamline of the Advanced Photon Source (APS) at the Argonne National Laboratory in collaboration with R.S. Tranter and A.L. Kastengren, a continuous beam

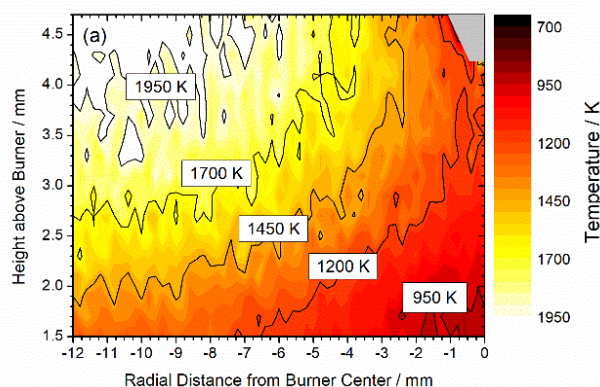


Figure 1: Two-dimensional temperature fields around the quartz probe at two different burner-probe separations: (a) 4.2 mm (reaction zone) and (b) 2.0 mm (preheat zone). Isotherms have been added to the images to guide the readers’ eyes.

of hard X-rays at 15 keV was used to excite krypton atoms that were added in a concentration of 5 vol.-% to the unburnt gas mixture and the resulting krypton fluorescence at 12.65 keV was subsequently collected. The highly spatially resolved signal was converted into the local flame temperature to obtain temperature fields at various burner-probe separations as functions of the distance to the burner surface and the radial distance from the centerline – see Fig. 1. Multiple measurements were performed with different probe geometries and these results clearly revealed the limitations of one-dimensional models for predicting flame-sampling experiments and provided guidance for model developments and validations based on quantitative speciation data from flames obtained via intrusive sampling techniques.

Design and construction of new time-resolved PEPICO apparatus:

Since 2006, both Sandia researchers and a diverse group of external collaborators have utilized the Sandia-designed multiplexed photoionization mass spectrometer (MPIMS) for time-resolved, isomer-specific investigations of unimolecular and bimolecular chemistry. In the quest for better molecular fingerprints, we designed a prototype time-resolved photoelectron photoion coincidence (PEPICO) spectrometer, whose core principles we tested in a series of experiments at the Swiss Light Source. We used the lessons from this prototype to design, over the past year, a new apparatus for time-resolved PEPICO, optimized for use at the Chemical Dynamics Beamline of the Advanced Light Source of Lawrence Berkeley National Laboratory. It will enable better molecular fingerprints to help resolve chemical reaction mechanisms that are beyond our capabilities at present. Much of the machining of this new apparatus is now complete, and we are beginning assembly.

PROPOSED WORK

Time-resolved PEPICO: The new time-resolved PEPICO apparatus was designed for a range of different experiments. First and foremost, it will allow an augmented version of our David Gutman-style flow-reactor for the study of unimolecular and bimolecular reactions in a collisional environment at well-defined temperatures (300 – 1000 K) and pressure (1 – 10 torr). This reactor, typically consisting of a quartz tube of 1.05 cm inner diameter, and 70 cm length, enables photochemical initiation of chemical reactions via a UV laser that propagates along the tube axis. Gases will be sampled into the PEPICO spectrometer via a pinhole in the side of the reactor. In addition to time-resolved mass spectra that reflect the evolving concentrations of neutrals in the chemical reactor, the datasets we generate will also comprise photoionization spectra (similar to those we now obtain with MPIMS), and mass-selected photoelectron spectra in coincidence with each mass selected ion. The fact that photoelectron spectra are comprised of peaks, whereas photoionization spectra are the integral of photoelectron spectra (in the limit of direct ionization processes), means that the new photoelectron spectra will provide better molecular fingerprints to make isomer specific assignments of species in chemical reactions. We anticipate many benefits from this higher information content. Most notably, in reactions where many isomers are likely at a given neutral mass, such as the propargyl + propargyl reaction, our prototype PEPICO spectrometer has shown great promise for disentangling and quantifying a mix of 5+ isomers observed at a single mass-to-charge ratio.

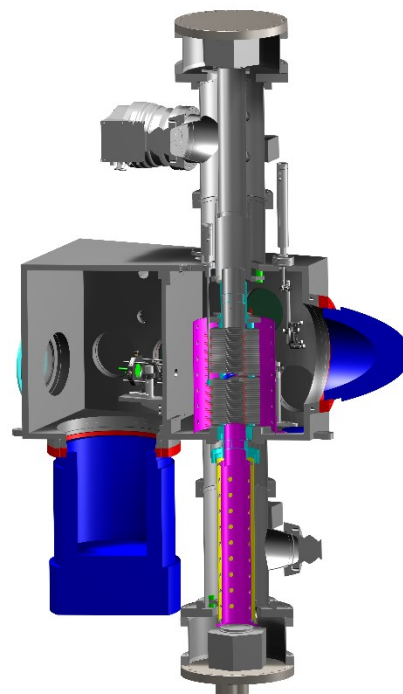


Figure 2: The new double-imaging photoelectron photoion coincidence spectrometer. A molecular beam source chamber is on the left. Ion and electron optics in the right side surround a quartz chemical reactor for studying reactions under thermal conditions. Electrons are sent downwards and cations upwards in the laboratory frame, detected by 2-D time- and position-sensitive delay line detectors.

Beyond chemistry taking place in our Gutman-style flow tube, the new PEPICO apparatus is also designed to accommodate a pinhole supersonic molecular beam valve, operating either in continuous or pulsed mode. This source can be coupled to either single-photon vacuum ultraviolet photoionization or resonance-enhanced multiphoton laser ionization (REMPI). In addition, the ionization step used as a probe of the neutral system can be preceded by a pump step that causes a vibrational or electronic excitation of a molecule. In this case the time-resolution of the instrument will be defined by the pulse widths of the pump and probe radiation, and the temporal records will be obtained by scanning the pump-probe delay. We expect this mode of operation will open up much faster timescales on the nanosecond, picosecond, and femtosecond domains, while retaining the multiplexed capabilities of PEPICO spectroscopy. We expect the instrument to be fully assembled by the end of summer 2019, and to generate its first data in fall 2019.

Tandem-mass spectrometry for gas-phase chemical physics: Through funds from Sandia's LDRD program we have modified a tandem mass spectrometer (provided from M. Ahmed at LBNL) to allow for sampling from reactive mixtures. This new MS-MS capability has been instrumental for detecting molecules containing multiple polycyclic aromatic hydrocarbon (PAH) cores, *i.e.* aliphatically bridged PAHs, in sooting flames. In this experiment the sampled gas-phase species are ionized using vacuum-ultraviolet photons of 10 eV, guided into the high-vacuum of the mass spectrometer, mass-selected using a quadrupole mass filter, and then dissociated through a collision-induced process. The fragment ions are subsequently detected using a reflectron time-of-flight mass spectrometer. The observed fragmentation patterns allow for elucidating structural information of the sampled molecules. We propose to use this tandem-mass spectrometric technique for assessing the role of PAH dimers in soot formation processes. The dimerization of PAHs has been discussed widely in combustion chemistry research as the critical step during the transition from gas-phase species to incipient soot-particles. This proposed scenario has been implemented in many combustion chemistry models, but latest theoretical work questions the feasibility of such an inception step. Flame-sampled MS-MS spectra of $m/z = 404.157$ ($C_{32}H_{20}$) across the two-dimensional flame space will provide experimental evidence for the identity of the sampled species.

Using the MS-MS tool, the formation and oxidation chemistry of aliphatically bridged PAH molecules will be studied systematically. We propose to use data science tools to explore the multi-dimensional parameter space effectively. We also envision to use tandem mass spectrometry to provide additional insights into the formation of the highly oxygenated species that have been observed in consecutive addition reactions of Criegee Intermediates to several compounds and during autooxidation processes at low temperatures. While we were able to detect the highly oxygenated species using our photoionization mass spectrometric approach, structural information could not be resolved from the respective photoionization efficiency curves. Tandem mass spectrometry has the potential to overcome this deficiency and to provide unprecedentedly detailed information about the chemical reaction pathways for the formation of these targeted species through structural information of the reactants, intermediates, and products.

High-harmonic generation for ultrafast chemistry: Equipment money from this program is being employed to purchase a high-energy carrier-envelope-phase stabilized ultrafast laser system. The laser system will produce 13 mJ sub-40 fs pulses, which will pump a commercial high-energy TOPAS to generate 2 mJ near-infrared pulses, tunable from 1.2 μm to 2.6 μm wavelengths. The near-infrared output from the TOPAS will drive table-top high harmonic generation in a gas cell filled with helium at pressures approaching an atmosphere to produce soft X-ray pulses with photon energies extending to 300 eV. These soft X-ray pulses will be coupled with UV excitation pulses to probe excited state non-adiabatic dynamics in gas phase small molecules, via the carbon 1s-to-valence (K-edge) and sulfur 2p-to-valence (L-edge) transitions at ~ 284 eV and ~ 165 eV, respectively.

BES-sponsored publications, 2017 – present

1. N. Hansen, R. S. Tranter, K. Moshhammer, J. B. Randazzo, J. P. A. Lockhart, P. G. Fugazzi, T. Tao and A. L. Kastengren, 2D-imaging of sampling-probe perturbations in laminar premixed flames using Kr X-ray fluorescence, *Combust. Flame*, **2017**, 181, 214-224.
2. N. Hansen, R. S. Tranter, J. B. Randazzo, J. P. A. Lockhart and A. L. Kastengren, Investigation of sampling-probe distorted temperature fields with X-ray fluorescence spectroscopy, *Proc. Combust. Inst.*, **2019**, 37, 1401-1408.
3. B. Sztaray, K. Voronova, K. G. Torma, K. J. Covert, A. Bodi, P. Hemberger, T. Gerber and D. L. Osborn, CRF-PEPICO: Double velocity map imaging photoelectron photoion coincidence spectroscopy for reaction kinetics studies, *J. Chem. Phys.*, **2017**, 147, 013944.
4. K. Voronova, K. M. Ervin, K. G. Torma, P. Hemberger, A. Bodi, T. Gerber, D. L. Osborn and B. Sztaray, Radical thermometers, thermochemistry, and photoelectron spectra: A photoelectron photoion coincidence spectroscopy study of the methyl peroxy radical, *J. Phys. Chem. Lett.*, **2018**, 9, 535.

CHEMICAL KINETICS FOR COMPLEX SYSTEMS

Nils Hansen, Habib N. Najm, David L. Osborn, Craig A. Taatjes, Judit Zádor

Sandia National Laboratories, MS 9055, Livermore, CA 94551-0969

nhansen@sandia.gov, hnnajm@sandia.gov, dlosbor@sandia.gov, cataatj@sandia.gov, jzador@sandia.gov

Program Scope

This program employs a unique set of experimental and theoretical studies with the goal of elucidating mechanisms of elementary chemical reactions, which impacts the research theme of *Reaction Pathways in Diverse Environments*. This task is linked with many other parts of the Sandia program; it extends the high-resolution view of the “Chemical Dynamics Methods and Applications” task to encompass complex interactions in collisional environments, and it provides a basis for the interface studies in the “Gas Phase Interactions with Other Phases” task. Methods developed under the “Advanced Mass Spectrometry and X-Ray Diagnostics” task that use tunable vacuum ultraviolet light from the Advanced Light Source (ALS) synchrotron at Lawrence Berkeley National Laboratory (LBNL) enable sensitive, isomer-specific ionization of reactant and product molecules sampled from chemical reactions. These individual reaction studies are linked to controlled measurements of more complex reaction systems as found in laboratory-scale flames and other reactors. Another important part of our strategy, especially for complex reaction systems, is using experimental data to test and refine detailed models, where the mechanism enables rigorous interpretation of experimental results and guides new measurements that will probe key aspects of potential energy surfaces. The experimental efforts are complemented by theoretical efforts to characterize the temperature and pressure dependence of reactions using quantum chemistry in a master equation framework, statistical theories, and experimental design strategies.

Recent Progress

Reaction of $\text{CH X}^{(2\Pi)}$ with ammonia and methyl-amines: We probed the reaction of $\text{CH X}^{(2\Pi)}$ with NH_3 and all the methyl amines [CH_3NH_2 , $(\text{CH}_3)_2\text{NH}$, and $(\text{CH}_3)_3\text{N}$] to understand how the increasing methyl substitution will affect the reaction outcome. Our results are consistent with a reaction mechanism in which the CH radical first creates a dative bond to the N atom, after which an H atom is lost. Molecular rearrangement can occur at the high energies made available by this dative bond formation. However, the dative bond formation pathway is not sufficient to explain all the detected products in the reaction of $\text{CH}+(\text{CH}_3)_3\text{N}$. We therefore proposed a C-H insertion mechanism that is likely to become favorable.

Reactions of carbonyl oxides: Our measurements of Criegee Intermediate (CI) reactions have highlighted the dominance of singlet association products, including insertion products, in reactions with stable species. We have measured insertion products in the reactions of CH_2OO with amines, hydroperoxides, and acids. Insertion forms products with an $-\text{OOH}$ functional group; as a result, carbonyl oxides can continue to insert into the O—H bonds and produce highly oxygenated oligomers. Measurements of ozone-initiated oxidation of ethylene has observed this sequential insertion mechanism. In these measurements, a network of CI reactions was identified, which can be described best by the sequential addition of CI with ethylene, water, formic acid, and other molecules containing hydroxy, aldehyde, and hydroperoxy functional groups. Species resulting from as many as four sequential CI addition reactions were observed.

Oxidation reactions at low temperatures: We have investigated the effects of resonance stabilization on hydrocarbon oxidation processes and the sequences of radical isomerization and O_2 addition that can lead to radical chain branching. Work with our collaborator B. Rotavera (U. Georgia) has focused on measuring products that are created via the second O_2 addition to QOOH radicals in the CI-initiated oxidation of cyclohexene. The relative ease of ketohydroperoxide formation is attributed to resonance stabilization of QOOH species increasing their lifetime against dissociation. This work was complemented by studies of the oxidation of *n*-butanal, 1,2-dimethoxyethane, dimethoxymethane, and acetaldehyde.

HCCH+HCCH: We used *ab initio* transition-state theory master equation (ME) methods to calculate rate coefficients for the association of two acetylene molecules and related reactions to unveil initiation

acetylene pyrolysis. Our calculations show that unimolecular initiation dominates H atom production only in dilute mixtures of acetylene. However, for more concentrated mixtures the bimolecular reactions dominate even at high temperatures, especially considering that the formed vinylacetylene, not included in this comparison, will also add to the chain-carrying H atom balance on a slightly longer time scale, diminishing the importance of the first-order initiation even further for these scenarios.

1-Pentanol pyrolysis and automated kinetics: We used KinBot to generate the *ab initio* data and to assemble the ME automatically for the $C_5H_{11}O$ potential energy surface relevant for 1-pentanol pyrolysis. We updated a comprehensive mechanism using our calculated rate coefficients and successfully simulated flow reactor experiments at U Ghent. We also carried out a joint study with the groups of Green and Suleimanov to compare various automated approaches.

New validation targets for the refinement of kinetic mechanisms through data research: Our work, which is based on a compilation of the chemical structures of 55 low-pressure premixed flames from various laboratories, unravels previously unexplored validation targets. We showed that the compiled set of more than 30,000 data points allows for the extraction of fuel-specific chemistry and can be used to identify inconsistent data, thus potentially improving the accuracy of the validation set. Most importantly, this large data set of flame structures was essential to discover that, despite the different fuels and flame conditions used in the individual flame studies, the maximum mole fractions of some intermediate species are correlated to each other in a systematic way. Additional targets for model refinement were reported for the pyrolysis of C_5 hydrocarbons.

Stochastic Chemical Systems: We used computational singular perturbation (CSP) to enable efficient explicit time integration of stiff chemical Langevin equations (CLEs). The construction advances a set of random sample paths of the CLE concurrently. At each time step, we eigen-decompose the Jacobian of the CLE drift term for each sample, and employ statistics across the samples to identify, in the mean, decoupled fast-exhausted and slow modes, providing the means for stable large-step explicit time integration. We demonstrated the performance and convergence of the construction, illustrating adaptive time-step growth as each mode is exhausted. We applied the construction for time integration of model stiff chemical systems.

Proposed Work

Chirped-pulse microwave spectroscopy: In collaboration with T. Zwier (Purdue University) we propose to develop chirped-pulse microwave spectroscopy into a sensitive analytical tool for investigation complex reaction systems. Microwave spectroscopy, which probes the rotational transitions of polar molecules in the gas-phase, is the most accurate method to determine chemical structures and it is proposed to probe the ozonolysis of ethylene and the low-temperature oxidation of DME using this technique.

Spin-forbidden chemistry: cyclopentene+O: We propose to study the reaction of cyclopentene + O initiated experimentally on the triplet surface. While the ethene + O reaction is dominated by chemistry happening on the singlet surface, the cyclopentene + O reaction, can proceed on the triplet surface as well due to submerged barriers belonging to the ring-opening of the initial C_5H_8O adduct and its further isomerization. Moreover, ISC is also possible via these open-chain isomers. We propose to explore the relevant parts of the PES with KinBot, and to match the predicted products and their branching ratios with the measured yields.

Oxidation of enols: We have succeeded in creating an intense source of ethenol and have observed preliminary data of its reaction with OH in the presence of O_2 . Although there is much work to be done, we have solid evidence for the production of glycoaldehyde and H_2CO , with some evidence for the production of formic acid ($HCOOH$). In future work, we will test whether these assignments are reproducible, and examine both the kinetics and the chemical pathways leading to their production.

The fate of α -QOOH radicals: To test this hypothesis that essentially all α -QOOH radicals will spontaneously decompose to $H_2C=O+OH$ by rotation about the C-OOH bond, we have begun a collaboration with Prof. Balint Sztaray's group (University of the Pacific) to study the reactions of OH and Cl with CH_3OOH (methyl hydroperoxide). In preliminary work, we see clear evidence of the CH_3OO

isomer, but no evidence of CH₂OOH. Instead, we observe formation of CH₂O and HO₂ radicals, the former likely arising from spontaneous decomposition of CH₂OOH. Thus, our preliminary results support the predictions that α -QOOH will in general be unstable to unimolecular decomposition.

Low-temperature and ozone-assisted oxidation and Criegee Intermediate reactions: We will continue to explore the reaction network of low-temperature and ozone-assisted oxidation processes. Specifically, the previously observed sequential addition of CIs to hydroperoxides will be investigated in more detail. Measurements of the reactions of unsaturated Criegee intermediates, which have additional biradical resonance structures, are being carried out in collaboration with M. Lester (U. Penn). Furthermore, the formation and reactions of ketohydroperoxides and other highly oxygenated intermediates in oxidation of substituted or oxygenated hydrocarbons will be explored in photolytically and thermally initiated reactions. Specifically, we target the isomer-selective detection of ketohydroperoxides in the oxidation of tetrahydrofuran, *n*- and *neo*-pentane.

Resonance stabilized carbonaceous radicals and their high-temperature reactions: Resonance stabilized carbonaceous radicals and their high-temperature reactions will be studied using pyrolytic and photolytic sources. First targets are the reaction sequences originating from C₃H₃ and C₅H₅ reactions and the importance of the C₃H₃+C₆H₅ and C₃H₃+C₇H₇ reaction on the formation of indene and naphthalene.

Stochastic chemical systems: In future work with stochastic chemical systems, we will work on ameliorating existing limitations of the CSP time integrator. We will explore suitable means of modeling the integration of the CLE diffusion term to relieve associated upper limits on the time step growth. We will also implement Jacobian eigensolve reuse strategies and explore the utility of eigensolvers that can make good use of a good initial guess. Finally, we will extend the construction to the "G-scheme" context, where both fast-exhausted and slow-inactive modes are dealt with separately, while only active modes are integrated using conventional methods, enabling the reduction of the size of the system in this last context.

Optimal experimental design: We are beginning a new effort, including both computational and experimental components, focusing on optimal experimental design. We will use a Bayesian formulation for the experimental design problem, and will target optimality in probabilistic terms, accounting for sources of noise and uncertainty, and arriving at robust designs.

List of Publications (2017-2019):

1. M. J. Al Rashidi *et al.*, *Elucidating reactivity regimes in cyclopentane oxidation: Jet stirred reactor experiments, computational chemistry, and kinetic modeling*, *Proc. Combust. Inst.*, **2017**, 36, 469-477.
2. T. J. Bannan *et al.*, *Seasonality of Formic Acid (HCOOH) in London during the ClearfLo Campaign*, *J. Geophys. Res. Atmos.*, **2017**, 122, 12488-12498.
3. M. Baroncelli *et al.*, *Investigating the effect of oxy-fuel combustion and light coal volatiles interaction: A mass spectrometric study*, *Combust. Flame*, **2019**, 204, 320-330.
4. J. Bourgalais *et al.*, *Product Detection of the CH Radical Reactions with Ammonia and Methyl-Substituted Amines*, *J. Phys. Chem. A*, **2019**, 123, 2178-2193.
5. M. Braun-Unkhoff *et al.*, *The influence of *i*-butanol addition to the chemistry of premixed 1,3-butadiene flames*, *Proc. Combust. Inst.*, **2017**, 36, 1311-1319.
6. R. L. Caravan *et al.*, *Products of Criegee intermediate reactions with NO₂: experimental measurements and tropospheric implications*, *Faraday Disc.*, **2017**, 200, 313-330.
7. R. L. Caravan *et al.*, *The reaction of hydroxyl and methylperoxy radicals is not a major source of atmospheric methanol*, *Nature Comm.*, **2018**, 9.
8. B. J. Chen *et al.*, *Ion chemistry in premixed rich methane flames*, *Combust. Flame*, **2019**, 202, 208-218.
9. M. W. Chen *et al.*, *Direct measurement of (OH)-O-center dot and HO₂ center dot formation in R-center dot + O-2 reactions of cyclohexane and tetrahydropyran*, *Phys. Chem. Chem. Phys.*, **2018**, 20, 10815-10825.
10. R. Chhantyal-Pun *et al.*, *Criegee Intermediate Reactions with Carboxylic Acids: A Potential Source of Secondary Organic Aerosol in the Atmosphere*, *ACS Earth Space Chem.*, **2018**, 2, 833-842.
11. R. Chhantyal-Pun *et al.*, *Experimental and computational studies of Criegee intermediate reactions with NH₃ and CH₃NH₂*, *Phys. Chem. Chem. Phys.*, **2019**, DOI: 10.1039/C8CP06810K.
12. R. Chhantyal-Pun *et al.*, *Direct Measurements of Unimolecular and Bimolecular Reaction Kinetics of the Criegee Intermediate (CH₃)₂COO*, *J. Phys. Chem. A*, **2017**, 121, 4-15.
13. J. Czekner *et al.*, *Study of low temperature chlorine atom initiated oxidation of methyl and ethyl butyrate using synchrotron photoionization TOF-mass spectrometry*, *Phys. Chem. Chem. Phys.*, **2018**, 20, 5785-5794.
14. J. C. Davis *et al.*, *Influence of Ether Functional Group on Ketohydroperoxide Formation in Cyclic Hydrocarbons: Tetrahydropyran and Cyclohexane*, *The J. Phys. Chem. A*, **2019**, DOI: 10.1021/acs.jpca.8b12510.
16. A. J. Eskola *et al.*, *Time-resolved measurements of product formation in the low-temperature (550-675 K) oxidation of neopentane: a probe to investigate chain-branching mechanism*, *Phys. Chem. Chem. Phys.*, **2017**, 19, 13731-13745.

17. A. J. Eskola *et al.*, Direct kinetics study of CH₂OO + methyl vinyl ketone and CH₂OO + methacrolein reactions and an upper limit determination for CH₂OO + CO reaction, *Phys. Chem. Chem. Phys.*, **2018**, 20, 19373-19381.
18. C. A. Grambow *et al.*, Unimolecular Reaction Pathways of a gamma-Ketohydroperoxide from Combined Application of Automated Reaction Discovery Methods, *J. Am. Chem. Soc.*, **2018**, 140, 1035-1048.
19. X. Han *et al.*, Explicit Time Integration of the Stiff Chemical Langevin Equations using Computational Singular Perturbation, *J. Chem. Phys.*, **2019**, in press.
20. N. Hansen *et al.*, Knowledge generation through data research: New validation targets for the refinement of kinetic mechanisms, *Proc. Combust. Inst.*, **2019**, 37, 743-750.
21. N. Hansen *et al.*, Investigating repetitive reaction pathways for the formation of polycyclic aromatic hydrocarbons in combustion processes, *Combust. Flame*, **2017**, 180, 250-261.
22. N. Hansen *et al.*, Microwave spectroscopic detection of flame-sampled combustion intermediates, *RSC Adv.*, **2017**, 7, 37867-37872.
23. M. A. H. Khan *et al.*, Investigating the Tropospheric Chemistry of Acetic Acid Using the Global 3-D Chemistry Transport Model, STOCHEM-CRI, *J. Geophys. Res. Atmos.*, **2018**, 123, 6267-6281.
24. M. A. H. Khan *et al.*, Criegee intermediates and their impacts on the troposphere, *Environm. Sci. Proc. Im.*, **2018**, 20, 437-453.
25. D. A. Knyazkov *et al.*, Photoionization mass spectrometry and modeling study of a low-pressure premixed flame of ethyl pentanoate (ethyl valerate), *Proc. Combust. Inst.*, **2017**, 36, 1185-1192.
26. A. L. Koritzke *et al.*, (Q) over dotOOH-mediated reactions in cyclohexene oxidation, *Proc. Combust. Inst.*, **2019**, 37, 323-335.
28. H. D. Liao *et al.*, Investigation of the low-temperature oxidation of n-butanal in a jet-stirred reactor, *Proc. Combust. Inst.*, **2019**, 37, 453-460.
30. K. Moshhammer *et al.*, Aromatic ring formation in opposed-flow diffusive 1,3-butadiene flames, *Proc. Combust. Inst.*, **2017**, 36, 947-955.
31. D. L. Osborn, Reaction Mechanisms on Multiwell Potential Energy Surfaces in Combustion (and Atmospheric) Chemistry *Ann. Rev. Phys. Chem.*, Vol 68, eds. M. A. Johnson and T. J. Martinez, 2017, vol. 68, pp. 233-260.
32. J. Pieper *et al.*, A high-temperature study of 2-pentanone oxidation: experiment and kinetic modeling, *Proc. Combust. Inst.*, **2019**, 37, 1683-1690.
33. B. Rotavera *et al.*, Influence of oxygenation in cyclic hydrocarbons on chain-termination reactions from R + O-2: tetrahydropyran and cyclohexane, *Proc. Combust. Inst.*, **2017**, 36, 597-606.
34. A. Roussio *et al.*, Identification of the Criegee intermediate reaction network in ethylene ozonolysis: Impact on energy conversion strategies and atmospheric chemistry, *Phys. Chem. Chem. Phys.*, **2019**, 21, 7341-7357.
35. A. C. Roussio *et al.*, Low-Temperature Oxidation of Ethylene by Ozone in a Jet-Stirred Reactor, *J. Phys. Chem. A*, **2018**, 122, 8674-8685.
36. L. Ruwe *et al.*, Consumption and hydrocarbon growth processes in a 2-methyl-2-butene flame, *Combust. Flame*, **2017**, 175, 34-46.
37. L. Ruwe *et al.*, Influences of the molecular fuel structure on combustion reactions towards soot precursors in selected alkane and alkene flames, *Phys. Chem. Chem. Phys.*, **2018**, 20, 10780-10795.
38. H. Selim *et al.*, Premixed flame chemistry of a gasoline primary reference fuel surrogate, *Combust. Flame*, **2017**, 179, 300-311.
41. L. Sheps *et al.*, The reaction of Criegee intermediate CH₂OO with water dimer: primary products and atmospheric impact, *Phys. Chem. Chem. Phys.*, **2017**, 19, 21970-21979.
42. W. Y. Sun *et al.*, Exploring the high-temperature kinetics of diethyl carbonate (DEC) under pyrolysis and flame conditions, *Combust. Flame*, **2017**, 181, 71-81.
43. W. Y. Sun *et al.*, Insights into the oxidation kinetics of a cetane improver-1,2-dimethoxyethane (1,2-DME) with experimental and modeling methods, *Proc. Combust. Inst.*, **2019**, 37, 555-564.
44. W. Y. Sun *et al.*, Exploration of the oxidation chemistry of dimethoxymethane: Jet-stirred reactor experiments and kinetic modeling, *Combust. Flame*, **2018**, 193, 491-501.
45. W. Y. Sun *et al.*, Probing fuel-specific reaction intermediates from laminar premixed flames fueled by two C-5 ketones and model interpretations, *Proc. Combust. Inst.*, **2019**, 37, 1699-1707.
46. W. Y. Sun *et al.*, The influence of dimethoxy methane (DMM)/dimethyl carbonate (DMC) addition on a premixed ethane/oxygen/argon flame, *Proc. Combust. Inst.*, **2017**, 36, 449-457.
48. C. A. Taatjes, Criegee Intermediates: What Direct Production and Detection Can Teach Us About Reactions of Carbonyl Oxides, *Ann. Rev. Phys. Chem.*, Vol 68, eds. M. A. Johnson and T. J. Martinez, 2017, vol. 68, pp. 183-207.
49. C. A. Taatjes *et al.*, Reaction of Perfluorooctanoic Acid with Criegee Intermediates and Implications for the Atmospheric Fate of Perfluorocarboxylic Acids, *Environm. Sci. Techn.*, **2019**, 53, 1245-1251.
50. C. A. Taatjes *et al.*, Hydroxyacetone Production From C-3 Criegee Intermediates, *J. Phys. Chem. A*, **2017**, 121, 16-23.
51. T. Tao *et al.*, A further experimental and modeling study of acetaldehyde combustion kinetics, *Combust. Flame*, **2018**, 196, 337-350.
52. T. Tao *et al.*, Exploring the negative temperature coefficient behavior of acetaldehyde based on detailed intermediate measurements in a jet-stirred reactor, *Combust. Flame*, **2018**, 192, 120-129.
53. T. Tao *et al.*, Investigation of the chemical structures of laminar premixed flames fueled by acetaldehyde, *Proc. Combust. Inst.*, **2017**, 36, 1287-1294.
54. R. Van De Vijver *et al.*, Decomposition and isomerization of 1-pentanol radicals and the pyrolysis of 1-pentanol, *Combust. Flame*, **2018**, 196, 500-514.
55. L. J. Wang *et al.*, Computational singular perturbation analysis of stochastic chemical systems with stiffness, *J. Comput. Phys.*, **2017**, 335, 404-425.
56. Z. Wang *et al.*, Exploring hydroperoxides in combustion: History, recent advances and perspectives, *Progr. Energy Combust. Sci.*, **2019**, 73, 132-181.
57. Z. D. Wang *et al.*, n-Heptane cool flame chemistry: Unraveling intermediate species measured in a stirred reactor and motored engine, *Combust. Flame*, **2018**, 187, 199-216.
58. Z. D. Wang *et al.*, New insights into the low-temperature oxidation of 2-methylhexane, *Proc. Combust. Inst.*, **2017**, 36, 373-382.
59. Z. D. Wang *et al.*, Unraveling the structure and chemical mechanisms of highly oxygenated intermediates in oxidation of organic compounds, *Proc. Nat. Acad. Sci.*, **2017**, 114, 13102-13107.
60. J. Zádor *et al.*, Initiation Reactions in Acetylene Pyrolysis, *J. Phys. Chem. A*, **2017**, 121, 4203-4217.
61. J. Zádor and J. A. Miller, Comment on "Influence of Multiple Conformations and Paths on Rate Constants and Product Branching Ratios. Thermal Decomposition of 1-Propanol Radicals", *J. Phys. Chem. A*, **2019**, 123, 1129-1130.

Theory of Electronic Structure and Chemical Dynamics

Martin Head-Gordon, Eric Neuscamman, David Prendergast

Chemical Sciences Division, Lawrence Berkeley National Laboratory, Berkeley, California 94720.

mhg@cchem.berkeley.edu, millerwh@berkeley.edu, eneuscamman@berkeley.edu, dgprendergast@lbl.gov

Scope of the Project: To expand knowledge of transient species such as radicals relevant to combustion chemistry, atmospheric photochemistry, and other areas including catalysis, new theoretical methods are needed for reliable computer-based prediction of their properties. The two main areas of relevant theory are electronic structure methods and techniques for chemical dynamics. Within electronic structure theory, focus centers on the development of new density functional theory methods and new wave function theories. Examples of current activity include the introduction of combinatorial design strategies for density functionals, and new quantum Monte Carlo approaches for excited states. Newly developed theoretical methods, as well as existing approaches, are employed to study prototype radical reactions, often in collaboration with experimental efforts in the related subtasks (see separate LBNL abstracts). These studies help to deepen understanding of the role of reactive intermediates in diverse areas of chemistry. They also sometimes reveal frontiers where new theoretical developments are needed in order to permit better calculations in the future.

Recent Progress

Due to length limitations, only a selection of projects can be summarized here.

High Accuracy Excited States and Novel Ansatzes. Neuscamman and co-workers have made substantial progress in both novel ansatz design and excited state methods. For excited states, we have developed a new quantum Monte Carlo methodology for the efficient evaluation and optimization of a rigorous excited state variational principle that allows all aspects of a wave function to be tailored for an individual excited state in much the same way as they have long been for ground states. In addition, the methodology can evaluate a rigorous measure of wave function error for ground and excited states alike and so can take a systematic approach to balancing descriptions of different states. These methods for variational excited state evaluations have been paired with cutting-edge quantum Monte Carlo wave function approximations. These include our own introduction of the variation-after-response ansatz that allows a wave function to fully relax itself within the presence of its own linear response, thus capturing important nonlinear effects that are absent in excited state descriptions such as configuration interaction singles and time-dependent density functional theory. Preliminary investigations have shown this approach to be effective in a number charge-transfer examples, where nonlinear orbital relaxations are especially important, and very recently we have demonstrated the approach to be compatible with diffusion Monte Carlo, which opens a clear path from quantum-chemistry-based initial guesses (e.g. TD-DFT) to exceptionally high accuracy Monte Carlo excited state predictions. Also on the excited state wave function front, we have now brought together recent advances in multi-determinant orbital optimization with our variational excited state methodology to show that it is possible to avoid state averaging in multi-reference treatments of excited states. In particular, we have demonstrated that this approach out-performs multi-reference state averaged perturbation theory in the context of a challenging charge transfer example thanks to its ability to fully relax *all* molecular orbitals and the correlation treatment after the charge transfer excitation changes the system's dipole. In addition to excited state methods, we have also developed new wave function approaches to strongly correlated ground states. In one case, new QMC technology has also allowed for the development of a polynomial-cost, variational analogue to pairwise coupled cluster theory. In another case, we have now successfully realized wave function stenciling in real space QMC where it can work in conjunction with diffusion Monte Carlo. This method has already proven capable of accurately dissociating a double bond using a single, restricted Slater determinant, a major simplification compared to traditional multireference approaches.

Density functionals. Head-Gordon and co-workers have been seeking the limit of transferable accuracy that can be achieved with current forms for density functionals. To achieve high accuracy,

non-local density-based corrections for long-range dispersion interactions are added, as well as the option of non-local range-separated hybrid (RSH) treatment of exact exchange. They introduced a novel “survival of the most transferable” (SOMT) procedure to achieve this goal. SOMT is a combinatorial design protocol that involves training a very large numbers of functionals using a fraction of the data, and then selecting the functional that performs best on the remaining data (with the fewest parameters). This approach has been used to create new density functionals (hybrids ω B97M-V, and ω B97X-V, the non-hybrid meta-GGA, B97M-V, and the double hybrid ω B97M(2)), each of which may be most accurate in its class for target problems in chemistry, as measured by performance on test data. A number of new assessments of density functionals have been completed, including for dipole moments, for static polarizabilities, as well as tests of delocalization error and errors associated with bond-breaking.

Electron correlation methods: Head-Gordon and co-workers are developing wavefunction-based electron correlation methods for problems where DFT suffers from self-interaction and/or strong correlation errors. The simplest such approach is a regularized orbital optimized MP2 method (κ -OOMP2) that removes static correlation contributions associated with small gaps. κ -OOMP2 thereby removes artificial symmetry-breaking associated with Hartree-Fock, while retaining essential symmetry-breaking as a signature of strong correlations. κ -OOMP2 has been applied to the fullerenes to address the debate over whether or not C60 is strongly correlated (we conclude it is not). Other noteworthy recent advances concern coupled cluster valence bond (CCVB) theory. CCVB is an inexpensive treatment of strong correlations that is particularly well-suited for describing strong spin correlations. The new extensions to CCVB theory enable any set of chemical bonds to be separated to Hartree-Fock level atoms, with pure spin, at polynomial effort.

Excited-state dynamics and transient inner-shell spectroscopy: Prendergast and co-workers are applying both linear response time-dependent DFT and wave-function methods in the context of fewest-switches surface hopping to explore excited-state dynamics of various small molecules. In particular, for photodissociated outcomes, moving beyond single-reference DFT to multireference methods is necessary. Multiconfigurational self-consistent field (MCSCF) using the restricted active space (RAS) SCF method has been effective in reproducing excited state dynamics induced by UV excitation, from equilibrium, through conical intersections and towards fragmentation. To provide interpretation of ultrafast pump-probe inner-shell transient spectroscopy, we have demonstrated how to effectively interpret such spectra from a physical perspective – separating peaks by species and explaining peaks shifts in terms of orbital character and localization, and exciton binding. We have also successfully extended the application of RASSCF to mixed core-valence excited states, as accessed in pump-probe experiments, and further employed RAS state interaction to include spin-orbit interactions for heavier atoms and to calculate transition amplitudes for transient absorption spectra that probe excited states with nontrivial angular momentum ($l=2$ here).

Future Plans:

(i) *High Accuracy Core Excitations:* Current efforts focus on extending our variational excited state work to core excitations, where the method's ability to capture secondary relaxations beyond the primary excitation will if anything be more relevant than in the charge transfer case. In this context, variation-after-response will be employed to deal with the large orbital relaxations that accompany a core excitation while, in contrast to delta SCF, maintaining a spin-pure structure for the excitation itself. Our accuracy balancing approach will be applied to the difficult problem of predicting peak positions in core spectra. All of these advantages will also be used together to prepare accurate nodal surfaces for use in core excitation diffusion Monte Carlo, thus expanding the remit of this high-accuracy method into a crucial area of chemical spectroscopy.

(ii) *Density functionals:* A series of new tests of density functionals, designed to provide reliable benchmark data that involves energy differences that are distinct from the normal chemical tests, is under construction. Examples include transition metal systems, and spin-gaps. These tests will

inform future development of density functionals, which continues with development of an opposite spin double hybrid that can be evaluated at only 4th order computational cost.

(iv) *Inner shell excitations and spectra*: Prendergast, Neuscamman and Head-Gordon will explore synergies around computational methods for inner-shell excitations. Prendergast will explore useful active space strategies for inner-shell excitations, and extend such techniques to larger systems, where DFT approaches employing final-state approximations have proven accurate for reproducing measurable spectra – X-ray absorption in particular.

Recent Publications Citing DOE Support (2016-2019)

- Blunt, N. S.; Neuscamman, E., Charge-transfer Excited States: Seeking a Balanced and Efficient Wave Function Ansatz in Variational Monte Carlo. *J. Chem. Phys.* **2017**, *147* (19), 194101. DOI: 10.1063/1.4998197.
- Blunt, N. S.; Neuscamman, E., Excited-state diffusion Monte Carlo calculations: a simple and efficient two-determinant ansatz. *J. Chem. Theory Comput.* **2019**, *15*, 178. DOI: 10.1021/acs.jctc.8b00879
- Cotton, S. J. and W. H. Miller, “The Symmetrical Quasi-Classical Model for Electronically Non-Adiabatic Processes Applied to Energy Transfer Dynamics in Site-Exciton Models of Light-Harvesting Complexes”, *J. Chem. Theory Comput.* **2016**, *12*, 983-991; doi: 10.1021/acs.jctc.5b01178
- Cotton, S.J. and W. H. Miller, “A New Symmetrical Quasi-Classical Model for Electronically Non-Adiabatic Processes: Application to the Case of Weak Non-Adiabatic Coupling”, *J. Chem. Phys.* **2016**, *145*, 144108.1-16; doi: 10.1063/1.4963914
- Cotton, S.J., R. Liang, and W. H. Miller, “On the Adiabatic Representation of Meyer-Miller Electronic-Nuclear Dynamics”, *J. Chem. Phys.* **2017**, *147*, 064112; doi: 10.1063/1.4995301
- Goetz, B. V. D.; Neuscamman, E., Suppressing Ionic Terms with Number-Counting Jastrow Factors in Real Space. *J. Chem. Theory Comput.* **2017**, *13*, 2035-2042. DOI: 10.1021/acs.jctc.7b00158
- Hait, D. and M. Head-Gordon, “How accurate is density functional theory at predicting dipole moments? An assessment using a new database of 200 benchmark values.” *J. Chem. Theory Comput.* *14*, 1969–1981 (2018); doi: 10.1021/acs.jctc.7b01252
- Hait, D. and M. Head-Gordon, “xDH double hybrid functionals can be qualitatively incorrect for non-equilibrium geometries: Dipole moment inversion and barriers to radical-radical association using XYG3 and XYGJ-OS”, *J. Chem. Phys.* *148*, 171102 (2018); doi: 10.1063/1.5031027
- Hait, D. and M. Head-Gordon, “Delocalization errors in density functional theory are essentially quadratic in fractional occupation number”, *J. Phys. Chem. Lett.* *9*, 6280–6288 (2018); doi: 10.1021/acs.jpcclett.8b02417
- Hait, D.; A. Rettig, and M. Head-Gordon, “Well-behaved versus ill-behaved density functionals for single bond dissociation: Separating success from disaster functional by functional for stretched H₂”, *J. Chem. Phys.* *150*, 094115 (2019); doi: 10.1063/1.5080122
- Lee, J. and M. Head-Gordon, “Distinguishing Artificial and Essential Symmetry Breaking in a Single Determinant: Approach and Application to the C₆₀, C₃₆, and C₂₀ Fullerenes”, *Phys. Chem. Chem. Phys.* *21*, 4763-4778 (2019); doi: 10.1039/c8cp07613h
- Johansson, K.O.; M. P. Head-Gordon, P.E. Schrader, K.R. Wilson, and H.A. Michelsen, “Resonance-stabilized hydrocarbon- radical chain reactions may explain soot inception and growth”, *Science* *361*, 997–1000 (2018); doi: 10.1126/science.aat3417
- Lee, J.; D.W. Small, and M. Head-Gordon, “Open-shell coupled-cluster valence-bond theory augmented with an independent amplitude approximation for 3-pair correlations: Application to a model oxygen-evolving complex and single molecular magnet”, *J. Chem. Phys.* *149*, 244121 (2018); doi: 10.1063/1.5052667
- Lee, J.; W. Huggins, M. Head-Gordon, and K.B. Whaley, “Generalized unitary coupled cluster wavefunctions for quantum computation”, *J. Chem. Theory Comput.* *15*, 311-324 (2019); doi: 10.1021/acs.jctc.8b01004
- Lehtola, S., M. Head-Gordon, and H. Jónsson, “Complex orbitals, multiple local minima and symmetry breaking in Perdew-Zunger self-interaction corrected density-functional theory calculations”, *J. Chem. Theory Comput.* **2016**, *12*, 3195-3207 (2016); DOI: 10.1021/acs.jctc.6b00347
- Lehtola, S., J.A. Parkhill and M. Head-Gordon, “Cost-effective description of strong correlation: efficient implementations of the perfect quadruples and perfect hexuples models”, *J. Chem. Phys.* **2016**, *145*, 134110 (2016); doi: 10.1063/1.4964317
- Lehtola, S., J.A. Parkhill and M. Head-Gordon, “Orbital optimization in the perfect pairing hierarchy. Applications to full-valence calculations on linear polyacenes”, *Mol. Phys.* *116*, 547-560 (2018); doi: 10.1080/00268976.2017.1342009

- M. Lucas, A.M. Thomas, T. Yang, R.I. Kaiser, A.M. Mebel, D. Hait, M. Head-Gordon, “Exotic Chemistry in the Phenyl - Silane System: Exploring the Prototype of a Radical Substitution Mechanism,” *J. Phys. Chem. Lett.* **9**, 5135–5142 (2018); 10.1021/acs.jpcclett.8b02303
- Mardirossian, N. and M. Head-Gordon, “ ω B97M-V: A combinatorially-optimized, range-separated hybrid, meta-GGA density functional with VV10 nonlocal correlation”, *J. Chem. Phys.* **144**, 214110 (2016); doi: 10.1063/1.4952647
- Mardirossian, N. and M. Head-Gordon, “How accurate are the Minnesota density functionals for thermochemistry, non-covalent interactions, isomerization energies & barrier heights of molecules containing main group elements?” *J. Chem. Theory Comput.* **2016**, *12*, 4303–4325; DOI: 10.1021/acs.jctc.6b00637
- Mardirossian, N. and M. Head-Gordon, “Note: The performance of new density functionals for a recent blind test of non-covalent interactions”, *J. Chem. Phys.* **2016**, *145*, 186101; DOI: 10.1063/1.4967424
- Mardirossian, N.; Pestana, L. R.; Womack, J. C.; Skylaris, C.-K.; Head-Gordon, T.; Head-Gordon, M., Use of the rVV10 Nonlocal Correlation Functional in the B97M-V Density Functional: Defining B97M-rV and Related Functionals. *J. Phys. Chem. Lett.* **2017**, *8*, 35-40; doi: 10.1021/acs.jpcclett.6b02527
- Mardirossian, N. and M. Head-Gordon, “Survival of the most transferable at the top of Jacob’s Ladder: Defining and testing the ω B97M(2) double hybrid density functional”, *J. Chem. Phys.* **148**, 241736 (2018); doi: 10.1063/1.5025226
- Miller, W.H. and S. J. Cotton, “Communication: Wigner Functions in Action-Angle Variables, Bohr-Sommerfeld Quantization, the Heisenberg Correspondence Principle, and a Symmetrical Quasi-Classical Approach to the Full Electronic Density Matrix”, *J. Chem. Phys.* **2016**, *145*, 081101; doi: 10.1063/1.4961551
- Miller, W.H. and S. J. Cotton, “Classical Molecular Dynamics Simulation of Electronically Non-Adiabatic Processes”, *Faraday Discuss.* **2016**, *195*, 9-30; doi: 10.1039/c6fd00181e
- Neuscamman, E. “Communication: Variation After Response in Quantum Monte Carlo” *J. Chem. Phys.* **2016**, *145*, 081103, <http://dx.doi.org/10.1063/1.4961686>
- Pestana, L. R.; Mardirossian, N.; Head-Gordon, M.; Head-Gordon, T., “Ab initio molecular dynamics simulations of liquid water using high quality meta-GGA functionals.” *Chem. Sci.* **2017**, *8*, 3554-3565; doi: 10.1039/c6sc04711d
- Pineda Flores, S. D. and E. Neuscamman, Excited State Specific Multi-Slater Jastrow Wave Functions. *J. Phys. Chem. A* **2019**, *123*, 1487. DOI: 10.1021/acs.jpca.8b10671
- Robinson, P. J.; Pineda Flores, S. D.; Neuscamman, E., Excitation Variance Matching with Limited Configuration Interaction Expansions in Variational Monte Carlo. *J. Chem. Phys.* **2017**, *147* (16), 164114. DOI: 10.1063/1.5008743
- Small, D. W.; Head-Gordon, M., Coupled cluster valence bond theory for open-shell systems with application to very long range strong correlation in a polycarbene dimer. *J. Chem. Phys.* **2017**, *147*, 024107; doi: 10.1063/1.4991797
- Small, D. W. and M. Head-Gordon, “Independent amplitude approximations in coupled cluster valence bond theory: Incorporation of 3-electron-pair correlation and application to spin frustration in the low-lying excited states of a ferredoxin-type tetrametallic iron-sulfur cluster”, *J. Chem. Phys.* **149**, 144103 (2018); doi: 10.1063/1.5046318.
- Stein, T., B. Bandyopadhyay, T. Troy, Y. Fang, O. Kostko, M. Ahmed, and M. Head-Gordon, “Ab initio dynamics and photoionization mass spectrometry reveal ion-molecule pathways from ionized acetylene clusters to benzene cation”, *Proc. Nat. Acad. Sci.* **2017**, *114*, E4125-E4133; doi: 10.1073/pnas.1616464114.
- Witte, J.; Mardirossian, N.; Neaton, J. B.; Head-Gordon, M., Assessing DFT-D3 Damping Functions Across Widely Used Density Functionals: Can We Do Better? *J. Chem. Theory Comput.* **2017**, *13*, 2043-2052; doi: 10.1021/acs.jctc.7b00176
- Witte, J.; Neaton, J. B.; Head-Gordon, M., Effective empirical corrections for basis set superposition error in the def2-SVPD basis: gCP and DFT-C. *J. Chem. Phys.* **2017**, *146*, 234105; doi: 10.1063/1.4986962
- Zhao, L. and Neuscamman, E. “An efficient variational principle for the direct optimization of excited states” *J. Chem. Theory Comput.* **2016**, *12*, 3436, DOI: 10.1021/acs.jctc.6b00508
- Zhao, L. and Neuscamman, E. “Equation of motion theory for excited states in variational Monte Carlo and the Jastrow antisymmetric geminal power in Hilbert space” *J. Chem. Theory Comput.* **2016**, *12*, 3719, DOI: 10.1021/acs.jctc.6b00480
- Zhao, L. and Neuscamman, E. “Amplitude determinant coupled cluster with pairwise doubles” *J. Chem. Theory Comput.* **2016**, *12*, 5841, DOI: 10.1021/acs.jctc.6b00812

Semiclassical Methods for Pressure Dependent Kinetics and Electronically Nonadiabatic Chemistry

Ahren W. Jasper
Chemical Sciences and Engineering Division
Argonne National Laboratory
ajasper@anl.gov

Program Scope

The outcome of a gas phase chemical reaction results from the competition of a variety of underlying microscopic processes, including collisional energy transfer, internal energy redistribution, bonding rearrangements, and inherently quantum mechanical events like electronic transitions. These same phenomena govern reactivity in more complex environments, and a major goal of the project is to develop a comprehensive set of semiclassical approaches for describing the fundamental chemical physics of these phenomena with high accuracy and that are broadly applicable throughout chemistry.

The improvement of first-principles theories via the construction of more and more detailed physical models benefits from the increasing impact of large-scale computing in chemistry, including Argonne's leadership-class resources. Our focus on the development of methods and codes for dynamics and kinetics recognizes that these approaches are now poised to take advantage of the tremendous advances made in electronic structure theory in recent decades. We pursue the development of semiclassical strategies, where the term is used to describe approaches that incorporate one or more quantum effect into simulations involving classical or nearly classical nuclear motion. Semiclassical methods offer a scalable balance of computational cost and accuracy and are well suited for high performance computing. We focus on the advancement of first-principles semiclassical approaches, i.e., methods that are systematically improvable and that may be assigned a priori error bars. We have demonstrated in a variety of contexts that our most detailed semiclassical models have accuracies that match and sometimes even exceed what is possible experimentally and approach the semiclassical accuracy limit of ~20%.

The increased accuracy of a priori theory and its use alongside experiment as an independent source of quantitative chemical and physical information may be anticipated to have a transformative effect in chemical modeling. Recent work supported by this project has continued the development of methods and codes for nonadiabatic dynamics and intersystem crossing, collisional energy transfer and transport, potential energy surface fitting, nonequilibrium reactivity, and rovibrational anharmonicity at high energies and temperatures.

Recent Progress

Using potentials developed by Harding and Georgievskii, Monte Carlo phase space integration (MCPSI) was used to compute full dimensional and fully anharmonic—but classical—rovibrational partition functions for 22 small- and medium-sized molecules and radicals. Several of the species featured multiple minima and low-frequency nonlocal motions, and efficiently sampling these systems was facilitated using curvilinear (stretch, bend, and torsion) coordinates. The curvilinear coordinate MCPSI method was demonstrated to be applicable to the treatment of fluxional species with complex rovibrational structures and as many as 21 fully coupled rovibrational degrees of freedom. Trends in the computed anharmonicity corrections were identified and discussed. In a follow-up study, we

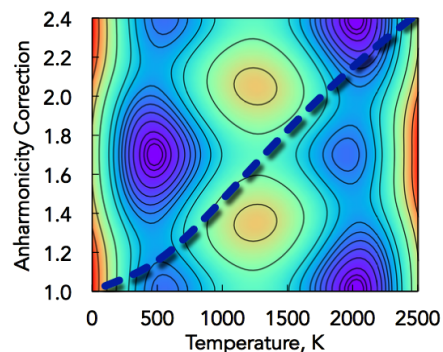


Fig. 1. Correction to the harmonic state count for NH_2OH overlaid over a contour plot of the PES as a function of the $-\text{NH}_2$ inversion and N-O torsion coordinates.

implemented our curvilinear coordinate MCPSI code “at scale” on Argonne’s petascale machine, Theta. There, we calculated semiclassical rovibrational state counts and partition functions for systems with two and three coupled torsions and as many as 30 rotational and vibrational modes. These results were used as benchmarks to quantify the accuracy of simpler reduced-dimensional approaches and analyzed for general physical insights about the nature of fluxional mode coupling at high temperatures and energies. For example, we identified and quantified the effect of low-frequency heavy-atom bends coupling to torsions.

In another project motivated in part by the modeling studies of Sivaramakrishnan, quasiclassical trajectories were used to compute nonthermal rate constants, k^* , for abstraction reactions involving

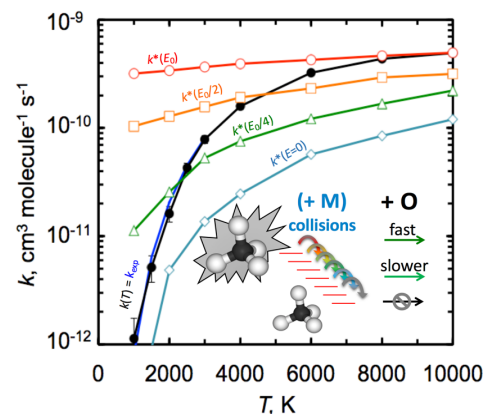


Fig. 2. Nonthermal, k^* , and thermal, k , rate constants for $\text{CH}_4 + \text{O}$. Nonthermal rate enhancements of more than two orders of magnitude are found at 1000 K.

highly-excited methane CH_4^* and the radicals H, O, OH, and O_2 . Several temperatures and internal energies of methane were considered, and significant nonthermal rate enhancements were found. With CH_4^* internally excited close to its dissociation threshold, its reactivity with H, O, and OH was shown to be collision-rate-limited and to approach that of comparably-sized radicals, such as CH_3 , with $k^* > 10^{-10} \text{ cm}^3 \text{ molecule}^{-1} \text{ s}^{-1}$ (see Fig. 2). Rate constants this large are more typically associated with barrierless reactions, and at 1000 K this represents nonthermal rate enhancements of more than two orders of magnitude. We showed that large nonthermal rate constants persisted even after significant internal cooling, and nonthermal channels were shown to account for up to 35–50% of the fate of the products of $\text{H} + \text{CH}_3 = \text{CH}_4^*$ under some conditions of practical relevance to combustion.

With Davis, several schemes for constructing intermolecular potentials using both class-based pairwise Buckingham representations and system-specific permutationally-invariant polynomials representations were automated and tested. We quantified efficiency and accuracy improvements related to the choice of sampling strategy and choice of functional form. In our first effort, we considered four sampling strategies: pseudorandom (P), Sobol quasirandom (S), and biased versions of each (bP and bS). Figure 3 shows the convergence in the out of sample (prediction) error as a function of the number of sampled geometries/energies M for each sampling type. For this system, the biased Sobol scheme is 10x more efficient than the unbiased pseudorandom scheme that is most often used. The optimized scheme requires just ~ 3 ab initio data per parameter. These trends persist both for larger alcohols and in the higher-dimensional fits required for larger bath gases.

With Tranter, the dissociation and the self-recombination of 2-methylallyl radicals were studied using ab initio, transition state theory, classical trajectory, and master equation calculations. The predicted pressure- and temperature-dependent kinetics for both reactions were found to agree very well with the accompanying shock tube measurements (within a factor of 2), with, notably, no adjustments to the theory required. The observed quantitative agreement is likely somewhat fortuitous, as one might expect significant uncertainty in the partition function for the self-recombination adduct (2,5-dimethyl-1,5-hexadiene). Nonetheless, the comparisons provide yet another example of the good accuracy that can be achieved with fully a priori kinetics calculations, including trajectory-based predictions of collisional energy transfer and pressure dependence.

The spin-forbidden and spin-allowed product branching of $^3\text{O} + \text{C}_2\text{H}_4$ was calculated using a combination of quantum

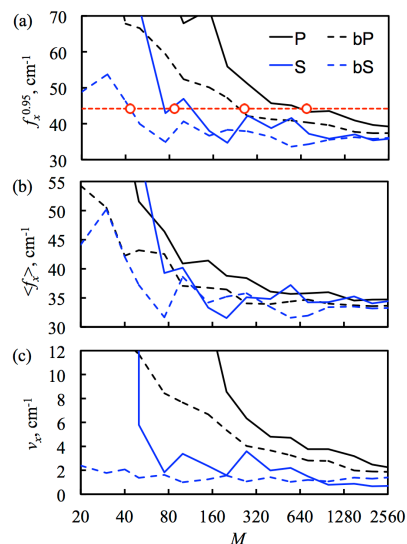


Fig. 3. (a) Convergence of the out of sample error $f_x^{0.95}$ for a separable pairwise $\exp/6$ fit of the $\text{CH}_3\text{OH} + \text{Ar}$ interaction PES as a function of the number of sampled data M . The (b) mean prediction error $\langle f_x \rangle$ and the (c) variance in the fitting error v_x converge at different rates for the four sampling types.

chemistry, master equation, classical trajectory, and nonadiabatic statistical theory calculations. This reaction has been widely studied, and it is known that product branching is largely controlled via the fate of the initial triplet adduct OC_2H_4 , where intersystem crossing (ISC) to the singlet surface competes with spin-allowed bimolecular channels on the triplet surface. Here we used a Landau-Zener statistical calculation for the ISC rate (sometimes called “nonadiabatic transition state theory”) alongside conventional TST to predict the temperature-dependent branching within a single master equation calculation. Product branching immediately following ISC was determined using short-time direct classical trajectories initiated at the crossing seam. Our predicted room temperature branching agreed well with available experimental results, as well as with a previous master equation study of Vereecken and co-workers, who used a more approximate treatment of ISC. The two studies predict different product branching at high temperatures, however.

Future Work

We will continue the development and application of practical predictive models for pressure-dependent chemical kinetics. In ongoing work, collision rates and efficiencies are being generated for hundreds of species with as many as 16 non-hydrogen atoms in three bath gases (He, Ar, and N_2). New potential energy parameterizations were obtained to allow for the treatment of alcohols and peroxides, and previously developed parameterizations were used for hydrocarbons. Analytic formulas for Lennard–Jones collision parameters σ and ε were determined for each of these three classes of systems as a function of the number of non-hydrogen atoms. Collision efficiency parameters ($\alpha = \langle \Delta E_d \rangle$) are being calculated for the normal alkanes, alcohols, and peroxides using a newly developed automation strategy. We find that trends in α can be rationalized based on the number and type of internal rotors, thus allowing for the estimation of collision parameters for species not explicitly considered.

We propose to characterize the low-pressure-limit microcanonical unimolecular rate coefficient, κ_0 , which is intermediate in complexity between the four-dimensional state-to-state rate coefficient $R = ZP$ and the thermal rate coefficient k_0 . The consideration of κ_0 has advantages over the more widely characterized k_0 or R . First, κ_0 may be calculated using classical trajectories without assuming a model for P , thus providing a direct test of the models for P that have been proposed. Second, the additional detail in κ_0 relative to k_0 is useful for rationalizing the often-puzzling trends in relative collision efficiencies that have been observed in k_0 . Finally, κ_0 is the low-pressure-limit analog of the high-pressure-limit’s $\kappa_\infty = N^\ddagger/h\rho$, and transition state theory has been shown to be particularly convenient and accurate for computing κ_∞ . The detailed characterization of κ_0 is a first step in the development of a transition state theory for collisional energy transfer, which is the bottleneck for low-pressure unimolecular reactivity.

We propose to continue to advance the applicability of MCPSI to include systems where the accuracy of existing anharmonicity approaches has not been well characterized, such as transition states and species involving constrained torsions and rings. In earlier work, we approximated the high-dimensional MCPSI integrals via a hierarchy of expressions based on so-called “ n -mode intrinsic” state densities. The 2-mode (pairwise) intrinsic state density Δ_{ij} , for example, is defined for each pair of coordinates i and j as the state density for those modes not represented by the convolution of the one-dimensional densities ρ_i . The full-dimensional density of states is then approximated through second order via convolutions of Δ_{ij} and ρ_k . Intractable high-dimensional integrals are thus computed from convolutions of readily obtained one- and two-dimensional ones. The 2nd-order result can be systematically improved via 3rd- and higher-order corrections. Despite the significant computational savings of this approach, the number of convolutions required can become cumbersome. We will explore approximations where terms are eliminated based on their order with respect to the number of intrinsics in the term. Preliminary studies for CH_4 show that retaining terms with just one 2nd-order intrinsic speeds up the calculation by two orders of magnitude with a negligible (2%) loss of accuracy. This strategy provides a route toward practical applications of MCPSI for very large molecular systems.

Publications supported by this project since 2017

1. A. W. Jasper, L. B. Harding, C. Knight, and Y. Georgievskii, Anharmonic rovibrational partition functions at high temperatures: Tests of reduced-dimensional models for systems with up to three fluxional modes. *J. Phys. Chem. A*, submitted (2019).
2. A. G. Dana, K. B. Moore III, A. W. Jasper, and W. H. Green, Large intermediates in hydrazine decomposition: A theoretical study of the N_3H_5 and N_4H_6 potential energy surfaces. *J. Phys. Chem. A*, submitted (2019).
3. A. W. Jasper and M. J. Davis, Parameterization strategies for intermolecular potentials for predicting trajectory-based collision parameters. *J. Phys. Chem. A*, online (2019). doi: 10.1021/acs.jpca.9b01918
4. A. C. Rousso, N. Hansen, A. W. Jasper, and Y. Ju, Identification of the Criegee intermediate reaction network in ethylene ozonolysis: Impact on energy conversion strategies and atmospheric chemistry. *Phys. Chem. Chem. Phys.* 21, 7341–7357 (2019).
5. A. W. Jasper, R. Sivaramakrishnan, and S. J. Klippenstein, Nonthermal rate constants for $\text{CH}_4^* + \text{X} = \text{CH}_3 + \text{HX}$, $\text{X} = \text{H}, \text{O}, \text{OH}, \text{and } \text{O}_2$. *J. Chem. Phys.* 150, 114112 (2019).
6. S. Elliott, Y.-P. Li, M. S. Johnson, C. Cavallotti, Y. Georgievskii, W. H. Green, M. Pelucchi, J. M. Wozniak, A. W. Jasper, and S. J. Klippenstein, Automated computational thermochemistry for butane oxidation: A prelude to predictive automated combustion kinetics. M. Keçeli, *Proc. Combust. Inst.*, 37, 363–371 (2019).
7. D. H. Bross, A. W. Jasper, B. Ruscic, and A. F. Wagner, Toward accurate high temperature anharmonic partition functions. *Proc. Combust. Inst.* 37, 315–322 (2019).
8. A. C. Rousso, N. Hansen, A. W. Jasper, and Y. Ju, Low-temperature oxidation of ethylene by ozone in a jet-stirred reactor. *J. Phys. Chem. A* 122, 8674–8685 (2018).
9. M. Pfeifle, Y.-T. Ma, A. W. Jasper, L. B. Harding, W. L. Hase, and S. J. Klippenstein, Nascent energy distribution of the Criegee intermediate CH_2OO from direct dynamics calculations of primary ozonide dissociation. *J. Chem. Phys.* 148, 174306 (2018).
10. S. J. Klippenstein, M. Pfeifle, A. W. Jasper, and P. Glarborg, Theory and modeling of relevance to prompt-NO formation at high pressure. *Combust. Flame.* 195, 3–17 (2018).
11. A. W. Jasper, Z. B. Gruey, L. B. Harding, Y. Georgievskii, S. J. Klippenstein, and A. F. Wagner, Anharmonic rovibrational partition functions for fluxional species at high temperatures via Monte Carlo phase space integrals. *J. Phys. Chem. A* 122, 1272–1740 (2018).
12. T. Tao, W. Sun, N. Hansen, A. W. Jasper, K. Moshhammer, B. Chen, Z. Wang, C. Huang, P. Dagaut, and B. Yang, Exploring the negative temperature coefficient behavior of acetaldehyde based on detailed intermediate measurements in a jet stirred reactor. *Combust. Flame.* 192, 120–129 (2018).
13. M. Pfeifle, Y. Georgievskii, A. W. Jasper, and S. J. Klippenstein, Theoretical investigation of intersystem crossing in the cyanonitrene molecule. $^1\text{NCN} \rightarrow ^3\text{NCN}$. *Chem. Phys.* 147, 084310 (2017).
14. D. Nurkowski, A. W. Jasper, J. Akroyd, and M. Kraft, Theoretical study of the Ti-Cl bond cleavage reaction in TiCl_4 . *Z. Phys. Chem.* 231, 1489–1506 (2017).
15. R. S. Tranter, A. W. Jasper, J. B. Randazzo, J. P. A. Lockhart, and J. P. Porterfield, Recombination and dissociation of 2-methyl allyl radicals: Experiment and theory. *Proc. Combust. Inst.* 36, 211–218 (2017).
16. X. Li, A. W. Jasper, J. Zádor, J. A. Miller, and S. J. Klippenstein, Theoretical kinetics of $\text{O} + \text{C}_2\text{H}_4$. *Proc. Combust. Inst.* 36, 219–227 (2017).
17. A. M. Mebel, Y. Georgievskii, A. W. Jasper, and S. J. Klippenstein, Temperature- and pressure-dependent rate coefficients for the HACA pathways from benzene to naphthalene. *Proc. Combust. Inst.* 36, 919–926 (2017).

ARGONNE-SANDIA CONSORTIUM ON HIGH-PRESSURE COMBUSTION CHEMISTRY

Ahren W. Jasper, Stephen J. Klippenstein (PI), Raghu Sivaramakrishnan, Robert S. Tranter,
Chemical Sciences and Engineering Division, Argonne National Laboratory, Argonne, IL, 60439

Leonid Sheps, Craig A. Taatjes (PI)
Combustion Research Facility, Mail Stop 9055, Sandia National Laboratories Livermore, CA 94551-0969
sjk@anl.gov; lsheps@sandia.gov; cataatj@sandia.gov

Program Scope: The goal of this project is to explore the fundamental effects of pressure on chemical kinetics and to employ that knowledge in the development of accurate models for combustion chemistry at the high pressures of current and future combustion devices. We design and implement novel experiments, theory, and modeling to probe high-pressure combustion kinetics from elementary reactions, to submechanisms, and eventual application to flames. We continue to invest in the development of sensitive time-resolved experimental probes of reaction kinetics that enable direct pressure-dependent studies of chemical systems of interest to high-pressure combustion chemistry and other DOE energy missions. Our experimental facilities include a miniature high-repetition rate shock tube (HRRST) and three variable-pressure flow reactors. Among them, these apparatuses cover a wide range of conditions (300 – 2500 K, 0.001 – 100 bar) and exploit complementary diagnostic methods: laser-induced fluorescence (LIF), broadband cavity-enhanced absorption spectroscopy (BB-CEAS), electron impact mass spectrometry, and photoionization mass spectrometry (PIMS). We aim to integrate modeling, experiment, and theory (MET) through feedback loops at all levels of chemical complexity. We are currently developing and testing the methodology for small alkanes, alcohols, and ethers as key prototype fuels. The consortium expands and enhances collaborations between Argonne’s Chemical Dynamics in the Gas Phase Group and the Combustion Chemistry Group in Sandia’s Combustion Research Facility.

Recent Progress:

Experimental method development We have extended the accessible experimental T and P range of an existing time-resolved BB-CEAS apparatus (L. Sheps, *J. Phys. Chem. Lett.* **4**, 4201-4205 (2013)) to perform measurements of pressure-dependent gas-phase chemical reactions of interest to HPCC. The apparatus consists of a laser photolysis flow reactor, housed inside an optical resonator cavity, and a unique detector which records the temporal evolution of the entire broadband absorption spectrum for each laser shot. The optical cavity uses “white-light” probe radiation from a Xe arc lamp and achieves effective optical path lengths of ~ 40 m over $\lambda = 300 - 450$ nm or $370 - 700$ nm simultaneously. Recent modifications to the apparatus include the introduction of an inline gas mixer (for on-the-fly mixing of multiple sample gases at P up to 1 atm) and a heating jacket with 4 independent sections (to ensure flat temperature profiles up to $T = 700$ K). The high sensitivity of this apparatus in the UV-VIS range will enable the time-resolved detection of key gas-phase radicals (e.g. formyl, vinyl, allyl, propargyl), and closed-shell species (e.g. formaldehyde, Criegee intermediates).

With the HRRST we have recently implemented a lab-scale photoionization source with a shock tube/TOFMS apparatus. The source consists of a resonance flow lamp in which a discharge is established in a low-pressure gas. In proof-of-concept experiments, argon has been shock heated in the HRRST and detected in the pre- and post-shock regimes. Good quality peaks for Ar^+ were obtained by averaging 100 experiments. Work is ongoing to find optimal conditions for ionizing/detecting organic species with this PI source and it is anticipated that lab HRRST/PIMS experiments will be a valuable complement to synchrotron PIMS.

Shock-tube measurements of pyrolysis Recent PIMS experiments with the HRRST at the ALS have focused on the pyrolysis of alcohols (1-butanol, 2-butanol, neopentanol), siloxanes (hexamethyldisiloxane and hexamethylcyclotrisiloxane) and the reactions of *i*-butyl radicals. These experiments are focused on examining competing elementary reaction paths and determining temperature and pressure dependencies of branching fractions. The experiments with neopentanol, *i*-pentyl nitrite and

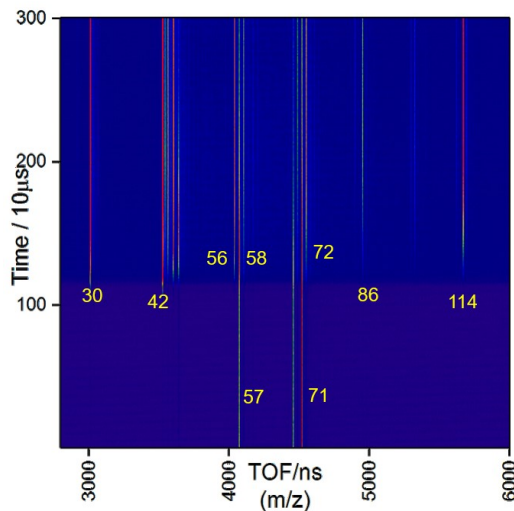


Figure 1: HRRST/PIMS 0.25% *i*-pentyl nitrite/ Ar . $T_5 \sim 880$ K, $P_5 \sim 8$ bar, I.E. 9-11 eV. Peaks are labeled with m/z . Parent ion (m/z 117) signal is weak and not visible on this plot.

the siloxanes complement lower pressure shock tube laser schlieren and TOFMS experiments. An example HRRST/PIMS result on the dissociation of *i*-pentyl nitrite, the source of *i*-butyl radicals, is shown in Fig. 1 and illustrates the type of data obtained at the ALS. *i*-Pentyl nitrite (m/z 117) decomposes to ultimately yield *i*-butyl radical (m/z 57), H_2CO and NO . Over the experimental range of 750-900K *i*-butyl radicals undergo dissociation to propene and methyl (m/z 42 and 15), recombination to 2,5-dimethylhexane (m/z 114) and disproportionation to propane and propene (m/z 58 and 56). *i*-Butyl also undergoes addition to methyl radicals. The products observed in the post-shock region ($t > 1000 \mu s$) are consistent with the above reactions and provide valuable insights into the complex chemistry occurring. In the pre-shock region ($t < 1000 \mu s$) m/z 57 and 71 are seen and arise from fragmentation of *i*-pentyl nitrite (m/z 117) in the ion source. Similar observations can be made about the results of the experiments with other molecules and they are leading to a deeper understanding of radical recombination chemistry, roaming reactions and the competition between pathways in multichannel reactions.

Thermal decomposition of Criegee Intermediates (i): Criegee intermediates (CI) are key atmospheric species because they oxidize trace inorganic compounds and because some isomers of CI with 2 or more C atoms decompose rapidly to OH + co-product even at atmospheric T . In contrast to their atmospheric impact, very little is known about CI reactivity at higher T and P , although the smallest CI, CH_2OO , was proposed as an intermediate in dimethyl ether (DME) combustion (Andersen, A.; Carter, E. A., *J. Phys. Chem. A*, **107**, 9463-9478 (2003); *Mol. Phys.* **106**, 367-396 (2008)). Although CH_2OO is thermally stable at room T , it may decompose rapidly at combustion conditions *via* dioxirane and formic acid intermediates, ultimately leading to either radical ($OH + HCO$) or closed shell products ($H_2 + CO_2$, $H_2O + CO$). Knowledge of the rates and products of CI decomposition is therefore important in modeling the combustion of DME and larger ethers.

We investigated the thermal decomposition of CH_2OO and its deuterated analog, CD_2OO , by time-resolved UV absorption spectroscopy using the upgraded TR-BB-CEAS apparatus at $T = 450 - 650$ K and $P = 10 - 350$ Torr. These experiments were combined with probing of the OH radical products from CH_2OO and with Master Equation modeling, led by collaborators at the University of Leeds, UK. We observed strongly T - and P -dependent decay timescales that spanned the low-pressure, falloff, and high-pressure regimes, allowing reliable benchmarking of the theoretical calculations. The decomposition rates of CH_2OO and CD_2OO range from $<< 1 s^{-1}$ at 300 K to $> 10^4 s^{-1}$ at 650K, which explains why CH_2OO has never been directly detected in DME combustion. The OH yield in CH_2OO decomposition is $< 1\%$, independent of T and P , meaning that closed-shell product channels are always dominant.

Low-temperature autoignition chemistry of ethers (j): We expanded on our earlier work on ether autoignition chemistry by comparing the competition among second O_2 addition and QOOH dissociation in the 6-membered cyclic ether tetrahydropyran and the analogous cyclic alkane cyclohexane. QOOH radicals are produced by isomerization of primary peroxy radicals in hydrocarbon oxidation; further oxidation of QOOH (the second O_2 addition) leads to radical chain branching *via* the ketohydroperoxide (KHP) intermediate.

We probed these reactions at $T = 500 - 700$ K, $P = 10$ and 1500 Torr, using the high-pressure PIMS apparatus, constructed in 2017 under the HPCC funding. We detected KHP – the key markers of second O_2 addition – in both tetrahydropyran and cyclohexane at $P = 1500$ Torr. However, although KHP signals persisted at T up to 700 K in cyclohexane, they disappeared by 650 K in tetrahydropyran and were instead replaced by products of QOOH decomposition: pentanedial, vinyl formate, and 3-buten-1-al. These results highlight an important feature of ether oxidation chemistry: the weak C-O bonds in the molecular backbone of ethers enable QOOH decomposition pathways at lower temperatures than in alkanes. These bond scission pathways compete with second O_2 addition to QOOH and hence reduce the reactivity of ether at combustion conditions, relative to alkanes.

Nonthermal Kinetics of Hot Stable Molecules (p): Recent theoretical studies have indicated that ephemeral radical collision complexes (formed by barrierless exothermic reactions of radicals with O_2 or other stable species) can undergo facile termolecular reactive collisions with radicals (another barrierless process). Such termolecular reactions were found to impact global reactivity in radical-rich combustion environments such as flames. Radical-radical recombination reactions (also barrierless processes) are typically more exothermic and can form highly energized stable species (potentially with longer lifetimes than ephemeral radical complexes). In this work, quasiclassical trajectory calculations, along with previously published potential energy surfaces, were used to compute nonthermal rate constants for $CH_4 + X$ ($X = H, O,$ and OH) as a function of temperature and of the vibrational energy of methane, E_{vib} . For large values of E_{vib} , CH_4^* was found to react with X as rapidly as a comparably sized radical (CH_3), with rate constants close to those of barrierless reactions (see Fig. 2) approaching the collision limit ($> 10^{-10} cm^3 molecule^{-1} s^{-1}$). These nonthermal rate constants represent an enhancement for near-threshold values of E_{vib} of more than two orders of magnitude at 1000 K. By varying the internal energy of CH_4^* , E_{vib} , we showed that fast nonthermal rate constants persist even after $\sim 100s$ of thermalizing collisions and significant cooling of CH_4 . Each abstractor showed a slightly different dependence on E_{vib} , which could be correlated with the different barriers for abstraction.

The competition between nonthermal reaction and collisional cooling was studied at 1000 K using a simple model. We showed that due to the fast nonthermal rates for H, O, and OH, as well as their weak dependence on collisional cooling at large E_{vib} , nonthermal reactions can account for from one-third to one-half (see Figure 3) of the fate of CH_4^* formed via $\text{H} + \text{CH}_3$ when the concentrations of the abstracting radicals are at their peak concentrations of $\sim 0.5\text{--}2\%$. A more limited study of $\text{X} = \text{O}_2$ was carried out. Although the nonthermal rates constants k^* are smaller for this system than for the other abstractors, the relative enhancement k^*/k is many orders of magnitude and the abundance of O_2 in flames is higher. Altogether, we found that around 10-15% of CH_4^* was diverted to $\text{CH}_3 + \text{HO}_2$ instead of stabilized CH_4 at 1000 K, which could nonetheless be an important source of radicals under some conditions.

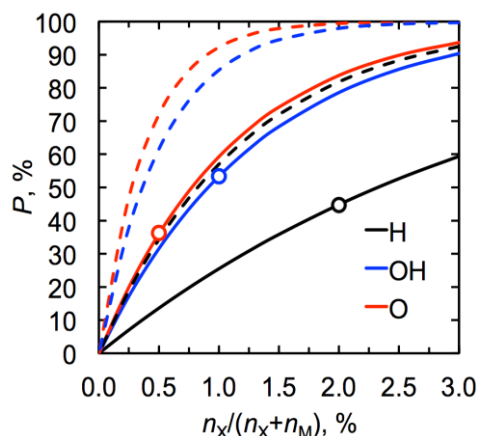


Fig. 3. Fraction P of CH_4^* that reacts with X before thermalizing vs. $[\text{X}]$. Results for estimated vibrational E (solid lines) and total E (dashed lines) cooling rates.

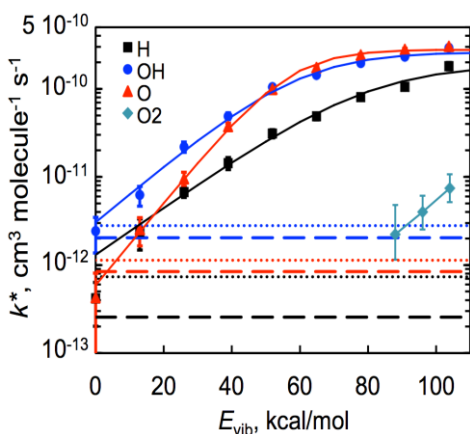


Fig. 2. k^* for $\text{CH}_4^* + \text{X}$ at 1000 K as a function of E_{vib} . Horizontal lines show computed (dotted) and experimental (dashed) thermal rate constants for comparison.

During the next year we will focus on linking the theory and experiments by developing a comprehensive model of DME oxidation. Furthermore, building on our previous studies of tetrahydropyran and tetrahydrofuran (THF), we will explore the autoignition of diethyl ether, $\text{CH}_3\text{CH}_2\text{OCH}_2\text{CH}_3$. This linear compound has key differences from the smaller DME, from similarly-sized cyclic ether THF, and from similarly-sized alkanes. It will therefore be an important point of comparison with propane, butane, DME, and THF in our efforts to understand the links between chemical structure and reactivity.

HRRST: We plan to extend the studies of reactions of alkyl and alkenyl radicals at high pressures and temperatures relevant to autoignition under conditions where addition/elimination reactions are largely suppressed. These will allow more accurate determinations of branching between recombination and disproportionation reactions and examine how these fractions change with molecular structure, size and reaction pressure. The pyrolysis experiments will also act as

These non-thermal reactions were represented as termolecular processes in detailed kinetics models. The inclusion of these termolecular processes along with a corresponding decrease ($\sim 10\text{--}30\%$) in the rate constants for the recombination reaction ($\text{H} + \text{CH}_3 \rightarrow \text{CH}_4$) led to noticeable ($\sim 10\%$) enhancements in laminar flame speeds for CH_4 -air at 1 atm, 300 K. An effective temperature model was also developed as part of this work. Preliminary results from this model indicate that termolecular reactions may also be effective in other radical recombinations (i. e. $\text{H} + \text{OH} + \text{M}$, $\text{OH} + \text{OH} + \text{M}$, $\text{H} + \text{HCO} + \text{M}$) forming stable species (with $\sim 7\text{--}8$ atoms or less). The ramifications of including these termolecular reactive processes and representing them properly in kinetic models will be explored in ongoing and future studies.

Future Directions:

Autoignition of hydrocarbon and oxygenated compounds: We plan to leverage our recent efforts in exploring the autoignition of alkanes (propane, n-butane) and ethers (DME, diethyl ether) to further develop a comprehensive understanding of the influence of molecular structure on low-temperature oxidation chemistry. We will extend our recent work on propane oxidation to higher pressures. The earlier studies at $P = 4$ Torr quantified the reaction flux through QOOH channels using PIMS probing (*J. Phys. Chem. A* **119**, 7095-7115, 7116-7129 (2015)) but did not reveal any evidence of second O_2 addition. Theory and modeling conducted by HPCP suggests that the second O_2 addition channels grow significantly in importance at $P = 10$ atm; thus, we propose to directly probe these chain-branching pathways at 10 atm and higher. Furthermore, in collaboration with A. Eskola (Helsinki) we plan to complete the ongoing study of n-butane oxidation using high- P PIMS. Our earlier work on n-butane (*J. Phys. Chem. A* **117**, 12216-12235 (2013); *Proc. Comb. Inst.* **35**, 291-298 (2015)) demonstrated the second- O_2 addition reactions by detection of the KHP intermediates. We will focus on the formation timescale and the subsequent decomposition products of KHP.

Similarly, we will complete our ongoing study of DME autoignition. We have already made significant progress in quantum chemical calculations of DME oxidation and have accumulated an extensive dataset from PIMS studies at up to 700 K and 40 atm.

a basis for oxidation of hydrocarbon radicals. Development of lab based PIMS source will continue as will efforts to develop methods to allow kinetic data to be extracted from PIMS data.

Non-thermal kinetics: Ongoing HPCC modeling suggests that prompt dissociation of oxygenated radicals is common at elevated temperatures. We plan to probe this prompt (non-thermal) decomposition of several prototypical radicals. We will investigate the decomposition of 1- and 2-hydroxyethyl radicals, formed by H atom loss from ethanol, which dissociate to $\text{CH}_2=\text{CHOH}$ or $\text{CH}_3\text{CHO} + \text{H}$ and to ethene + OH, respectively. We will also study the radicals CH_3OCO and CH_2OCHO , derived from methyl formate. These species are predicted to decompose to $\text{CH}_3 + \text{CO}_2$ and $\text{CH}_2\text{O} + \text{HCO}$, respectively. We will quantify the yields and formation timescales for the products of these decomposition reactions by PIMS as a function of T and P ; the experimental measurements will then benchmark preliminary calculations, which are already underway. Detailed comparisons will be made with theory-based models to provide definitive descriptions of the prompt dissociation process.

We propose to continue dynamical and modeling studies of hydrocarbon radical prompt dissociations. While our prior combustion modeling studies focused on prompt dissociation of HCO, it is evident that prompt dissociation is a common feature in the dissociations of most weakly-bound hydrocarbon and oxygenated radicals. We propose to extend our combustion modeling studies by characterizing the role of prompt dissociations of all weakly-bound radicals in the high temperature oxidations of primary reference fuels such as n-heptane and iso-octane. Preliminary simulations are also being performed using our core mechanism to design PIMS experiments to probe thermal decompositions (and potentially prompt dissociations) of radicals generated with CI abstractions from ethanol and methyl formate. Lastly, recent theoretical dynamical studies have postulated the role of alternative (i. e. isomerization, H_2 elimination via roaming) reaction pathways to explain the observations from photodissociation studies of energized C_2H_5 radicals. In high temperature combustion, the addition process in $\text{H} + \text{C}_2\text{H}_4$ is a dominant process and is an important source for C_2H_5 radicals. We propose to experimentally and theoretically characterize the dissociation pathways of potentially energized ethyl radicals formed under such conditions.

A priori pressure-dependent kinetics: We will apply our a priori trajectory methods for predicting collisional energy transfer and our two-dimensional master equation methods for predicting pressure dependent kinetics. Specifically, we will fully characterize from first-principles the temperature and bath gas dependence of the important combustion reactions $\text{H} + \text{O}_2$ (+M), $\text{H} + \text{OH}$ (+M), and $\text{OH} + \text{OH}$ (+M). We will also predict pressure-dependent kinetics for a series of spin-forbidden reactions: $\text{O} + \text{CO}$ (+M), $\text{O} + \text{N}_2$ (+M), $\text{NH} + \text{CO}$ (+M), and $\text{NH} + \text{N}_2$ (+M). These studies will make use of our recent advances in potential energy surface fitting, automation, predicting rovibrational anharmonicity, and statistical theories for intersystem crossing.

Publications acknowledging support from this program, 2017-Present

- a. **From Theoretical Reaction Dynamics to Chemical Modeling of Combustion**, S. J. Klippenstein, *Proc. Comb. Inst.* **36**, 219-227 (2017).
- b. **Ramifications of Including Non-Equilibrium Effects for HCO in Flame Chemistry**, N. J. Labbe, R. Sivaramakrishnan, C. F. Goldsmith, Y. Georgievskii, J. A. Miller, S. J. Klippenstein, *Proc. Comb. Inst.* **36**, 525-532 (2017).
- c. **Influence of Oxygenation in Cyclic Hydrocarbons on Chain-Termination Reactions from $\text{R} + \text{O}_2$: Tetrahydropyran and Cyclohexane**. B. Rotavera, J. D. Savee, I. O. Antonov, R. L. Caravan, L. Sheps, D. L. Osborn, J. Zádor, and C. A. Taatjes. *Proc. Combust. Inst.*, **36**, 597-606 (2017).
- d. **Direct Experimental Probing and Theoretical Analysis of the Reaction between the Simplest Criegee Intermediate CH_2OO and Isoprene**, Z. C. J. Decker, K. Au, L. Vereecken, L. Sheps, *Phys. Chem. Chem. Phys.*, **19**, 8541-8551 (2017).
- e. **Time-Resolved Measurements of Product Formation in the Low-Temperature (550 – 675 K) Oxidation of Neopentane: a Probe to Investigate Chain-Branching Mechanism**. A. J. Eskola, I. O. Antonov, L. Sheps, J. D. Savee, D. L. Osborn, and C. A. Taatjes. *Phys. Chem. Chem. Phys.*, **19**, 13731-13745 (2017).
- f. **High Pressure Oxidation of Ethane**, H. Hashemi, J. G. Jacobsen, C. T. Rasmussen, J. M. Christensen, P. Glarborg, S. Gersen, M. van Essen, H. B. Levinsky, S. J. Klippenstein, *Combust. Flame*, **182**, 150-166 (2017).
- g. **Modeling Nitrogen Chemistry in Combustion**, P. Glarborg, B. Ruscic, J. A. Miller, S. J. Klippenstein, *Prog. Energy Combust. Sci.*, **67**, 31-68 (2018).
- h. **Theory and Modeling of Relevance to Prompt-NO Formation at High Pressure**, S. J. Klippenstein, M. Pfeifle, A. W. Jasper, P. Glarborg, *Combust. Flame* **195**, 3-17 (2018).
- i. **Unimolecular decomposition kinetics of the stabilised Criegee intermediates CH_2OO and CD_2OO** , D. Stone, K. Au, S. Sime, D. J. Medeiros, M. Blitz, P. W. Seakins, Z. Decker and L. Sheps, *Phys. Chem. Chem. Phys.* **20**, 24940-24954 (2018).
- j. **The reaction of hydroxyl and methylperoxy radicals is not a major source of atmospheric methanol**, R. L. Caravan, M. A. H. Khan, J. Zador, L. Sheps, I. O. Antonov, B. Rotavera, K. Ramasesha, K. Au, M. W. Chen, D. Rosch, D. L. Osborn, C. Fittschen, C. Schoemaeker, M. Duncianu, A. Griira, S. Dusanter, A. Tomas, C. J. Percival, D. E. Shallcross and C. A. Taatjes, *Nature Communications* **9**, (2018).
- k. **Kinetics of 1-Butyl and 2-Butyl Radical Reactions with Molecular Oxygen: Experiment and Theory**, A. J. Eskola, T. T. Pekkanen, S. P. Joshi, R. S. Timonen, S. J. Klippenstein, *Proc. Combust. Inst.*, **37**, 291-298 (2019).
- l. **High-Pressure Oxidation of Propane**, H. Hashemi, J. M. Christensen, L. B. Harding, S. J. Klippenstein, P. Glarborg, *Proc. Combust. Inst.*, **37**, 461-468 (2019).
- m. **Direct Measurements of Channel Specific Rate Constants in $\text{OH} + \text{C}_3\text{H}_8$ illuminates prompt dissociations of propyl radicals**, R. Sivaramakrishnan, C. F. Goldsmith, S. L. Peukert, J. V. Michael, *Proc. Combust. Inst.*, **37**, 231-238 (2019).
- n. **Reference Natural Gas Flames at Nominally Autoignitive Engine-Relevant Conditions**, A. Krisman, C. Mounaim-Rousellet, R. Sivaramakrishnan, J. A. Miller, J. H. Chen, *Proc. Combust. Inst.*, **37**, 1631-1638 (2019).
- o. **Comment on "Influence of Multiple Conformations and Paths on Rate Constants and Product Branching Ratios. Thermal Decomposition of 1-Propanol Radicals"**, J. Zador, J. A. Miller, *J. Phys. Chem. A*, **123**, 1129-1130 (2019).
- p. **Nonthermal Rate Constants for $\text{CH}_4^* + \text{X} \rightarrow \text{CH}_3 + \text{HX}$, $\text{X} = \text{H}, \text{O}, \text{OH}$, and O_2** . A. W. Jasper, R. Sivaramakrishnan, S. J. Klippenstein, *J. Chem. Phys.* **150**, 114112 (2019).
- q. **Influence of ether functional group on ketohydroperoxide formation in cyclic hydrocarbons: tetrahydropyran and cyclohexane**, J. C. Davis, A. L. Koritzke, R. L. Caravan, I. O. Antonov, M. G. Christianson, A. C. Doner, D. L. Osborn, L. Sheps, C. A. Taatjes, and B. Rotavera, *J. Phys. Chem. A* doi:10.1021/acs.jpca.8b12510 (2019).

Probing the Reaction Dynamics of Hydrogen-Deficient Hydrocarbon Molecules and Radical Intermediates via Crossed Molecular Beams

Ralf I. Kaiser

Department of Chemistry, University of Hawai'i at Manoa, Honolulu, HI 96822

ralfk@hawaii.edu

1. Program Scope

The major goals of this project are to explore experimentally by exploiting molecular beams the fundamental reaction dynamics and underlying potential energy surfaces (PESs) of hydrocarbon molecules and their corresponding (resonantly free stabilized and aromatic) radical precursors, which are relevant to the formation and molecular growth of polycyclic aromatic hydrocarbons (PAHs). First, reactions are initiated in a crossed molecular beams machine under single collision conditions by crossing two supersonic reactant beams containing radicals and/or closed shell species under a well-defined collision energy and intersection angle. By recording angular-resolved time of flight (TOF) spectra, we obtain information on the reaction products, intermediates involved, branching ratios of competing reaction channels, reaction energetics, and on the underlying reaction mechanisms. Second, in collaboration with Dr. Musahid Ahmed (Advanced Light Source, Lawrence Berkeley Laboratory), reactions are carried out in a chemical reactor at well characterized pressure and temperature distributions with reaction products interrogated isomer-selectively by tunable vacuum ultraviolet light (VUV) via photoionization (PI) coupled with a reflectron time of flight mass spectrometer (ReTOFMS). Merged with electronic structure calculations (Prof. Alexander M. Mebel, Florida International University), these data are of crucial importance to comprehend the detailed formation mechanisms of two key classes of molecules involved in mass-growth processes leading to carbonaceous nanostructures from the bottom up: resonantly stabilized free radicals (RSFRs) and polycyclic aromatic hydrocarbons (PAHs).

2. Recent Progress

2.1. Formation of Resonantly Stabilized Free Radicals (RSFRs)

The energetics and dynamics involved in the formation of resonantly stabilized free radicals (RSFRs) are of paramount importance in untangling the formation of soot particles, polycyclic aromatic hydrocarbons (PAHs), and their hydrogen deficient precursors from the 'bottom up' in combustion processes. Here, we investigated the formation and stability of two key classes of resonantly stabilized free radicals (RSFR) under single collision conditions via crossed molecular beam studies through the reactions of ground state carbon atoms ($C(^3P)$) as well as ground and excited state dicarbon molecules ($C_2(X^1\Sigma_g^+/a^3\Pi_u)$): C_8H_7 [P7] and C_5H_3 [P9]. Besides the first gas phase synthesis of the elusive cyclooctatetraenyl radical (C_8H_7) via (non) aromatic triplet cyclooctatriene intermediates (C_8H_8) [P7], these investigations revealed the involvement of resonantly stabilized acyclic doublet radicals by exploiting a novel supersonic dicarbon source [P9]: 1,4-pentadiynyl-3 [$HCCCHCCH(X^2B_1)$], 2,4-pentadiynyl-1 [$H_2CCCCCH(X^2B_1)$], and the previously unknown doublet penta-1-yn-3,4-dienyl-1 [$H_2CCCHCC(X^2A)$] radical.

2.2. Reaction Dynamics of the 1-Propynyl Radical ($CH_3CC(X^2A_1)$) – An Isomer of the Resonantly Stabilized Free Propargyl (H_2CCCH) Radical with Acetylene (C_2H_2) and 1,3-Butadiene (C_4H_6)

First, we investigated the 1-propynyl (CH_3CC ; X^2A_1) plus acetylene/acetylene- d_2 ($HCCH/DCCD$; $X^1\Sigma_g^+$) system under single-collision conditions using the crossed molecular beams method. The reaction was found to produce C_5H_4 plus atomic hydrogen (H) via an indirect reaction mechanism with a reaction energy of -123 ± 18 kJ mol $^{-1}$. Using D1-acetylene ($HCCD$), we confirmed that the hydrogen atom is lost from the acetylene reactant. Our computational analysis suggests the reaction proceeds by the barrierless addition of the 1-propynyl radical to acetylene, resulting in C_5H_5 intermediate(s) that dissociate(s) preferentially to methylidyne (CH_3CCCCH ; X^1A_1) via hydrogen atom emission with a computed reaction energy of -123 ± 4 kJ mol $^{-1}$. The barrierless nature of this reaction scheme suggest the 1-propynyl radical may be a key intermediate in hydrocarbon chain growth even in low temperature environments at temperatures as low as 10 K [P12].

Second, the crossed beams reactions of the 1-propynyl radical (CH_3CC ; X^2A_1) with 1,3-butadiene ($\text{CH}_2\text{CHCHCH}_2$; X^1A_g), 1,3-butadiene- d_6 ($\text{CD}_2\text{CDCDCD}_2$; X^1A_g), 1,3-butadiene- d_4 ($\text{CD}_2\text{CHCHCD}_2$; X^1A_g), and 1,3-butadiene- d_2 ($\text{CH}_2\text{CDCDC}_2$; X^1A_g) were performed under single collision conditions at collision energies of about 40 kJ mol^{-1} . The underlying reaction mechanisms were unraveled through the combination of the experimental data with electronic structure calculations at the CCSD(T)-F12/cc-pVTZ-f12//B3LYP/6-311G(d,p) + ZPE(B3LYP/6-311G(d,p)) level of theory along with statistical Rice-Ramsperger-Kassel-Marcus (RRKM) calculations. Experimentally, the data suggests the reaction involves two product channels indirectly via hydrogen atom (H) emission with representative reaction energies of $-108 \pm 21 \text{ kJ mol}^{-1}$ ($62 \pm 10 \%$) and $-373 \pm 37 \text{ kJ mol}^{-1}$ ($38 \pm 10 \%$). Our electronic structure calculations suggest these channels correspond to the formation of 1,3-heptadien-5-yne (**p1** + H; $-117 \pm 4 \text{ kJ mol}^{-1}$) and toluene (**p2** + H; $-368 \pm 4 \text{ kJ mol}^{-1}$) via the barrierless addition of 1-propynyl to the 1,3-butadiene terminal carbon atoms forming a low-lying C_7H_9 intermediate that dissociates to **p1** plus atomic hydrogen or undergoes multiple isomerization steps resulting in cyclization and ultimately aromatization following hydrogen atom elimination to form **p2**. This is further supported by RRKM theory, where **p1** and **p2** hold a respective 57.9 % and 15.5 % of the C_7H_8 yield at the experimental collision energy and are the most abundant of six considered C_7H_8 isomers. Since the 1-propynyl radical may be present in extreme environments such as high temperature combustion systems and in low temperature molecular clouds, it could potentially serve as a carrier of the methyl group incorporating itself into methyl-substituted (poly)acetylenes or aromatic systems such as toluene via overall exoergic reaction mechanisms that are uninhibited by an entrance barrier. Such pathways are a necessary alternative to existing high energy reactions leading to toluene that are formally closed in the cold regions of space and are an important step toward understanding the synthesis of polycyclic aromatic hydrocarbons (PAHs) in its harsh extremes [P17].

2.3. Formation Mechanisms and Reaction Dynamics of PAHs Carrying Three Rings

Having elucidated the formation mechanisms and chemical dynamics leading to (hydrogenated and substituted) PAHs carrying two rings, i.e. naphthalene (two six membered rings; C_{10}H_8) and indene (one six and one five membered ring; C_9H_8) [P1, P4, P11], we elucidated fundamental reaction mechanisms leading to the formation of three-ring PAHs carrying three six membered rings [phenanthrene ($\text{C}_{14}\text{H}_{10}$) and anthracene ($\text{C}_{14}\text{H}_{10}$) [P5, P13] within a pyrolytic reactor [P14]. These studies revealed that the hydrogen abstraction acetylene addition (HACA) mechanism starting from non-PAH radicals such as biphenyl (C_{12}H_9) reacting with acetylene (C_2H_2) can synthesize via bay-closure phenanthrene ($\text{C}_{14}\text{H}_{10}$), but not the anthracene isomer ($\text{C}_{14}\text{H}_{10}$) [P5]. On the other hand, the hydrogen abstraction vinylacetylene addition (HAVA) mechanism commencing from 1- and 2-naphthyl radicals (C_{10}H_7) reacting with vinylacetylene (C_4H_4) can form via ring annulation phenanthrene ($\text{C}_{14}\text{H}_{10}$) and anthracene ($\text{C}_{14}\text{H}_{10}$) (Figure 1) via barrierless reactions of aryl-type aromatic radicals with vinylacetylene [P13]. These studies highlight the complementary nature of HACA and HAVA to two dimensional (planar) PAHs via bay-closure and barrierless ring annulation with HAVA operating even at ultralow temperatures such as 10 K.

2.4. Formation Mechanisms and Reaction Dynamics to PAHs Carrying Four Rings

We expanded our studies on the growth of PAHs to PAH systems carrying four six membered rings utilizing pyrene ($\text{C}_{16}\text{H}_{10}$) as a prototype [P10]. By exploring the reaction of the 4-phenanthrenyl radical ($[\text{C}_{14}\text{H}_9]'$) with acetylene (C_2H_2) under conditions prevalent in high temperature combustion systems, we provide testimony on a facile, isomer-selective formation of pyrene ($\text{C}_{16}\text{H}_{10}$). Along with the Hydrogen Abstraction – Vinylacetylene Addition (HAVA) mechanism, molecular mass growth processes from pyrene may lead through systematic ring expansions not only to more complex PAHs, but ultimately to two-dimensional graphene-type structures thus facilitating an understanding toward soot growth in combustion systems. This research was carried out in collaboration with Dr. Ahmed (ALS) and Profs. Mebel (FIU; computations) and Fischer (UC Berkeley; synthesis of precursor). Recently, these studies were expanded to unravel the formation of [4]-helicene [P15] and triphenylene ($\text{C}_{18}\text{H}_{12}$) [P16].

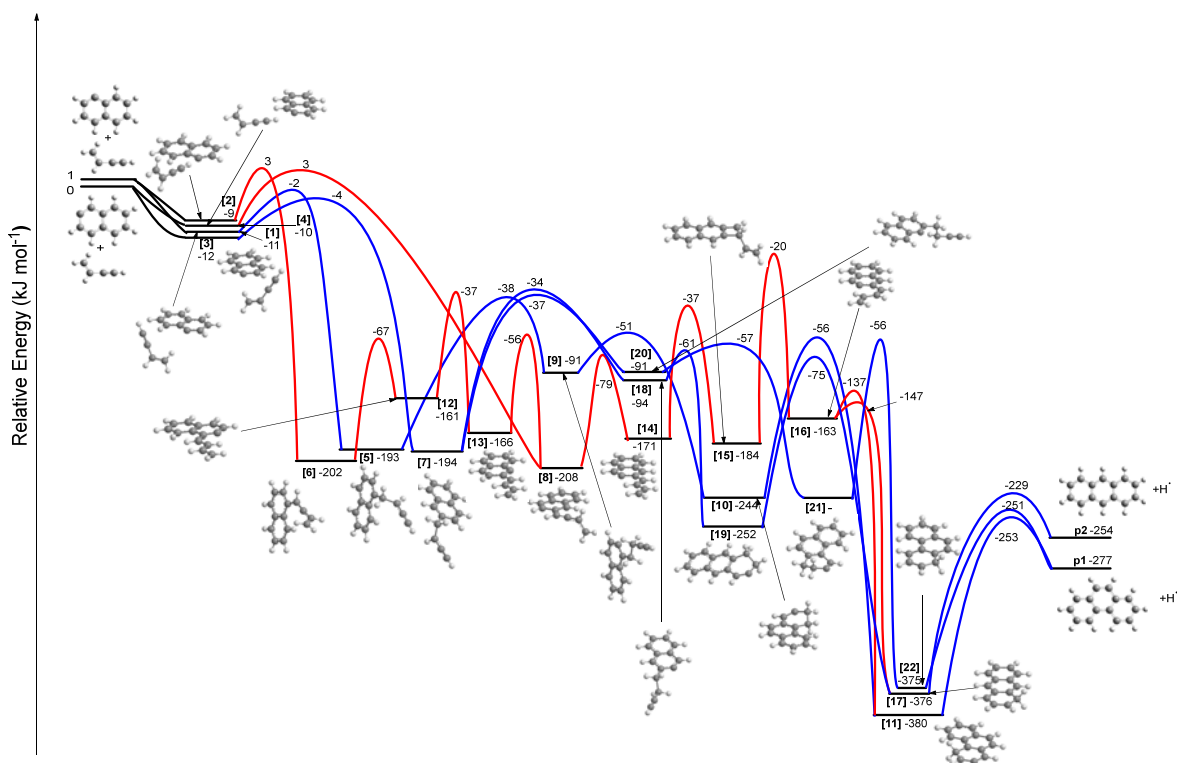


Figure 1: Potential energy surfaces of the reactions of 1-naphthyl and 2-naphthyl radicals with vinylacetylene leading to phenanthrene (p1) and anthracene (p2). The barrier-less pathways highlighted in blue dominate the anthracene and phenanthrene formation in cold environments. The pathways denoted in red have entrance barriers and hence are only relevant at elevated temperatures as present, for instance, in combustion flames, but closed at low temperatures due to the inherent barriers to reaction.

3. Future Plans

Having established synthetic pathways to PAHs carrying up to four rings (naphthalene, indene, phenanthrene, anthracene, acenaphthylene, pyrene, [4]-helicene, triphenylene), we will expand our studies to the formation of more complex PAHs (four rings) along with [5]-helicene (five rings), corannulene and [6]-helicene (six rings) as well as coronene (seven rings) as building blocks to two and three dimensional carbon nanostructures. Further, our molecular beam studies plan unravelling the synthesis of the simplest representatives of key classes of PAHs: phenacenes, acenes, and helicenes. Electronic structure calculations are conducted by Prof. Mebel (Florida International University). Commercially unavailable precursors are synthesized by Prof. Felix Fischer (UC Berkeley). This also helps to define the role and complementary nature of three reaction mechanisms in PAH growth: the Hydrogen Abstraction – acetylene Addition mechanism (HACA), the Hydrogen Abstraction – Vinylacetylene Addition mechanism (HAVA), and the Phenyl Addition – dehydroCyclization pathway (PAC).

4. Acknowledgements

This work was supported by US Department of Energy (Basic Energy Sciences; DE-FG02-03-ER15411).

5. Publications Acknowledging DE-FG02-03ER15411 (6/2016 – now)

P1 T. Yang, T. P. Troy, B. Xu, O. Kostko, M. Ahmed, A.M. Mebel, R.I. Kaiser, Hydrogen-Abstraction/Acetylene-Addition Exposed. *Angew. Chemie Int. Ed.* 55, 14983-14987 (2016).

P2 A.M. Thomas, T. Yang, B.B. Dangi, R.I. Kaiser, G.-S. Kim, A.M. Mebel, Oxidation of the Para-Tolyl Radical by Molecular Oxygen Under Single-Collision Conditions: Formation of the Para-Toloxyl Radical. *J. Phys. Chem. Lett.* 7, 5121-5127 (2016).

- P3** D.S.N. Parker, R.I. Kaiser, On the Formation of Nitrogen-Substituted Polycyclic Aromatic Hydrocarbons (NPAHs) in Circumstellar and Interstellar Environments. *Chem. Soc. Rev.* 46, 452 - 463 (2017).
- P4** A.M. Mebel, A. Landera, R.I. Kaiser, Formation Mechanisms of Naphthalene and Indene: From the Interstellar Medium to Combustion Flames. *J. Phys. Chem. A* 121, 901–926 (2017).
- P5** T. Yang, R.I. Kaiser, T.P. Troy, B. Xu, O. Kostko, M. Ahmed, A.M. Mebel, M.V. Zagidullin, V.N. Azyazov, HACA's Heritage: A Free-Radical Pathway to Phenanthrene in Circumstellar Envelopes of Asymptotic Giant Branch Stars. *Angew. Chemie Int. Ed.* 56, 4515-4519 (2017).
- P6** A.M. Thomas, M. Lucas, T. Yang, R.I. Kaiser, L. Fuentes, D. Belisario-Lara, A.M. Mebel, A Free Radical Pathway to Hydrogenated Phenanthrene in Molecular Clouds - Low Temperature Growth of Polycyclic Aromatic Hydrocarbons. *Chem. Phys. Chem.* 18, 1971-1976 (2017).
- P7** M. Lucas, L. Zhao, A.M. Thomas, R. I. Kaiser, A.M. Mebel, Gas Phase Synthesis of the Elusive Cyclooctatetraenyl Radical (C_8H_7) *Angewandte Chemie – International Edition* 44, 13533-13897 (2017).
- P8** M. Lucas, A.M. Thomas, R. I. Kaiser, A.M. Mebel, A Combined Experimental and Computational Investigation of the Elementary Reaction of Ground State Atomic Carbon ($C; ^3P_j$) with Pyridine ($C_5H_5N; X^1A_1$) via Ring Expansion and Ring Degradation Pathways. *The Journal of Physical Chemistry A* 122, 3128-3139 (2018).
- P9** A.M. Thomas, M. Lucas, L. Zhao, J. Liddiard, R.I. Kaiser, A.M. Mebel, A Combined Crossed Molecular Beams and Computational Study on the Observation of the Penta-1-yn-3,4-dienyl-1 (C_5H_3) Radical from Dissociating Triplet C_6H_6 Collision Complexes. *Physical Chemistry Chemical Physics* 20, 10906-10925 (2018).
- P10** L. Zhao, R.I. Kaiser, B. Xu, M. Ahmed, F. Fischer, A.M. Mebel, On the Synthesis of Pyrene in Circumstellar Envelopes and Its Role in the Formation of 2D Nanostructures. *Nature Astronomy* 2, 413-419 (2018).
- P11** L. Zhao, R.I. Kaiser, B. Xu, U. Ablikim, M. Ahmed, M.V. Zagidullin, V.N. Azyazov, A.H. Howlader, S.F. Wnuk, A.M. Mebel, VUV Photoionization Study on the Formation of the Simplest Polycyclic Aromatic Hydrocarbon: Naphthalene ($C_{10}H_8$). *J. Phys. Chem. Lett.* 9, 2620–2626 (2018).
- P12** A.M. Thomas, L. Zhao, C. He, A.M. Mebel, R. Kaiser, A Combined Experimental and Computational Study on the Reaction Dynamics of the 1-Propynyl (CH_3CC) - Acetylene (C_2H_2) System and the Formation of Methylidyne (CH_3CCCCH). *J. Phys. Chem. A* 122, 6663-6672 (2018).
- P13** L. Zhao, R.I. Kaiser, B Xu, U. Ablikim, M. Ahmed, M. Evseev, E.K. Bashkirov, V.N. Azyazov, A.M. Mebel, Low-Temperature Formation of Anthracene and Phenanthrene and Implications to the Synthesis of Polycyclic Aromatic Hydrocarbons in Titan's Atmosphere. *Nature Astronomy* (2018).
- P14** M. V. Zagidullin, R. I. Kaiser, D. P. Porfiriev, I. P. Zavershinskiy, M. Ahmed, V. N. Azyazov, A. M. Mebel Functional Relationships Between Kinetic, Flow, and Geometrical Parameters in a High Temperature Chemical Micro-Reactor. *J. Phys. Chem. A* 122, 8819–8827 (2018).
- P15** L. Zhao, R.I. Kaiser, B. Xu, U. Ablikim, M. Ahmed, M. Evseev, E. K. Bashkirov, V.N. Azyazov, A.N. Morozov, A.H. Howlader, S.F. Wnuk, A.M. Mebel, D. Joshi, G. Veber, F. R. Fischer, Gas Phase Synthesis of [4]-Helicene via a Versatile Vinylacetylene-Mediated Free Radical Ring Annulation. (submitted 2018).
- P16** L. Zhao, R.I. Kaiser, B. Xu, U. Ablikim, M. Ahmed, A.M. Mebel., On the Synthesis of Triphenylene ($C_{18}H_{12}$). (submitted 2019).
- P17** A.M. Thomas, C. He, L. Zhao, A.M. Mebel, R.I. Kaiser, A Combined Experimental and Computational Study on the Reaction Dynamics of the 1-Propynyl (CH_3CC) – 1,3-butadiene ($CH_2CHCHCH_2$) System and the Formation of Toluene Under Single Collision Conditions. (submitted 2019).

IMAGING THE NEAR-SURFACE GAS PHASE: A NEW APPROACH TO COUPLED GAS-SURFACE CHEMISTRY

Christopher J. Kliewer, David L. Osborn, Farid El Gabaly, Jonathan H. Frank, Nils Hansen
Sandia National Laboratories, Livermore, CA

Coleman Kronawitter, and Ambarish Kulkarni

Department of Chemical Engineering, University of California, Davis

cjkliew@sandia.gov, dlosbor@sandia.gov

PROGRAM SCOPE

The chemical reactivity of gases with solid surfaces is ubiquitous in natural and industrial energy transformation and is crucial to the synergistic research themes of *Chemistry at Complex Interfaces* and *Reaction Pathways in Diverse Environments*. Cooperative effects that couple gas phase chemistry with surface chemistry are critical for foundational understanding but challenging to probe experimentally and theoretically. Heterogeneous catalysis is an ideal field to expose and isolate the fundamental chemical physics of these cooperative effects. We have recently started a program to characterize gas-surface coupling, through chemically specific, temporally and spatially resolved probes of both reacting surfaces and the near-surface gas phase. This work links to the tools developed in Sandia tasks “Ultrafast Physics: Nonlinear Optical Spectroscopy and Diagnostics” and “Advanced Mass Spectrometry and Diagnostics” and complements work related to other surfaces in “Gas Phase Interactions with Other Phases.” The program combines linear and non-linear optical spectroscopies, universal photoionization mass spectrometry, and surface-specific spectroscopies at ambient pressures. Coherent nonlinear spectroscopic imaging methods will enable mapping of surface-gas exchange, which, combined with *in operando* surface spectroscopy, will correlate reaction rates with local surface structure, composition, and oxidation state during catalytic chemical transformations. These correlated measurements in self-organized oscillatory reaction systems will directly quantify how different surface domains communicate via chemical transport and are linked by chemical feedback. We will observe reactive intermediates above surfaces, establishing the critical mechanistic links between surface and gas-phase reactivity, and providing detailed species maps to inform microkinetic models. The long-term goal of the proposed work is to elucidate the fundamental mechanisms of cooperative gas-surface chemistry, influencing DOE mission research in catalysis, synthesis, and energy transformation.

This program comprises two interrelated thrusts, examples of which are illustrated in Fig. 1. The thrusts are distinguished by the physical mechanism of gas-surface coupling – transport or reaction – and

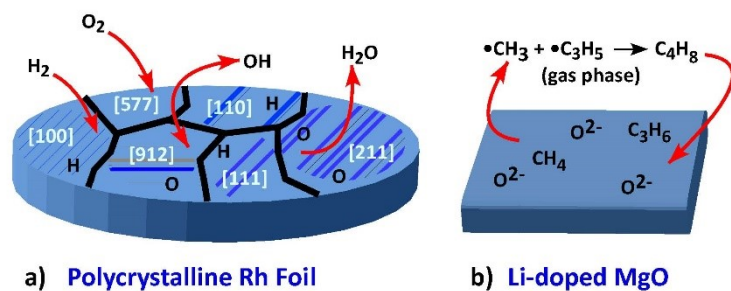


Figure 1: a) Oscillating reaction of H_2 oxidation over a polycrystalline Rh foil, depicting chemical waves of different wavelength. Miller indices label different domains. We will directly measure the gas-phase concentrations in the near-surface region of reactants, products, and reactive intermediates such as OH radical, resolving the spatially localized reactive gas-surface exchange rate. b) Oxidative coupling of methane and propene on Li-doped MgO. We hypothesize that methyl and allyl radicals are ejected from the surface and combine in the gas phase to form butene, which may later adsorb on the surface.

employ differing degrees of chemical complexity and control over the model catalyst surface. The first thrust (Fig. 1a) explores how molecular transport in the gas phase may mediate coupling between different domains on a surface without gas-phase chemical reactions, and employs well-controlled reactions over atomically cleaned crystalline and polycrystalline surfaces prepared under UHV conditions, with reactivity studied under pressures of 10^{-6} to 760 torr. The second thrust (Fig. 1b) adds the complexity of reactive coupling, with bond breaking and formation among intermediates occurring in the gas phase as well as on the surface. Thrust 2 will utilize both single crystal

metal oxide and more complex surfaces (e.g., doped metal oxides, and bifunctional supported catalysts), with reactivity studied at elevated temperatures (700 - 1250 K) and pressures of 1 – 1500 torr.

RECENT PROGRESS

Imaging of Gas-Phase Species in Catalytic Oxidation of Methanol

Improved understanding of interactions between gas-phase and surface chemistry requires direct temporally and spatially resolved measurements of the gas above a reacting surface. Fundamental chemical physics has established that the observation of reactive intermediates is key to establishing mechanistic pathways. Despite this experimental need, such measurements are relatively rare in coupled gas-surface chemistry. We are employing proven techniques from gas-phase chemical physics to quantify reactants, products, and reactive intermediates in the near-surface region, in chemical systems that exhibit interrelated gas-phase and surface chemistry. As an initial testbed for imaging gas-phase species in catalytic reactions, we have constructed a prototype laminar flow reactor for combined 2-D planar laser-induced fluorescence (PLIF) and 1-D spontaneous Raman scattering in gases flowing over a catalyst (Fig. 2). The target reaction for these initial experiments is the catalytic partial oxidation of methanol over Ag, a widely used process for formaldehyde production.

The catalytic reactor consists of a stainless-steel cube with optical access for PLIF and Raman scattering through opposing optical ports. A third diagnostics port is available for future coupling to a molecular beam mass spectrometer (described below). A laminar flow of methanol, oxygen, and nitrogen is supplied across a heated catalytic surface, consisting of a 150 nm silver film deposited via magnetron sputtering on an undoped silicon wafer, provided by collaborator Coleman Kronawitter (UC Davis). The wafer is affixed to an unreactive boron nitride holder.

As the silver surface is heated to 350-700 C, catalytic production of formaldehyde progresses via two main pathways of partial oxidation: dehydration, $2CH_3OH + O_2 \rightarrow 2H_2CO + 2H_2O$, and dehydrogenation, $CH_3OH \rightarrow H_2CO + H_2$. The branching ratio of these pathways is highly dependent on the catalyst temperature and reactant mixture. Our newly established capability for imaging gas-phase species in a catalytic reactor will enable us to map interactions between gas-phase and surface catalyzed chemistry to address fundamental questions in the feedback between the two phases. Computational investigations (Kulkarni) using Density Functional Theory (DFT) are currently underway to understand the mechanism of surface-mediated oxidation of methanol to formaldehyde on various Ag facets.

PROPOSED WORK

Transport-Mediated Gas-Surface Coupling and Domain-Specific Chemistry

Resolving the local reaction kinetics and mechanism during surface catalyzed reactions as they vary from one crystallographic domain to the next, under ambient pressure conditions, is a foundational but elusive measurement for understanding gas-surface catalytic reactions. We aim to accomplish this task by directly monitoring local gas-surface reactive exchange rate across the many crystallographic domains of a typical polycrystalline catalyst. These measurements will show the effects that the local crystallographic termination, structure, and oxidation state, or the local average concentration of steps and defects within a domain, have on the product formation rate for polycrystalline (nonuniform) catalysts. Gas-phase composition measurements will also determine which key species are transported via the gas-phase to other crystallographic domains. To accomplish this task, we are currently assembling an instrument, unique in

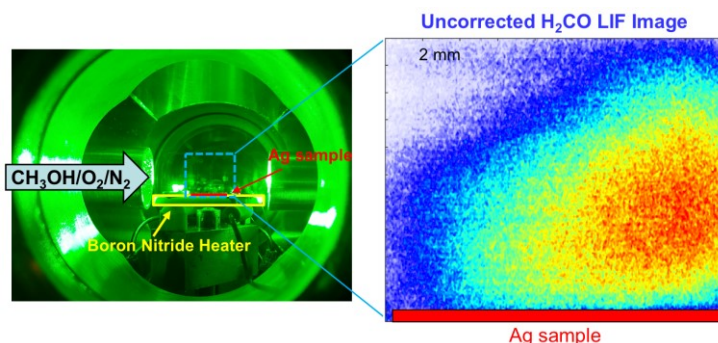


Fig. 2. Laser-induced fluorescence image of formaldehyde shows the growth in formaldehyde production as the reactants flow from left to right across the heated silver catalyst. Raw LIF image does not include corrections for spatial variations in the laser beam profile, optical throughput, or temperature.

the world, which will couple surface-sensitive spectroscopy with a range of gas phase optical spectroscopies.

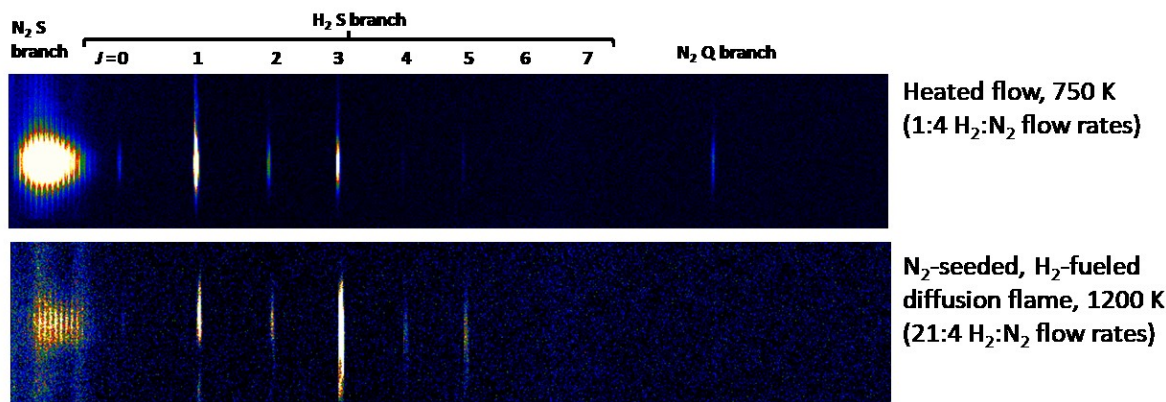


Figure 3. CARS image of molecular H₂ in a bath of N₂ at two different gas-phase temperatures, demonstrating the spatially resolved detection of gas phase H₂.

The instrumental capabilities required for the gas-surface chemical mapping reactor including an experimental chamber that can accommodate simultaneous laser access and ambient-pressure X-ray photoelectron spectroscopy (XPS) under relevant gas-surface conditions. For example, the combination of a focusing monochromatic X-ray source and a differentially-pumped electron spectrometer with a 2D detector will allow mapping surface domains while 2-dimensional Coherent Anti-Stokes Raman Spectroscopy (2D-CARS) and/or PLIF spectroscopy images the gas phase speciation with 10 μm spatial resolution.

The first set of experiments in the new instrument will involve joint gas-surface measurements of H₂-D₂ exchange over patterned Pd samples to form HD. We anticipate that the local crystal structure will influence reaction rates, and that this physics could be directly measured by monitoring the gas-surface exchange and product formation rates, along with surface characterization with ambient pressure XPS to monitor oxidation state. The resulting dataset will provide a complete picture of the gas-surface chemistry for that catalytic process and will help validate microkinetic models.

Coupling Photoionization Mass Spectrometry to Optical Laser Diagnostics

Although recent modeling of heterogeneous reactions include feedback between surface- and gas-phase reactions, direct temporally and spatially resolved experimental measurements of the gas above a reacting surface are still rare. To address this scarcity, we will employ our mass spectrometric techniques from gas-phase chemical physics to quantify reactants, products, and reactive intermediates in the near-surface region in chemical systems that exhibit interrelated gas-phase and surface chemistry. The goal of this project is to explore gas-surface reaction systems in which bond breaking and/or formation occurs in both the gas phase and on surfaces.

We envision two different experimental configurations. In the first apparatus, we employ molecular-beam sampling mass spectrometry to provide two-dimensional, spatially resolved concentration maps of reactants, intermediates, and products above a reactive surface at pressures ranging from 20 to 760 Torr. Because of known issues with the quantification of the mass spectrometric signal for OH, this apparatus allows for simultaneous measurements of PLIF signal from this very reactive radical. The catalytic surface can be translated underneath a fixed sampling cone to measure reactants, intermediates, and products as a function of time (by varying bulk flow velocity), pressure, and temperature. The custom-built mass spectrometer needed for this work already exists at Sandia and we will use electron-ionization, laboratory-based sources of non-tunable vacuum ultraviolet (VUV) radiation for photoionization, and the more powerful tunable VUV radiation from the Chemical Dynamics Beamline of LBNL's Advanced Light Source for ionization of the sampled gas-phase molecules.

In the second approach, a catalytic surface in a jet-stirred reactor coupled to the same molecular-beam mass spectrometer is being designed to allow for well-defined residence times and averaging of the

gas phase completely over the spatial dimension (a 0-D approach), thus enabling the most straightforward comparison with chemistry models. The simultaneous observation of both the free radicals and their closed-shell reaction products will provide kinetic links between reactants and products.

Mechanistic Studies of Oxidative Coupling of Methane

Concurrent to efforts in technique development, our UC Davis collaborators are designing and fabricating new catalysts to facilitate mechanistic studies of a more complex reaction – the oxidative coupling of methane (OCM) – which involves dynamic exchange of intermediates between the surface and gas phase. Because most known OCM catalysts are complex oxides with ill-defined surface composition, they are not well-suited for investigation of fundamental structure-activity relationships, which typically require higher degrees of uniformity. Therefore our Davis colleagues are developing single-site catalysts of well-defined structure for more uniform surface active sites.

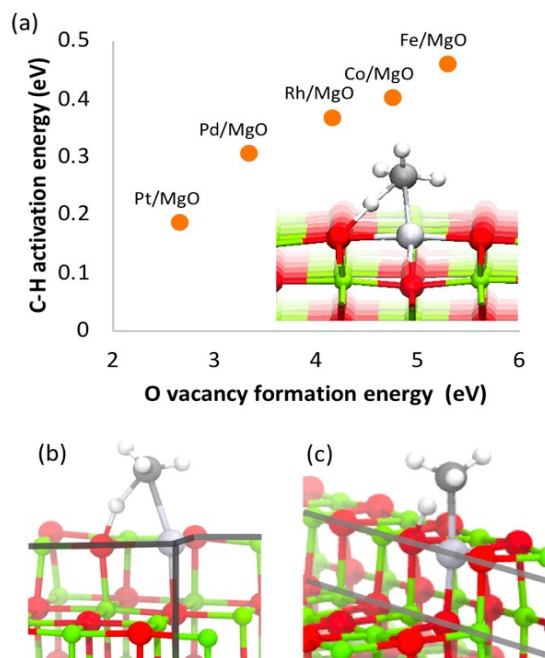


Figure 4. (a) Preliminary DFT calculations showing the correlation between C-H bond activation energy and O vacancy formation energy for a range of TM/MgO(110) surfaces. Geometry of the transition state for (b) (100) corner sites and (c) (100) step sites.

for different facets. By comparison with experiments, we will test how the gas phase composition immediately above the surface is altered by the change of transition metal site and activation energy. Using the MgO(110) surface as an example, the preliminary data in Fig. 4 shows the inverse relationship between the C-H activation barrier and the surface reducibility (*i.e.* the oxygen vacancy formation energy). These data show that the weaker Pt-O bond is more reactive than the Fe-O bond in doped MgO(110), suggesting a higher rate of $\bullet\text{CH}_3$ generation for Pt/MgO.

BES-sponsored publications, 2017 – present

- 1) The project was funded in September 2018. No peer-reviewed articles have yet been published under this Field Work Proposal

ULTRAFAST PHYSICS: NONLINEAR OPTICAL SPECTROSCOPY AND DIAGNOSTICS

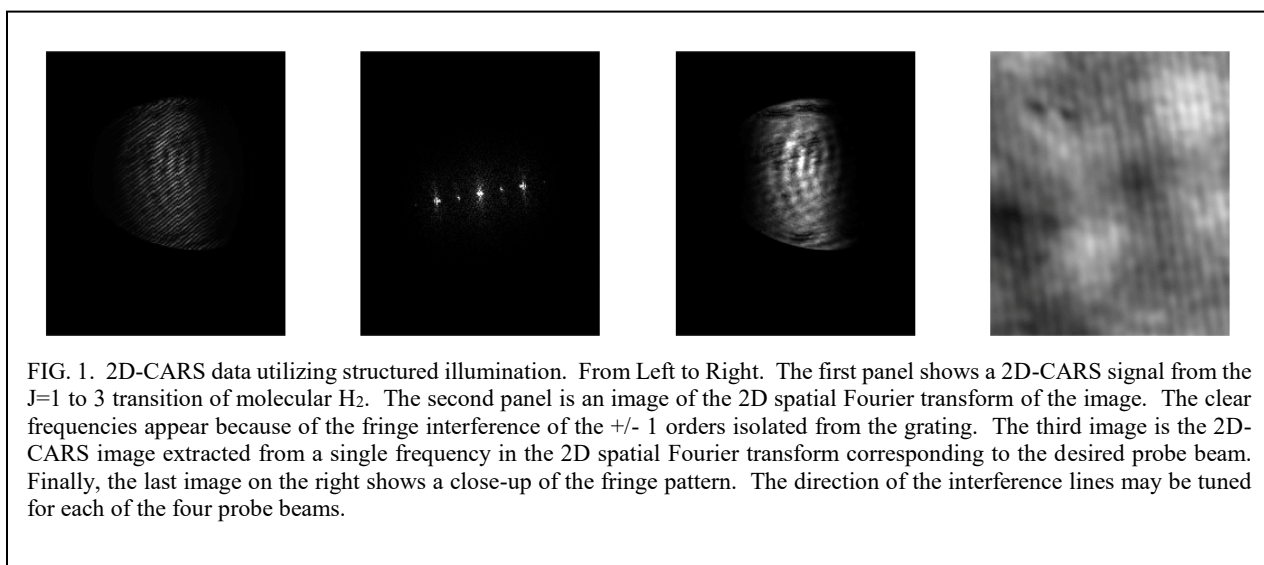
Christopher J. Kliewer, David W. Chandler, Krupa Ramasesha, Jonathan H. Frank
Sandia National Laboratories, MS 9051, Livermore, CA 94551-0969
cjkliew@sandia.gov, chand@sandia.gov, kramase@sandia.gov, jhfrank@sandia.gov

Program Scope

This program focuses on the development of innovative laser-based techniques for measuring temperature and concentrations of important gas phase molecular species as well as the investigation of fundamental physical and chemical processes that directly affect quantitative application of these techniques. The physics and spectroscopy developed in this task are employed in the “Chemical Dynamics Methods and Applications,” “Ultrafast Chemistry: Spectroscopic Probes of Non-Adiabatic Dynamics,” and “Gas Phase Interactions with Other Phases” tasks. Our recent development efforts focus on crossed-beam approaches such as time-resolved nonlinear wave-mixing. A critical aspect of our research includes the study of fundamental spectroscopy, energy transfer, molecular dynamics, and photochemical processes. This aspect of the research is essential to the development of accurate models and quantitative application of techniques to the complex environments encountered in combustion systems. These investigations use custom-built tunable picosecond (ps) and commercial femtosecond lasers, which enable efficient nonlinear excitation, provide high temporal resolution for pump/probe studies of collisional processes, and are amenable to detailed physical models of laser-molecule interactions. The fundamental studies of this subtask directly tackle the quantum control and interrogation of gas-phase molecules in ground and excited electronic states, one of the essential topics enumerated as a Grand Challenge for Basic Energy Sciences.

Recent Progress

Coherence Lifetime Imaging. In collaboration with Lund University Professors Joakim Bood, Per-Erik Bengtsson, and Elias Kristensson, we are developing a single laser shot coherence lifetime imaging experiment. Coherence lifetime imaging, similar to fluorescence lifetime imaging, provides a unique glimpse of spatially resolved energy transfer and dephasing in a sample. In combustion applications, this could yield information on molecular species concentrations, mixing, and temperature without the need for a hyperspectral image deconvolution. We were able to achieve this deconvolution for N_2 systems at ambient pressure, but high-pressure situations with line-broadening or multi-species interactions would rule

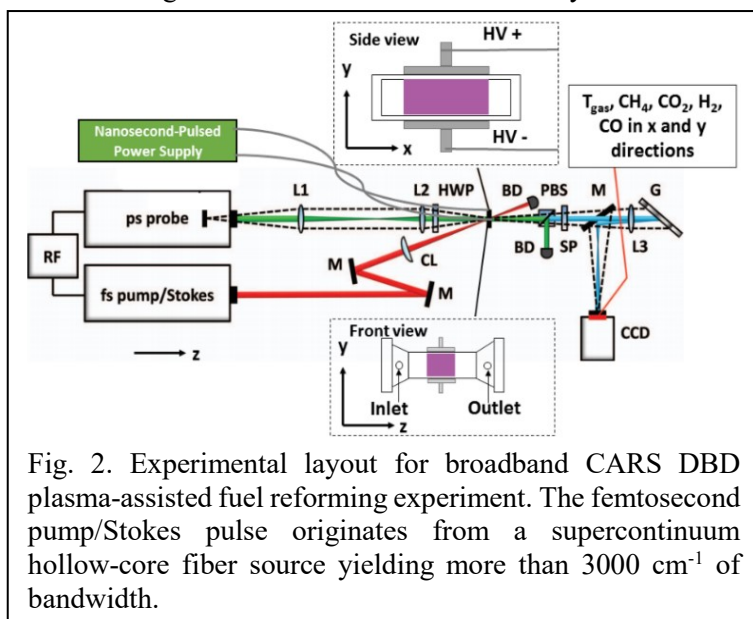


out such a setup. Further, applications for such a metric extend far beyond combustion. In the life sciences, cell imaging and biomedical research microscopy methods seek new contrast mechanisms to decipher one local chemical environment from another – coherence lifetime imaging with single-shot implementation will be a major break-through for this community. To accomplish this, we have designed an experimental approach that combines 2D-CARS (developed in our lab at Sandia) with SLIPI, structured laser illumination methods developed at Lund University. In this approach, the two-beam CARS pump/Stokes pulse intersects the sample. The probe beam, however, is separated via beam-splitters into four separate beams. Each of these beams propagates through a time-of-flight optical delay stage and is then passed through a transmission grating. These gratings are designed to optimize the ± 1 orders. The position of the grating is relay imaged to the experiment. In this way, each of the four probe beams gets imprinted with a fringe pattern at a controllable angle. The CARS beams are recombined into a single beam and scattered from the sample. The resulting image contains four separate probe delays, with independent spatial frequencies, which can be extracted through spatial Fourier transform. A sample set of data is shown in Figure 1.

Future Work

Simultaneous species and temperature measurements of plasma-catalytic CH₄ dry reforming using 2D-CARS (Collaboration with Yiguang Ju and Timothy Chen, Princeton University). Plasma-assisted catalytic fuel reforming is an attractive alternative to large-scale reforming facilities to process methane. The chemical kinetic mechanism and physical understanding of the interaction of the plasma with the sheath layer and catalyst are poorly understood. Our lab has pioneered in recent years the invention of nonlinear optical imaging and broadband detection methods capable of probing harsh environments, such as those encountered in and following a plasma discharge, on a single-laser shot basis. This is important for tracking transient processes such as those following a dielectric barrier discharge (DBD) plasma breakdown. The vibrational excitation of molecules may enhance dissociation and act as an additional catalyst to the overall reaction. To characterize these effects, direct measurements of chemical speciation and vibrational/rotational energy distribution in the near surface region following plasma excitation are needed. Timothy Chen from Yiguang Ju's group at Princeton will be visiting Sandia to perform these measurements.

In this study, we will track the spatio-temporal evolution of rotational and vibrational energy distributions as well as chemical speciation in the dry reforming of CH₄ using plasma assisted catalysis, while resolving the transition from the sheath layer to the bulk using 1D and 2D ultrabroadband CARS.



We will detect CH₄, CO₂, H₂, CO, CH₂O with this method. It is important to characterize the vibrational and rotational energy distributions of the CH₄ and CO₂ following the plasma discharge. The time-domain CARS code developed over the past several years at Sandia under this BES program currently contains validated models for H₂, N₂, and O₂. For this study, we will add time-domain molecular response models for CH₄, CO, and CO₂. Temperature-dependent measurements in a heated cell will provide the baseline for validation of the spectroscopic model. Figure 2 displays the experimental layout for these experiments.

Heterodyne Detection of Cavity-Ring-Down Spectroscopy. Cavity-ring-down spectroscopy is a popular technique for recording weak absorption signals. It has the advantages of long path length and is generally laser bandwidth limited in resolution. One way we have overcome this limitation in resolution in the past was to use the cavity as an etalon and then resolve the etalon modes. In this manner, one is limited by the etalon mode spacing and not the laser resolution for the spectroscopy. In addition, by resolving the modes we were able to simultaneously record the absorption spectra at multiple wavelengths. Our earlier effort was dubbed a Dual-Etalon, Frequency-Comb, Cavity-Ring-Down spectrometer. A single laser pulse, 3 mJ per pulse with 6 ns pulse length, obtained from a Lambda Physik dye laser pumped by a coherent Infinity Nd:YAG laser was split into two pulses and used as the light source for the spectrometer. The spectrometer was comprised of two optical paths each containing an etalon. The etalons were of slightly different lengths and therefore had slightly different free spectral ranges. The outputs were combined and the cross beat was recorded. This was a version of a dual frequency comb laser experiment that Drs. Picque and Hensch had previously published. We propose here a hybrid version of these experiments. We will take a pulse-amplified Ti-Sapphire laser and use the pulse-amplified pulse to seed an etalon. We will take light from the femtosecond high-rep-rate seed laser output that fed the amplifier to heterodyne with the output of the cavity. For any 30 μ s period of time (a very good cavity ring down life time) even a non-carrier-envelope-phase stabilized femtosecond laser is an excellent frequency comb for this length of time. In this manner we will be able to measure the broad band absorption of molecules in the frequency range of the fundamental of the pulse amplified laser without the need for locking and

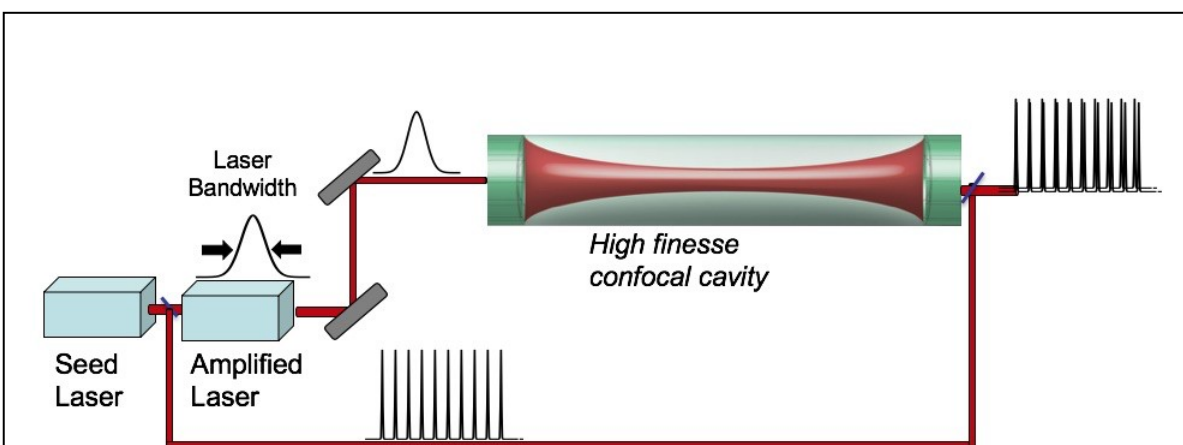


Fig. 3. Heterodyne Cavity Ring-Down Spectrometer. The output of a femtosecond oscillator is split into a reference arm and a second arm which is pulse-amplified at 1 kHz. The amplified arm is then fed into the cavity ring-down cavity. The output of the cavity is joined with the reference arm. The interference between the two arms allows high-resolution spectroscopy

matching the FSR of the etalon to the laser. A preliminary goal will be to show that there is enough light in the cavity modes of the etalon and in the light from the seed laser to obtain a heterodyne signal.

Direct visualization of $O_2(a^1\Delta_g)$ using nonlinear optical methods

The direct time-resolved and spatially-resolved detection and visualization of the concentration of singlet oxygen, $O_2(a^1\Delta_g)$, has been a challenging goal for many years. A weak absorption cross-section for excitation to the next lowest-lying electronic state requires a cavity ring-down or cavity-enhanced type setup for detection. Such methods have very long effective path lengths and are line-of-sight limited and are thus not applicable to many areas of gas phase chemical physics (such as combustion and plasma-assisted chemistry) where $O_2(a^1\Delta_g)$ is known or suspected to play a major kinetic role. We have recently

developed a technique to directly visualize $O_2(a^1\Delta_g)$ with excellent spatial resolution based upon time-domain coherent Raman spectroscopy. In the coming months we will demonstrate this technique by measuring $O_2(a^1\Delta_g)$, quantifying the detection limits, and then applying the method in measurements of plasma generated $O_2(a^1\Delta_g)$.

Molecular alignment and coherence: strong-field effects. We have recently observed unique changes to the H_2 time-domain coherent Raman signal as a function of the strength of a strong-field alignment pulse in the nanosecond regime. We plan to use a nanosecond laser with programmable pulse shape as the strong field. The benefit of this experiment is that a very well-defined field strength may be used to study the effects that a strong adiabatic laser field has on the nonadiabatic alignment of molecules. Instead of having a Gaussian time-profile, a flat-top time profile may be used. This allows for an electric field strength that is constant on the time scales of the femtosecond nonadiabatic molecular alignment probe, even with the standard timing jitter expected from nanosecond pulsed lasers. Fundamental questions we plan to answer involve: How do adiabatic and nonadiabatic molecular alignment processes interact with one another? How are ultrafast coherent scattering signals affected by some level of pre-alignment in the molecules?

High-pressure diagnostics development. We have recently completed the construction of an optical high pressure cell capable of up to 100 atm pressure and up to 1000 K temperature, and incorporated an active pulse-shaper into our femtosecond laser setup to correct for higher order chirp in the cell windows. We plan to continue development of high pressure nonlinear mixing strategies, and tailored probe arrangements for multiplex coherent imaging of temperature and species concentrations at high pressure. Nonlinear optical strategies benefit from a squared number density dependence at high pressure, but fast dephasing requires the use of tailored probe pulses. We plan to develop molecular phase-mask pulse shaping for excitation of only the species of interest, while eliminating the broad signal from neighboring transitions of other species which are collisionally broadened.

Direct measurement of N_2 -Fuel and N_2 - H_2O broadening coefficients. With the successful development of the time-domain technique for acquiring high-accuracy S-branch broadening coefficients, demonstrated thus far for the N_2 - N_2 and N_2 - H_2 collisional systems, we propose to continue the collaboration with Per-Erik Bengtsson of Lund University, Sweden, to tackle the relative paucity of broadening coefficient data in the literature for air-fuel collisional systems. Initial studies will focus on the collisional broadening of N_2 and O_2 when perturbed by DME, ethane, ethylene, propane, and propylene. Accurate broadening models must be developed for these collisional environments, especially at elevated pressures. We will alter our current time-domain CARS code to implement these new linewidth libraries and test the validity of the model in our newly constructed high-pressure, high-temperature cell.

Journal publications supported by this BES project (2017-2019)

1. A. Bohlin, C. Jainski, B.D. Patterson, A. Dreizler, and C.J. Kliewer, "Multiparameter spatio-thermochemical probing of flame-wall interactions advanced with coherent Raman imaging," *Proc. Combust. Inst.* **36**, 4557-4564 (2017)
2. T.L. Courtney, A. Bohlin, B.D. Patterson, C.J. Kliewer, "Pure-Rotational H_2 Thermometry by Ultrabroadband Coherent Anti-Stokes Raman Spectroscopy," *J. Chem. Phys.* **146**, 224202 (2017)
3. A. Bohlin, B.D. Patterson, C.J. Kliewer, "Dispersive Fourier Transformation for Megahertz Detection of Coherent Raman Spectra," *Optics Communications* **402**, 115-118 (2017)

THEORETICAL CHEMICAL KINETICS

Stephen J. Klippenstein
Chemical Sciences and Engineering Division
Argonne National Laboratory
Lemont, IL, 60439
sjk@anl.gov

Program Scope

The focus of this program is the development and application of theoretical methods for exploring gas phase chemical kinetics. The research involves a combination of *ab initio* electronic structure calculations, variational transition state theory (TST), classical trajectory simulations, and master equation (ME) calculations. Detailed applications, including careful comparisons with experiment as feasible, are used to (i) develop a deeper understanding of the applicability of various foundational principles of gas phase chemical kinetics, (ii) motivate improvements in theoretical chemical kinetics methodologies, and (iii) enhance our understanding of various aspects of combustion, atmospheric, and interstellar chemistry. The specific reactions studied are generally motivated by global modeling efforts and state-of-the-art experimental observations.

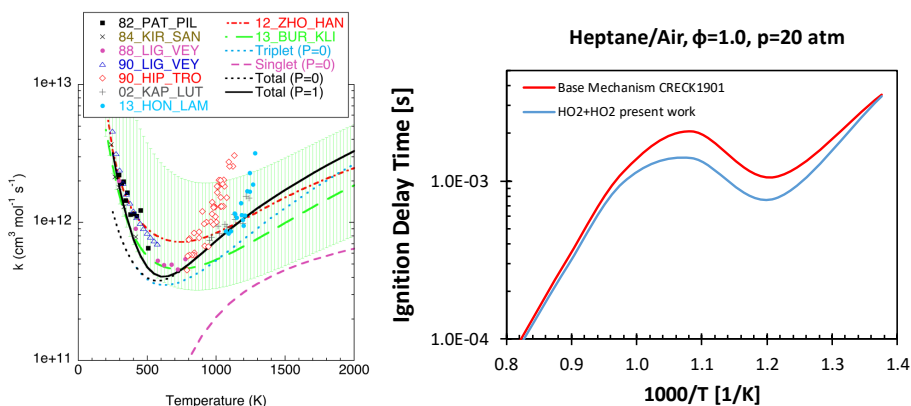
Recent Progress

$HO_2 + HO_2$: The self-reaction of hydroperoxy radicals is important in both atmospheric and combustion chemistry. It has generally been presumed to occur as an abstraction on the triplet surface to produce $H_2O_2 + {}^3O_2$. We employed a combination of high level electronic structure theory (ANL0 and multireference as appropriate), sophisticated TST (vibrationally adiabatic torsions, variational, and variable reaction coordinate), and ME analyses to predict the thermal kinetics on the H_2O_4 surface. Notably, this analysis suggests a significant branching to $HO_3 + OH$ near 1000 K via reaction on the singlet surface; a channel that does not appear to have

been considered in prior combustion models. HO_3 itself is a metastable complex (bound by only 3 kcal/mol) that rapidly dissociates to $OH + {}^3O_2$. Thus, the net reaction for this channel, $HO_2 + HO_2 \rightarrow OH + OH + O_2$, converts two low

reactivity radicals into two highly reactive radicals. The ramifications of these newly derived rate expressions were explored through modeling studies of H_2/O_2 , CH_3OH , n-heptane, and iso-octane, all at high pressures.

Automated Kinetics. We reported the development of a new computational environment, namely EStokTP (electronic structure to temperature and pressure dependent rate constants), that reduces the human effort involved in the rate prediction for single channel reactions essentially

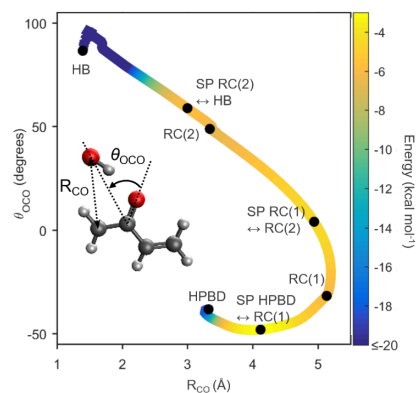


to the specification of the reactant structures and the methodologies (electronic structure, TST, ME) to be employed. It focuses on generating, extracting, and organizing the necessary structural properties from a sequence of calls to electronic structure codes, with robust automatic failure recovery options to limit human intervention. The code implements one or multi-dimensional hindered rotor treatments of internal torsional modes (with automated projection from the Hessian, and with optional vibrationally adiabatic corrections), Eckart and multidimensional tunneling models (such as small curvature theory), and variational treatments (based on intrinsic reaction coordinate following). This focus on a robust implementation of high level TST methods allows the code to be used in high accuracy studies of large sets of reactions, as was illustrated through sample studies of a few hundred reactions. At present the following reaction types are implemented in EStokTP: abstraction, addition, isomerization, and beta-decomposition.

Titan Chemistry: In collaboration with a group of leading astrochemistry modelers, (Vuitton, Yelle, Horst, and Lavvas), we published a comprehensive modeling study of Titan's atmospheric chemistry from the surface to the exobase. The chemical network includes reactions and photochemistry for neutrals, cations, and anions of hydrocarbons, nitrogen, and oxygen bearing species. Detailed comparisons were made with the full set of observational data from the Cassini-Huygen mission. We contributed a large number of (on the order of 100) *ab initio* kinetics calculations. Fortunately, many of these calculations involved simple extrapolations from models previously developed in our group for studying combustion processes. This publication, which represents the culmination of many years of collaborative effort by each of the authors, demonstrates considerable progress in our level of understanding Titan's atmospheric chemistry, although a number of issues remain unresolved.

Criegee Intermediates: Ozonolysis leads to the formation of chemically activated carbonyl oxides that may either directly dissociate or be collisionally stabilized, with the branching between these products having an important impact on atmospheric chemistry. The ozonolysis of isoprene, which is one of the most abundant volatile organic compounds in the atmosphere, produces three distinct carbonyl oxide species (RR'COO) known as Criegee intermediates: formaldehyde oxide (CH₂OO), methyl vinyl ketone oxide (MVK-OO), and methacrolein oxide (MACR-OO). The unimolecular decay of MVK-OO is predicted to be the major source of hydroxyl radicals (OH) in isoprene ozonolysis. In a collaboration led by Lester, we reported the initial laboratory synthesis and direct detection of MVK-OO utilizing infrared action spectroscopy, as well as collaborative experimental and theoretical studies of its dissociation. For *syn*-MVK-OO, the rate of appearance of OH products agrees with the unimolecular decay rate predicted using statistical theory with tunneling. Interestingly, theoretical calculations reveal an additional roaming pathway between the separating radical fragments, which results in other products. Master equation modeling yields a thermal unimolecular decay rate for *syn*-MVK-OO of 33 s⁻¹ (298 K, 1 atm). For *anti*-MVK-OO, theoretical exploration of several unimolecular decay pathways predicts that isomerization to dioxole is the most likely initial step to products.

For ethylene ozonolysis, we used a combination of high level electronic structure evaluations (including multireference treatments as necessary), direct dynamics simulations, and ME calculations to explore this branching. This analysis included treatments of both concerted



and sequential/diradical steps. For the concerted pathway, the CI average internal energies from molecular dynamics were significantly lower than statistical model expectations (which provided the basis for all prior theoretical treatments). For the stepwise pathway, either an under- or overestimation of the yields was observed, depending on the statistical model that was employed. By combining the channel-specific stabilized CI yields with the channel branching fractions, an overall stabilized CI yield of $(48 \pm 5)\%$ was obtained, in good agreement with measured literature values ranging from 35 to 54%. Within the experimental data set, our calculations favor those clustered at the upper end of this spectrum.

Future Directions

We continue to work toward implementing automated high-level theoretical thermochemical kinetics to improve our understanding of classic combustion mechanisms. Currently, those efforts are focused on developing computationally based thermochemical properties for the ANL0 set of species, and for a range of RH/R/RO2/QOOH/O2QOOH alkane species up to iso-octane.

We are currently studying the kinetics of the larger Creigee intermediates, which are of greater interest to atmospheric chemists. For example, in collaboration with Lester and Taatjes, we are in the process of studying the kinetics of MVK-OO and MACR-OO with species such as H₂O, OCHOH, and SO₂. We are also exploring the oligomerization of CH₂OO through its successive additions to OCHOH, for example.

DOE Supported Publications, 2017-Present

1. **From Theoretical Reaction Dynamics to Chemical Modeling of Combustion**, S. J. Klippenstein, *Proc. Combust. Inst.* **36**, 77-111 (2017).
2. **Recombination of Aromatic Radicals with Molecular Oxygen**, F. Zhang, A. Nicolle, L. Xing, S. J. Klippenstein, *Proc. Combust. Inst.* **36**, 169-177 (2017).
3. **Theoretical Kinetics of O + C₂H₄**, X. Li, A. W. Jasper, J. Zádor, J. A. Miller, S. J. Klippenstein, *Proc. Combust. Inst.* **36**, 219-227 (2017).
4. **Temperature- and Pressure-Dependent Rate Coefficients for the HACA Pathways from Benzene to Naphthalene**, A. M. Mebel, Y. Georgievskii, A. W. Jasper, S. J. Klippenstein, *Proc. Combust. Inst.* **36**, 919-926 (2017).
5. **First-Principles Chemical Kinetic Modeling of Methyl Trans-3-Hexenoate Epoxidation by HO₂**, S. Cagnina, A. Nicolle, T. de Bruin, Y. Georgievskii, S. J. Klippenstein, *J. Phys. Chem. A* **121**, 1909-1915 (2017).
6. **Tunneling Effects in the Unimolecular Decay of (CH₃)₂COO Criegee Intermediates to OH Radical Products**, Y. Fang, V. P. Barber, S. J. Klippenstein, A. B. McCoy, Marsha I. Lester, *J. Chem. Phys.* **146**, 134307 (2017).
7. **Accurate Anharmonic Zero Point Energies for some Combustion Related Species from Diffusion Monte Carlo**, L. B. Harding, Y. Georgievskii, S. J. Klippenstein, *J. Phys. Chem. A* **121**, 4334-4340 (2017).
8. **Ephemeral Collision Complexes Mediate Chemically Termolecular Transformations that Affect System Chemistry**, M. P. Burke, S. J. Klippenstein, *Nature Chem.* **9**, 1078-1082 (2017).
9. **Ab Initio Computations and Active Thermochemical Tables Hand in Hand: Heats of Formation of Core Combustion Species**, S. J. Klippenstein, L. B. Harding, B. Ruscic, *J. Phys. Chem. A* **121**, 6580-6602 (2017).
10. **Theoretical Investigation of Intersystem Crossing in the Cyanonitrene Molecule, ¹NCN → ³NCN**, M. Pfeifle, Y. Georgievskii, A. W. Jasper, S. J. Klippenstein, *J. Chem. Phys.* **147**, 084310 (2017).

11. **Theoretical Kinetics Analysis for H-atom Addition to 1,3-Butadiene and Related Reactions on the \dot{C}_4H_7 Potential Energy Surface**, Y. Li, S. J. Klippenstein, C.-W. Zhou, H. J. Curran, *J. Phys. Chem. A* **121**, 7433-7445 (2017).
12. **Selective Deuteration Illuminates the Importance of Tunneling in the Unimolecular Decay of Criegee Intermediates to Hydroxyl Radical Products**, A. M. Green, V. P. Barber, Y. Fang, S. J. Klippenstein, M. I. Lester, *Proc. Nat. Acad. Sci.* **114**, 12372-12377 (2017).
13. **Dynamic Time-Resolved Chirped-Pulse Rotational Spectroscopy of Vinyl Cyanide Photoproducts in a Room Temperature Flow Reactor**, D. P. Zaleski, L. B. Harding, S. J. Klippenstein, B. Ruscic, K. Prozument, *J. Phys. Chem. Lett.* **8**, 6180-6188 (2017).
14. **Anharmonic Rovibrational Partition Functions for Fluxional Species at High Temperatures via Monte Carlo Phase Space Integrals**, A. W. Jasper, Z. B. Gruey, L. B. Harding, S. J. Klippenstein, A. F. Wagner, *J. Phys. Chem. A* **122**, 1727-1740 (2018).
15. **Modeling Nitrogen Chemistry in Combustion**, P. Glarborg, B. Ruscic, J. A. Miller, S. J. Klippenstein, *Prog. Energy Combust. Sci.* **67**, 31-68 (2018).
16. **H-Abstraction Reactions by OH, HO₂, O, O₂, and Benzyl Radical Addition to O₂ and Their Implications for Kinetic Modelling of Toluene Oxidation**, M. Pelucchi, C. Cavallotti, T. Faravelli, S. J. Klippenstein, *Phys. Chem. Chem. Phys.* **20**, 10607-10627 (2018).
17. **Unimolecular Decay of Criegee Intermediates to OH Radical Products: Prompt and Thermal Decay Processes**, M. I. Lester, S. J. Klippenstein, *Acc. Chem. Res.* **51**, 978-985 (2018).
18. **Nascent Energy Distribution of the Criegee Intermediate CH₂OO from Direct Dynamics Calculations of Primary Ozonide Dissociation**, M. Pfeifle, Y.-T. Ma, A. W. Jasper, L. B. Harding, W. L. Hase, S. J. Klippenstein, *J. Chem. Phys.* **148**, 174306 (2018).
19. **Four-Carbon Criegee Intermediate from Isoprene Ozonolysis: Methyl Vinyl Ketone Oxide Synthesis, Infrared Spectrum, and OH Production**, V. P. Barber, S. Pandit, A. M. Green, *J. Am. Chem. Soc.* **140**, 10866-10880 (2018).
20. **Automated Computational Thermochemistry for Butane Oxidation: A Prelude to Predictive Automated Combustion Kinetics**, M. Keceli, S. Elliott, Y.-P. Li, M. S. Johnson, C. Cavallotti, Y. Georgievskii, W. H. Green, M. Pelucchi, J. M. Wozniak, A. W. Jasper, S. J. Klippenstein, *Proc. Combust. Inst.* **37**, 363-371 (2019).
21. **Small Ester Combustion Chemistry: Computational Kinetics and Experimental Study of Methyl Acetate and Ethyl Acetate**, A. Ahmed, W. J. Pitz, C. Cavallotti, M. Mehl, N. Lokachari, E. J. K. Nilsson, J.-Y. Wang, A. A. Konnov, S. W. Wagnon, B. Chen, Z. Wang, H. J. Curran, S. J. Klippenstein, W. J. Roberts, S. M. Sarathy, *Proc. Combust. Inst.* **37**, 419-428 (2019).
22. **Simulating the Density of Organic Species in the Atmosphere of Titan with a Coupled Ion-Neutral Photochemical Model**, V. Vuitton, R. V. Yelle, S. J. Klippenstein, P. Lavvas, S. M. Horst, *Icarus*, **324**, 120-197 (2019).
23. **EStokTP: Electronic Structure to Temperature- and Pressure-Dependent Rate Constants – A code for Automatically Predicting the Thermal Kinetics of Reactions**, C. Cavallotti, M. Pelucchi, Y. Georgievskii, S. J. Klippenstein, *J. Chem. Theory Comp.* **15**, 1122-1145 (2019).
24. **HO₂ + HO₂: High Level Theory and the Role of Singlet Channels**, S. J. Klippenstein, R. Sivaramakrishnan, U. Burke, K. P. Somers, H. J. Curran, L. Cai, H. Pitsch, M. Pelucchi, T. Faravelli, P. Glarborg, *11th U. S. National Combustion Meeting*, Paper 1A13 (2019).
25. **Ab Initio Kinetics for Pyrolysis and Combustion Systems**, S. J. Klippenstein, C. Cavallotti; in: *Mathematical Modeling of Complex Reaction Systems: Pyrolysis and Combustion*, T. Faravelli, F. Manenti, and E. M. Ranzi, Eds. Computer Aided Chemical Engineering Series, Elsevier: New York, *in press* (2019).

A Coupled Theoretical and Experimental Approach to Elucidating the Mechanisms of Methyl Esters

Nicole J. Labbe,¹ G. Barney Ellison,² John W. Daily¹

¹Department of Mechanical Engineering

²Department of Chemistry

University of Colorado Boulder

UCB 427, 1111 Engineering Drive, Boulder, CO 80301-0427

Nicole.Labbe@colorado.edu, John.Daily@colorado.edu, Barney@jila.colorado.edu

Program Scope

Methyl esters of fatty acids are believed to have similar combustion properties to petroleum-based fuels, making them a promising class of biofuels which are amenable for use in existing engine technology. Such biofuels are derived from the triglyceride esters of fatty acids such as those found in biological membranes of algae. Due to their promise as drop in fuel replacements, it is desirable to understand the fundamental kinetics of methyl esters and the fundamental implications of burning such fuels for health and the environment. In this study, we aim to answer many of the fundamental questions surrounding the kinetics of methyl ester reactivity. In particular, through a combined experimental, theoretical, and computational approach, this project aims to create and test new kinetic models that accurately reflect the chemistry of two model methyl esters, methyl hexanoate ($\text{CH}_3\text{CH}_2\text{CH}_2\text{CH}_2\text{COOCH}_3$), and methyl 5-hexenoate ($\text{CH}_2=\text{CHCH}_2\text{CH}_2\text{COOCH}_3$) to address uncertainties regarding unsaturation in methyl esters and the potential impact degree of saturation has on subsequent pollutant formation.

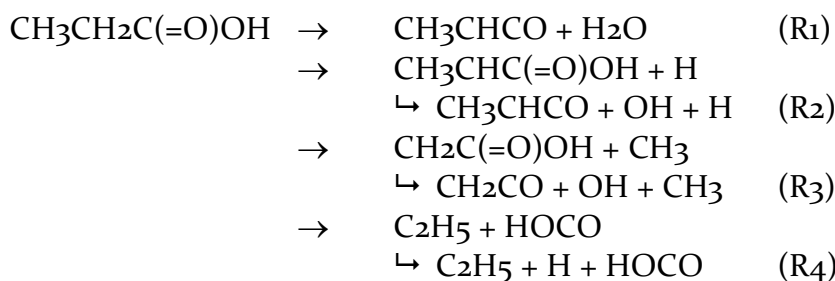
In order to address this problem, the goal of our program is to utilize a our new approach to using the microreactors first utilized by Barney Ellison for pyrolysis to probe \ the fundamental reactions of gas phase chemically reacting systems. A combination of system upgrades to better control the conditions within the microreactor itself for studying reactions at targeted temperature and pressure conditions and the simultaneous employment of kinetic theory to elucidate mechanisms in tandem with photo ionization mass spectrometry data is used to elucidate the reaction mechanisms of complex fuels.

Recent Progress

Experimental-Theory Hybrid Approach to Mechanisms using Microreactors: A significant amount of the past year has focused on improving the microreactor experiment for gas phase chemical kinetics studies. In particular, the system has been upgraded to operate under continuous flow conditions, a gas rig was created for multicomponent reactant mixtures, and the ionization chamber was reworked for improved signal. The ultimate goal of these improvements is to establish a method by which the experimental apparatus may

be used in tandem with theory to quickly and accurately determine gas phase kinetic mechanisms.

Ethyl propanoate and propionic acid were chosen to test the viability of this particular method. Ethyl propanoate pyrolysis has been well studied,¹⁻⁷ and nearly all thermal decomposition proceeds via water elimination to produce propionic acid. Figure 1-top shows that propionic acid (m/z 74) is indeed the only major product we see until subsequent decomposition of the propionic acid begins to play a role at 1200 K. Propionic acid has been significantly less studied and the thermal decomposition pathways are presently uncertain due to discrepancies between published models.^{6,7} Four major products appear in the spectra for propionic acid pyrolysis (Fig. 1-bottom), including methyl radical (m/z 15), ethylene (m/z 28), ketene (m/z 42) and methyl ketene (m/z 56). Multiple kinetic pathways can result in these products including:



A potential energy surface (PES) for propionic acid decomposition (Fig. 2) reveals that while methyl ketene can only be formed directly from propionic acid via R1 or R2, additional pathways are energetically favored. One favored reaction includes R5, although it is important to note that we see no evidence of ethane production in the experiments.

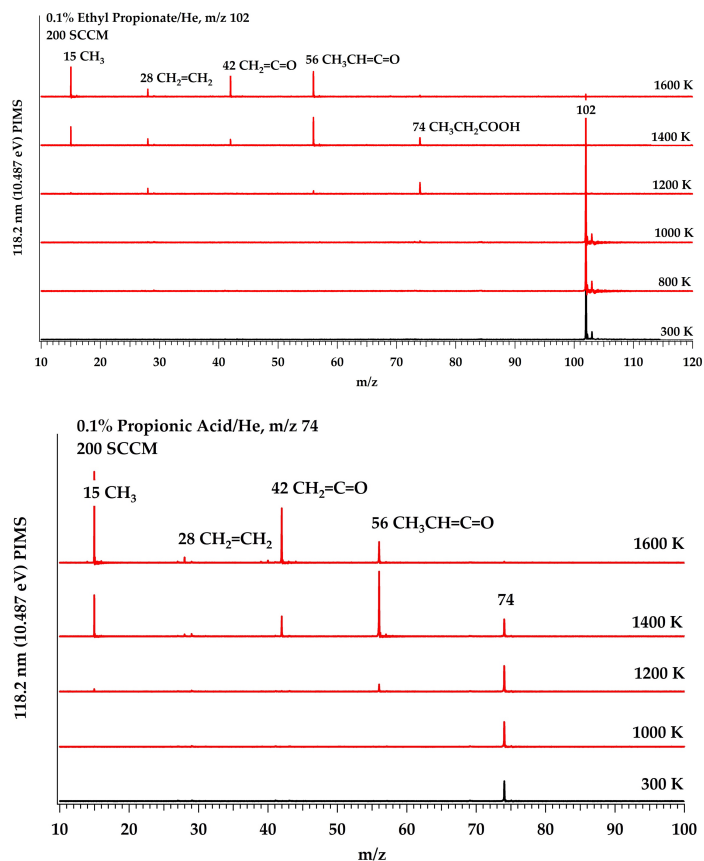


Figure 1: Observed masses for pyrolysis of 0.1% ethyl propanoate in He (*top*) and for 0.1% propionic acid in He (*bottom*).

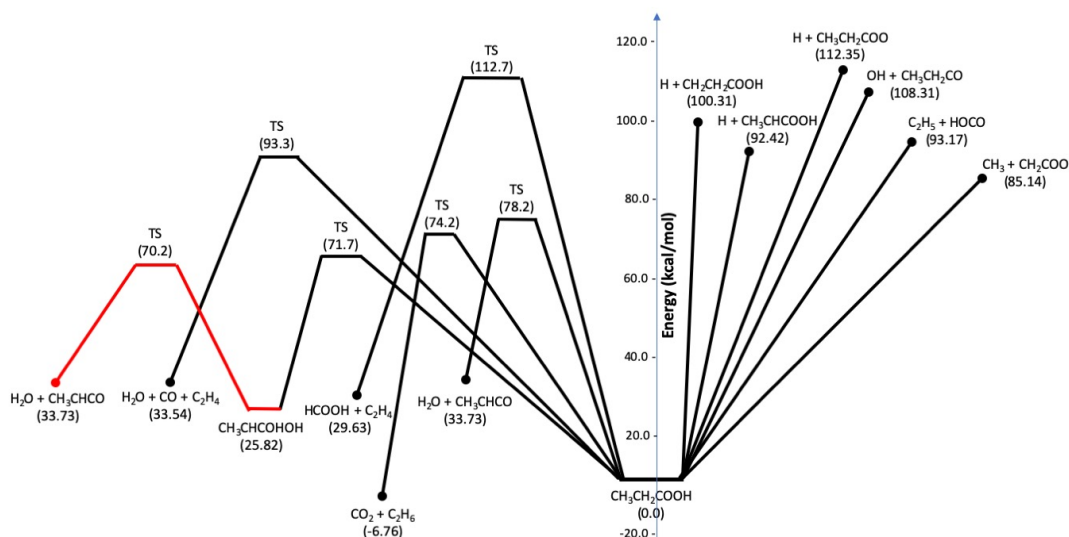


Figure 2: PES of propionic acid decomposition (*bottom*) obtained at the CCSD(T)/cc-pV ∞ Z//Mo6-2X/cc-pVTZ level of theory reveals importance of the well-skipping pathway highlighted in red.

Careful consideration of the observed products with the PES revealed an alternative pathway to methyl ketene via a well-skipping reaction through the diol product (see R6).

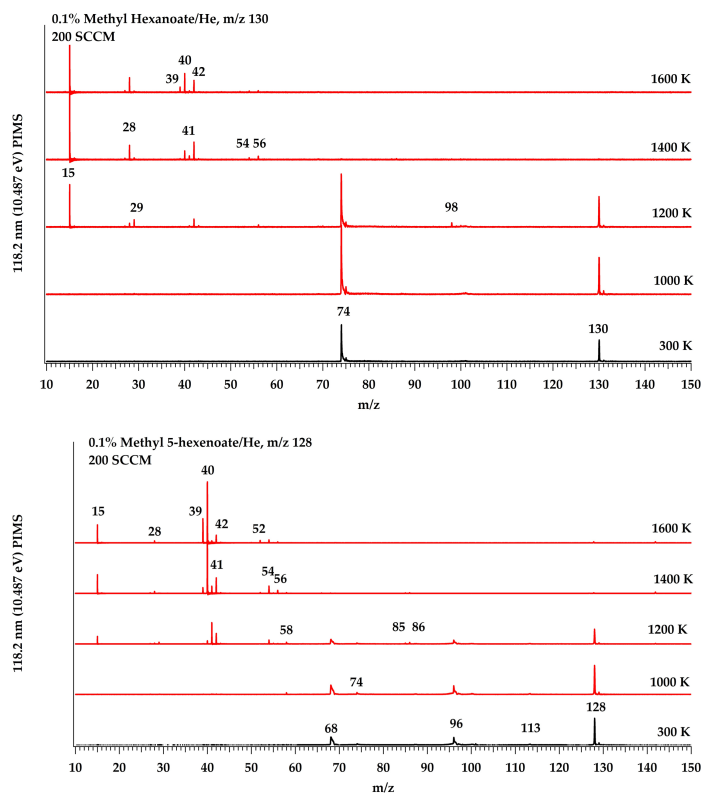
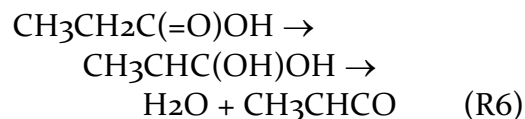


Figure 3: Observed masses for pyrolysis of 0.1% methyl hexanoate in He (*top*) and for 0.1% methyl hexenoate in He (*bottom*).

The tandem approach of theory and experiment resulted in revealing the true mechanism for propionic acid decomposition, when the well skipping pathway may not have otherwise been considered.



Methyl Hexanoate / Methyl 5-Hexenoate: Recently, we have performed photo-ionization mass spectrometry experiments on methyl hexanoate and the unsaturated methyl 5-hexenoate to understand the kinetic role of the double bond within the alkyl chain on methyl hexenoate. The results of these experiments can be found in Figure 3. In Figure 3-top, the spectra of methyl hexanoate is shown and possible identification for each peak is listed

in Table 1. At 300 K, the presence of dissociative ionization is detected and a fragment ion at m/z 74 appears. Thermal decomposition does not occur until around 1200 K, when m/z 98 (likely butyl ketene) emerges.

The peaks between the fully saturated methyl hexanoate (Figure 3-top) and the unsaturated methyl hexenoate (Figure 3-bottom) are similar, yet some distinct differences emerge. The ionization fragmentation pattern is distinctly different and several new species emerge at masses greater than m/z 50. While identification of these species and the mechanism through which they arise is ongoing, of note is the difference in intensity of m/z 40 and 39, which likely correspond to allene and propargyl, respectively. The double bond increases the selectivity towards these soot precursor molecules, which may have implications for pollutant formation.

Table 1: Possible Identifications of Species in Figure 3-top

m/z	Identification
130	Methyl hexanoate
98	Butyl ketene
74	$\text{CH}_2=\text{C}(\text{OH})\text{OCH}_3^+$
56	Butene
54	Butyne/Butadiene/Propadienal
42	Ketene/Propene
41	Allyl
40	Allene
39	Propargyl
29	Ethyl radical/HCO
28	Ethylene
15	Methyl radical

Future Plans

Work resolving the chemistry of methyl hexanoate and methyl 5-hexenoate is ongoing. A PES for both methyl esters is currently under development to elucidate the exact pathways for the products observed in the microreactor and for generation of rate constants for kinetic model development. Furthermore, a series of experiments has begun to study the H- and OH-abstraction products of these two methyl esters by using thermal radical sources such as ethyl iodide or tert-butyl hydroperoxide as a co-reactant within the microreactor.

Publications, Presentations, and Submitted Articles Acknowledging This Grant

C. Rogers, K. Cummins, J. Porterfield, J. W. Daily, G. B. Ellison, N. J. Labbe, “*The Pyrolysis Chemistry of Propionic Acid and Ethyl Propionate in a Microreactor*” Oral Presentation at the US National Combustion Meeting, Pasadena, CA, March 2019.

References

- [1] J. A. Barnard, et al. *J. Chem. Soc. Faraday Transactions 1*, 72 (1976) 1456-1463.
- [2] W. K. Metcalfe, et al. *J. Phys. Chem. A*, 111 (2007) 4001-4014.
- [3] W. K. Metcalfe, et al. *Combust. and Flame*, 156 (2009) 250-260.
- [4] S. M. Walton, et al. *Proc. of the Combust. Inst.*, 32 (2009) 255-262.
- [5] B. Yang, et al. *Phys. Chem. Chem. Phys.*, 13 (2011) 6901-6913.
- [6] A. Farooq, et al. *Fuel*, 134 (2014) 26-38.
- [7] G. Dayma, et al. *Energy & Fuels*, 26 (2012) 6669-6677.

Fundamental Molecular Spectroscopy and Chemical Dynamics

Stephen R. Leone and Daniel M. Neumark

Lawrence Berkeley National Laboratory and Departments of Chemistry and Physics, University of California, Berkeley, California 94720 (510) 643-5467 srl@berkeley.edu, 510-642-3502
dmneumark@berkeley.edu

Scope of the Project: Decades of research into molecular dynamics, including branching fractions, dissociation dynamics, and energetics, have vastly improved our fundamental understanding of chemical processes. Measurements of radical spectroscopy, ions and excited state dynamics comprise key future goals of the effort, especially the development of new ways to probe excited-state dynamics and photoproducts by the program of Leone and Neumark. The Leone group has pioneered femtosecond time-resolved table-top x-ray spectroscopic investigations of chemical dynamics at sufficiently high photon energies to access the carbon K-edge. Ultrafast x-ray transient absorption spectroscopy based on this methodology investigates transition states and products. The Neumark program uses a suite of experimental methods aimed at the spectroscopy and photodissociation dynamics of reactive free radicals: slow electron velocity-map imaging of cryogenically cooled anions (cryo-SEVI), a high resolution variant of photoelectron spectroscopy, fast radical beam (FRBM) studies of radical photodissociation, in which a beam of radicals is generated by negative ion photodetachment, and molecular beam photodissociation of radicals (XBeam) carried out on species generated by flash pyrolysis of suitable precursors.

Recent Progress:

Femtosecond Soft X-ray Transient Absorption Experiments

A unique femtosecond soft x-ray transient absorption spectroscopy apparatus with x-ray probe energies up to 300 eV is used to characterize the electronic structure of transient intermediates of chemical reactions. The ultrafast photoinduced ring-opening reaction of 1,3-cyclohexadiene, a fundamental prototype of photochemical pericyclic reactions, was investigated. The key step in this reaction is the ultrafast relaxation from the initial 1B excited state through a transient 2A excited-state intermediate known as the pericyclic minimum, which leads to isomerization onto the ring-opened product or the ground state with internal excitation. With the capability of femtosecond soft x-ray transient absorption spectroscopy near the carbon K-edge (284 eV), the electronic structure of the transient intermediate state is observed and a limit is put on the yield of ring-opened product.

In another ring opening study, x-ray transient absorption spectroscopy at the carbon K-edge provides spectral fingerprints of ring-opened isomers of organic heterocycles such as furfural. The unique differences in the electronic structure between a carbon atom bonded to an oxygen in the ring versus a carbon atom set free of the oxygen in the ring-opened product are readily apparent in the x-ray spectra. Ultrafast ring opening via C–O bond fission occurs within ~350 fs in 266-nm photoexcited furfural, as evidenced by fingerprint core (carbon 1s) electronic transitions into a nonbonding orbital of the open-chain carbene intermediate at 283.3 eV.

The ultrafast excited state non-adiabatic dynamics of acetylacetone (pentane-2,4-dione) is directly probed up to 150 ps after excitation at 266 nm using time-resolved x-ray absorption spectroscopy near the carbon K-edge (284 eV). At this wavelength, the enolic tautomer of the molecule is excited to the S_2 ($^1\pi\pi^*$) electronic state, from which it undergoes internal conversion to the lower-lying singlet states and intersystem crossing to the triplet states. Aided by density functional theory, the evolution of the core-to-valence resonances at the carbon K-edge directly establishes an ultrafast population of the T_1 state ($^3\pi\pi^*$) in acetylacetone via intersystem crossing from the S_2 state on a 1.5 ± 0.2 ps timescale.

Taking advantage of the broad bandwidth of the soft x-ray probe, the CH_2Cl radical generated by the ultrafast photodissociation of CH_2ICl at 266 nm is investigated at both the carbon K edge (~284 eV) and chlorine $L_{2,3}$ edge (~200 eV). The CH_2Cl radical is characterized by a prominent new carbon 1s

→ 2p feature at 282.8 eV, due to a transition to the half-filled frontier carbon 2p orbital (singly occupied molecular orbital SOMO), in addition to the shifts in the energies of core-level transitions from carbon 1s and chlorine 2p to the same $\sigma^*(\text{C}-\text{Cl})$ antibonding valence orbital. Characterizing these energy shifts provides a complete construction of the energy level diagram for the bonding and antibonding orbital changes before and after the C-I bond is broken. The removal of the I atom returns electron density to the carbon atom, causing a large energy shift due to the change in shielding around the carbon, while the C-Cl bond energy increases in energy, causing the antibonding orbital energy to increase significantly in energy.

A new type of experiment involves the ability to acquire detailed x-ray spectra of ions for the first time. Two-photon (1+1) ionization with 266 nm is used to prepare benzene cations in the ground state, a cation that undergoes well-known Jahn-Teller splitting. The ionization from the degenerate highest occupied π orbitals of neutral benzene leads to two cations, $\text{Bz}^+(\text{B}_{2g})$ and $\text{Bz}^+(\text{B}_{3g})$, with different partially occupied electronic states, $\pi(\text{b}_{2g})$ and $\pi(\text{b}_{3g})$, and consequently different geometries. Although the energetic splitting between the minima of these two states is very small, about 0.001 eV, the transitions from the C K-edge to the $\pi(\text{b}_{2g})$ and $\pi(\text{b}_{3g})$ orbitals indicates an ~ 1 eV difference. The large splitting of the x-ray transitions is confirmed by theoretical calculations by the group of A. Krylov at USC and S. Coriani at DTU (Denmark). The result presents an observation of Jahn-Teller splitting based on electronic spectroscopy, revealing the sensitivity of core orbitals to valence states and geometry changes. The remarkable sensitivity not only leads to a novel approach for observation of Jahn-Teller distortion, but it also provides a new concept of the core level sensitivity to C-C bond length and electronic structure of the valence states.

In order to access even faster electronic dynamics, a new beamline has been designed for attosecond and few-femtosecond soft x-ray transient absorption experiments. In this lab, 1300 nm pulses are compressed down to 9 fs few cycle pulses and used to generate a soft x-ray continuum up to 375 eV. This will be used to observe electronic dynamics at the carbon K-edge ultimately with attosecond time resolution. In addition to this unique probe, versatile pumping schemes are developed, namely few-cycle near infrared pulses and sub-20 fs UV pulses, to initiate, respectively, strong-field and one-photon excited state dynamics in molecules.

Free radical spectroscopy and dynamics

The spectroscopy and photodissociation dynamics of several free radicals are studied using slow photoelectron velocity-map imaging of cryogenically-cooled anions (cryo-SEVI), fast radical beam (FRBM) dissociation, and molecular beam photodissociation (XBeam). In cryo-SEVI, mass-selected anions are stored in an rf ion trap at $T=5$ K and cooled by collisions with a low pressure buffer gas. Ions are then extracted and photodetached, and the resulting slow photoelectrons are selectively analysed with velocity-map imaging, yielding photoelectron spectra with energy resolution as high as $1\text{-}2\text{ cm}^{-1}$ for complex species. The application of this method to two isomers of the pyridyl anion yields highly resolved vibrational structure of the corresponding radicals along with precise electron affinities.

Photodissociation of the phenoxy radical ($\text{C}_6\text{H}_5\text{O}$) is investigated using fast beam photofragment translational spectroscopy. Phenoxy radicals are generated through photodetachment of phenoxide anions at 532 nm. Following photoexcitation of the radicals at 225 nm, 290 nm, or 533 nm, photofragments are collected in coincidence to determine their masses, translational energy, and scattering angle for each dissociation event. Two-body dissociation yields exclusively $\text{CO} + \text{C}_5\text{H}_5$, while three-body dissociation to $\text{CO} + \text{C}_2\text{H}_2 + \text{C}_3\text{H}_3$ and $\text{CO} + \text{C}_5\text{H}_4 + \text{H}$ is also observed at the two higher photon energies. The translational energy distributions for two-body dissociation suggest that dissociation occurs via internal conversion to the ground electronic state followed by statistical dissociation. The absorption of an additional 532 nm photon in the photodetachment region provides some $\text{C}_6\text{H}_5\text{O}$ radicals with an additional 2.33 eV of energy, leading to much of the two-body dissociation observed at 533 nm and the three-body dissociation at the two higher excitation energies.

On the XBeam experiment, the photodissociation dynamics of jet-cooled methylsulfinyl radicals, CH_3SO , at 248 nm have been investigated using molecular beam photofragment translational spectroscopy. The primary channel is $\text{CH}_3\text{S} + \text{O}$, which occurs via the initially prepared excited CH_3SO state by rapid cleavage of the S-O bond to produce ground state products. The minor $\text{SO} + \text{CH}_3$ channel has two components in comparable proportions: a fast feature corresponding to rapid C-S cleavage on the excited state to produce CH_3 and electronically excited SO , and a slow feature due to internal conversion of CH_3SO followed by statistical dissociation on the ground electronic state. Statistical ground state dissociation also produces small amounts of CH_2SO , likely sulfine, and H-atoms.

Future Plans:

The UV-pump, soft x-ray-probe apparatus will be used to spectroscopically investigate fundamental hydrocarbon photochemical processes including radical formation, decomposition of carbonyl compounds, predissociation of aromatic systems, and isomerization of heterocyclic rings. Future investigations include cyclopentadiene, pentamethylcyclopentadiene, heptatriene, and pyrazine, involving characterization of rapid return to internally excited ground states, H migration, and possible isomerization channels. Future efforts will extend the soft x-ray probe to obtain energy-tunable pulses covering the nitrogen K-edge (410 eV) as well as the temporal resolution to achieve few-femtosecond timescales. The new attosecond soft X-ray apparatus will be combined with the short UV pump to provide the temporal resolution to resolve excited state dynamics through conical intersections in, e.g., methyl iodide, pyrazine and thymine. Coherent wave packet dynamics will be explored to detail the impact of vibrational wave packets on x-ray core-level absorption spectroscopy with attosecond resolution.

Neumark is transitioning the XBeam experiment to investigate the elastic, inelastic, and reactive scattering of atoms and reactive free radicals from flat liquid jets of water and other volatile solvents. The incorporation of flat jet technology into the molecular beam scattering instrument will build on the pioneering liquid scattering experiments carried out by Nathanson and co-workers. The proposed experiments will provide unprecedented insights into how the well-understood binary interactions that govern gas phase collision dynamics are modified when one of the scattering partners is a liquid. In addition, the flat jet geometry is suitable for carrying out transient absorption experiments in liquids at photon energies at or above the carbon K-edge, so mastering this technology will enable time-resolved x-ray experiments that will be of interest in the CPIMS and AMO programs in the DOE Basic Energy Sciences portfolio.

Recent Publications Acknowledging DOE GPCP Support (2016-2019):

- E. N. Sullivan, B. Nichols, D. M. Neumark, "Fast beam photofragment translational spectroscopy of the phenoxy radical at 225 nm, 290 nm, and 533 nm" *Phys. Chem. Chem. Phys.* (2019). DOI: 10.1039/c8cp06818f
- I. Ramphal, C. Lee, D. M. Neumark, "Photodissociation dynamics of the methylsulfinyl radical at 248 nm" *Molec. Phys.* (2019). DOI:10.1080/00268976.2019.1580781
- K. Schnorr, A. Bhattacharjee, K. J. Oosterbaan, M. G. Delcey, Z. Yang, T. Xue, A. R. Attar, A. S. Chatterley, M. Head-Gordon, S. R. Leone, and O. Gessner, "Tracing the 267 nm-Induced Radical Formation in Dimethyl Disulfide Using Time-Resolved X-ray Absorption Spectroscopy," *J. Phys. Chem. Lett.* 10, 1382–1387 (2019).
- A. Bhattacharjee, and S. R. Leone, "Ultrafast X-ray Transient Absorption Spectroscopy of Gas-Phase Photochemical Reactions - A New Universal Probe of Photoinduced Molecular Dynamics," *Acc. Chem. Res.* 51, 3203–3211 (2018).
- Z. Yang, K. Schnorr, A. Bhattacharjee, P. L. Lefebvre, M. Ephstein, T. Xue, J. F. Stanton, and S. R. Leone, "Electron-withdrawing effects in the photodissociation of CH_2ICl to form CH_2Cl radical, simultaneously viewed through the carbon K and chlorine $L_{2,3}$ X-ray edges," *J. Am. Chem. Soc.* 140, 13360 (2018).

- A. Bhattacharjee, K. Schnorr, S. Oesterling, Z. Yang, T. Xue, R. Vivie-Riedle, and S. R. Leone, "Photoinduced heterocyclic ring opening of furfural: distinct open-chain product identification by ultrafast X-ray transient absorption spectroscopy," *J. Am. Chem. Soc.* 140, 12538 (2018).
- P. M. Kraus, M. Zürch, S. K. Cushing, D. M. Neumark, and S. R. Leone, "The ultrafast X-ray spectroscopic revolution in chemical dynamics," *Nat. Rev. Chem.* 2, 82 (2018).
- E. N. Sullivan, B. Nichols, D. M. Neumark, "Photodissociation dynamics of the simplest alkyl peroxy radicals, CH_3OO and C_2H_5OO , at 248 nm," *J. Chem. Phys.* 148, 033409 (2018).
- B. Nichols, E. N. Sullivan, M. Ryazanov, C. M. Hong, D. M. Neumark, "Investigation of the two- and three-fragment photodissociation of the tert-butyl peroxy radical at 248 nm," *J. Chem. Phys.* 147, 134304 (2017).
- J. A. DeVine, M. L. Weichman, M. C. Babin, Daniel M. Neumark, "Slow photoelectron velocity-map imaging of cold tert-butyl peroxide," *J. Chem. Phys.* 147, 013915 (2017).
- M. L. Weichman, L. Cheng, J. B. Kim, J. F. Stanton, D. M. Neumark, "Low-lying vibronic level structure of the ground state of the methoxy radical: Slow electron velocity-map imaging (SEVI) spectra and Koppel-Domcke-Cederbaum (KDC) vibronic Hamiltonian calculations," *J. Chem. Phys.* 146, 224309 (2017).
- Z. Wang, D. M. Popolan-Vaida, B. Chen, K. Moshhammer, S. Y. Mohamed, H. Wang, S. Sioud, M. A. Raji, K. Kohse-Höinghaus, N. Hansen, P. Dagaut, S. R. Leone, and S. M. Sarathy, "Unraveling the structure and chemical mechanisms of highly oxygenated intermediates in oxidation of organic compounds," *PNAS* 114, 13102 (2017).
- I. A. Ramphal, M. Shapero, C. Haibach-Morris, D. M. Neumark, "Photodissociation dynamics of fulvenallene and the fulvenallenyl radical at 248 and 193 nm," *Phys. Chem. Chem. Phys.* 19, 29305 (2017).
- A. Bhattacharjee, C. D. Pemmaraju, K. Schnorr, A. R. Attar, and S. R. Leone, "Ultrafast intersystem crossing in acetylacetone via femtosecond x-ray transient absorption at the carbon K-edge," *J. Am. Chem. Soc.* 139, 16576 (2017).
- Z. Wang, D. M. Popolan-Vaida, B. Chen, K. Moshhammer, S. Y. Mohamed, H. Wang, S. Sioud, M. A. Raji, K. Kohse-Höinghaus, N. Hansen, P. Dagaut, S. R. Leone, and S. M. Sarathy, "Unraveling the structure and chemical mechanisms of highly oxygenated intermediates in oxidation of organic compounds," *PNAS* 114, 13102 (2017).
- S. Chambreau, D. Popolan-Vaida, G. Vaghjiani, and S. R. Leone, "Catalytic decomposition of hydroxylammonium nitrate ionic liquid: enhancement of NO formation," *J. Phys. Chem. Lett.* 8, 2126 (2017).
- S. D. Chambreau, D. M. Popolan-Vaida, G. L. Vaghjiani, S. R. Leone, "Catalytic Decomposition of Hydroxylammonium Nitrate Ionic Liquid: Enhancement of NO Formation," *J. Phys. Chem. Lett.* 8, 2126-2130 (2017).
- A. R. Attar, A. Bhattacharjee, C. D. Pemmaraju, Kirsten Schnorr, Kristina D. Closser, David Prendergast, and S. R. Leone, "Femtosecond x-ray spectroscopy of an electrocyclic ring-opening reaction," *Science* 356, 54 (2017).
- B. Nichols, E. N. Sullivan, M. Ryazanov, D. M. Neumark, "Photodissociation dynamics of the i-methylvinoxy radical at 308, 248, and 225 nm using fast beam photofragment translational spectroscopy" *J. Phys. Chem. A* 121, 579 (2017).
- J. A. DeVine, M. L. Weichman, S. J. Lyle, D. M. Neumark, "High-resolution photoelectron imaging of cryogenically cooled α - and β -furanil anions" *J. Mol. Spec.* 332, 16 (2017).
- A. W. Harrison, M. Ryazanov, E. N. Sullivan, D. M. Neumark, "Photodissociation dynamics of the methyl perthiyl radical at 248 and 193 nm using fast-beam photofragment translational spectroscopy" *J. Chem. Phys.* 145, 024305 (2016).
- N. C. Cole-Filipiak, M. Shapero, C. Haibach-Morris, D. M. Neumark, "Production and Photodissociation of the Methyl Perthiyl Radical" *J. Phys. Chem. A* 120, 4818 (2016).
- A. Bhattacharjee, A. R. Attar, and S. R. Leone, "Transition-state region in the A-band photodissociation of Allyl Iodide – A femtosecond extreme ultraviolet transient absorption study", *J. Chem. Phys.* 144, 124311 (2016).
- A. D. Dutoi, S. R. Leone, "Simulation of x-ray transient absorption for following vibrations in coherently ionized F_2 molecules," *Chem. Phys.* 482, 249 (2016).

SPECTROSCOPY AND DYNAMICS OF REACTION INTERMEDIATES IN COMBUSTION CHEMISTRY

Marsha I. Lester
Department of Chemistry
University of Pennsylvania
Philadelphia, PA 19104-6323
milester@sas.upenn.edu

I. Program Scope

Carbonyl oxides (Criegee intermediates), important intermediates in tropospheric hydrocarbon oxidation and some combustion reactions, and related isomeric species are being examined to determine their intrinsic stability and explore dynamical pathways.

II. Recent Progress

A. Electronic spectroscopy and dynamics

Recently, the Lester group generated and characterized a four-carbon unsaturated Criegee intermediate in the laboratory for the first time. The laboratory synthesis differs from previous studies,¹ since an analogous *gem* diiodo precursor cannot be readily synthesized. Instead, we demonstrated that photolysis of 1,3-diiodobut-2-ene generates a resonance-stabilized monoiodoalkene radical that reacts with O₂ to produce methylvinylketone oxide ((CH₂=CH(CH₃)COO, MVK-oxide).^{2,3} This four-carbon unsaturated Criegee intermediate is of particular significance because it accounts for 23% of the Criegee intermediates formed in the ozonolysis of isoprene, which is the most abundant non-methane hydrocarbon in the atmosphere. In the past year, we have explored the UV-vis and IR spectroscopy of MVK-oxide, along with its photochemical and unimolecular decay pathways.^{2,3} MVK-oxide is predicted to have four conformers with similar ground state energies (within ca. 3.2 kcal mol⁻¹) that are separated by significant barriers to isomerization.

The UV-vis spectrum of MVK-oxide was recorded on its first $\pi^* \leftarrow \pi$ electronic transition under isolated conditions following supersonic jet cooling. Resonant UV-vis laser excitation induces a ground state depletion and an associated reduction of the VUV (10.5 eV) photoionization signal on the *m/z* 86 parent mass. The strong depletion (up to 25%) of one or more of the four MVK-oxide conformers peaks at 388 nm in a one-photon absorption process. The experimental spectrum is broad and unstructured, spanning from at least 300 to 430 nm, with an asymmetric profile that falls off sharply on the long wavelength side. Additional velocity map imaging experiments reveal an anisotropic distribution of O ¹D products, demonstrating that electronic excitation of MVK-oxide to the 1¹ $\pi\pi^*$ excited state results in rapid dissociation (≤ 100 ps). The prompt excited state dynamics assures that the UV-vis spectrum obtained by the depletion method is equivalent to a direct absorption measurement.

Complementary electronic structure calculations (CASPT2(12,10)/AVDZ) predict two $\pi^* \leftarrow \pi$ transitions with significant oscillator strength for each of the four conformers of MVK-oxide with vertical excitation energies (and corresponding wavelengths) at 3.1-3.6 eV (350-400 nm), in good accord with experiment, and 4.5-5.5 eV (220-280 nm). These two optically bright transitions are nominally associated with the carbonyl oxide and vinyl groups. The computed electronic absorption profile of MVK-oxide, based on a Wigner distribution of ground state

configurations and summed over the four conformers, is predicted to peak at 397 nm. Electronic excitation of MVK-oxide to the $1^1\pi\pi^*$ state accesses a repulsive region of the excited state potential energy surface, leading to conical intersections with repulsive potentials that result in dissociation.

The first $\pi^*\leftarrow\pi$ electronic transition of MVK-oxide is shifted to longer wavelength than previously studied Criegee intermediates due to extended conjugation across the carbonyl oxide and vinyl groups. Our recent identification of the UV-vis spectrum of MVK-oxide is expected to enable future studies of its photochemistry, unimolecular decay processes, and bimolecular reactions. These ongoing and future studies may, in turn, help unravel the contributions of the four conformers of MVK-oxide to the UV-vis spectrum.

In earlier work, we utilized velocity map imaging to demonstrate the prompt release of O 1D products upon UV excitation of the CH₂OO Criegee intermediate in the long wavelength tail region (364 to 417 nm) of the B¹A' - X¹A' spectrum.⁴ The VMI images exhibit anisotropic distributions indicating that dissociation to H₂CO X¹A₁ + O 1D products is rapid compared to the rotational period of CH₂OO and occurs on a picosecond timescale. As a result, the broad oscillatory structure reported previously by several groups⁵⁻⁷ in the long wavelength tail region of the UV absorption spectrum is attributed to short-lived resonances associated with the excited B¹A' state of CH₂OO, in accord with theoretical predictions.⁸

The total kinetic energy release distributions show that the available energy is nearly equally partitioned, on average, between product translational energy and internal excitation of the H₂CO co-fragments. The anisotropy and energy partitioning are unchanged with excitation wavelength, and consistent with previously reported experimental and theoretical findings of the CH₂OO B-X transition moment and dissociation energy to H₂CO X¹A₁ + O 1D products.^{9,10} Thus, the strong UV absorption spectrum over the entire wavelength range (308 to 417 nm)^{5-7,11} arises from electronic excitation of CH₂OO from its ground X¹A' state to a single excited electronic state, namely the B¹A' state, which couples to repulsive singlet states and results in rapid O-O bond breakage and dissociation.

B. Photoionization mass spectrometry studies

In collaboration with Taatjes and coworkers, we have also carried out experiments on hydroxyacetone (CH₃C(O)CH₂OH) formation using the multiplexed photoionization mass spectrometer at the Chemical Dynamics Beamline with tunable VUV radiation from the Advanced Light Source.¹² Hydroxyacetone was identified as a stable product from reactions of the (CH₃)₂COO Criegee intermediate in a flow tube. In the experiment, the two isomers at m/z 74 are distinguished by their different photoionization spectra and reaction times. Hydroxyacetone was observed as a persistent signal at m/z 74 at longer (≥ 5 ms) reaction times and higher photoionization energies starting at ca. 9.7 eV. Complementary electronic structure calculations by Kumar and Thompson have revealed multiple reaction pathways for hydroxyacetone formation including a unimolecular isomerization mechanism involving hydrogen atom transfer and -OH group migration as well as self-reaction of the Criegee intermediates. Varying the concentration of Criegee intermediates suggests contributions from both unimolecular and self-reaction pathways to hydroxyacetone. The unimolecular mechanism is more likely to occur for alkene ozonolysis reactions, where hydroxyacetone can potentially be monitored as a stable end product.

Further theoretical work by Kuwata et al.¹³ has shown that a roaming-induced isomerization pathway provides an explanation for the observation of hydroxyacetone in our recent experiments on the thermal decay of (CH₃)₂COO.¹² In collaboration with Klippenstein, we have mapped out an analogous roaming pathway for *syn*-conformers of MVK-oxide.² In addition to unimolecular decay of *syn*-MVK-oxide to OH radicals, the OH radical may roam in a relatively flat potential region and react with the co-fragment to form 1-hydroxybut-3-en-2-one. By contrast, *anti*-conformers of MVK-oxide are predicted to undergo rapid unimolecular decay via an electrocyclic ring-closing reaction to form dioxole.² While these and other isomers could be ionized at 10.5 eV, none are predicted to absorb in the 300-430 nm region observed for MVK-oxide.

III. Future Work

A new line of research is being pursued in our laboratory to generate hydroperoxyalkyl radicals in a pulsed supersonic expansion, and characterize them spectroscopically. In addition, we will be continuing research at Penn and in collaboration with Taatjes and coworkers at the Advanced Light Source on critical reaction intermediates derived from ozonolysis of isoprene. Novel unimolecular decay pathways and key bimolecular reactions will be examined. The highly isomer- and conformer-specific chemistry of four-carbon unsaturated carbonyl oxide intermediates will be unraveled using the Sandia multiplexed photoionization mass spectrometer interfaced with tunable VUV output of beamline 9.0.2.

IV. References

1. O. Welz, J. D. Savee, D. L. Osborn, S. S. Vasu, C. J. Percival, D. E. Shallcross and C. A. Taatjes, *Science* 335, 204-207 (2012).
2. M. F. Vansco, B. Marchetti, and M. I. Lester, *J. Chem. Phys.* 149, 244309 (2018).
3. V. P. Barber, S. Pandit, A. M. Green, N. Trongsirawat, P. J. Walsh, S. R. Klippenstein, and M. I. Lester, *J. Am. Chem. Soc.* 140, 10866–80 (2018).
4. M. F. Vansco, H. Li and M. I. Lester, *J. Chem. Phys.* 147, 013907 (2017).
5. L. Sheps, *J. Phys. Chem. Lett.* 4, 4201 (2013).
6. W.-L. Ting, Y.-H. Chen, W. Chao, M. C. Smith and J. J.-M. Lin, *Phys. Chem. Chem. Phys.* 16, 10438 (2014).
7. E. S. Foreman, K. M. Kapnas, Y. Jou, J. Kalinowski, D. Feng, R. B. Gerber and C. Murray, *Phys. Chem. Chem. Phys.* 17, 32539 (2015).
8. R. Dawes, B. Jiang and H. Guo, *J. Am. Chem. Soc.* 137, 50 (2015).
9. J. H. Lehman, H. Li, J. M. Beames and M. I. Lester, *J. Chem. Phys.* 139, 141103 (2013).
10. H. Li, Y. Fang, J. M. Beames and M. I. Lester, *J. Chem. Phys.* 142, 214312 (2015).
11. J. M. Beames, F. Liu, L. Lu, and M. I. Lester, *J. Am. Chem. Soc.* 134, 20045-48 (2012).
12. C. A. Taatjes, F. Liu, B. Rotavera, M. Kumar, R. Caravan, D. L. Osborn, W. H. Thompson, and M. I. Lester, *J. Phys. Chem. A* 121, 16-23 (2017).
13. K. T. Kuwata, L. Luu, A. B. Weberg, K. Huang, A. J. Parsons, L. A. Peebles, N. B. Rackstraw, and M. J. Kim, *J. Phys. Chem. A* 122, 2485-2502 (2018).

V. Publications supported by this DOE project (2016-present)

1. M. F. Vansco, B. Marchetti, and M. I. Lester, "Electronic spectroscopy of methyl vinyl ketone oxide: A four-carbon unsaturated Criegee intermediate from isoprene ozonolysis", [*J. Chem. Phys.* 149, 244309 \(2018\)](#).

2. V. P. Barber, S. Pandit, A. M. Green, N. Trongsiwat, P. J. Walsh, S. R. Klippenstein, and M. I. Lester, "Four carbon Criegee intermediate from isoprene ozonolysis: Methyl vinyl ketone oxide synthesis, infrared spectrum, and OH production", [*J. Am. Chem. Soc.* **140**, 10866–80 \(2018\)](#).
3. M. F. Vansco, H. Li, and M. I. Lester, "Prompt release of O ¹D products upon UV excitation of CH₂OO Criegee intermediates", [*J. Chem. Phys.* **147**, 013907 \(2017\)](#).
4. C. A. Taatjes, F. Liu, B. Rotavera, M. Kumar, R. Caravan, D. L. Osborn, W. H. Thompson, and M. I. Lester, "Hydroxyacetone production from C₃ Criegee intermediates", [*J. Phys. Chem. A* **121**, 16-23 \(2017\)](#).
5. H. Li, N. M. Kidwell, X. Wang, J. M. Bowman, and M. I. Lester, "Velocity map imaging of OH radical products from IR activated (CH₃)₂COO Criegee intermediates", [*J. Chem. Phys.* **145** 104307 \(2016\)](#).
6. A. M. Green, F. Liu, and M. I. Lester, "UV + VUV double-resonance studies of autoionizing Rydberg states of the hydroxyl radical", [*J. Chem. Phys.* **144**, 184311 \(2016\)](#).
7. N. M. Kidwell, H. Li, X. Wang, J. M. Bowman, and M. I. Lester, "Unimolecular dissociation dynamics of vibrationally activated CH₃CHOO Criegee intermediates to OH radical products", [*Nat. Chem.* **8**, 509-14 \(2016\)](#).

Advanced Nonlinear Optical Methods for Quantitative Measurements in Flames

Robert P. Lucht

School of Mechanical Engineering, Purdue University

West Lafayette, IN 47907-2088

Lucht@purdue.edu

I. Program Scope

Nonlinear optical techniques such as laser-induced polarization spectroscopy (PS), resonant wave mixing (RWM), and ultrafast coherent anti-Stokes Raman scattering (CARS) are techniques that show great promise for high-repetition-rate temperature measurements and sensitive measurements of transient gas-phase species, and diagnostic applications of these techniques are being pursued actively at laboratories throughout the world. The objective of this research program is to develop and test strategies for quantitative concentration and temperature measurements using nonlinear optical techniques in flames and plasmas. We have continued our fundamental theoretical and experimental investigations of these techniques. In recent years our theoretical and experimental efforts have been focused on investigating the potential of femtosecond (fs) laser systems for sensitive and accurate CARS measurements in gas-phase media. In the last few years we have demonstrated the acquisition of single-shot temperature measurements at data rates of 5 kHz in highly turbulent, swirl-stabilized methane-air flames and then in pilot-stabilized jet flames with both gaseous and liquid fuels (these measurements are described in P2 and P5-P7) using N₂ chirped-probe-pulse (CPP) fs CARS. Our recent efforts have focused on the CPP fs CARS spectroscopy of other species such as CO₂ and O₂. We have also performed measurements on these species in a high-pressure, high-temperature gas cell and have observed very significant self-phase modulation of the pump and Stokes beams, with consequent significant impact on the CPP fs CARS spectra. Although our initial ultrafast spectroscopy efforts have been focused on fs CARS, ultrafast laser systems will be useful for a wide range of future diagnostic techniques involving two-photon-induced processes including fluorescence and RWM.

We are investigating the physics of both fs CARS and two-color PS by direct numerical integration (DNI) of the time-dependent density matrix equations for the resonant interaction. Significantly fewer restrictive assumptions are required using this DNI approach compared with the assumptions required to obtain analytical solutions. We are concentrating on the accurate simulation of two-photon processes, including Raman transitions, where numerous intermediate electronic levels contribute to the two-photon transition strength. Recent progress has been much more rapid in our modeling efforts after my PhD student Mingming Gu parallelized the time-dependent density matrix code with the assistance of my faculty colleague Prof. Carlo Scalo. The code was parallelized such that different computer nodes performed independent calculations for separate Q-branch transitions. The calculated electric field amplitude of the signal from each of these transitions was then added to give us the time-dependent CARS signal amplitude, and the spectrum was then calculated by Fourier transforming the time-dependent CARS signal amplitude. Using this parallelized computer code, we have investigated in detail the effects of chirp in the pump and Stokes beams on the Raman excitation efficiency and on signal generation for chirped-probe-pulse (CPP) fs CARS.

We also began a theoretical analysis of Raman transitions, in particular pure rotational Raman transitions for the nitric oxide molecule. The theoretical approach is very similar to that employed to calculate two-photon absorption line strengths for nitric oxide described in paper P1. The theoretical results have been compared with pure rotational CARS measurements performed several years ago on this project, and we have determined a new value for the anisotropic molecule-fixed tensor invariant that gives rise to the electronic Raman transition at 121 cm⁻¹ between the spin split ²Π_{1/2} and ²Π_{3/2} ground electronic levels.

II. Recent Progress

A. Advances in CPP Fs CARS

Fs CARS offers several major potential advantages compared with nanosecond (ns) CARS; i.e., CARS as usually performed with nanosecond pump and Stokes lasers. These potential advantages include an elimination of collisional effects in the signal generation and the capability of performing real-time temperature and species measurements at data rates of 1 kHz or greater as compared to 10-50 Hz for ns CARS. Our Coherent ultrafast laser system operates at 5 kHz with a fundamental pulse width of 55-60 fs and pulse energy of over 2 mJ.

After we parallelized our time-dependent density matrix code for fs CARS, we were able to speed up the calculations by a factor of almost 100 by parallelizing and rewriting the code using the Python programming language. This in turn has allowed us to extract much more physical insight from our computer calculations because we can perform parametric variation studies much faster.

We have completed an investigation of the effects of moderate chirp in the pump and Stokes beams on the Raman excitation efficiency and signal generation for CPP fs CARS. This may be very significant for projected future applications of the technique to high pressure systems, where the beams may have to propagate through thick windows which will induce significant chirp. The key result of our study of pump and Stokes chirp effects is that as long as the sign and magnitudes of the chirp are nearly equal for the pump and Stokes beams, the bandwidth of Raman excitation efficiency envelope decreases only slightly. This effect must be taken into account to extract accurate temperatures from either CPP fs CARS, performed in our laboratory, or hybrid fs/ps CARS. We explored the effects of inducing moderate chirp in the pump and Stokes beams by placing SF11 disks with thicknesses of 10, 20, or 30 mm in the pump and Stokes beam paths. Our results indicate that inducing moderate levels of chirp appears to actually enhance, albeit slightly, the temperature accuracy and precision of the CPP fs CARS technique.

In our most recent work we are exploring the potential for measuring temperature and concentrations from CPP fs CARS for species such as CO_2 and O_2 . These studies are significant for future measurements in oxy-fuel flames or in pressure gain combustion devices where N_2 may not be present in high concentrations for CARS temperature measurements. While the spectral model for O_2 is very similar to that for N_2 , the spectral model for CO_2 is significantly more complicated. Some results of our initial experimental and theoretical results for CO_2 CPP fs CARS are shown in Fig. 1.

B. Self-Phase Modulation Effects in Femtosecond CARS

Several years ago we measured the CPP fs CARS spectra of methane and ethylene at room temperature and at pressures ranging from 1 to 7 bar. The methane spectrum was essentially unchanged as a function of pressure, but the ethylene spectrum changed drastically as the pressure was increased from 1 to 7 bar. We were not able to explain this effect at that time, but last year we again

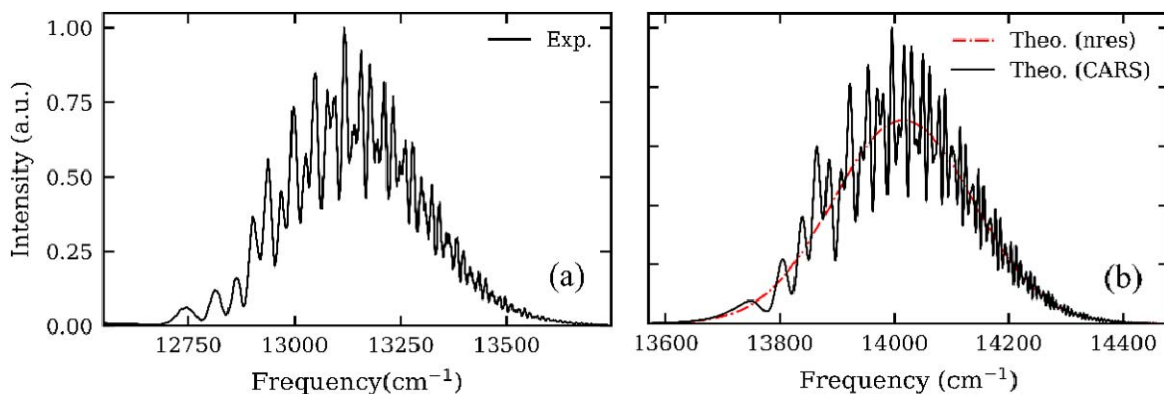


Fig. 1. CPP fs CARS spectra of CO_2 at room temperature and pressure. (a) Experiment (b) Theory.

started to investigate high-pressure effects for N_2 , CO_2 , O_2 , CH_4 and C_2H_4 in a new high-pressure, high-temperature cell at pressures from 1 to 10 bar. We observed that at high pulse energies that the spectra of all of these species were very pressure dependent, even though the characteristic collisional times were much longer than the chirped probe pulse time duration of ~ 3 ps. We measured the spectra of the pump and Stokes beams before and after the cell and observed a drastic change in the spectrum for high cell pressures due to self-phase modulation (SPM). This effect is shown in Fig. 2 for CO_2 CPP fs CARS. The SPM effects for molecules such as CO_2 and N_2 with pure rotational spectra include both broadening and a shift of the pump and Stokes spectra, whereas for a spherically symmetric molecule such as CH_4 the pump and Stokes spectra broaden but the central frequency does not shift. The shift in the CO_2 CPP fs CARS spectrum towards lower frequencies as pressure increases is clearly evident in both panels of Fig. 2. We are able to model the SPM effects with two parameters (electronic and pure rotational) and obtain good fits to the SPM-altered pump and Stokes spectra at the gas cell exit. Furthermore we are able to obtain good fits to the SPM-altered N_2 CPP fs CARS spectra using the SPM parameters at the cell exit, divided by a factor of 2, to calculate the pump and Stokes spectra at the CARS probe volume.

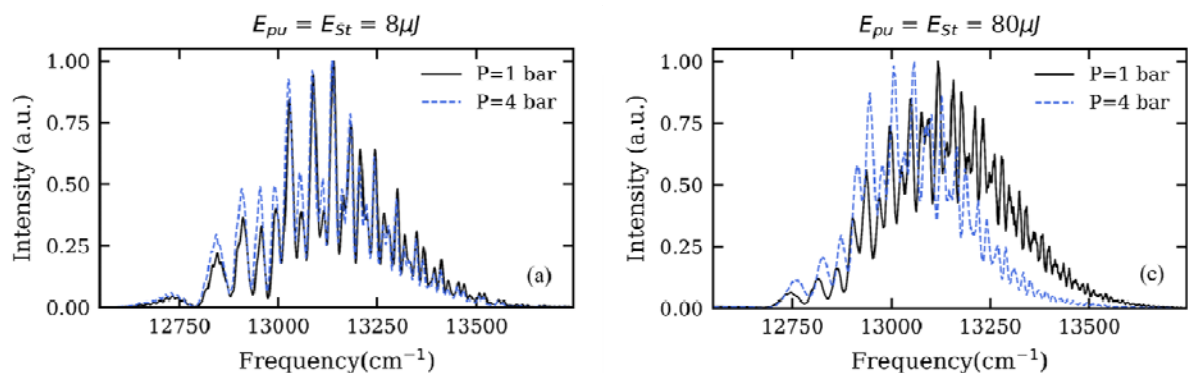


Fig. 2. CPP fs CARS spectra of CO_2 at room temperature. (a) Low pump and Stokes pulse energies. (b) High pump and Stokes pulse energies.

C. Pure Rotational Raman Spectroscopy of Nitric Oxide

We have performed pure rotational CARS measurements mixture of nitric oxide and nitrogen at room temperature. The simultaneous acquisition of pure rotational CARS spectra from known mixtures of these two species will enable us to determine with excellent accuracy the pure rotational Raman cross section for nitric oxide, given that the pure rotational Raman cross section of nitrogen is so well known. The theoretical analysis of the pure rotational Raman process in nitric oxide is based both on a density matrix analysis where the intermediate electronic levels of the molecule are taken into account and on a polarizability analysis where the intermediate levels are not explicitly included. This last analysis is very similar to the two-photon transition analysis described in paper P1.

D. CARS Temperature Measurements in Sooting Ethylene/Nitrogen Diffusion Flames

Temperature measurements were performed in sooting ethylene-air co-flow diffusion flames stabilized over a Yale burner. The Yale burner also known as Smooke/Long burner is identified as the third target flame by the international sooting flame workshop. Measurements were performed using a dual-pump vibrational CARS system to obtain temperature measurements, without soot interference, with high spatial and temporal resolution. We were able to obtain excellent quality spectra in all parts of the flame including the highly sooting region and near the tip of the fuel nozzle where the nonresonant modulation of the CARS spectra is strong. Large discrepancies, in both peak temperature and temperature profiles, were observed between CARS measurements and previously performed CFD calculations. Paper P8 describing this work has been submitted to Combustion and Flame.

III. Future Work

We will continue to perform fs CARS experiments using the Coherent ultrafast laser system. Our studies of temperature measurements using CPP fs CARS will continue. We continue to investigate the effect of laser system parameters on the CPP fs CARS spectrum to improve the temperature accuracy of the technique. We will explore the potential for using CPP fs CARS for accurate concentration measurements for polyatomic species such as CO₂ and hydrocarbons. We will make full use of the high-temperature, high-pressure gas cell that we have fabricated for fundamental studies of the effects of temperature and pressure on CPP fs CARS spectra. We will explore further the effects of soot and droplets on the CPP fs CARS process, and use a Pockels cell between crossed polarizers as a fast electronic shutter for the 5 kHz fs CARS measurements.

Our theoretical studies of the physics of fs CARS will continue. The parallelization of our density matrix computer code will allow us to explore effects such as collisional narrowing that was simply not possible using the serial version of our code. The study of collisional narrowing requires communication between different computational nodes due to the transfer of coherence during collisions. We are still developing the numerical code for the collisional narrowing studies.

Our investigation of two-color PS and 6WM for species such as NO will continue. We will explore collisional effects on the PS and 6WM processes in much more detail using a two-dye laser system that is just becoming operational. We will explore further the effects of buffer gas collisions on collision-induced resonances in single-photon, two-color PS of NO. We will continue to use the density matrix code to gain insight into the physics of the PS and 6WM processes.

Our theoretical studies of the physics of two-photon resonances will also continue. We will also initiate an investigation of two-photon-induced fluorescence for species such as NO. The broadband excitation provided by fs pulses will be a significant advantage for these measurements.

IV. Refereed publications and submitted journal articles supported by this project 2017-2019

- P1. W. D. Kulatilaka and R. P. Lucht, "Two-Photon-Absorption Line Strengths for Nitric Oxide: Comparison of Theory and Sub-Doppler, Laser-Induced Fluorescence Measurements," *Journal of Chemical Physics* **146**, 124311 (2017). DOI: 10.1063/1.4978921
- P2. L. M. Thomas, A. Satija, and R. P. Lucht, "Technique Developments and Performance Analysis of Chirped-Probe-Pulse Femtosecond Coherent Anti-Stokes Raman Scattering Combustion Thermometry," *Applied Optics* **56**, 8797-8810 (2017). DOI: 10.1364/AO.56.008797
- P3. D. Han, A. Satija, J. Kim, Y. Weng, J. P. Gore, R. P. Lucht, "Dual-Pump Vibrational CARS Measurements of Temperature and Species Concentrations in Turbulent Premixed Flames with CO₂ Addition," *Combustion and Flame* **181**, 239-250 (2017). DOI: 10.1016/j.combustflame.2017.03.027
- P4. D. Han, J. Kim, A. Satija, J. P. Gore, and R. P. Lucht, "Experimental Study of CO₂ Diluted, Piloted, Turbulent CH₄/Air Premixed Flames using High-Repetition-Rate OH PLIF," *Combustion and Flame* **193**, 145-156 (2018). DOI: 10.1016/j.combustflame.2018.03.012
- P5. A. Lowe, L. M. Thomas, A. Satija, R.P. Lucht, and A.R. Masri, "Chirped-Probe-Pulse Femtosecond CARS Thermometry in Turbulent Spray Flames," *Proceedings of the Combustion Institute* **37**, 1383-1391 (2019). DOI: 10.1016/j.proci.2018.06.149
- P6. L. M. Thomas, A. Lowe, A. Satija, A.R. Masri, and R.P. Lucht, "5 kHz Thermometry in Turbulent Spray Flames Using Chirped-Probe-Pulse Femtosecond Coherent Anti-Stokes Raman Scattering, Part I: Processing and Interference Analysis," *Combustion and Flame* **200**, 405-416 (2019). DOI: [10.1016/j.combustflame.2018.11.004](https://doi.org/10.1016/j.combustflame.2018.11.004)
- P7. A. Lowe, L. M. Thomas, A. Satija, R.P. Lucht, and A.R. Masri, "Chirped-Probe-Pulse Femtosecond CARS Thermometry in Turbulent Spray Flames," *Proceedings of the Combustion Institute* **37**, 1383-1391 (2019). DOI: 10.1016/j.proci.2018.06.149
- P8. A. Satija, Z. Chang, A. Lowe, L. M. Thomas, A. Masri, and R. P. Lucht, "CARS Thermometry in Laminar Sooting Ethylene-Air Co-Flow Diffusion Flames with Nitrogen Dilution," *Combustion and Flame*, submitted for publication (2019).

Thermal Decomposition of Cyclic, Oxygenated Hydrocarbons

Laura R. McCunn
Chemistry Department, Marshall University
1 John Marshall Dr.
Huntington, WV 25755
mccunn@marshall.edu

Program Scope

The objective of this project is to elucidate how chemical structure affects the thermal decomposition mechanisms of cyclic, oxygenated hydrocarbons that are relevant to biofuels and combustion. The primary specific aim of the proposed experiments is to identify the thermal decomposition products of dihydro-2-furanone, dihydro-3-furanone, 2-cyclopentenone, 3-cyclopentenone, 2-pyrone, and 4-pyrone. A pulsed hyperthermal nozzle will be used to induce gas-phase pyrolysis at temperatures up to 1600 K. Product detection will be accomplished with a matrix-isolation FTIR spectrophotometer. A second specific aim of the project is to construct a mass spectrometer with tunable low-energy electron-impact ionization that can be used with the same hyperthermal nozzle. The introduction of a new detection technique will complement the FTIR experiments and provide a more complete characterization of the pyrolysis products, which is essential to the development of accurate thermal decomposition mechanisms.

The experiments are designed to probe the early steps in the pyrolysis mechanism, with the possibility of capturing radical intermediates. Two goals can be accomplished by this approach. First, the results will augment the existing body of knowledge created by shock-tube and static pyrolysis experiments, which typically probe the ultimate products of thermal decomposition on long time scales. Adding to the variety of techniques in the literature will clarify pyrolysis mechanisms, which can include dozens of elementary steps. Second, identifying pyrolysis products of compounds that are intermediates or by-products in the production or combustion of new fuels will enable the prediction of pollutants from these fuels. The experimental results will contribute to the elucidation of pyrolysis mechanisms and enable the assessment of the environmental impact of various fuels. The completed research will build a foundation of knowledge for overcoming challenges to the nation's energy supply and environmental quality.

The project period began in April 2019 and continues for two years. The early months of the project will be devoted to design and construction of the mass spectrometer. Concurrently, experiments will be conducted using the existing hyperthermal nozzle and matrix-isolation FTIR instrument.

Methodology

The laboratory has an established instrument consisting of a pulsed hyperthermal nozzle coupled to a matrix-isolation FTIR spectrophotometer. The hyperthermal nozzle consists of a pulsed valve (Parker Series 9) coupled to a resistively heated silicon carbide pyrolysis tube that is 3.8 cm in length, with a 1 mm inner diameter. In typical operation, a dilute mixture of a chemical sample (approximately 0.01% to 1%) and argon is supersonically expanded from the pulsed valve and immediately enters the pyrolysis tube. The pyrolysis tube is heated resistively and regulated by a Love Controls Series 16A temperature controller. The gas-phase products of pyrolysis exit the silicon carbide tube and are deposited in an argon matrix on a cesium iodide window that is

mounted inside a liquid-helium cooled cryostat (Janis Research and SHI Cryogenics) with exterior KBr windows suitable for FTIR. The CsI window is maintained at 15 K during deposition, then 4 K during spectral measurement.

A separate detection apparatus including a quadrupole mass filter will be constructed with DOE support. (Figure 1) The pulsed hyperthermal nozzle described above will be coupled to this apparatus and operate similarly as in the FTIR experiments, but helium will be used instead of argon as a buffer gas. Pyrolysis products will be skimmed following the supersonic expansion and subsequently ionized with tunable electron-impact ionization. The electron impact ionizer will be tunable over the range 5-70 eV, which will help prevent dissociative ionization of many of the products. A quadrupole mass filter and electron multiplier will record the ion signal. The addition of a mass spectrometer to the laboratory is important because it will enable identification of the full range of pyrolysis products when FTIR is not sufficient. The combination of mass spectrometry and matrix-isolation FTIR techniques will provide a complete view of the pyrolysis products, including intermediates, which will provide critical information for the development of pyrolysis mechanisms.

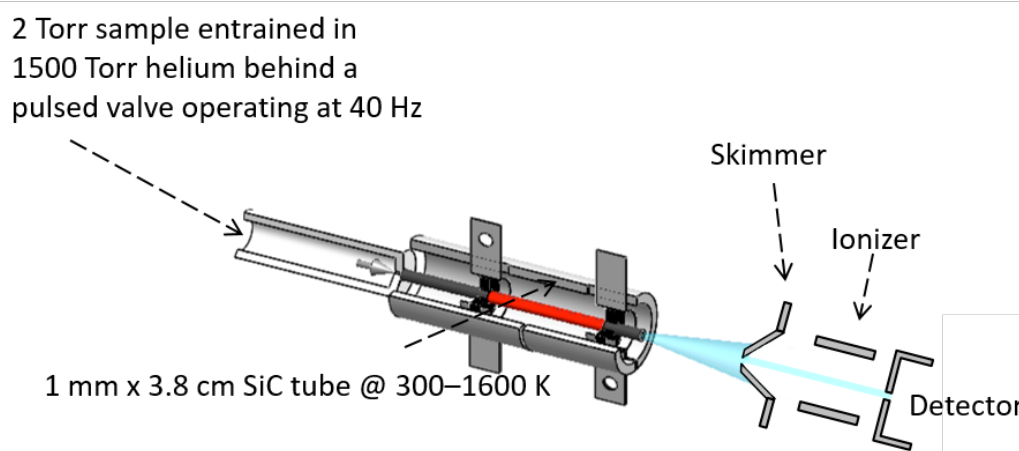


Figure 1. Schematic hyperthermal nozzle coupled to planned mass spectrometer

Estimation and Analysis of Uncertain Chemical Models

Habib N. Najm

Sandia National Laboratories
P.O. Box 969, MS 9051, Livermore, CA 94551

hnnajm@sandia.gov

I. Program Scope

The goal of this research program is to improve fundamental understanding of chemical models. The work involves developing numerical methods for uncertainty quantification (UQ) in chemical system computations, estimation of uncertain chemical model parameters, and UQ studies in computations of chemical systems. In the following, recent progress in these areas is discussed.

II. Recent Progress

A. Model Error

Statistical inference techniques for model calibration and parameter estimation typically ignore errors associated with the model itself – i.e., the model is assumed to be correct. However, every model has assumptions and therefore model error. If unaccounted for, model error can introduce bias in calibration and handicap predictive utility of the model. Conventional statistical approaches for capturing model error typically estimate error correlations from observational data employing *ad hoc* covariance structures on quantities of interest (QoIs). This subsequently burdens the model with additive statistical mismatch terms that are QoI-specific, and lead to predictions that can violate the underlying physical constraints imposed through the models, unless appropriately corrected via requisite priors.

We have previously developed an approach for handling model error where we embed a statistical construction for model error in model components, such as constitutive laws or phenomenological parameterizations, rather than as additive corrections to model outputs. Specifically, we focus on an approach where corrections are added to select model input parameters, therefore allowing the model to be treated as a black-box. The framework is developed in a general Bayesian context, where existing model parameters are inferred simultaneously along with parameters that characterize model error. Additionally, we employ Polynomial Chaos (PC) to represent the augmented inputs, permitting effortless extraction and propagation of uncertainties, eventually leading to efficient Bayesian computation. The approach leads to a model error representation that is consistent with the underlying model physics, and can be employed as a diagnostic device to enable attribution of model errors to specific submodels, thus enabling targeted model improvement and optimal experimental design. The strength of the developed framework is highlighted in model-to-model calibration studies where the classical independent Gaussian discrepancy models are not defensible.

Recently [B7], we extended the above probabilistic framework of to enable calibration with respect to noisy observational data, and to provide a principled way of attributing predictive uncertainties to components due to data noise/error, model error, as well as errors associated with the lack-of-information. This generalization allows the utilization of the construction with both computational and/or experimental data, while retaining the non-intrusive PC construction and the facile implementation of the method with black-box models. We also outlined a range of options for construction of likelihoods for model error estimation, and highlighted some of them in different scenarios. Overall, our recent work provided solid foundations for earlier developments, and extended them to more general practical contexts. In particular, we extended and applied the construction in the calibration of a chemical model for hydrocarbon ignition.

We considered the ignition of n-dodecane in air, and pursued calibration of a simple global 2-step mechanism [2] employing (a) experimental data, and (b) more complex model [1] predictions, with the key observable being ignition time.

Calibration with experimental data employed a noise model, such that the uncertainty accounting involved contributions due to data-noise, data-volume, and model-error. With the inclusion of model-error, we showed that the analysis provides estimation of noise model parameters with significant reduction in bias compared to the classical construction. Further, we reported the three indicated contributions to uncertainty providing pushed forward posterior (PFP) predictive uncertainties that span the discrepancy from the data in the L2 sense, for two equivalence ratio conditions.

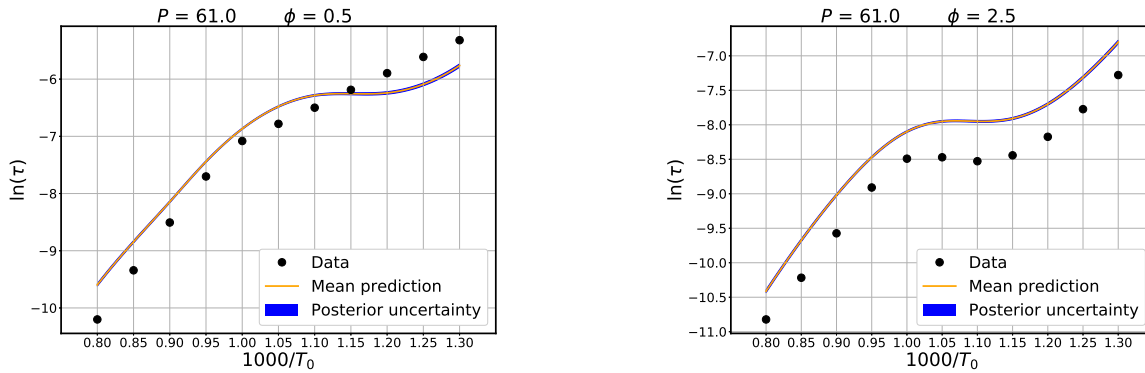


Figure 1: Demonstration of PFP uncertainties of classical calibration. The output of interest, $\ln(\tau)$, where τ is the ignition time, is shown as a function of the inverse initial temperature, for given values of the two other operating conditions, the equivalence ratio ϕ and the pressure P (atm).

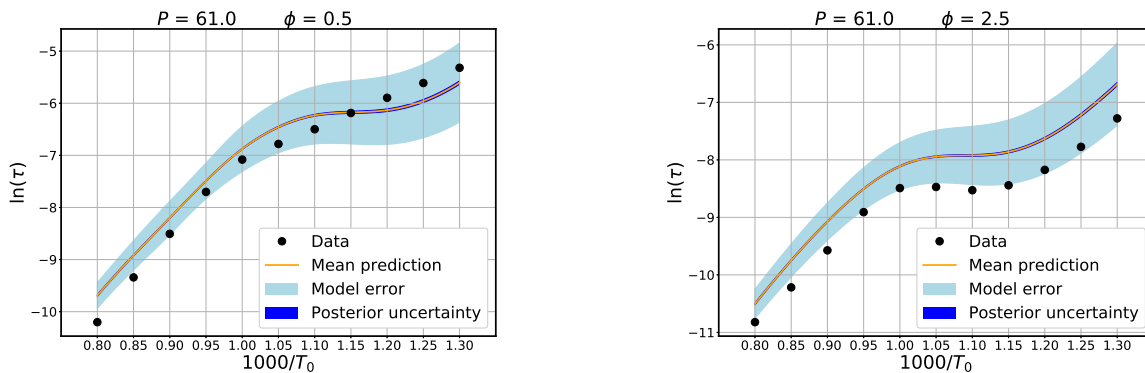


Figure 2: Demonstration of PFP uncertainties of calibration with model error embedding. The output of interest, $\ln(\tau)$, where τ is the ignition time, is shown as a function of the inverse initial temperature, for given values of the two other operating conditions, the equivalence ratio ϕ and the pressure P (atm).

Demonstrations with respect to the more complex model [1] covered a range of operating conditions in pressure, equivalence ratio, and initial temperature. Here again we targeted ignition time as the key QoI. Results showed clearly the impact of accounting for model error, in terms of more meaningful uncertainties on model parameters, and associated predictive uncertainties that are consistent in a root-mean-square sense with the range of the discrepancy between mean global model predictions and data from the complex model. Results without accounting for model error are shown in Figure 1, while those including accounting for model error are shown in Figure 2. We note that, without model error, the predictive uncertainty in the calibrated model is negligible, and yet there are large disagreements with the data. This misguided overconfidence in calibrated model predictions is a typical result when model error exists but is unaccounted for. On the other hand, the results with model error include a sizeable degree of uncertainty, on the scale of discrepancy from the data, such that predictive uncertainties provide a meaningful guide as to the confidence that may be placed in model predictions.

B. Statistical Inference of Reaction Rate Coefficients with Missing Data

We have continued to extend our “Data Free Inference” (DFI) method for statistical estimation of uncertain chemical rate coefficients from summary information without direct access to actual measurement data. DFI is necessary to provide for correlations among uncertain Arrhenius rate expression parameters, which are necessary for accurate prediction using chemical models with uncertainty quantification. Correlations and/or the joint probability density function on parameters could be obtained using Bayesian inference with the original raw experimental data. However, such data is rarely available, and certainly not for older measurements reported in the literature. Hence the need for this procedure, employing a combination of maximum entropy and approximate Bayesian computation methods, to translate reported statistics (e.g. nominal values and error bars) into a consistent joint posterior density on the uncertain parameters.

In recent work [B1], we revisited the analysis of the H_2O_2 thermal decomposition reaction using DFI, invoking data fusion and model replacement concepts, which we deployed in the multi-reaction analysis of dominant chain branching reactions in the $\text{H}_2\text{-O}_2$ system. This analysis of the chain branching reactions resulted in a representation of the relevant chemical kinetic parameters with correlated uncertainty that enabled predictions of important quantities of interest, e.g. homogeneous ignition time, with both more accurate and drastically lower uncertainty than obtainable when operating with uncorrelated uncertain parameters (see results in Fig. 3).

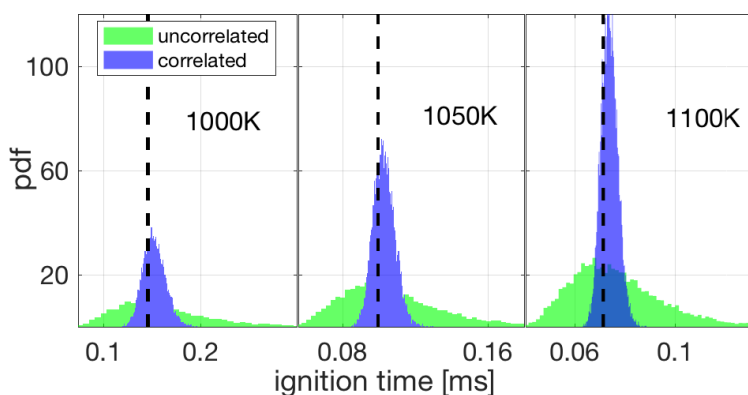


Figure 3: Comparison of uncertain homogeneous ignition time estimates in stoichiometric H_2 -air mixtures at various temperatures, contrasting the results using correlated uncertainty information as delivered by our statistical inference procedure to a case where correlations are ignored or otherwise unknown.

Using this new approach, the nominal reaction rate constants at each temperature, as determined by the experimentalists by fitting a first-order rate law model to their data, are used, in concert with reported error measures on these rate constants in the form of temperature-dependent symmetric error bars, in the DFI procedure. An ensemble of separate data inference problems is defined across multiple temperatures and the two experimental pressures employed in the experiment. By pooling this data together, and invoking a new model that was not considered by the original experimentalists, namely the pressure-dependent Lindemann mechanism, we refit the data at all reported temperatures and pressures to arrive at uncertain chemical model parameters that respect the pressure variation, and are appropriate for deployment in standard chemical mechanisms for modeling purposes. This construction allows for the evaluation of rate constants with joint uncertainty at arbitrary pressures (Fig. 4), whereas the original Arrhenius fitting performed by the experimentalists (whose summary statistics were used for the initial data inference effort) only delivered uncorrelated parameters at the isolated experimental pressures, which is of limited utility for use in predictive models and for quantifying uncertainty in variable pressure contexts.

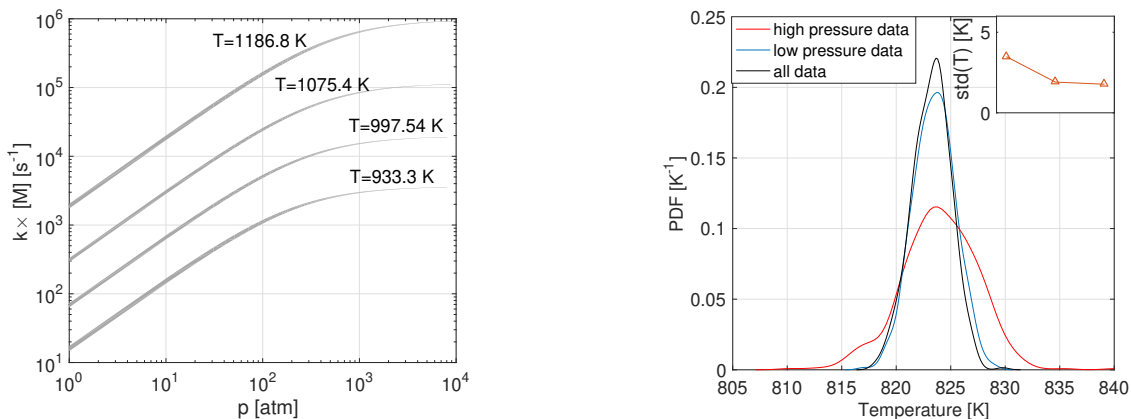


Figure 4: Left: Uncertain rate constant across pressure and temperature in the context of the Lindemann model obtained with DFI. Right: Explosion temperature of 1 atm $\text{H}_2\text{-O}_2$ mixtures, accounting for uncertainty in the H_2O_2 thermal decomposition rate. Depending on which data is considered, both the mean and variance of the estimate change, with minimum variance arising when all available data is considered.

References

- [1] K. Narayanaswamy, P. Pepiot, and H. Pitsch. A chemical mechanism for low to high temperature oxidation of n-dodecane as a component of transportation fuel surrogates. *Comb. Flame*, 161:867–884, 2014.
- [2] C.K. Westbrook and F.L. Dryer. Simplified Reaction Mechanisms for the Oxidation of Hydrocarbon Fuels in Flames. *Combustion Science and Technology*, 27:31–43, 1981.

BES-Supported Published/In-Press Publications [2017-2019]

- [B1] T. A. Casey and H.N. Najm. Estimating the joint distribution of rate parameters across multiple reactions in the absence of experimental data. *Proc. Combust. Inst.*, 37(1):797–805, 2019.
- [B2] L. Hakim, G. Lacaze, M. Khalil, K. Sargsyan, H. Najm, and J. Oefelein. Probabilistic parameter estimation in a 2-step chemical kinetics model for n-dodecane jet autoignition. *Combustion Theory and Modeling*, 22(3):446–466, 2018.
- [B3] M. Khalil, K. Chowdhary, C. Safta, K. Sargsyan, and H.N. Najm. Inference of reaction rate parameters based on summary statistics from experiments. *Proc. Comb. Inst.*, 36(1):699–708, 2017.
- [B4] M. Khalil and H.N. Najm. Probabilistic Inference of Reaction Rate Parameters from Summary Statistics. *Combustion Theory and Modeling*, 22(4):635–665, 2018.
- [B5] R. Malpica-Galassi, M. Valorani, H.N. Najm, C. Safta, M. Khalil, and P.P. Ciottoli. Chemical Model Reduction under Uncertainty. *Combustion and Flame*, 179:242–252, 2017.
- [B6] C. Safta, M. Blaylock, J. Templeton, S. Domino, K. Sargsyan, and H. Najm. Uncertainty quantification in les of channel flow. *International Journal for Numerical Methods in Fluids*, 83:376–401, 2017.
- [B7] K. Sargsyan, X. Huan, and H. Najm. Embedded model error representation for Bayesian model calibration. *Int. J. UQ*, 2019. in press.

Spectroscopy, Kinetics and Dynamics of Combustion Radicals

David. J. Nesbitt

Our research program involves experimental and theoretical study of transient chemical species relevant to fundamental combustion and atmospheric chemical processes. The work focuses on spectroscopy and unimolecular/bimolecular dynamics of highly reactive radical intermediates, combining i) high-resolution direct IR laser absorption methods with quantum shot noise limited detection, ii) high densities (10^{12} - 10^{14} #/cm³) of jet-cooled hydrocarbon radicals and molecular ions in slit supersonic discharge expansions, accompanied by iii) high-level *ab initio* potential surface and multidimensional quantum mechanics calculations. Advantages of the slit discharge expansion techniques are i) generation of high concentrations of chemically reactive species yet ii) rapid subsequent cooling of these transient intermediates to $T_{\text{rot}} \approx 15$ -30 K in a collisionally collimated multipass geometry ideal for “reduced-Doppler” direct absorption spectroscopy with quantum shot-noise limited detection sensitivity. Over the past year, our group has explored multiple jet-cooled transients such as highly reactive singlet carbenes (e.g., HCF), oxyradical adducts (e.g., *trans*-DOCO), high energy oxyhydrocarbon conformers e.g., (*cis*-formic acid), Criegee intermediate precursor halocarbon radicals (e.g., CH₂Br) and molecular ions (e.g., NH₃D⁺, ND₃H⁺) via high-resolution IR laser spectroscopy. In the interest of space, two examples will be briefly discussed below.

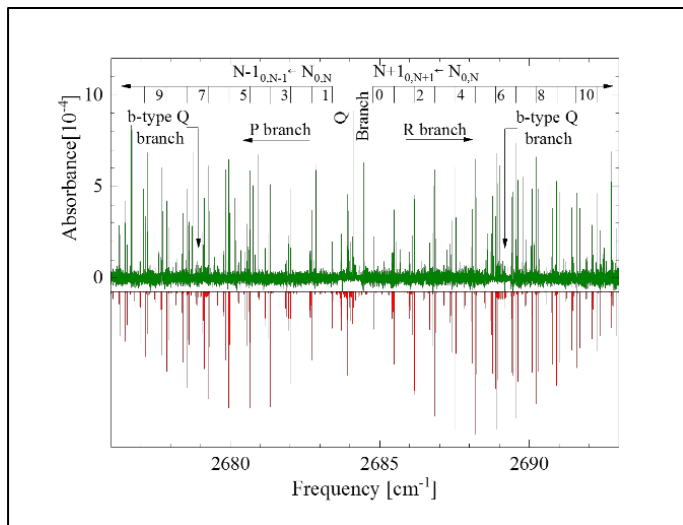
A. Rovibrational Spectroscopy and RRKM Dynamics of Jet Cooled *trans*-DOCO

The role of hydrocarboxyl radical (HOCO) as an intermediate in the OH oxidation of CO to CO₂ has made HOCO a subject of vigorous inquiry. The OH + CO reaction is involved in the burning of all hydrocarbon fuels and has been described as being among the most important of combustion reactions.¹ As expected for a free radical, HOCO is highly reactive, having reaction rates with common radical species one to three orders of magnitude larger than the reaction rate for OH + CO. Of greatest relevance is the OH + CO oxidation reaction itself, which critically controls the concentration of hydroxyl radicals in the atmosphere. The first evidence that HOCO plays an important role as an intermediate in this reaction came from early low temperature kinetic studies, which revealed rate constants with a highly non-Arrhenius temperature dependence and an inverse dependence on pressure,² with a long-lived collision complex mechanism



proposed to explain the anomalous behavior. Recent modeling strongly supports this hypothesis,³ with the presence of a HOCO intermediate directly observed during the OH + CO reaction.⁴ Central to the HOCO story line is the presence of two different geometries, the *trans*- and *cis*-HOCO isomers. The *trans*-HOCO radical is thought to form from entrance channel attack of the HO radical oxygen atom on CO, with the *cis*-HOCO isomer separated from the initial *trans*-HOCO adduct by a substantial barrier to internal rotation. *Trans*-HOCO was first observed spectroscopically in rare gas matrices⁵, with many subsequent *ab initio* studies indicating that both the *trans* and the *cis* conformers have submerged potential wells and barriers deep enough with respect to the reactants and products to allow collisional stabilization of HOCO into a long lived transient species. The *trans*-HOCO species is the more tightly bound of the two HOCO isomers, with a measured well depth of 42.7 ± 0.3 kJ/mole relative to the lowest dissociation product (H + CO₂)⁶ and the *cis*-HOCO isomer less tightly bound by

about 10 kJ/mole.⁷ Thermalization of the OH + CO reactants into a deep *trans*-HOCO entrance channel complex occurs with high efficiency under matrix isolation conditions, which is the plausible reason why the *trans*-HOCO isomer has proven experimentally more accessible. Indeed, a high resolution gas phase IR spectrum of *cis*-HOCO remains unobserved to this day. Interestingly, electron photodetachment from the corresponding HOCO⁻ anionic species shows a clear propensity for *cis*-vs. *trans*-HOCO formation.⁸ As a small step towards obtaining high-resolution IR spectroscopy data on *cis*-DOCO, we have pursued measurements on the *trans*-DOCO IR spectrum under supersonically cooled conditions, building on the room temperature frequency comb work by Ye *et al.* as well as the extensive LMR/diode laser work by Sears *et al.*⁹⁻¹¹

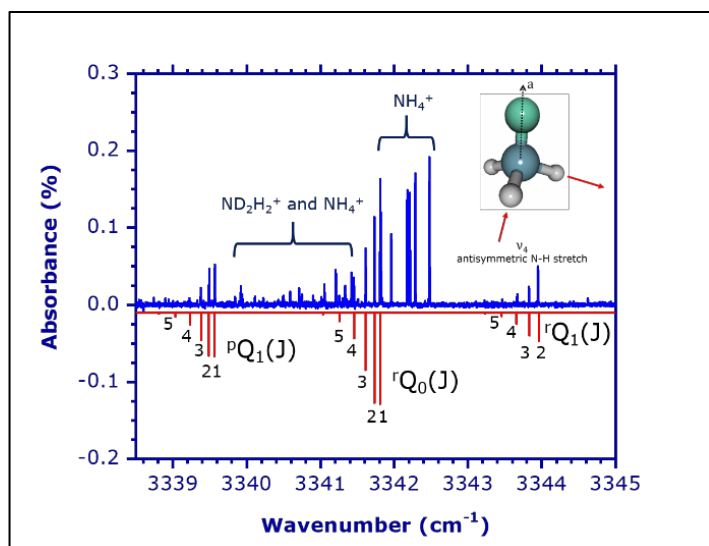


Specifically, we have measured the rotationally-resolved ν_1 O-D stretch spectrum of DOCO generated in a pulsed supersonic discharge of OD + CO and collisionally stabilized to $T_{\text{rot}} \approx 32$ K in the subsequent slit-jet expansion. Spectra with reduced Doppler widths are obtained via direct IR laser absorption parallel to the slit axis, with careful subtraction of laser amplitude noise achieving sensitivities within a factor of three of the shot-noise limit. By combining our data with data from previously published millimeter and microwave rotational studies, we fit ground-state combination differences to an improved non-rigid rotor Hamiltonian with spin-rotation coupling. For the vibrationally excited state, we unambiguously determine the eigenvalues of a non-rigid rotor Hamiltonian with spin-rotation coupling included, thereby improving upon the precision of recent and past measurements. By careful Boltzmann analysis of both *a*- and *b*-type band intensities, the direction of the transition dipole moment in the molecule fixed frame can be determined and compared with predictions from *ab initio* theory. The current high-resolution spectral results are in excellent agreement with recent studies of the *trans*-DOCO radical by infrared frequency comb spectroscopy under room temperature conditions. Combined with previous microwave/millimeter wave rotational studies, the reduced-Doppler infrared data permit characterization of the vibrational ground state, improved structural parameters for the OD stretch vibrational level, and *trans*-DOCO spin-rotation information in both ground and excited vibrational states. Of dynamical interest is whether the nascent *trans*-DOCO complex formed in the entrance channel has sufficient time to convert into the *cis*-DOCO isomer, or whether this is quenched by rapid stabilization into the *trans*-DOCO well. *Ab initio* and RRKM analysis of the intrinsic reaction coordinate (IRC) for *trans*-DOCO to *cis*-DOCO interconversion rates supports the latter scenario, which helps explain the failure of previous high resolution infrared efforts to detect *cis*-HOCO.

B. Slit Jet Infrared Spectroscopy of Molecular Cations: Symmetric (ν_1) and Antisymmetric (ν_4) NH Stretching Modes in NH_3D^+

The suppressed-Doppler infrared spectrum of NH_3D^+ , a partially deuterated isotopologue of ammonium ion, has been obtained on the ν_1 (symmetric) and ν_4 (antisymmetric) N-H stretch bands using a slit jet discharge expansion in a direct absorption high

resolution IR laser spectrometer. The ion is efficiently generated by H_3^+ protonation of NH_2D in a slit jet discharge of $\text{H}_2/\text{NH}_2\text{D}$, with the resulting slit jet expansion rapidly cooling the molecular ions into low rotational states. The first high-resolution infrared spectrum of ν_1 is reported, as well as many previously unobserved transitions in the ν_4 rovibrational manifold. Simultaneous observation of both ν_1 and ν_4 permits elucidation of both the vibrational ground and excited state properties of the ion, including tests of these band origins against high-level anharmonic *ab initio* theoretical predictions as well as determination of the $\nu_1:\nu_4$ intensity ratio for comparison with bond-dipole model predictions. Ground-state two-line combination differences from known transitions observed in this work and previous studies permit the rotational constants of NH_3D^+ to be determined to unprecedented accuracy, the results of which support previous laboratory and astronomical assignment of the 1_0-0_0 pure rotational transition and should aid future searches for other rotational transitions as well.



The ammonium ion, NH_4^+ , is considered to be an abundant or even dominant ion in a variety of astrochemical environments.¹² In hot cores, for example, the ion's neutral precursor NH_3 desorbs in large concentrations from the surfaces of icy grains,¹² where it is readily protonated by H_3^+ ions thought to be ubiquitous in the interstellar medium.¹³ In cold clouds, on the other hand, NH_4^+ is formed by successive hydrogenation of atomic N^+ ions by H_2 .¹⁴ Whatever the synthesis pathway, the NH_4^+ ion is thermodynamically extremely stable due to ammonia's high proton affinity ($\Delta\text{H}^0 = 853$ kJ/mol), which is the largest of any small polyatomic molecule in the interstellar medium. As a result, NH_3 acts as an extremely aggressive proton sink, which in turn suppresses the formation of many other ions. The predominant decomposition pathway for NH_4^+ is dissociative recombination with electrons, either on the surfaces of negatively charged grains or via oxidation of other species such as neutral metals.

In spite of its central role in ion-molecule astrochemistry, NH_4^+ has a net zero dipole moment and therefore is effectively invisible to pure rotational spectroscopy. However, all of the partially-deuterated isotologues of NH_4^+ (i.e., NH_3D^+ , ND_2H_2^+ , and ND_3H^+) break this spherical top molecular symmetry and thereby generate nonvanishing dipole moments. As a result, these species can be detected via radio/microwave/mm-wave rotational spectroscopy, provided their rotational transition energies are known with sufficient precision. Spectroscopic detection of these partially deuterated ions is therefore desirable as a valuable proxy for NH_4^+ ; moreover, these deuterated species provide an experimental probe of the interstellar kinetics and dynamics driving deuterium uptake. In particular, the high vapor pressure of neutral $\text{NH}_x\text{D}_{3-x}$ makes it an excellent carrier of information on temperature dependent kinetics in interstellar regions where other species are largely frozen out. Also of dynamical significance, ammonia exhibits unexpectedly large deuterium fractionation effects in the interstellar medium.¹⁵ This fractionation is believed to arise by D^+ transfer from

deuterated variants of H_3^+ ($\text{H}_x\text{D}_{3-x}^+$) to form the $\text{NH}_y\text{D}_{4-y}^+$ ion which eventually decomposes to form $\text{NH}_{y-1}\text{D}_{4-y}$.¹³ The unusual isotopic abundance of $\text{H}_x\text{D}_{3-x}^+$, in turn, is driven by subtle isotopic differences in zero-point energies. For instance, the reaction $\text{H}_3^+ + \text{HD} \rightarrow \text{H}_2\text{D}^+ + \text{H}_2$ is exothermic by nearly 2 kJ/mol, which seems modest but is enormously significant at low interstellar temperatures.¹⁶ Experimental quantification of these and related processes demands unambiguous detection of $\text{NH}_y\text{D}_{4-y}^+$ by rotational spectroscopy, which in turn requires *terrestrial* laboratory studies to specify the precision spectral signatures of these marker ion species.

In the last granting period, we reported the first observation of rovibrational transitions in the symmetric N-H stretch vibration of NH_3D^+ , ν_1 . We also further complement the previous work of Doménech et al. and of Nakanaga and Amano by reporting new transition energies in the antisymmetric N-H stretch vibration, ν_4 . This data allows us to significantly improve both the accuracy and precision of the ground state spectroscopic constants, as well as explore the rovibrational properties of NH_3D^+ upon symmetric and antisymmetric NH stretch excitation. This work also significantly increases the total number of available 2-line combination differences and thus yields much tighter constraints on spectroscopic parameters for the ground and vibrationally excited states. In addition, our measurements allow us to test simple “bond-dipole” model predictions for relative intensities of the two NH stretch vibrational bands, as well as to probe for possible H atom ortho-para nuclear spin relaxation dynamics on the time scale of the slit jet discharge expansion.

- 1 J. A. Miller, R. J. Kee, and C. K. Westbrook, *Annu. Rev. Phys. Chem.* **41**, 345 (1990).
- 2 I. W. M. Smith, *Chem. Phys. Lett.* **49** (1), 112 (1977).
- 3 J. R. Barker and D. M. Golden, *Chem. Rev.* **103** (12), 4577 (2003).
- 4 N. F. Scherer, C. Sipes, R. B. Bernstein, and A. H. Zewail, *J. Chem. Phys.* **92** (9), 5239 (1990).
- 5 D. E. Milligan and M. E. Jacox, *J. Chem. Phys.* **54** (3), 927 (1971).
- 6 B. Ruscic, M. Schwarz, and J. Berkowitz, *J. Chem. Phys.* **91** (11), 6780 (1989).
- 7 C. J. Johnson, R. Otto, and R. E. Continetti, *Phys. Chem. Chem. Phys.* **16** (36), 19091 (2014).
- 8 C. J. Johnson, M. E. Harding, B. L. J. Poad, J. F. Stanton, and R. E. Continetti, *J. Am. Chem. Soc.* **133** (49), 19606 (2011).
- 9 T. Q. Bui, B. J. Bjork, P. B. Changala, T. L. Nguyen, J. F. Stanton, M. Okumura, and J. Ye, *Science Adv.* **4** (1), eaao4777 (2018).
- 10 H. E. Radford, M. A. Moore, T. J. Sears, J. Grussdorf, J. Nolte, and F. Temps, *J. Mol. Spectrosc.* **165** (1), 137 (1994).
- 11 T. J. Sears, W. M. Fawzy, and P. M. Johnson, *J. Chem. Phys.* **97** (6), 3996 (1992).
- 12 Y. Aikawa, K. Furuya, V. Wakelam, F. Hersant, T. Matsumoto, K. Saigo, K. Tomida, K. Tomisaka, R. Garrod, and E. Herbst, *Proc. Int. Astron. Union* **7** (s280), 33 (2011).
- 13 T. Oka, *Chem. Rev.* **113** (12), 8738 (2013).
- 14 J. Le Bourlot, *Astron. & Astrophys.* **242**, 235 (1991).
- 15 D. C. Lis, M. Gerin, E. Roueff, C. Vastel, and T. G. Phillips, *Astrophys. J.* **636** (2), 916 (2006).
- 16 D. Gerlich, E. Herbst, and E. Roueff, *Planet. Space Sci.* **50**, 1275 (2002).

State-to-State Molecular Reactions in the Ultracold Regime

Kang-Kuen Ni

Department of Chemistry and Chemical Biology, Harvard University

12 Oxford St., Cambridge, MA 02138

ni@chemistry.harvard.edu

Research Scope:

We aim to gain state-to-state experimental data for both the AB + CD and AB + C types of reactions that can be compared to advanced theoretical calculations and elucidate the role of quantum mechanics in the processes of bond breakage and formation. Our approach is to conduct experiment with reactants prepared at ultracold temperatures ($< 1\mu K$) such that quantum effects of translational motion are an important factor. Specific examples of the potassium-rubidium metathesis reaction $KRb + KRb \rightarrow K_2 + Rb_2$ and the atom exchange reaction $K + KRb \rightarrow K_2 + Rb$ are chosen because the technology of quantum internal and motional state control of these types of molecules is ripe. We have constructed a new quantum degenerate gas apparatus that integrates ion detection and velocity map imaging capabilities and began to explore the bimolecular reaction. Reactions in this regime will serve as a sensitive probe to compare to high accuracy *ab initio* potentials and quantum scattering calculations. This work will advance both our intuition about and ability to perform chemistry at ultracold temperatures and to control chemistry at the most basic quantum level.

Recent Progress:

We report recent result during the funding period since last year where we provide the first direct observation of KRb+KRb reaction. We begin our work by implementing the steps and techniques of Ref. [1] to create an optically trapped gas of ultracold KRb molecules. In brief, ultracold K and Rb atoms are first converted to weakly-bound “Feshbach” molecules by a magnetic field sweep through a Fano-Feshbach resonance at 546 G. Then a pair of Raman beams are applied in a STIRAP pulse sequence as shown in Fig. 1b to coherently transfer weakly-bound Feshbach molecules into the ro-vibrational and electronic ground state. Because the STIRAP transfer is coherent, the reverse is also coherent. To image the ground-state molecules which are dark to our imaging beams, a reversed STIRAP sequence is applied to transfer them back to Feshbach molecules for absorption imaging (Fig. 1a) on an atomic transition. The population of Feshbach molecules exposed to the STIRAP pulse sequence is shown in Fig. 1c.

Once the ground-state KRb molecules are created, chemical reactions take place continuously [2]. The absorption imaging technique described so far is only sensitive to reveal the population of $v'' = 0, N'' = 0$ of $X^1\Sigma^+$ KRb molecules. Chemical reaction products cannot be probed with this specialized absorption imaging. To detect products, we instead use single UV photon ionizations and direct the ions toward the MCP ion detector inside the chamber to extract both their mass through time-of-flight and their velocity through Velocity Map Imaging (VMI) [3]. The KRb

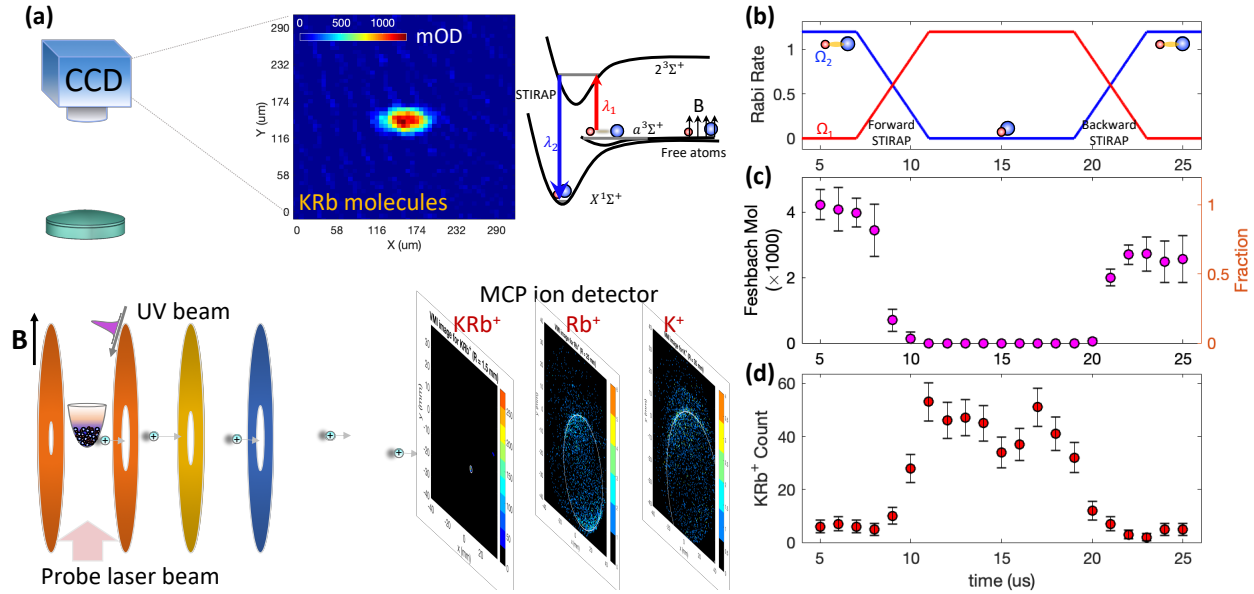


Figure 1: **Creation and detection of an ultracold KRb gas.** (a) KRb molecules are created from ultracold gases of K and Rb atoms and optically trapped inside a vacuum chamber. The molecules can be probed through resonant absorption imaging (after coherent converting them to atoms) or direct ionization. (b) STIRAP pulse sequence that coherently converts KRb Feshbach molecules (formed from K and Rb atoms) to ground-state molecules and then back to Feshbach molecules (then atoms) for imaging. (c) Absorption detection of Feshbach molecule population exposed to the STIRAP pulse sequence in (b). (d) Ionization detection of KRb ground-state molecules population exposed to the STIRAP pulse sequence. Forward STIRAP transfers Feshbach molecules to the ground-state and backward STIRAP reverses the process.

molecule creation process (through the STIRAP pulse sequence) can be probed directly with ionization detection as shown in Fig. 1d. As expected, direct detection of KRb shows the opposite population as Feshbach molecules because STIRAP coherently transfers population between the ground-state and the Feshbach molecular state.

To probe reaction products and to reduce perturbation to the reactants during ionization, we shape our ionization beam to be “hollow-bottled” such that it is dark at the location of the reactants with concentrated laser intensity outside the region of the reactants (Fig. 2a). To further reduce the hollow area for higher efficiency ionization, we cross two hollow-bottled beams at a 40-degree angle centered at the optical dipole trap (ODT). Because our ionization laser runs at a repetition rate of 10 Hz with a beam diameter of about 0.5 mm, the beams only catch products that occur about 5 μ s preceding the laser pulse. Therefore, the detection statistics would be very low, and sufficient data accumulation could take a week. We optimize our system carefully for robust operation and collect data for one week continuously at a time.

Our data accumulation KRb with a 285 nm ionization beam is shown in Fig. 2b and c. The dominant observed peaks are KRb^+ , from one-photon ionization of KRb, and K^+ and Rb^+ , from two-photon dissociative ionization. Although the ionization laser is supposed to be dark in the center, the in-

tensity is not completely extinguished and therefore, KRb can still be ionized with a much reduced efficiency.

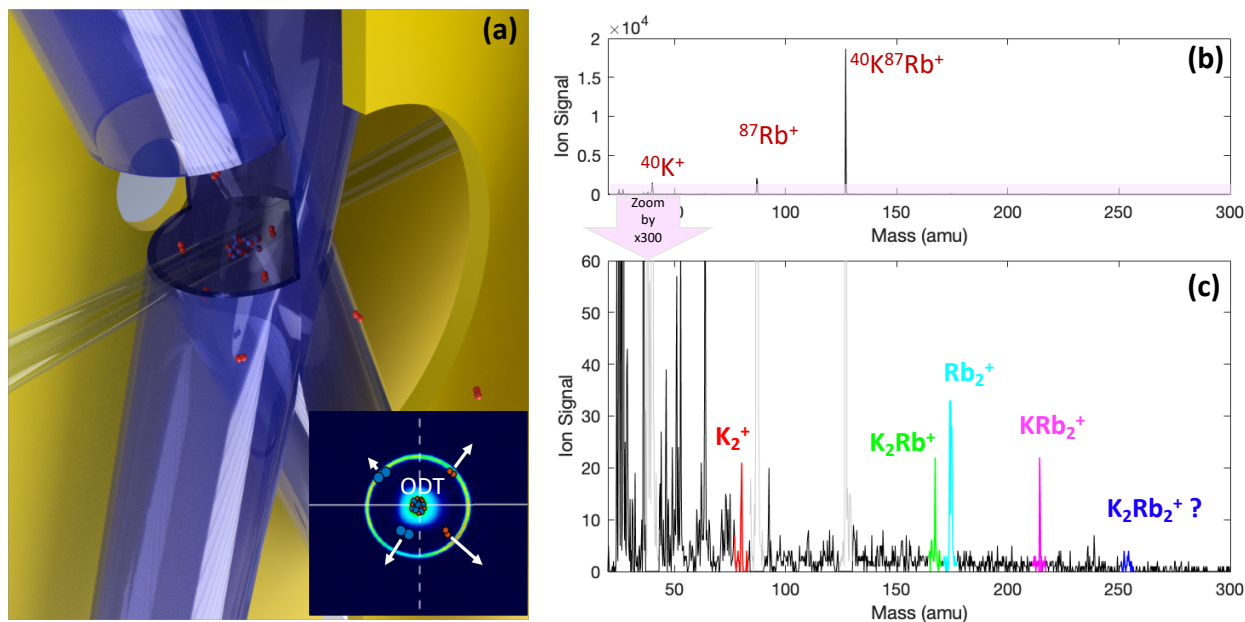


Figure 2: **Probing KRb+KRb reaction products.** (a) Two crossed hollow-bottled ionization beams are centered around the optical dipole trap where the reactants (KRb) are held. Once a reaction takes place, products fly out and can be intercepted by the ionization beams. Subsequently, the ionized products travel through a 1 meter long time-of-flight (TOF) tube before reaching the MCP detector. (b) The largest TOF signals are KRb^+ , K^+ , and Rb^+ . (c) Zoomed in (b) by 300, we see peaks corresponding to K_2^+ , K_2Rb^+ , Rb_2^+ , and K^2Rb_2 . Other prominent peaks in black are background peaks that are present even in the absence of the ultracold atom and molecule gases.

Zooming into the signal near the floor, we observe K_2^+ and Rb_2^+ which come from ionization of reaction products, K_2 and Rb_2 . This is the first time such an ultracold chemical reaction is directly observed! The low count rate is understood to be from the low repetition rate of the ionization laser and the limited beam coverage size. In the same spectrum, we also observe strong K_2Rb^+ and KRb_2^+ signals, which are not from ionization of K_2Rb and KRb_2 because these products are energetically forbidden in the reaction. One likely origin of them is from dissociative ionization of the intermediate K_2Rb_2 complex. Furthermore, all of this information is cross checked with VMI to further validate our signals. We are preparing a manuscript detailed this result.

Future Plans:

Combining ionization detection with a sample of ultracold molecules, we have unambiguously provided the first direct observation of ultracold chemical reactions through the detection of reaction products. We speculate that the unexpected trimer ion signal (trimer products are energetically forbidden) comes from dissociative 4-atom reaction intermediates. Further investigation to prove the signal origin by varying ionization wavelengths is underway.

From a theoretical estimate based on RRKM theory, we indeed expect the reaction intermediate of the bimolecular reaction to be long-lived ($\sim 4 \mu\text{s}$) [4], which makes direct observation of the

intermediate complex plausible and an exciting goal. The long complex lifetime is due partly to the ultracold nature of the reaction that imposes an energetic constraint to a small number of entrance and exit channels.

Furthermore, we plan to gain state-to-state reaction information of the bimolecular reaction by tuning the VMI to a configuration to map the small exothermic kinetic energy ($\sim 10.4 \text{ cm}^{-1}$) to a much larger radius to resolve their rotational quantum states. We will work with theory collaborators, Hua Guo and Svetlana Kotochigova, to understand such reactions in the ultracold regime.

Reference

- [1] K.-K. Ni, S. Ospelkaus, M. H. G. de Miranda, A. Pe'er, B. Neyenhuis, J. J. Zirbel, S. Kotochigova, P. S. Julienne, D. S. Jin, and J. Ye. A High Phase-Space-Density Gas of Polar Molecules. *Science*, 322(5899):231–235, 2008.
- [2] S. Ospelkaus, K.-K. Ni, D. Wang, M. H. G. de Miranda, B. Neyenhuis, G. Quéméner, P. S. Julienne, J. L. Bohn, D. S. Jin, and J. Ye. Quantum-state controlled chemical reactions of ultracold potassium-rubidium molecules. *Science*, 327(5967):853–857, 2010.
- [3] André T. J. B. Eppink and David H. Parker. Velocity map imaging of ions and electrons using electrostatic lenses: Application in photoelectron and photofragment ion imaging of molecular oxygen. *Review of Scientific Instruments*, 68(9):3477–3484, 1997.
- [4] Michael Mayle, Goulven Quéméner, Brandon P. Ruzic, and John L. Bohn. Scattering of ultracold molecules in the highly resonant regime. *Phys. Rev. A*, 87:012709, Jan 2013.

Chemical Kinetic Modeling of Combustion Chemistry

William J. Pitz, Charles K. Westbrook
Lawrence Livermore National Laboratory, Livermore, CA 94550
pitz1@llnl.gov

1. Program Scope

We develop chemical kinetic reaction models to describe the combustion of hydrocarbons and other related fuels, including bio-derived fuels. The models also describe reactions important for the formation of emissions such as PAHs. These models are validated through comparisons between simulations and experimental results in carefully controlled laboratory-scale facilities including shock tubes, stirred reactors, flow reactors, premixed flames, diffusion flames, and rapid compression machines. After validation, these models are then used to understand more complex combustion phenomena in practical combustion systems. We identify particularly sensitive parts of these models and provide that information to other DOE/GPCP researchers who can use theory and new experiments to refine the kinetic models. We try to anticipate kinetic modeling needs of the DOE combustion community, so other researchers can have accurate models to assist in their own research projects. Our kinetic models are freely available at <https://combustion.llnl.gov/> and provide a valuable service to the combustion community.

2. Recent Progress

Our work has focused on developing and improving the chemical kinetic models of transportation fuels, including the formation of PAHs which are important precursors in the formation of soot emissions. These kinetic models use fuel-component surrogate mixtures to represent the properties of complex gasoline and diesel fuels. We also develop kinetic models for new bio-derived fuels with properties that are attractive for blending into gasoline and diesel fuels.

A. Development of an improved PAH model

Polycyclic aromatic hydrocarbons (PAHs) are precursor species in the formation of soot particles. An accurate and validated chemical kinetic model for PAHs is needed for use in simulating soot formation from the combustion of hydrocarbon and alternative fuels. At LLNL, a PAH mechanism was developed on top of our recent aromatic mechanism [1]. The mechanism describes the formation of PAH containing up to 24 carbon (coronene and ethnylnaphthotetraphene) using various repetitive reaction schemes that connect smaller PAHs to larger ones. The reaction pathways and the associated reaction rates for the different various repetitive reactions are largely taken from recent ab-initio and experimental studies mentioned below. Reaction rates and product channels were updated for both the formation of the first aromatic ring and for PAHs up to coronene.

For the formation of the first aromatic ring, molecular growth reactions were added, and kinetic rates were updated for existing reactions. In particular, molecular growth reactions of propargyl radical with acetylene, allyl radical, cyclopentadienyl radical and itself were reviewed and updated. The reaction of propargyl radical with acetylene was added according to recent findings of da Silva 2017. The recombination of propargyl and allyl, and the self-recombination of propargyl radicals were taken from Miller et al. 2010 and Miller and Klippenstein 2003. The reaction of propargyl

and cyclopentadiene radicals was added from Sharma, Harper and Green 2010. The reaction of allyl radical addition to propene was added from Wang, Villano and Dean 2015.

For the formation of the second aromatic ring and larger rings, the hydrogen-abstraction, H-atom-addition (HACA) scheme has been described using the recent works of Mebel et al. 2017 and Frenklach et al. 2018. Mebel et al. studied the reactions of phenyl radicals with acetylene molecules to understand the role of different variations of HACA in the growth of large PAHs. For addition of acetylene to radicals at zig-zag sites which result in production of cyclopentafused PAHs, we have used the rates from Frenklach et al. 2012. For addition of acetylene to radical on arm-chair sites, we have used the rates from Yang et al. 2017. Many other molecular growth reactions for the formation of second ring and higher PAHs were added and updated. Another notable update is the inclusion of reactions of phenyl radicals with C₃ species from Mebel et al. 2017, and from Morozov and Mebel 2019. For PAH oxidation, the oxidation reactions on 5- and 6- membered rings from Singh, Mebel and Frenklach 2015 were added.

The updated PAH model was compared to experiments performed by Nils Hansen on allene and propyne flames in a counterflow burner at 700 Torr at SNL. The flame structure was measured with a quartz microprobe and analyzed using high-resolution mass spectrometry with single-photon ionization employing synchrotron-generated vacuum-ultraviolet radiation. Results of the kinetic model were compared to measurements of stable C₂-C₄ intermediates and of PAHs. A comparison for C₁₀H₈ species profiles (includes naphthalene) is shown in Fig. 1. The peak mole fractions of the simulated profiles agree with the experiments within the 30% estimated uncertainty for major intermediates in experiments. There is a shift in the peak location between the simulations and the experiments and we are investigating this discrepancy. The experimental and simulated results in Fig. 1 show that the allene flame produces higher amounts of PAH than the propyne flame.

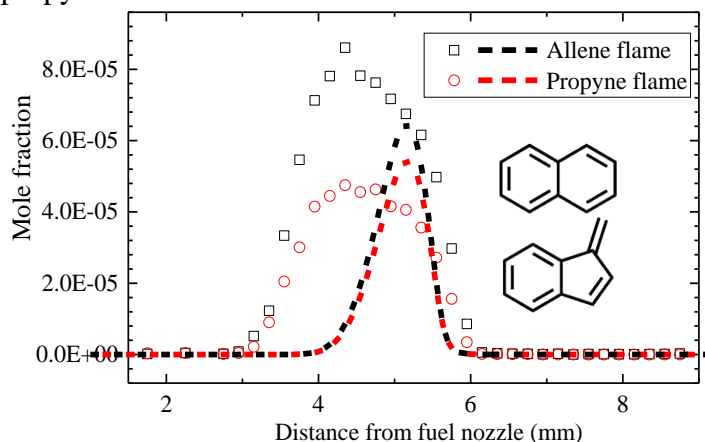


Figure 1: Comparison of the simulated (curves) and measured (symbols) mole fractions of C₁₀H₈ of allene and propyne counter flow diffusion flames.

A. Development of accurate reaction-rate rules for the low temperature chemistry of highly branched iso-alkanes

We are working on developing accurate reaction-rate rules for large, highly-branched iso-alkanes. For these large iso-alkanes, new reaction classes were added that were not previously

included in LLNL models. They are concerted HO₂ elimination from hydroperoxy alkylperoxy radicals (commonly referred as OOQOOH radicals), as well as the alternative isomerization reactions of OOQOOH radicals producing the dihydroperoxy alkyl radicals (commonly referred as P(OOH)₂ radicals). Those additional low temperature reaction pathways revise the details of the chain branching, chain propagation, and chain termination channels in the kinetic model. Currently, we have developed chemical kinetic models for iso-nonane (2,2,4,4-tetramethylpentane) and iso-dodecane (2,2,4,6,6-pentamethylheptane), and compared simulated results to experimentally-measured autoignition times in a rapid compression machine by Sung's group at University of Connecticut. The simulations of iso-dodecane compare well with the experiments, but the simulated autoignition times of iso-nonane are too short compared to the experiments near the high-temperature end of the negative temperature coefficient (NTC) region. Iso-nonane (2,2,4,4-tetramethylpentane) has a unique molecular structure that does not allow alkylperoxy radical (RO₂) ⇌ alkene + HO₂ elimination reactions and requires further investigation of its chemistry to resolve the autoignition-time discrepancy.

B. Reactions and thermodynamic properties for further fundamental study

Our work has identified reactions for further fundamental experimental and theoretical studies by DOE/GPCP and other researchers. For PAH chemistry, the following reactions need further study. The reactions of resonantly-stabilized fulvenallenyl radical (C₇H₅) with propargyl, and of cyclopentadienyl and itself are needed because these reactions could facilitate the formation of two- and three- ring PAHs. Currently, we are using rate constant expressions based on the propargyl + propargyl reaction. Additionally, the reaction of naphthalenyl radicals with allyl and propargyl (C₃H₃) radicals could facilitate an understanding the growth of larger PAHs. We currently model these last two classes using analogies from reactions of phenyl radical, but the rate constants and product species are speculative.

In the chemical kinetic modeling of the low temperature oxidation of large iso-alkanes, reaction rate expressions for alkyl-peroxy radical (RO₂) isomerization reactions for iso-nonane (2,2,4,4-tetramethylpentane) and the thermodynamic properties of associated species have significant uncertainties and literature values are incomplete. This creates difficulties in developing an accurate chemical kinetic model for this highly-branched iso-alkane.

3. Future Plans

In the future, we plan to continue our development of chemical kinetic models for fuel components present in gasoline, diesel and alternative fuels. We also will continue our work on the development of an accurate PAH kinetic model and soot model.

Acknowledgements

This work was performed under the auspices of the U.S. Department of Energy by Lawrence Livermore National Laboratory under Contract DE-AC52-07NA27344.

References

1. Kukkadapu, G., Kang, D., Wagnon, S. W., Zhang, K., Mehl, M., Monge-Palacios, M., Wang, H., Goldsborough, S. S., Westbrook, C. K. and Pitz, W. J., "Kinetic Modeling Study of Surrogate

Components for Gasoline, Jet and Diesel Fuels: C7-C11 Methylated Aromatics," *Proc. Combust. Inst.* 7 (1) (2019) 521-529.

Published papers in 2017 to 2019

1. Westbrook, C. K., Mehl, M., Pitz, W. J., Kukkadapu, G., Wagnon, S. and Zhang, K., "Multi-Fuel Surrogate Chemical Kinetic Mechanisms for Real World Applications," *Physical Chemistry Chemical Physics* 20 (16) (2018) 10588-10606.
2. Zhang, K., Lokachari, N., Ninnemann, E., Khanniche, S., Green, W. H., Curran, H. J., Vasu, S. S. and Pitz, W. J., "An Experimental, Theoretical, and Modeling Study of the Ignition Behavior of Cyclopentanone," *Proceedings of the Combustion Institute* 37 (1) (2019) 657-665.
3. Ahmed, A., Pitz, W. J., Cavallotti, C., Mehl, M., Lokachari, N., Nilsson, E. J. K., Wang, J.-Y., Konnov, A. A., Wagnon, S. W., Chen, B., Wang, Z., Kim, S., Curran, H. J., Klippenstein, S. J., Roberts, W. L. and Sarathy, S. M., "Small Ester Combustion Chemistry: Computational Kinetics and Experimental Study of Methyl Acetate and Ethyl Acetate," *Proc. Combustion Inst.* 37 (1) (2019) 419-428.
4. Wagnon, S. W., Thion, S., Nilsson, E. J. K., Mehl, M., Serinyel, Z., Zhang, K., Dagaut, P., Konnov, A. A., Dayma, G. and Pitz, W. J., "Experimental and Modeling Studies of a Biofuel Surrogate Compound: Laminar Burning Velocities and Jet-Stirred Reactor Measurements of Anisole," *Combustion and Flame* 189 (2018) 325-336.
5. Reference 1 above.
6. Zhang, K., Banyon, C., Burke, U., Kukkadapu, G., Wagnon, S. W., Mehl, M., Curran, H. J., Westbrook, C. K. and Pitz, W. J., "An Experimental and Kinetic Modeling Study of the Oxidation of Hexane Isomers: Developing Consistent Reaction Rate Rules for Alkanes," *Combustion and Flame*, Accepted (2019).
7. Guzman, J., Kukkadapu, G., Brezinsky, K. and Westbrook, C., "Experimental and Modeling Study of the Pyrolysis and Oxidation of an Iso-Paraffinic Alcohol-to-Jet Fuel," *Combustion and Flame* 201 (2019) 57-64.
8. Westbrook, C. K., Sjöberg, M. and Cernansky, N. P., "New Chemical Kinetic Method of Determining RON and MON Values for Single Component and Multicomponent Mixtures of Engine Fuels," *Combust. Flame* 195 (2018) 50-62.
9. Padilla, R. E., Escofet-Martin, D., Pham, T., Pitz, W. J. and Dunn-Rankin, D., "Structure and Behavior of Water-Laden CH₄/Air Counterflow Diffusion Flames," *Combustion and Flame* 196 (2018) 439-451.
10. Westbrook, C. K., Mehl, M., Pitz, W. J. and Sjöberg, M., "Chemical Kinetics of Octane Sensitivity in a Spark-Ignition Engine," *Combustion and Flame* 175 (2017) 2-15.
11. Fridlyand, A., Johnson, M. S., Goldsborough, S. S., West, R. H., McNeely, M. J., Mehl, M. and Pitz, W. J., "The Role of Correlations in Uncertainty Quantification of Transportation Relevant Fuel Models," *Combustion and Flame* (2017).
12. Zhang, Y., Somers, K. P., Mehl, M., Pitz, W. J., Cracknell, R. F. and Curran, H. J., "Probing the Antagonistic Effect of Toluene as a Component in Surrogate Fuel Models at Low Temperatures and High Pressures. A Case Study of Toluene/Dimethyl Ether Mixtures," *Proceedings of the Combustion Institute* 36 (1) (2017) 413-421.
13. Al Rashidi, M. J. A., Thion, S., Togbé, C., Dayma, G., Mehl, M., Dagaut, P., Pitz, W. J., Zádor, J. and Sarathy, S. M., "Elucidating Reactivity Regimes in Cyclopentane Oxidation: Jet Stirred Reactor Experiments, Computational Chemistry, and Kinetic Modeling," *Proceedings of The Combustion Institute* Volume 36, Issue 1, 2017, Pages 469-477.
14. Sun, W., Wang, G., Li, S., Zhang, R., Yang, B., Yang, J., Li, Y., Westbrook, C. K. and Law, C. K., "Speciation and the Laminar Burning Velocities of Poly (Oxymethylene) Dimethyl Ether 3 (POMDME₃) Flames: An Experimental and Modeling Study," *Proceedings of the Combustion Institute* 36 (1) (2017) 1269-1278.

INVESTIGATION OF NON-PREMIXED TURBULENT COMBUSTION

Grant: DE-FG02-90ER14128

Stephen B. Pope & Perrine Pepiot
Sibley School of Mechanical & Aerospace Engineering
Cornell University, Ithaca, NY 14853
s.b.pope@cornell.edu, pp427@cornell.edu

1 Scope of the Research Program

The underlying theme of this work is the development of computational approaches which allow our detailed knowledge of the chemical kinetics of combustion to be applied to the modeling and simulation of combustion devices. The principal modeling approaches used are large-eddy simulation (LES) to describe the flow and turbulence, and particle-based probability density function (PDF) methods to treat the turbulence-chemistry interactions. Research is currently focused on the development and validation of a pre-partitioned adaptive chemistry (PPAC) approach [4] for use in LES-PDF simulations, in which individual particles evolve according to a reduced set of kinetic equations tailored for their specific compositions, thereby significantly reducing both the time and memory required for a computation with a given kinetic mechanism, and enabling affordable computations with significantly more detailed chemistry descriptions.

2 Recent Progress - A Pre-Partitioned Adaptive Chemistry (PPAC) Methodology to Implement Detailed Chemistry in LES/PDF

The initial development of the pre-partitioned adaptive chemistry methodology has been done using a partially stirred reactor (PaSR). The PaSR serves as a computationally inexpensive surrogate for a transported PDF computation. Recent efforts have focused on the development of a state-of-the-art LES/PDF code and coupling it holistically to PPAC. The LES/PDF code is developed within the discretely conservative, variable density low Mach solver NGA [1]. The mean estimation is performed using the cloud-in-cell approach and the interpolation to particle locations is performed using linear-splines [2]. Additionally, the smoothing algorithm of Viswanathan et al. [2] has been implemented for variance reduction, enabling the use of a smaller number of particles per cell. The two-way coupling with the flow solver is achieved using the transported specific volume approach of Popov et al [3]. The mixing fractional step uses the classical implementation of the interaction by exchange with the mean (IEM) mixing model. The transport in physical space is performed using a simple first-order Euler scheme.

The runtime dynamic procedure detailed in Liang et al. [4] is implemented in the LES/PDF code, to demonstrate and quantify the performance of the coupled PPAC LES/PDF methodology. We note that since the mixing fractional step is performed in the full composition space with the IEM model, scalar fields corresponding to all the species need to be retained at runtime. However,

particle specific compositions can be maintained in their reduced skeletal form, with the reconstruction to their full representation being performed only before the mixing step.

The coupled PPAC LES/PDF methodology has been tested using a domain of size $18D$ in the streamwise direction and $10D$ in the cross-stream directions, D being diameter of the fuel jet). The domain is discretized using a uniform Cartesian grid with 90 cells in the axial or streamwise direction and 100 cells in the cross-stream direction. The use of this relatively small domain and modest spatial resolution allows us to directly use the detailed mechanism and perform a rigorous evaluation of PPAC. The 38 species detailed mechanism of Esposito and Chelliah [5] is used for the current computation. The initial database of detailed compositions for the preprocessing stage is obtained by down sampling compositions from the LES/PDF computation using the detailed mechanism. The number of regions used for partitioning the composition space is 10 and targets used for reduction are CH_4 , CO , OH , HO_2 , and heat release rate. We generate 5 sets of reduced models, each of which correspond to a specified DRGEP error tolerance. The specified DRGEP error tolerances are 5×10^{-4} , 10^{-4} , 10^{-5} , 5×10^{-5} and 10^{-6} . Each of these 5 reduced models are utilized to perform a LES/PDF computation, in order to assess their performance.

Figure 1 shows the notional particles colored by their temperature (K) on the left and for the same time instant particles colored by the number of reactions, relative to the detailed mechanism, belonging to the reduced model used for integrating the particle compositions. The stream-wise direction is from the bottom to the top of the page. We observe that particles having unmixed compositions in the core of the fuel jet and in the co-flow are being resolved by models with zero reactions.

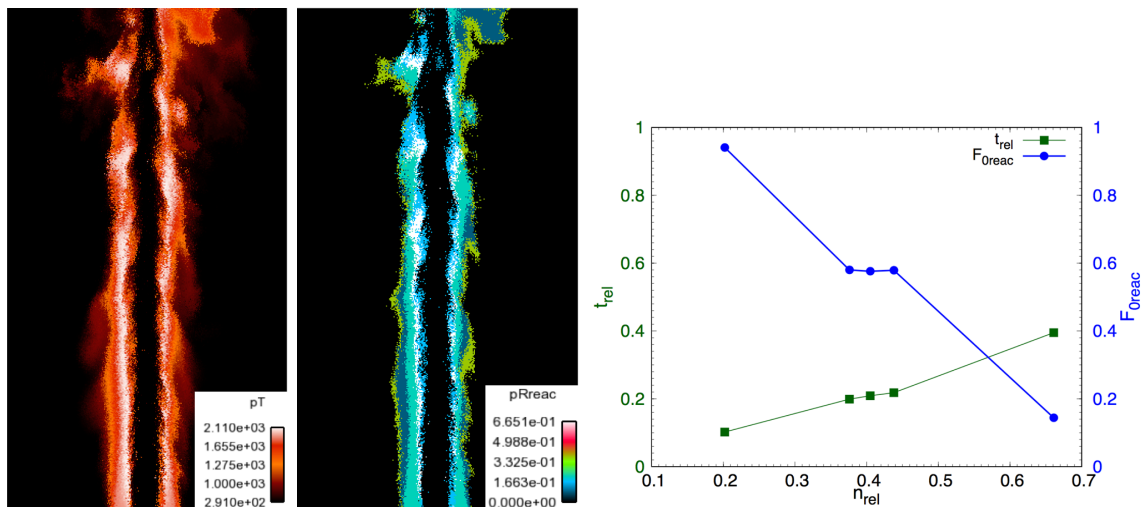


Figure 1: Notional particles colored by particle temperature (K) (left) and relative number of reactions (middle). Relative time and fraction of compositions resolved using models with zero reactions versus relative number of species for various adaptive LES/PDF runs (right).

A quantitative assessment of the performance of PPAC is provided in Figure 1 (right), showing the relative time for the adaptive LES/PDF runs, along with the relative fraction of compositions resolved using models with zero reactions as a function of the relative number of species. The

relative time is defined as average wall clock time per time step of the adaptive LES/PDF run relative to its analog of a LES/PDF run using the detailed mechanism. The relative number of species is the average fraction of the species present in the reduced models used in the reaction fractional step. The compositions that are resolved using reduced models with zero reactions are highlighted here as their state after the reaction fractional step is trivially known. Consequently these compositions are resolved without entering the actual reaction fractional step code, sparing the time required for communicating these compositions.

A quantitative assessment of the accuracy of PPAC is provided in Figure 2, comparing the conditional means for the mass fraction of OH between the non-adaptive and adaptive runs. We observe that barring the adaptive run with largest DRGEP reduction threshold, there is excellent agreement between the non-adaptive and adaptive runs. Finally, we recall that PPAC incurs conservation errors during conversion from the detailed to skeletal representations for particle compositions. Figure 2 shows the time-averaged elemental conservation for the various adaptive LES/PDF runs. We observe that all the conservation errors are bounded below 3×10^{-5} are deemed to be acceptable.

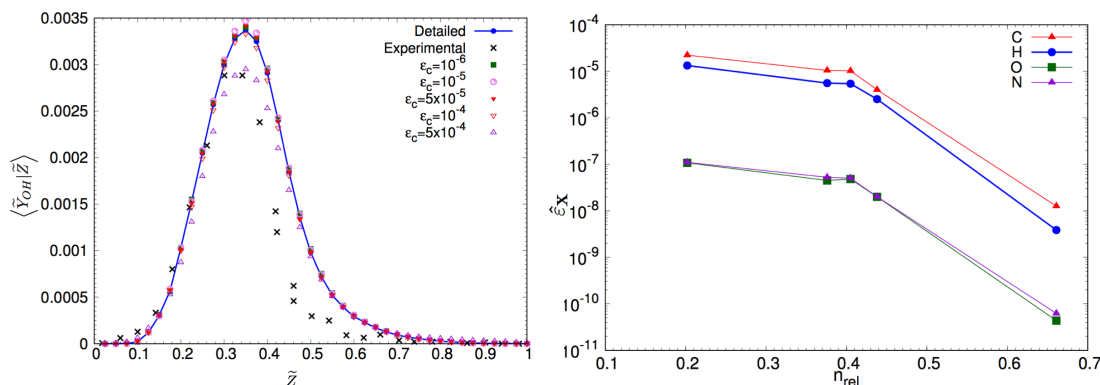


Figure 2: Conditional means for OH mass fraction at $x/D = 15$ (left) and conservation errors versus relative number of species (right).

3 Future Plans

Work in near future will focus on the performance of the coupled PPAC-ISAT approach, which will be assessed in the same configuration, as well as in a full-scale LES/PDF computation of Sandia flame D. An ongoing side effort on developing error-control strategies for PPAC will continue, with implementation and assessment planned for both partially stirred reactor models and large scale turbulent flame simulations.

4 Publications from DOE Research 2013-2019

- A.S. Newale, Y. Liang, S.B. Pope, P. Pepiot (2019) “A combined PPAC-RCCE-ISAT methodology for efficient implementation of combustion chemistry”, *Combust. Th. Modell.*, accepted.
- A. Felden, B. Cuenot, L. Esclapez, P. Pepiot, E. Riber (2018) “Including analytically reduced chemistry (ARC) in CFD applications”, *Acta Aeronautica*, accepted.
- F. Tagliante, T. Poinot, L.M. Pickett, P. Pepiot, L.-M. Malbec, G. Bruneaux, C. Angelberger (2019) “A conceptual model of the flame stabilization mechanisms for a lifted Diesel-type flame based on

direct numerical simulation and experiments”, *Combust. Flame* 201, 65 – 77.

- Jaravel, T., Riber, E., Cuenot, B., Pepiot, P. (2018) “Large Eddy Simulation of the Sandia flame D using reduced mechanism for accurate pollutant prediction”, *Combust. Flame* 188,180 – 198.
- R.R. Tirunagari, S.B. Pope (2016) “Characterization of extinction/re-ignition events in turbulent premixed counterflow flames using strain-rate analysis”, *Proc. Combust. Inst.*, accepted.
- R.R. Tirunagari, S.B. Pope (2016) “An Investigation of Turbulent Premixed Counterflow Flames using Large-Eddy Simulations and Probability Density Function Methods”, *Combust. Flame* 166, 229–242.
- R.R. Tirunagari, M.W.A. Pettit, A.M. Kempf, S.B. Pope (2015) “A Simple Approach for Specifying Velocity Inflow Boundary Conditions in Simulations of Turbulent Opposed-Jet Flows”, *Flow, Turb. Combust.*, submitted for publication.
- R.R. Tirunagari, S.B. Pope (2015) “LES/PDF for Premixed Combustion in the DNS Limit”, *Combust. Th. Model.*, submitted for publication.
- Y. Liang, S. B. Pope, and P. Pepiot (2015) “An adaptive methodology for the efficient implementation of combustion chemistry in particle PDF methods”, *Combust. Flame* 162, 3236–3253.
- M. Mehta, R. O. Fox, and P. Pepiot. (2015) “Reduced chemical kinetics for the modeling of TiO₂ nanoparticle synthesis in flame reactors”, *Ind. Eng. Chem. Res.* 54, 5407–5415.
- K. Narayanaswamy, P. Pitsch, and P. Pepiot (2015) “A chemical mechanism for low to high temperature oxidation of methylcyclohexane as a component of transportation fuel surrogates”, *Combust. Flame*, 162, 1193–1213.
- Pope, S. B. (2014) “The determination of turbulence-model statistics from the velocity-acceleration correlation”, *J. Fluid Mech.* 757, R1, DOI:10.1017/jfm.2014.563.
- Pope, S. B. and R. Tirunagari (2014) “Advances in probability density function methods for turbulent reactive flows”, In *Proceedings of the Nineteenth Australasian Fluid Mechanics Conference*. RMIT University, Melbourne.
- Popov, P. and S. B. Pope (2014) “Large eddy simulation/probability density function simulations of bluff body stabilized flames”, *Combust. Flame* 161, 3100–3133.
- K. Narayanaswamy, P. Pepiot, and P. Pitsch (2014) “A chemical mechanism for low to high temperature oxidation of *n*-dodecane as a component of transportation fuel surrogates”, *Combust. Flame*, 161, 866–884.
- Hiremath, V., S. R. Lantz, H. Wang, and S. B. Pope (2013) “Large-scale parallel simulations of turbulent combustion using combined dimension reduction and tabulation of chemistry”, *Proc. Combust. Inst.* 34, 205–215.
- Hiremath, V. and S. B. Pope (2013) “A study of the rate-controlled constrained-equilibrium dimension reduction method and its different implementations”, *Combust. Theory Modelling* 17, 260–293.
- Pope, S. B. (2013) “A model for turbulent mixing based on shadow-position conditioning”, *Phys. Fluids* 25, 110803.
- Pope, S. B. (2013) “Small scales, many species and the manifold challenges of turbulent combustion”, *Proc. Combust. Inst.* 34, 1–31.
- Ren, Z., G.M. Goldin, V. Hiremath, S.B. Pope (2013) “Simulations of a turbulent non-premixed flame using combined dimension reduction and tabulation for combustion chemistry”, *Fuel* 105, 636–644.

References

- [1] O. Desjardins, G. Blanquart, G. Balarac, and H. Pitsch. *J. Comput. Phys.*, 227 (2008) 7125–7159.
- [2] S. Viswanathan, H. Wang, and S.B. Pope. *J. Comput. Phys.*, 230(17):6916–6957, 2011.
- [3] P. P. Popov, H. Wang, and S.B. Pope. *J. Comput. Phys.*, 294:110–126, 2015.
- [4] Y. Liang, S.B. Pope, and P. Pepiot. *Combust. Flame*, 162(9):3236–3253, 2015.
- [5] G. Esposito and H.K. Chelliah. *Combust. and Flame*, 158(3):477–489, 2011.

OPTICAL PROBES OF ATOMIC AND MOLECULAR DECAY PROCESSES

S.T. Pratt
Building 200, B-125
Argonne National Laboratory
9700 South Cass Avenue
Lemont, Illinois 60439
E-mail: stpratt@anl.gov

PROGRAM SCOPE

The study of molecular photoabsorption, photoionization, and photodissociation dynamics can provide insight into how energy and angular momentum flow among the electronic, vibrational, and rotational degrees of freedom in isolated, highly energized molecules. This project is focused on these dynamics in small molecules, with the goal of determining the mechanisms of these decay processes and their product branching distributions. In addition to intramolecular dynamics, a second aspect of this work involves the determination of absolute photoabsorption and photoionization cross sections, as well as the general principles that determine them. The experimental approach uses both laboratory-based laser techniques for single- and multiphoton excitation of valence-shell processes, and facilities-based vacuum-ultraviolet (VUV) and x-ray techniques for the excitation of both valence-shell and inner-shell processes. The detection methods include mass spectrometry, photoion- and photoelectron-imaging, high-resolution photoelectron spectroscopy, photoelectron-photoion coincidence techniques, and VUV Fourier-transform absorption spectroscopy. Photoelectron imaging is also being explored for circular dichroism studies of photoelectron angular distributions as a means to characterize chiral molecules. Finally, time-domain experiments enabled by new VUV and x-ray free electron laser sources are being performed to complement ongoing frequency-domain work.

RECENT PROGRESS

Over the past year, new experiments have been performed both in the laboratory at Argonne and at the SOLEIL synchrotron facility. The work at SOLEIL is performed with the team of researchers acknowledged below, and focused on several different projects using both the VUV Fourier-transform absorption spectrometer (FTS) and the photoelectron-photoion coincidence spectrometer at the DESIRS beamline. In addition, I participated in new time-resolved experiments at the FERMI free-electron laser facility in Trieste, Italy. I have also spent time analyzing results from previous experiments and preparing them for publication. The work at Argonne has focused on double-resonance studies of the photoionization of molecular nitrogen, N_2 , and on preliminary polarization studies with chiral molecules.

Photoabsorption studies using the FTS

In the last year, we had two sets of beamtime to use the FTS. First, working with A. Heays (University of Arizona), we recorded comprehensive absorption data on nitric oxide at several different pressures and temperatures. While the VUV absorption spectrum of nitric oxide is one of the best studied of all molecules, the focus of this work was on recording absolute photoabsorption cross sections at high resolution. These measurements will complement the existing relative cross section data, and provide a challenging task for theoretical predictions. Leveraging the work of E. Miescher and his students, Ch. Jungen (Laboratoire Aimé Cotton) and his collaborators have used multichannel quantum defect theory (MQDT) to provide a comprehensive analysis for the energetics of the Rydberg states of NO. He is interested in seeing how well this approach can do for the transition intensities, and we will work with him on this effort.

As an extension of our earlier work on the linear alkyne molecules, we have recorded comprehensive absorption spectra of a set of branched, C_6H_{10} 1-alkyne molecules, including 1-hexyne, 3-methyl-1-pentyne, 4-methyl-1-pentyne, and 3,3-dimethyl-1-butyne. Strong similarities are observed in the spectra of the first three molecules, both with each other and with those of the smaller 1-alkynes. On the other hand, the spectrum of 3,3-dimethyl-1-butyne (a.k.a. t-butyl acetylene) is quite different. This difference almost certainly results from the higher symmetry of the latter molecule, and the similarities between its

spectrum and that of propyne (i.e., methyl acetylene) are being explored. While some of these observations were first noted some time ago (for example, in the classic books of M. Robin), their detailed analysis has not yet been presented.

Finally, we recorded very high-resolution photoabsorption measurements on N_2 from the lowest Rydberg states up to the $B\ ^2\Sigma_u^+$ threshold. The spectra were recorded at room temperature, liquid nitrogen temperature, and in a jet, and with a resolution across the full region of $\sim 0.7\text{ cm}^{-1}$. As discussed below, when combined with new double-resonance experiments and a full MQDT treatment, we hope to make a comprehensive assignment of the valence-shell photoionization spectrum.

Photoionization of C_4H_5 and other small radicals

In collaboration with J. C. Loison (ISM, Bordeaux), we had previously recorded coincidence spectra of C_4H_5 radicals produced from 2-butyne by using a fluorine abstraction reaction at the SOLEIL synchrotron. This approach has allowed detailed photoelectron-photoion coincidence studies of the valence shell photoionization of C_4H_5 radicals. In particular, we recorded a high-resolution photoionization spectrum that shows considerable structure resulting from electronic autoionization of Rydberg series converging to excited electronic states of the corresponding radical cation. This structure is closely related to that observed for the propargyl radical. (The 2-butyne-1-yl radical is methyl-propargyl.) We also made a measurement of the photoionization cross section to put the full spectrum on an absolute scale. The data also allow the extraction of a slow photoelectron spectrum of C_4H_5 with high signal-to-noise ratio, from the first ionization threshold near 8 eV up to 11.5 eV. This energy range is sufficient to reveal two electronically excited states of the cation for the first time. While there have been previous studies of the photoionization of C_4H_5 [(see, for example, N. Hansen et al., *J. Phys. Chem. A* **110**, 3670 (2006) and M. Lang et al., *J. Phys. Chem. A* **119**, 3995 (2015).], the present data provide a more information on the excited states of the cations. In future work, we hope to complement these data with results on the other C_4H_5 isomers, and to use fixed-photon-energy photoelectron spectroscopy to help identify the autoionizing resonances.

In a beamtime led by B. Gans (ISMO, France) in early 2018, we used the same approach to record slow photoelectron spectra, photoionization spectra, and absolute photoionization cross sections for a number of free radicals and reactive species, including HNC, CH_3 , C_2H_5 , $C_6H_5CH_2$, and OH. The initial results on HNC and OH have been published, and the remainder of the data is still being analyzed.

Photoionization of Molecular Nitrogen

Last year we performed preliminary double-resonance experiments on the autoionizing states of N_2 by using the $a\ ^1\Sigma_g^+$ intermediate state. We have now completed our study of the "new Ogawa bands," providing a definitive assignment for these spectral features. We also used photoelectron imaging to determine the electron energy and angular distributions for the autoionization process. We are now moving on to explore other regions of the spectrum, in particular, the "cathedral" bands between 126100 cm^{-1} and 126500 cm^{-1} and other intense features that have not been definitively assigned previously. We are also working to provide Ch. Jungen experimental input for his comprehensive MQDT analysis of the N_2 spectrum.

In time-resolved experiments at FERMI, we prepared a wavepacket made up of several bound Rydberg states, and probed the wavepacket evolution as a function of time delay by using photoelectron imaging. This approach provided both the electron energy and angular distributions. The time-dependent distributions reflect the composite character of the initially prepared wavepacket, and can be understood in terms of a simple model for the intermediate state. Our work on the absorption spectroscopy of N_2 should allow us to make a more quantitative model for the observed behavior.

I have also been collaborating with the group of A. Stolow (University of Ottawa) on the interpretation of time-resolved photoelectron spectra of electronic coherences in NH_3 . In many ways, these experiments are similar to those performed on N_2 at FERMI. As in the N_2 work, high-resolution photoabsorption data

on NH₃ recorded at SOLEIL helped us understand the states that made up the wavepacket prepared in the new time-resolved experiments, and helped in the interpretation of the spectra.

Inner-shell and inner-valence processes in methyl iodide

I have continued my collaboration with D. Holland (STFC, UK) and R. Forbes (University College London) on the photoelectron spectroscopy of the inner-shell and inner-valence shells of methyl iodide. Papers were published on 3d and 4d subshells and on Auger spectroscopy of the 3d states. A third paper combining theoretical calculations and new experimental data on the shake-up processes near the 1s ionization threshold was recently submitted. It appears that spin-orbit interactions are responsible for the observation of one of the most intense shake-up states. Additional experiments on methyl iodide are planned to pin down this mechanism, and complementary experiments on lighter alkyl halides (e.g., methyl bromide and methyl chloride) are also planned. Our new data should be helpful for many new experiments with free-electron lasers, in which methyl iodide often serves as the prototypical sample of choice.

FUTURE PLANS

In the coming year, I will work to bring together all of the different threads of research on the valence-shell photoabsorption and photoionization spectrum of N₂, with the goal of providing a comprehensive analysis between the X ²Σ_g⁺ threshold and the B ²Σ_u⁺ threshold. This effort will include working on the analysis of our very-high resolution photoabsorption spectra, the analysis of our existing double-resonance spectra via the a" ¹S_g⁺ state, additional double-resonance spectra to probe selected regions of the spectrum, and working to develop a model for the time-resolved measurements from the FERMI experiments. I will also work with Christian Jungen on his multichannel quantum defect theory analysis of this spectrum. While this analysis is a long-term effort, I believe that significant progress will be made in the coming year. I will also use the double-resonance approach with photoelectron imaging to learn more about the autoionization dynamics and photoelectron angular distributions of rotationally selected resonances. I will also investigate the possibility of using an additional laser to detect N atoms to address the predissociation processes that compete with autoionization for some resonances. Finally, I will apply for additional beamtime at FERMI to pursue a broader range of time-resolved experiments on N₂. I have already applied for additional beamtime at the FERMI FEL with Katharine Reid, David Holland, and Henrik Stapelfeldt (Aarhus University). This proposal focuses on photoelectron angular distributions from dissociating, fixed-in-space Br₂ molecules. In these experiments, the Br₂ will be impulsively aligned by using an ultrafast near-infrared laser, excited to a dissociative state with a second optical laser, and probed by the vacuum-ultraviolet FEL pulse.

Although a paper was published about our work on C₄H₅ this past year, we still have significant data on C₄H₄ and C₄H₃ produced by sequential H-atom abstraction from our 2-butyne starting material, and I will continue to work on their analysis. In an effort to provide more definitive assignment for the resonances in the 2-butyne-1-yl spectrum, we will also record photoelectron images with improved resolution and signal-to-noise ratio. We are also planning new experiments to investigate the other C₄H₅ isomers that will be produced by H atom abstraction from other C₄H₆ precursors (e.g., 1-butyne, 1,2-butadiene, and 1,3-butadiene). We are particularly interested to see how the resonance structure changes in the different C₄H₅ isomers. This work should also allow us to compare the absolute photoionization cross sections of the different C₄H₅ isomers. In my laboratory work at Argonne, I will work to complete my double-resonance studies on N₂.

I will continue to work on the analysis of my existing data on the photoabsorption spectra of branched alkyne molecules, the inner-shell spectra of CH₃I, and the photoabsorption cross section of NO. This past year, we had beamtime at SOLEIL to perform coincidence measurements on the photoionization of HBr, but the instrument was suffering from poor resolution at that time. We have new beamtime to address these issues in June, and we hope to have rotationally resolved photoelectron images near the first ionization threshold.

Finally, I am initiating some new experiments to observe polarization effects in the photoionization and photodissociation of chiral molecules, and we are hoping to see our first meaningful results in the coming year.

ACKNOWLEDGEMENTS

This work was performed in collaboration with my postdoc, Ananya Sen. Work on oriented NO was performed in collaboration with K. L. Reid (Nottingham). Work at Soleil was performed in collaboration with S. Boyé-Péronne and B. Gans (Institut des Sciences Moléculaires d'Orsay), J. -C. Loison (University of Bordeaux), D. M. P. Holland (STFC, Daresbury), U. Jacovella (ETH-Zürich), E. F. McCormack (Bryn Mawr College), G. Garcia (SOLEIL), L. Nahon (SOLEIL), and N. de Oliveira (SOLEIL). The work at FERMI was performed in collaboration with a large international group of researchers led by K. Ueda (Tohoku University, Japan). Theoretical work on N₂ was performed in collaboration with Ch. Jungen (Laboratoire Aimé Cotton). This work was supported by the U.S. Department of Energy, Office of Science, Office of Basic Energy Sciences, Division of Chemical Sciences, Geosciences, and Biological Sciences under contract No. DE-AC02-06CH11357.

DOE-SPONSORED PUBLICATIONS SINCE 2017

1. A. Sen, S. T. Pratt, and K. L. Reid, Circular dichroism in photoelectron images from aligned nitric oxide molecules, *J. Chem. Phys.* **147**, 013927 (2017).
2. A. M. Chartrand, E. F. McCormack, U. Jacovella, D. M. P. Holland, Bérenger Gans, Xiaofeng Tang, G. A. Garcia, L. Nahon, and S. T. Pratt, Photoelectron angular distributions from rotationally resolved autoionizing states of N₂, *J. Chem. Phys.* **147**, 224303 (2017).
3. Min Xie, Zhitao Shen, S. T. Pratt, and Yuan-Pern Lee, Vibrational autoionization of state-selective jet-cooled methanethiol (CH₃SH) investigated with infrared + vacuum-ultraviolet photoionization *Phys. Chem. Chem. Phys.* **19**, 29153-29161 (2017).
4. R. Forbes, A. De Fanis, C. Bomme, D. Rolles, S. T. Pratt, I. Powis, N. A. Besley, S. Nandi, A. R. Milosavljević, C. Nicolas, J. D. Bozek, J. G. Underwood, and D. M. P. Holland, Auger electron angular distributions following excitation or ionization of the I 3d level in methyl iodide, *J. Chem. Phys.* **149**, 094304 (2018).
5. R. Forbes, A. De Fanis, C. Bomme, D. Rolles, S. T. Pratt, I. Powis, N. A. Besley, M. Simon, S. Nandi, A. R. Milosavljevic, C. Nicolas, J. D. Bozek, J. G. Underwood, and D. M. P. Holland Photoionization of the iodine 3d, 4s and 4p orbitals in methyl iodide, *J. Chem. Phys.* **149**, 144311 (2018).
6. A. Sen and S. T. Pratt, Double-resonance studies of electronically autoionizing states of molecular nitrogen, *Mol. Phys.*, DOI: [10.1080/00268976.2018.1544672](https://doi.org/10.1080/00268976.2018.1544672)
7. H. R. Hrodmarsson, J.-C. Loison, U. Jacovella, D. M. P. Holland, S. Boyé-Péronne, B. Gans, G. A. Garcia, L. Nahon, and S. T. Pratt, Valence-shell photoionization of the C₄H₅ radical, *J. Phys. Chem. A* **123**, 1521-1528 (2019).
8. B. Gans, G. A. Garcia, S. Boyé-Péronne, S. T. Pratt, J.-C. Guillemin, A. Aguado, O. Roncero, and J.-C. Loison, Origin band of the first photoionizing transition of hydrogen Isocyanide, *Phys. Chem. Chem. Phys.* **21**, 2337-2344 (2019).
9. O. J. Harper, M. Hassenfratz, J.-C. Loison, G. A. Garcia, N. de Oliveira, H.R. Hrodmarsson, S. T. Pratt, S. Boyé-Péronne, and B. Gans, Quantifying the photoionization cross section of the hydroxyl radical, *J. Chem. Phys.* (in press).

Reaction Mechanisms Studied with Chirped-Pulse Rotational Spectroscopy

Kirill Prozument
Argonne National Laboratory
Chemical Sciences and Engineering Division
Lemont, IL 60439
prozument@anl.gov

1. Scope of the Program

The goal of the Program is to gain detailed understanding of the dynamical processes that govern chemical reactivity. Oftentimes, the rates predicted for even simple reactions are in disagreement with experimental observations. The discrepancy may arise because such effects as roaming dynamics, tunneling reaction mechanism, lack of thermal equilibration of reaction intermediates and others are often neglected in kinetics models. We investigate the pyrolysis and photolysis reactions that help us reveal these mechanisms. We aim at generalizing our findings to broad classes of reactions. The experimental approach in this Program is based on chirped-pulse Fourier transform millimeter-wave (CP-FTmmW) spectroscopy. The reaction products are detected non-destructively, with quantum state specificity and time resolution. Because CP-FTmmW spectroscopy is also quantitative, branching ratios are measured and can be compared with theoretical models. The versatility of the CP-FTmmW technique is sufficient for its application to a wide range of experiments in reaction dynamics and kinetics in the gas phase. The program is currently focused of two experimental directions: i) investigation of pyrolysis chemistry in the microtubular reactor at 1000–1800 K, and ii) *in situ* time-resolved chirped-pulse spectroscopy of photoproducts at room temperature. The third direction of the Program is development of the Artificial Intelligence (AI) methods for automation of spectroscopic assignment. The need for that component is pressing as vast amounts of potentially useful spectroscopic data are generated in broadband rotational experiments, but rarely are fully analyzed. The goal of the AI thrust is that vast amounts of *spectroscopic* data becomes the *chemical* information, ready for reaction mechanisms discovery.

2. Recent Progress

Pyrolysis in microtubular reactor

Quantitative detection of the pyrolysis reaction products, including the free radical intermediates, has been demonstrated. Figure 1 shows the branching of the following products of the CH₃ONO pyrolysis: CH₂O, HNO, CH₃O, HCNO, CH₃OCH₃, HCO, CH₃NO, *trans*-HONO, HCN, HNCO, and HNC. The dynamic range of the detected products' concentrations is $\sim 10^5$, and the mole fraction of the least abundant product HNC is 2×10^{-8} or 20 ppb. We have demonstrated the outstanding sensitivity, multiplexed detection of multiple reaction products, including the radicals, with their branching ratios in our CP-FTmmW/pyrolysis experiments.

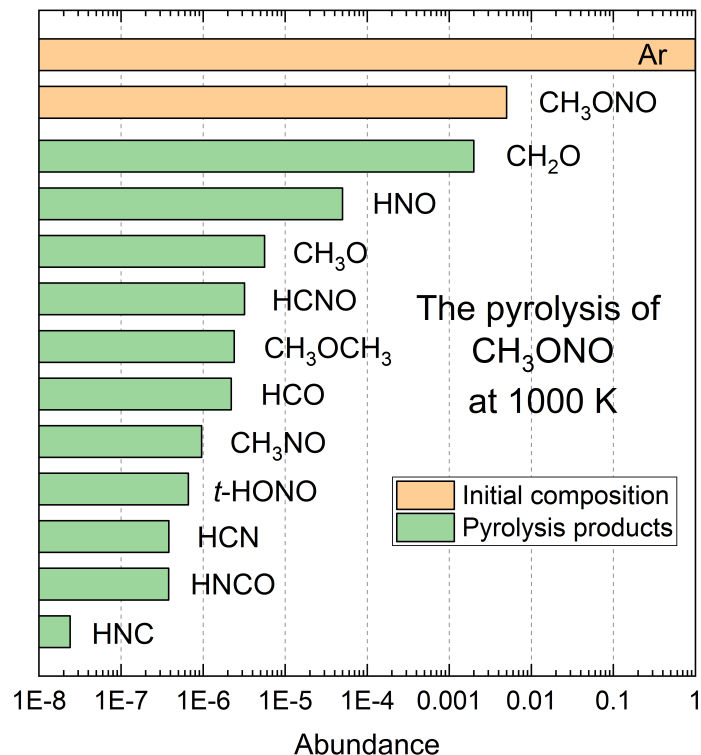


Figure 1. The branching of the pyrolysis products following thermal decomposition of methyl nitrite. The experiment is utilizing the 75–110 GHz BrightSpec CP-FTmmW spectrometer¹ coupled to the continuous flow Chen-type pyrolysis reactor. CH₃ONO is initially entrained in argon carrier gas at 0.5% by mole (both are shown in orange bars). A variety of pyrolysis products are quantified and shown in green bars.

These experiments reveal that the chemistry of methyl nitrite pyrolysis in this type of reactors is much richer than it was previously assumed. The notion that the residence time of 10–100 μ s in the microtubular reactor allows to isolate the initial unimolecular decomposition reactions and is too short for the consecutive bimolecular chemistry to occur must be gauged by the sensitivity of the measurement. We find it to be an advantage rather than an unwanted complication that we can observe apparently complex networks of chemical reactions. Multiple experimental branching ratios can better constrain a kinetic model and lead to understanding of the underlying reaction dynamics. However, in order to reach that goal, the thermodynamic conditions in the reactor need to be characterized.

We have been working with the group of Robert Kee of Colorado School of Mines on the boundary-layer model that provides an efficient way to simultaneously simulate chemistry and the gas flow in these microtubular reactors.² The results of the simulation of acetaldehyde pyrolysis is demonstrated in Figure 2.

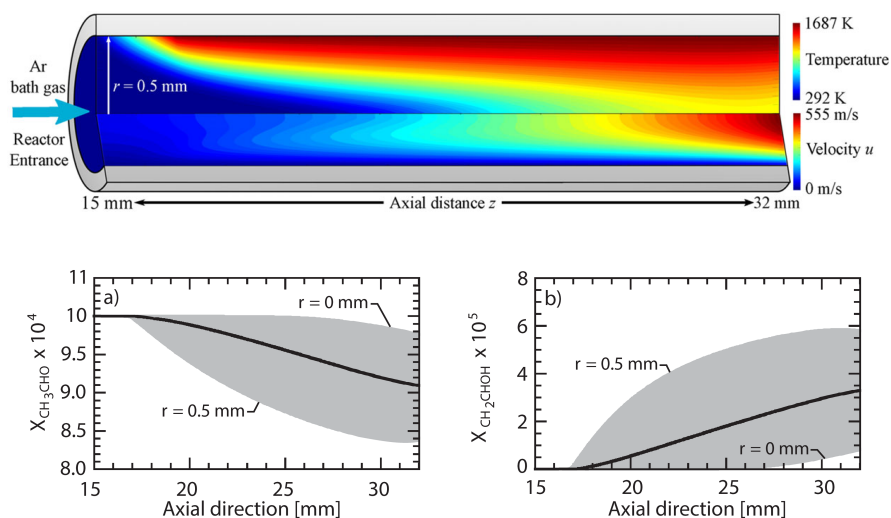


Figure 2. Simulation of the gas flow and the pyrolysis of acetaldehyde in the Chen-type microtubular reactor. The heat map is showing the distribution of temperature (top) and velocity (bottom) inside the reactor. The bottom graphs show a) consumption of the precursor and b) formation of vinyl alcohol product. Adapted from Ref. 1.

Assignment of Rotational Spectra using Artificial Neural Networks

The Rotational Assignment and Identification Network (RAINet) has been developed with the goal of automating assignment of the broadband rotational spectra.³ RAINet is trained to recognize patterns of lines in rotational spectra. Those patterns can then be used to identify the types of molecules present and their rotational constants and other parameters of the Hamiltonian (at present, the distortion constant and the electric quadrupole hyperfine constant).

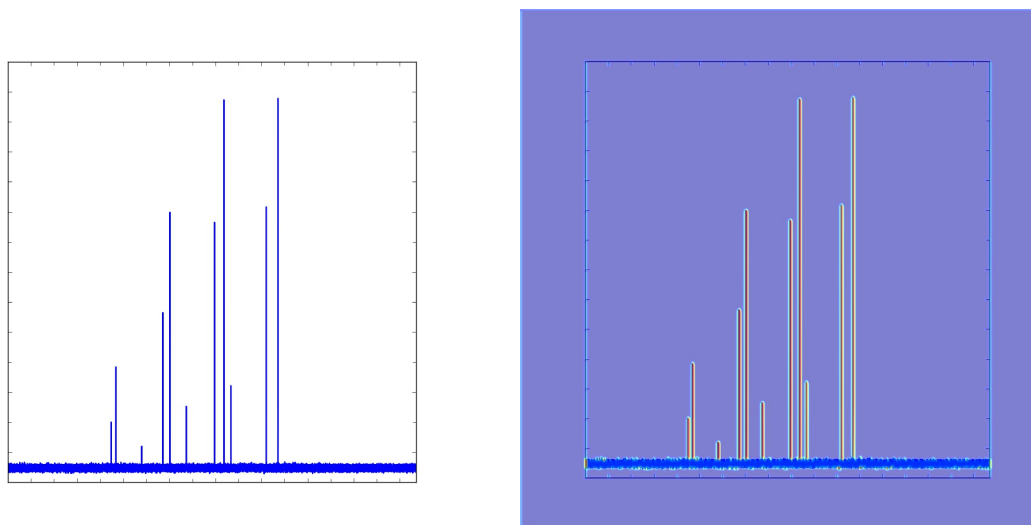


Figure 3. In image of a spectrum of a symmetric top molecule (left). The heat map generated by the trained CNN from the spectral image. The "hot" regions indicate high probability to contain a rotational line as perceived by the CNN. Adapted from Ref. 2.

The present most significant limitation of RAINet is its inability to localize and separate the rotational transitions that belong to different species. One of the approaches in solving that problem is utilization of convolutional neural networks (CNNs). Unlike the feed forward neural networks that operated with transition frequencies, a CNN is trained to recognize the rotational lines in images of the spectra (Figure 3). Although this approach was found useful in separating the noise, the background and the spurious lines, we were not able to localize the lines of different molecules.

3. Future Plans

Having established the branching of the methyl nitrite products, we will be able to complete, in collaboration with Raghu Sivaramakrishnan, the kinetic model describing the complex chemistry of methyl nitrite that we are observing in the microtubular reactor.

We plan to shift the emphasis of the Program from the AI thrust to the time-resolved kinetic chirped-pulse (TReK-CP) experiments⁴ during the next year. The plans are to extend the present spectrometer⁵ to 260 – 290 GHz range and thus increase the TReK-CP sensitivity by at least a factor of 10. With the new spectrometer, we plan to initiate H-atom abstraction reactions by OH or CN radicals (193 nm photolysis of H₂O₂ or NCCN) from, for example, CH₃OH. We will then study the consecutive chemistry of CH₃O and CH₂OH *in situ* and with time and vibrational state resolution. Because rotational and vibrational relaxations can be directly observed and may play an important role in products branching, we anticipate a close collaboration with Ahren Jasper on this project.

DOE-Sponsored Publications Since 2017

¹ D. P. Zaleski, C. Duan, M. Carvajal, I. Kleiner, and K. Prozument. The broadband rotational spectrum of fully deuterated acetaldehyde (CD₃CDO) in a CW supersonic expansion. *J. Mol. Spectrosc.* **342**, 17 (2017)

² P. J. Weddle, C. Karakaya, H. Y. Zhu, R. Sivaramakrishnan, K. Prozument, and R. J. Kee. Boundary-Layer Model to Predict Chemically Reacting Flow within Heated, High-Speed, Microtubular Reactors. *Int. J. Chem. Kinet.* **50**, 473 (2018)

³ D. P. Zaleski, and K. Prozument. Automated assignment of rotational spectra using artificial neural networks. *J. Chem. Phys.* **149**, 104106 (2018)

⁴ D. P. Zaleski, L. B. Harding, S. J. Klippenstein, B. Ruscic, and K. Prozument. Time-Resolved Kinetic Chirped-Pulse Rotational Spectroscopy in a Room-Temperature Flow Reactor. *J. Phys. Chem. Lett.* **8**, 6180 (2017)

⁵ D. P. Zaleski, and K. Prozument. Pseudo-equilibrium geometry of HNO determined by an E-Band CP-FTmmW spectrometer. *Chem. Phys. Lett.* **680**, 101 (2017)

ULTRAFAST CHEMISTRY: SPECTROSCOPIC PROBES OF NON-ADIABATIC DYNAMICS

Krupa Ramasesha, Christopher J. Kliewer

Combustion Research Facility, Mail Stop 9055; Sandia National Laboratories, Livermore, CA 94550

kramase@sandia.gov, cjkliew@sandia.gov

I. Program Scope

This program aims to apply ultrafast spectroscopy to follow fundamental gas-phase chemical dynamics. The work develops molecular structure-specific probes to follow coupled electronic and nuclear motion on femtosecond to picosecond timescales in gas-phase small molecules. The work in this task has strong connections to the laser spectroscopy investigated under the “Ultrafast Physics: Nonlinear Optical Spectroscopy and Diagnostics” subtask, and the high photon-energy techniques developed in the “Advanced Mass Spectrometry and X-Ray Diagnostics” task. The coupling of electronic and nuclear degrees of freedom, representing a breakdown of the Born-Oppenheimer approximation, gives rise to complex pathways of non-radiative energy dissipation in electronically excited molecules, often involving participation of several electronic states. Identifying the motions that couple electronic states, the timescales and dynamics of excited state population relaxation, and the role of the coupled vibrational modes of a molecule in guiding energy flow is crucial to our understanding of non-equilibrium dynamics, and it forms the mainstay of this program. This task extends the “Chemical Dynamics Methods and Applications” work down to the fundamental timescales of vibrational or electronic motion. *Ultrafast Chemistry* is one of the synergistic, fundamental research themes of CSGB and this work addresses two key aspects of the Grand Challenges for Basic Energy Sciences: (1) investigating the nature of electronic excited states, and (2) exploring the breakdown of the Born-Oppenheimer approximation during non-radiative relaxation through conical intersections.

II. Recent Progress

(a) Transient broadband infrared spectroscopy of non-adiabatic dynamics:

Over the last year, we have progressed towards developing broadband infrared (BBIR) spectroscopy as a method for probing excited state structural dynamics in polyatomic molecules. The goal of these experiments is to use BBIR pulses to probe high-frequency molecular vibrations as reporters of delocalized structural deformations following electronic excitation. These experiments are performed in a pump-probe transient absorption scheme, where a UV pulse electronically excites the system of interest and a BBIR pulse interrogates changes to molecular vibrations in the entire mid-infrared region.

The experimental set-up uses the output of a commercial ultrafast Ti:Sapphire laser system, generating 3 mJ/pulse, 55 fs pulses at 1 kHz repetition rate. The laser output is split into two arms, where one arm generates BBIR pulses and the other arm generates UV pulses. The BBIR arm constitutes a series of optics to generate doubled light at 400 nm. A Type I BBO crystal cut at 29.2° doubles the 800 nm output of the laser to 400 nm, a calcite crystal

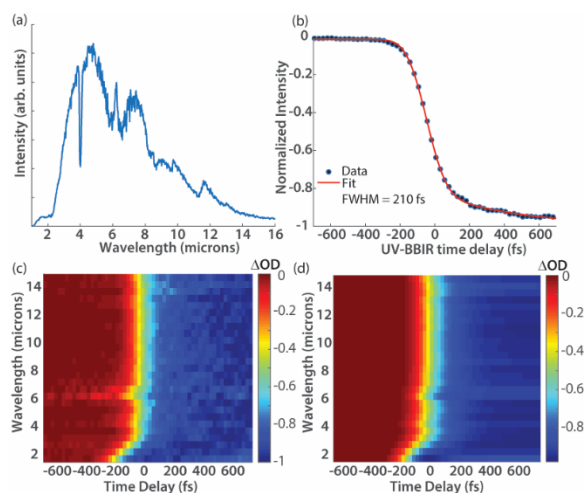


Figure 1: (a) Spectrum of plasma-generated BBIR.

The long wavelength cut-off is imposed by the detector response; (b) Frequency-integrated cross-correlation of BBIR with UV in 500 micron thick Ge wafer, yielding a half-width-at-half-maximum of 105 fs; (c) Frequency-resolved cross-correlation of BBIR with UV in Ge, revealing minimal spectral dispersion at wavelengths larger than 3000 nm. (d)

Fit to the frequency-resolved cross-correlation, yielding a wavelength-independent half-width-half-maximum of 73 fs.

compensates for temporal walk-off between the 800 nm and 400 nm pulses, and a dual-waveplate rotates the 800 nm polarization onto the polarization of 400 nm. The beam is then focused into a stream of flowing nitrogen gas using a $f = 50$ mm broadband concave dielectric mirror coated for high reflectivity at 800 nm and 400 nm, creating a plasma. The plasma radiates nearly linearly polarized broadband mid-infrared^{1,2}, which is separated from the visible plasma emission using a 500 μm thick undoped high-resistivity silicon wafer placed at Brewster's angle. Figure 1a displays the spectrum of the BBIR pulse measured by dispersing onto a 64-element liquid nitrogen cooled HgCdTe array detector, showing that these pulses span from <800 cm^{-1} to ~ 5000 cm^{-1} . In the UV arm, the 800 nm beam is first sent onto a motorized delay stage for controlling the UV-BBIR time delay, and then into the UV generation set-up. UV pulses at 262 nm with pulse energies of 10 μJ are collinearly generated using crystals identical to the BBIR arm, with the addition of a BBO crystal cut at 44.26° to sum the 800 nm and 400 nm pulses following timing and polarization compensation. The cross-correlation between the UV and BBIR pulses in a 500 μm thick undoped germanium wafer is displayed in Figure 1b, showing a half-width-at-half-maximum of ~ 100 fs. The negligible spectral dispersion in the absence of additional transmissive optics in the BBIR path is displayed in Figure 1c, and its fit reconstruction is shown in Figure 1d. Frequency-dependent cross correlation reveals a wavelength-independent half-width-at-half-maximum of ~ 70 fs.

The BBIR is focused by a 90° off-axis parabolic mirror with a 101.6 mm effective focal length into a gas sample cell. The UV is loosely focused into the sample by a 1000 mm focal length CaF_2 lens through a hole in the center of the parabolic mirror, in a collinear beam geometry for the UV pump and BBIR probe pulses. The apparatus allows for flexibility in focusing conditions of the UV and BBIR beams, required for minimizing multi-photon excitation processes while not jeopardizing transient IR absorption signal significantly. The gas sample cell contraption contains two CaF_2 windows at the entrance and exit ports for the beams, and the windows are placed far away from the focus in order to minimize time-resolved resonant response of the window material interfering with the resonant signal from the sample. The windows are heated and are continuously purged with flowing nitrogen gas to suppress the deposition of sample and photoproducts. The gas cell itself at the center of the contraption allows for path lengths in the range of 3 mm to 10 mm. Following the interaction region, the UV is blocked by a silicon wafer, and the BBIR is collimated by a second off-axis parabolic mirror, and routed, focused and dispersed onto one stripe of a 2 x 64 element HgCdTe array detector. The spectral resolution for IR detection ranges from 7 nm/pixel to 22 nm/pixel depending on the grating used. In order to correct for shot-to-shot variation in the BBIR intensity, we have implemented a referencing scheme where a small portion of the BBIR is picked off by a ZnSe plate and sent onto the second stripe of the array detector, for pixel-by-pixel noise suppression.

(b) Harmonic frequency calculations of acetylacetone

Acetylacetone (AcAc), with a strong O-H---O=C intramolecular hydrogen bond in its gas phase “enolone” conformation, is one of our first targets for studying non-equilibrium vibrational dynamics. While anharmonic frequency calculation is more accurate for estimating vibrational frequencies particularly involving O-H and C=O stretching modes in this molecule, we performed harmonic frequency calculations of the AcAc molecular vibrations in the ground and excited singlet and triplet electronic states as a first step to obtain preliminary estimates for the frequencies of the vibrational transitions. Electronic structure calculations were performed at the B3LYP/cc-pVDZ level and molecular geometries on S_0 , T_1 , S_1 and S_2 were taken from Ref. 3. Not surprisingly, many vibrational frequencies showed marked changes on all calculated electronic states, with the O-H and C=O stretch-containing normal mode vibrations displaying the most dramatic shifts. The O-H stretching vibrational frequency predicted by these calculations on S_0 is 2838 cm^{-1} , on S_2 is 1673 cm^{-1} , on S_1 is 4090 cm^{-1} , and on T_1 is 4062 cm^{-1} . The normal mode frequencies involving the C=O stretching vibration on S_0 is predicted at 1666 cm^{-1} , 1573 cm^{-1} on S_2 , 1475 cm^{-1} on S_1 , and 1616 cm^{-1} on T_1 . Given the magnitude of shifts to the vibrational frequencies, the broad bandwidth of the BBIR pulses is essential for capturing structural and vibrational dynamics in electronically excited AcAc.

III. Future Work

(a) Transient broadband infrared absorption spectroscopy of electronically excited molecules

AcAc displays a strong UV absorption at 262 nm, where one-photon absorption results in electronic excitation to the S_2 ($\pi\pi^*$) state. Poisson et al. performed ultrafast multiphoton ionization to probe ultrafast dynamics following 266 nm excitation, and the results suggested that the population evolves to the S_1 on timescales 1.4 ps⁵, while more recent soft X-ray transient absorption spectroscopy at the carbon K-edge by Bhattacharjee et al. indicated that the 1.5 ps timescale is due to intersystem crossing to the T_1 state.⁴ Recent work by Sheps, Osborn and co-workers using multiplexed photoionization mass spectrometry, photoelectron photoion coincidence spectroscopy and multi-pass infrared spectroscopy on microsecond to millisecond timescales has revealed many photoproduct channels, involving both one-photon and multiphoton absorption at pump energy fluences far less than those used in previous ultrafast spectroscopy measurements where one-photon excitation was assumed. We aim to perform UV pump-BBIR probe spectroscopy on AcAc using large spot sizes for the pump and probe beams and perhaps using temporally dispersed UV pump to drive down the excitation power density as much as possible to approach the one-photon absorption limit.

Theoretical work on AcAc has indicated that relaxation of electronically excited AcAc from S_2 ($\pi\pi^*$) involves significant changes to the backbone structure as it traverses through conical intersections, accessing lower-lying singlet and triplet states^{6,7}. While the ground state AcAc molecular structure involves a strong hydrogen bond, the predicted molecular geometry in the S_2 state is characterized by an even stronger hydrogen bond with the hydrogen atom almost equidistant from the oxygen and carbon atoms. The molecular structure on S_1 , on the other hand, involves a strained hydrogen bond with the O-H stretching frequency approaching that of a “free” O-H stretch. Probing the evolution of high frequency vibrations in the molecule can effectively constrain possible backbone structures as a function of time. O-H and C=O stretching vibrations are particularly advantageous for probing since their vibrational frequencies are highly sensitive to their local bonding environment and their infrared cross-sections are relatively high. The O-H stretching vibrations on S_0 , S_1 and T_1 are spectrally isolated from the fingerprint region, making it a particularly valuable reporter of structural dynamics. The UV-BBIR apparatus we have built offers sufficient time and frequency resolution, and will allow simultaneous detection of all infrared active vibrations in the mid-IR, making this a potentially powerful source for probing structural and vibrational dynamics.

Over the next year, we will also build a 200 nm pulse generation set-up to enable electronic excitation of a host of small molecules, and will start by coupling this source with BBIR probing to investigate excited state vibrational dynamics of molecules such as acrolein and methyl vinyl ketone. These systems also exhibit complex non-adiabatic dynamics involving delocalized twist/pyramidalization motion of the molecular structure at conical intersections, and have been previously studied using electronic probes such as femtosecond photoelectron spectroscopy.⁸

(b) Ultrafast electron diffraction probing of non-adiabatic dynamics

We will initiate a collaboration with SLAC to study the structural evolution of electronically excited small molecules using ultrafast electron diffraction⁹, which will serve as a useful complement to vibrational spectroscopy. Our first target system for this technique is carbonyl sulfide (OCS), since it has been extensively studied using nanosecond laser spectroscopy, has straightforward photodissociation dynamics when excited in the deep UV involving cleavage of only the C=S bond, and is amenable to laser alignment. Yet, the structural dynamics associated with the bending deformation of the molecule as it rapidly traverses excited electronic states has largely been derived from theoretical studies with no experimental benchmarks to date. Electronic excitation at 220 nm promotes OCS from the ground state to the $2^1A'$ electronic state, where the molecule evolves from a linear to a bent geometry. Theoretical calculations indicate that subsequent dynamics results in the sampling of significantly bent geometries prior to the dissociation of the C=S bond¹⁰, experimentally evidenced by high rotational excitations of the C=O photofragment.¹¹ Using a short 220 nm excitation pulse and mega-electron-volt kinetic energy electron probe pulse, we will follow the evolution of the molecular geometry on a picosecond timescale by measuring the time-dependent

behavior of the pair distribution functions of the O=C and C=S bonds. These studies will further complement the planned ultrafast soft X-ray spectroscopy of OCS, where core-level transitions from the carbon 1s and sulfur 2p orbitals to the valence states will also report on structural dynamics.

IV. References

1. Ramasesha, K., De Marco, L., Mandal, A. & Tokmakoff, A. Water vibrations have strongly mixed intra- and intermolecular character. *Nat. Chem.* **5**, 935–940 (2013).
2. Petersen, P. B. & Tokmakoff, A. Source for ultrafast continuum infrared and terahertz radiation. *Opt. Lett.* **35**, 1962–4 (2010).
3. Chen, X. B., Fang, W. H. & Phillips, D. L. Theoretical studies of the photochemical dynamics of acetylacetone: Isomerization, dissociation, and dehydration reactions. *J. Phys. Chem. A* **110**, 4434–4441 (2006).
4. Bhattacharjee, A., Pemmaraju, C. Das, Schnorr, K. & Attar, A. R. Ultrafast Intersystem Crossing in Acetylacetone via Femtosecond. *J. Am. Chem. Soc.* **139**, 16576–16583 (2017).
5. Poisson, L. *et al.* Ultrafast Dynamics of Acetylacetone (2 , 4-Pentanedione) in the S₂ State. *J. Am. Chem. Soc.* **130**, 2974–2983 (2008).
6. Coe, J. D. & Martínez, T. J. Ab initio molecular dynamics of excited-state intramolecular proton transfer around a three-state conical intersection in malonaldehyde. *J. Phys. Chem. A* **110**, 618–630 (2006).
7. Upadhyaya, H. P., Kumar, A. & Naik, P. D. Photodissociation dynamics of enolic acetylacetone at 266, 248, and 193 nm: Mechanism and nascent state product distribution of OH. *J. Chem. Phys.* **118**, 2590 (2003).
8. Schalk, O. *et al.* Internal Conversion vs . Ultrafast Intersystem Crossing – What Drives the Dynamics of Cyclic α , β - Enones? *J. Phys. Chem. A* **118**, 2279–2287 (2014).
9. Yang, J. *et al.* Imaging CF₃I conical intersection and photodissociation dynamics with ultrafast electron diffraction. *Science* **361**, 64–67 (2018).
10. Suzuki, T., Katayanagi, H., Nanbu, S. & Aoyagi, M. Nonadiabatic bending dissociation in 16 valence electron system OCS. *J. Chem. Phys.* **109**, 5778–5794 (1998).
11. Katayanagi, H. & Suzuki, T. Non-adiabatic bending dissociation of OCS: The effect of bending excitation on the transition probability. *Chem. Phys. Lett.* **360**, 104–110 (2002).

Photoinitiated Reactions of Radicals and Diradicals in Molecular Beams

Hanna Reisler

Department of Chemistry, University of Southern California

Los Angeles, CA 90089-0482

reisler@usc.edu

Program Scope

Open shell species such as radicals, diradicals and molecules in excited electronic states are central to reactive processes in combustion and environmental chemistry. Our program is concerned with photo-initiated reactions of radicals, carbenes, and other open shell species. The goal is to investigate the detailed dissociation dynamics of species in which multiple pathways participate, including molecular rearrangements, and compare them to high-level calculations. Studies include unimolecular reactions on the ground state as well as photodissociation dynamics on excited Rydberg and valence states that involve multiple potential energy surfaces.

Recent Progress

One- and Two-Photon Dissociation of Pyruvic Acid

Pyruvic acid (PA) is an atmospherically important α -keto carboxylic acid, and as such its UV absorption spectrum and decomposition in the gas phase have been studied extensively at wavelengths similar to the solar radiation.¹⁻³ Its longest wavelength absorption system lies at 300-380 nm, accessing the first excited singlet state (S_1) via a $\pi^* \leftarrow n$ transition.⁴ Several photolysis studies of PA at 298 K reported that decarboxylation leading to CO_2 and CH_3CHO final products is the predominant photodissociation pathway. Although a mechanism for the formation of these products has been proposed, the contributions of S_1 , T_1 and highly vibrationally excited levels of S_0 to the photodissociation are still under debate. The photodissociation of PA was also investigated at atmospheric pressure in the presence of O_2 , N_2 and air.^{1,2} These studies identified several stable products and showed that the photodissociation quantum yield depended on the initial concentration of PA and the pressure and nature of the buffer gas. The experiments, however, have been carried out in static gas cells where nascent products were likely to undergo secondary reactions and multiple collisions. Under these conditions, the final products and their yields depended on the concentration of PA, the pressure in the reaction chamber, and the specific experimental arrangement used in each study. Understandably, they do not always agree with one another on the relative abundance of the final products. We carried out the first study of the photodissociation of PA in a molecular beam and measured the $S_1 \leftarrow S_0$ absorption spectrum. In the course of these experiments we discovered an efficient two-photon dissociation process via the S_1 state, and used velocity map imaging (VMI) to characterize the reaction products.

H-photofragment yield spectra of PA at 330-380 nm reveal narrow rovibronic bands that are well separated up to ~ 400 cm^{-1} above the 26,710 cm^{-1} band origin. Progressions in the C-C and CH_3 torsional modes are tentatively assigned. The spectrum is complicated by splittings due to the methyl group, and theoretical calculations are needed to firm the assignments. From the linewidths of the vibronic bands, we conclude that the S_1 state lives longer than a picosecond, a result that is supported by a previous observation of fluorescence following $S_1 \leftarrow S_0$ excitation.³

Electronic structure calculations show that the oscillator strength of the $S_2 \leftarrow S_1$ transition is more than two orders of magnitude larger than that of the $S_1 \leftarrow S_0$ transition, while the $S_3 \leftarrow S_1$ oscillator strength is

much smaller. We conclude that a two-photon transition via S_1 (mainly to S_2) is facile, and in fact hard to suppress in focused laser beam experiments.

Indeed, in our experiments we observed H, HOCO, CH_3CO , CO and CH_3 dissociation products, which exhibit a quadratic dependence on laser fluence. H, CO, and CH_3 fragments were detected by state-selective 2+1 REMPI, and HOCO and CH_3CO , by non-resonant multiphoton ionization. Kinetic energy release (KER) distributions of these fragments were determined, confirming the two-photon nature of the dissociation. The angular distributions of the H and CH_3CO products were anisotropic, indicating that dissociation on the S_2 surface is fast.

The KER distributions of H and CH_3CO fragments displayed in Figure 1 are multimodal, suggesting that more than one dissociation pathway contributes to the observed products. As the S_1 state of PA lives longer than a picosecond and fluoresces, PA is likely to undergo rovibrational motions before dissociating or absorbing another photon. These motions should affect the product angular distributions, which likely reflect mostly the transition dipole moment of the $S_2/S_3 \leftarrow S_1$ transition(s).

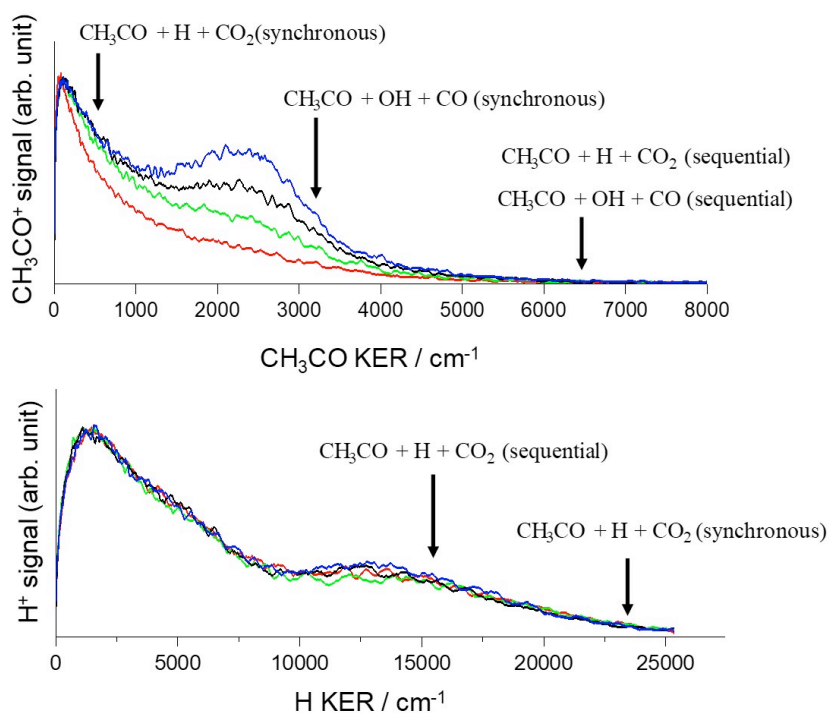


Figure 1. Kinetic energy release (KER) distributions of CH_3CO (top) and H (bottom) fragments at several excitation energies. In the top figure the red, green, black and blue curves depict progressively increasing excitation energy. The arrows point to the fragments' maximum energy release (KE_{max}) allowed for the indicated three-body fragmentation reactions assuming that the fragments have no internal energy. KER values lower than KE_{max} indicate that the products possess internal energy.

Our theoretical calculations show that the direction of the transition dipole moment for the $S_2 \leftarrow S_1$ transition is parallel with respect to the molecular plane whereas it is perpendicular for $S_3 \leftarrow S_1$. The high KER component of the CH_3CO distribution shown in Figure 1 has a positive recoil anisotropy parameter ($\beta = 1.4-1.5$), which is consistent with fast dissociation on the S_2 surface. The low KER component has lower anisotropy ($\beta = 0.2-0.5$), and some of it may derive from dissociation of vibrationally excited PA in the S_1 or T_1 states reached via nonradiative transitions from S_2 .⁵ This scenario is also consistent with the observation that the fraction of the high KER component increases with increasing excitation energy; at higher excitation energies, direct dissociation on S_2 can compete effectively with couplings to lower electronic states.

Interpretation of the angular distribution of the H fragment, which shows an overall negative anisotropy ($\beta = -0.2 - -0.6$) is more complicated because several two- and three-body fragmentation processes can contribute to it. For example, the angular distributions of H fragments produced via O-H bond fission ($\text{CH}_3\text{COCOOH} \rightarrow \text{CH}_3\text{COCOO} + \text{H}$) and the synchronous three-body fragmentation reaction $\text{CH}_3\text{COCOOH} \rightarrow \text{CH}_3\text{CO} + \text{H} + \text{CO}_2$ will depend on the angle between the transition dipole moment vector and the H-fragment recoil direction. On the other hand, the secondary dissociation of rovibrationally excited HOCO to $\text{H} + \text{CO}_2$ is likely to lead to H products with an isotropic angular distribution and a broad range of kinetic energies. We also cannot rule out that some dissociation via the S_3 state (a perpendicular transition) contributes to the observed value of β .

Following the treatment of Maul and Gericke,⁶ we analyzed the feasibility of the energetically allowed two- and three-body fragmentation processes, and found out that both are feasible routes to the observed products. While we cannot determine branching ratios, we have gained insights into the dissociation mechanism by estimating the maximum allowed kinetic energy release, KE_{max} , for the synchronous and sequential three-body fragmentation pathways leading to each product. These values are compared to the computed KE_{max} values for two-body fragmentation processes and the observed KER distributions of the fragments. The analyses show that several three-body fragmentation processes, both synchronous and sequential, contribute significantly to the observed products. Some of the computed KE_{max} values are indicated by arrows in Figure 1.

We also conclude that most of the CH_3CO and HOCO fragments are generated with significant internal energies and many of them further dissociate. For example, CO fragments with high KER are observed when the internal energy of the CH_3CO cofragment is above its barrier to dissociation, supporting a sequential dissociation mechanism. On the other hand, we find that synchronous three-body fragmentation of PA is likely to contribute to the low KER component of the CH_3CO distribution (see Figure 1).

Taking into account the available energy for each dissociation reaction, the KE_{max} values for each fragment generated in these reactions, and the observed fragments' KER and angular distributions, we reach the conclusion that three-body fragmentation processes, synchronous and sequential, are major contributors to the CH_3O , HCOH, CH_3 , H, and CO products generated by two-photon dissociation. Considering the two-photon energy of $\sim 54,000 \text{ cm}^{-1}$ and the high available energy for each dissociation pathway, it is not surprising that both two- and three-body fragmentation pathways are feasible. It took us a long time to figure out the dissociation mechanism, but all the results are self-consistent and support the proposed pathways. This work has been submitted for publication.

In spite of many attempts, we were unable to detect the proposed nascent CO_2 and methylhydroxycarbene (CH_3COH) dissociation products of the one-photon dissociation of PA on S_1 ,³ probably due to a combination of insufficient sensitivity of the employed REMPI detection schemes and the fairly long lifetime of the S_1 state. To investigate further the nascent one-photon dissociation products, we are collaborating with Dr. David Osborn of the Sandia Combustion Research Facility to carry out experiments at the ALS with their mass spectrometer system by employing tunable VUV ionization. These experiments are performed at 298 K, 4 torr total pressure (He), and 0.01 torr partial pressure of PA. The laser fluence is more than two orders of magnitude smaller than the one used in the molecular beam experiments. Using tunable VUV from the ALS, we are able to observe the depletion of PA, and detect CO_2 as a reaction product. We have also detected the more stable isomers of CH_3COH , namely, acetaldehyde and syn- and anti-vinyl alcohol. Our most recent results suggest the formation of a short-lived methylhydroxycarbene, which quickly isomerizes. In addition, we have detected, even at these low pressures, products

of bimolecular reactions. Surprisingly, one of these products has mass 88, the same as PA ($C_3H_4O_3$), but much lower ionization energy. High-resolution mass spectroscopy shows that the molecular formula of this product is, in fact, $C_4H_8O_2$. Experiments to characterize the reaction(s) leading up to this product are planned.

Future work

The work on the photodissociation of pyruvic acid will continue, and in the next year we will focus on publishing the large body of work that we have acquired. We have carried out similar experiments on glyoxylic acid, and this work will be published as well. Being smaller than pyruvic acid, we hope that theoretical work will help us assign the spectrum and describe the two-photon dissociation mechanism. We are especially excited about the collaboration with David Osborn on pyruvic acid, and these studies will be extended to one-photon dissociation at 193 nm. Pyruvic acid is known to slowly react with water, and we plan to study this reaction. We will also examine dimers and larger clusters of pyruvic acid with water by using VMI to detect the water moiety. We will determine bimolecular reaction rates of short-lived species and detect reaction products by using tunable VUV at the ALS. Studies of the production and photochemistry of hydroxycarbenes will continue as well.

References

1. Reed Harris, A.E.; Doussin, J.-F.; Carpenter, B.K.; Vaida, V., *J. Phys. Chem. A* **2016**, *120*, 10123–10133.
2. Reed Harris, A. E.; Cazaunau, M.; Gratien, A.; Pangui, E.; Doussin, J.-F.; Vaida, V. *J. Phys. Chem. A* **2017**, *121* (44), 8348–8358.
3. Yamamoto, S.; Back, R.. *Can. J. Chem.* **1985**, *63* (2), 549–554.
4. H Horowitz, A.; Meller, R.; Moortgat, G. K. *J. Photochem. Photobiol. A: Chemistry* **2001**, *146*, 19–27.
5. Chang, X.-P.; Fang, Q.; Cui, G. *J. Chem. Phys.* **2014**, *141* (15), 15431
6. Maul, C.; Gericke, K.-H. *Int. Rev. Phys. Chem.* **1997**, *16* (1), 1–79.

Publications 2016-2018

1. S. Sutradhar, B.R. Samanta, A.K. Samanta, and H. Reisler, “Temperature dependence of the photodissociation of CO_2 from high vibrational levels: 205-230 nm imaging studies of $CO(X^1\Sigma^+)$ and $O(^3P, ^1D)$ products”, *J. Chem. Phys.* **147**, 013916 (2017).
2. B.R. Samanta, S. Sutradhar, R. Fernando, A.I. Krylov, A. I. and Reisler, “Electronic structure and Rydberg-core interactions in hydroxycarbene and methylhydroxycarbene”, *J. Phys. Chem. A* **122**, 6176-6182 (2018).

Active Thermochemical Tables

Branko Ruscic
Chemical Sciences and Engineering Division, Argonne National Laboratory,
9700 South Cass Avenue, Lemont, IL 60439
ruscic@anl.gov

Program Scope

The *spiritus movens* of this program is the need to provide the scientific community with accurate and reliable thermochemical information on chemical species that are relevant in energy-generating chemical processes or play prominent roles in subsequent environmental chemistry. Detailed knowledge of thermodynamic parameters for a broad array of stable and ephemeral chemical species is pivotal to chemistry and essential in many industries. In particular, the availability of accurate, reliable, and internally consistent thermochemical values is a *conditio sine qua non* in kinetics, reaction dynamics, formulation of plausible reaction mechanisms, and construction of predictive models of complex chemical environments. In addition, the availability of accurate thermochemical values has historically been the prime driver for steady advancements of increasingly sophisticated electronic structure theories.

The focus of this program is on bringing substantial innovations to the thermochemical field through development of new methodologies, and utilizing them to systematically improve both the quality and quantity of available thermochemical data relevant to energy-producing processes. In order to achieve the stated goals, this program has developed a novel approach that is centered on analyzing and optimally utilizing the information content of *all available* thermochemically relevant determinations. The aim is not only to dynamically produce the best currently possible thermochemical parameters for the targeted chemical species, but also to allow efficient updates with new knowledge, properly propagating its consequences through all affected chemical species, as well as to provide critical tests of new experimental or theoretical data, and generate pointers to new determinations that are most likely to efficiently improve the overall thermochemical knowledge base. In order to provide a broad perspective of this area of science, the effort of this program is synergistically coordinated with related experimental and theoretical efforts within the Chemical Dynamics Group at Argonne.

Recent Progress

Over the past year we have continued the development of Active Thermochemical Tables (ATcT). Briefly, ATcT are a new paradigm for developing accurate and reliable thermochemical values for stable and reactive chemical species. Thermochemical determinations (reaction enthalpies, equilibrium constants, bond dissociation energies, etc.) by definition involve several chemical species, and thus define the enthalpy of formation of the target chemical species *relative* to other species. Consequently, enthalpies of formation generally do not correspond to directly measured quantities; rather, they are indirectly defined via complex manifolds of thermochemical dependencies. Historically, extracting the enthalpies of formation from intertwined (and frequently inconsistent) dependencies was an intractable proposition, resulting in a simplified *sequential* approach of inferring the enthalpies of formation one at the time (A begets B, B begets C, etc.), delivering static sets of values that contain hidden progenitor-progeny relationships and cannot be updated with new knowledge without introducing inconsistencies. The success of ATcT is rooted in treating the intertwined determinations as a network of simultaneous dependences that is amenable to mathematical and statistical manipulation, converting the originally intractable problem to an information-rich environment that produces a quantum leap in the quality and reliability of the resulting thermochemistry. The Thermochemical Network (TN) corresponds to a system of qualified constraints that must be simultaneously satisfied in order to produce enthalpies of formation that correctly reflect the epistemic content of the TN. Because of the unavoidable presence of determinations with ‘optimistic’ uncertainties (a.k.a. erroneous determinations), ATcT first performs an iterative statistical analysis, which isolates them and brings the TN to self-consistency. Once self-consistency is achieved, ATcT proceeds to solve the TN simultaneously for all included species.

Probably the most important vehicle for dissemination of ATcT results is the ATcT website, ATcT.anl.gov, which keeps growing in popularity as a reliable source of enthalpies of formation for key species relevant in combustion and atmospheric chemistry, as well as in other areas of chemistry. The website has been lately attracting upwards of 25,000 monthly visitors.

The most recent public version of ATcT results, ATcT TN ver. 1.122d, which was released in September 2018, covers 1414 chemical species. This version has been obtained by expansion of the predecessor ver. 1.122b (1199 species), which was partially motivated by the needs of a broad collaborative study [Cheng et al., *J. Chem. Theory Comput.* **13**, 1044 (2017)] that combined experiment and theory and produced benchmark scalar-relativistic coupled-cluster calculations for dissociation energies of 20 diatomic molecules containing 3d transition metals, but required reference benchmark thermochemical values for heterolytic C-H bond dissociation energies in mono-, di-, and trimethylamine.

We are currently preparing for web release the successor version, ATcT TN ver. 1.122e, which covers > 1600 species; the targeted web release date is June 2019. This version is an expansion of ver. 1.122d, largely driven by the needs of a collaborative study involving members of the ATcT Task Force One (J. F. Stanton and his group at UF, T. L. Nguyen at UF, G. B. Ellison and his group at UC Boulder, B. Changala at JILA, J. Baraban at Ben-Gurion), related to combined experimental and theoretical activities involving the thermal decomposition of methyl acetate and methyl butanoate, which are representative of the chemistry of ester biofuels [Porterfield et al. *J. Chem. Phys. A* **121**, 4658 (2017)].

The coverage of the current developmental version of the ATcT TN, 1.122r, has recently reached 2000 species, intertwined by >25,000 active determinations (as well as several thousand additional determinations that have been rendered inactive during various analyses and TN improvements).

In parallel to the mentioned expansions of coverage of ATcT, another important activity during the last year relates to improving the thermophysical properties (i.e. properties derivable directly from the partition function) of the species included in the ATcT TN. Namely, when ATcT were in their infancy, the original plan was to focus on the TN and the resulting enthalpies of formation, while simply adopting the required auxiliary thermophysical properties from the best available external sources. However, it quickly became clear that relying on external sources is a rather limiting strategy, since for most species of interest there are either no tabulated thermophysical properties, or they are based on the RRHO model. While the ubiquitous RRHO model is in many cases acceptable for approximate conversions of thermochemical properties between 0 and 298.15 K, it is demonstrably inadequate for extending these properties to temperatures relevant in combustion. In principle, the best thermophysical properties would be obtained by direct count, but this is limited to just a handful of species, given that for proper convergence this would require a complete set of rovibronic levels up to at least 30,000 - 35,000 cm^{-1} for combustion-related applications, and up to 40,000 cm^{-1} and even higher if explosions are to be also considered. Short of having the luxury of being able to perform a direct count, the next best approach is the implementation of a two-pronged strategy, as currently implemented in ATcT. In this strategy, the potential energy surface involving large-amplitude motions is projected out and solved to obtain the relevant energy levels, allowing the estimation of the related contribution by direct count. For the other, more rigid modes, the strategy employs computing non-rigid rotor anharmonic oscillator (NRRAO) corrections to the RRHO thermophysical properties, which account for the effects of vibrational anharmonicity, vibration-rotation interaction, centrifugal stretching, resonances, as well as low-temperature effects. The strategy has been regularly used in ATcT for rigid chemical species and for floppy species in which the large-amplitude motion(s) were deemed to be reasonably separable. We have very recently successfully tested this strategy on a more challenging case, CH_2OH , in collaboration with D. H. Bross and L. B. Harding (ANL) and H.-G. Yu (BNL). In CH_2OH , the CH_2 wag and the OH torsion are tightly coupled and thus inseparable. In fact, the historical value of $\Delta_f H^\circ_{298}(\text{CH}_2\text{OH})$ that could be extracted from experiments (and computations) depended critically on how correctly these two modes were treated (free torsion vs. pseudo-vibration vs. hindered torsion vs. coupled wag-torsion manifold).

Another activity worth mentioning here is related to the discovery in the ATcT TN of cases where ostensibly accurate experimental determinations (involving, e.g., combustion calorimetry of the

condensed phase, and a determination of the vaporization enthalpy from vapor pressure measurements) imply a gas-phase enthalpy of formation that differs significantly from prevailing theoretical value(s). In general, if the TN contains inconsistent thermochemical pathways, ATcT tries to arbitrate between them based on statistical plausibility. However, if the associated TN is underdeveloped (i.e. sparse), then the pathway that claims to be nominally more accurate (though not necessarily actually more accurate) may end up prevailing, since there is insufficient data that would challenge its veracity. Evidently, such cases require additional scrutiny in order to home onto the correct values. One such recent case was the enthalpy of formation of oxalic acid, where two combustion calorimetries were contradicting each other, with the older (but nominally more accurate) determination prevailing. Extended ATcT analyses (using the ATcT capability to test hypotheses) ruled in favor of mid-level theory and the nominally less-accurate of the two calorimetries, and this conclusion was further confirmed by state-of-the-art high-level theory.

We have a broad range of ongoing collaborations, both outside (nationally and internationally) and inside the Gas-Phase Chemical Dynamics Group at ANL. While these are reflected in the list of publications given at the end of the current abstract, but otherwise not discussed in detail, we would like to explicitly mention here one collaboration with P. Glarborg (DTU), J. A. Miller and S. J. Klippenstein (ANL), in which ATcT has provided consistent thermochemistry for a comprehensive systematization of the current state of modeling nitrogen chemistry in combustion, which summarizes decades of dedicated research in the area of formation and destruction of NO_x, and draws on recent advances in the knowledge of thermochemistry and theoretical reaction rates. This study, published in 2018, examined different mechanisms for formation and consumption of NO_x, evaluated key reaction steps, and validated the predictive capabilities of various subsets of the model against experimental data.

Future Plans

Future plans of this program pivot around further development and expansion of the Active Thermochemical Tables approach, continuing to provide accurate thermochemistry to the scientific community, and driving targeted thermochemically-relevant theoretical and experimental investigations of radicals and transient species that are intimately related to combustion and post-combustion atmospheric processes. A significant part of the effort will be focused on continued ‘finalization’ and dissemination of the resulting ATcT thermochemistry, typically involving groups of related chemical species. One important component of this process, focused on their enthalpies of formation, consists of testing and analyzing the TN dependencies, using tools such as the variance/covariance decomposition approach and analyses of the influence of relevant determinations via the hat-matrix, followed by improving the connectivity within the TN and adding new high-quality results (either virtual, i.e. computational, or actual, i.e. experimental) to coerce the resulting thermochemistry toward stable, ‘release quality’ values. This iterative process unavoidably results in an expansion of the TN with new related chemical species, which is an added benefit. Another equally important component focuses on enhancing the accuracy of the partition functions, typically by upgrading RRHO partition functions to NRRAO partition functions, which is a currently ongoing effort. Future plans invariably incorporate a continuation of the current effort of expanding our web site (ATcT.anl.gov) that displays the ATcT thermochemistry together with ever increasing amounts of pertinent metadata. Pertinent metadata that we will continue generating aims to adequately document the provenance of each thermochemical value, entailing a variance decomposition analysis for each of the chemical species. Finally, another long-term component of future progress consists of enhancing the underlying ATcT software, making it more efficient as well as user-friendly.

This work is supported by the U.S. Department of Energy, Office of Basic Energy Sciences, Division of Chemical Sciences, Geosciences, and Biosciences, under Contract No. DE-AC02-06CH11357.

Publications resulting from DOE sponsored research (2016 – present)

- *Active Thermochemical Tables: The Partition Function of Hydroxymethyl (CH₂OH) Revisited*, D. H. Bross, H.-G. Yu, L. B. Harding, and B. Ruscic, *J. Phys. Chem. A* **123**, in press (2019); DOI: 10.1021/acs.jpca.9b02295 (*Hanna Reisler Festschrift*)

- *Enthalpy of Formation of C₂H₂O₄ (Oxalic Acid) from High-Level Calculations and the Active Thermochemical Tables Approach*, D. Feller, D. H. Bross, and B. Ruscic, *J. Phys. Chem. A* **123**, in press (2019); DOI: 10.1021/acs.jpca.8b12329
- *Thermochemistry*, B. Ruscic and D. H. Bross, Ch. 1 in: *Mathematical Modeling of Complex Reaction Systems: Pyrolysis and Combustion*, T. Faravelli, F. Manenti, and E. M. Ranzi, Eds., *Computer Aided Chemical Engineering Series* Vol. **45**, Elsevier: New York 2019 (in press); DOI: 10.1016/B978-0-444-64087-1.00001-2
- *A Master Equation Simulation for the •OH + CH₃OH Reaction*, T. L. Nguyen, B. Ruscic, and J. F. Stanton, *J. Chem. Phys.* **150**, 084105/1-8 (2019); DOI: 10.1063/1.5081827
- *Toward Accurate High Temperature Anharmonic Partition Functions*, D. H. Bross, A. W. Jasper, B. Ruscic, and A. F. Wagner, *Proc. Combust. Inst.* **37**, 315-322 (2019); DOI: 10.1016/j.proci.2018.05.028
- *Unimolecular Reaction of Methyl Isocyanide to Acetonitrile: A High-Level Theoretical Study*, T. L. Nguyen, J. H. Thorpe, D. H. Bross, B. Ruscic, and J. F. Stanton, *J. Phys. Chem. Lett.* **9**, 2532-2538 (2018); DOI: 10.1021/acs.jpcllett.8b01259
- *Active Thermochemical Tables (ATcT) Enthalpies of Formation Based on version 1.122d of the Thermochemical Network*, B. Ruscic and D. H. Bross, Argonne National Laboratory, Argonne, Ill. (2018); <https://atct.anl.gov/Thermochemical%20Data/version%201.122b/>
- *Modeling Nitrogen Chemistry in Combustion*, P. Glarborg, J. A. Miller, B. Ruscic, and S. J. Klippenstein, *Progress Energy Combust. Sci.* **67**, 31-68 (2018); DOI: 10.1016/j.peccs.2018.01.002
- *Time-Resolved Kinetic Chirped-Pulse Rotational Spectroscopy in a Room-Temperature Flow Reactor*, D. P. Zaleski, L. B. Harding, S. J. Klippenstein, B. Ruscic, and K. Prozument, *J. Phys. Chem. Lett.* **8**, 6180-6188 (2017); DOI: 10.1021/acs.jpcllett.7b02864
- *Post-Transition State Dynamics and Product Energy Partitioning Following Thermal Excitation of the F··HCH₂CN Transition State: Disagreement with Experiment*, S. Pratihari, X. Ma, J. Xie, R. Scott, E. Gao, B. Ruscic, A. J. A. Aquino, D. W. Setser, and W. L. Hase, *J. Chem. Phys.* **147**, 144301/1-15 (2017); DOI: 10.1063/1.4985894
- *Active Thermochemical Tables: The Adiabatic Ionization Energy of Hydrogen Peroxide*, P. B. Changala, T. L. Nguyen, J. H. Baraban, G. B. Ellison, J. F. Stanton, D. H. Bross, and B. Ruscic, *J. Phys. Chem. A* **121**, 8799-8806 (2017); DOI: 10.1021/acs.jpca.7b06221 (highlighted on the journal cover, see <https://pubs.acs.org/toc/jpcafh/121/46#>)
- *Ab Initio Computations and Active Thermochemical Tables Hand in Hand: Heats of Formation of Core Combustion Species*, S. J. Klippenstein, L. B. Harding, and B. Ruscic, *J. Phys. Chem. A* **121**, 6580-6602 (2017); DOI: 10.1021/acs.jpca.7b05945
- *Enthalpy of Formation of N₂H₄ (Hydrazine) Revisited*. D. Feller, D. H. Bross, and B. Ruscic, *J. Phys. Chem. A* **121**, 6187-6198 (2017); DOI: 10.1021/acs.jpca.7b06017
- *Thermal Decomposition of Potential Ester Biofuels, Part I: Methyl Acetate and Methyl Butanoate*, J. P. Porterfield, D. H. Bross, B. Ruscic, J. H. Thorpe, T. L. Nguyen, J. H. Baraban, J. F. Stanton, J. W. Daily, and G. B. Ellison, *J. Chem. Phys. A* **121**, 4658-4677 (2017); DOI: 10.1021/acs.jpca.7b02639 (Veronica Vaida Festschrift)
- *An Experimental and Theoretical Study of the Thermal Decomposition of C₄H₆ Isomers*, J. P. A. Lockhart, C. F. Goldsmith, J. B. Randazzo, B. Ruscic, and R. S. Tranter, *J. Phys. Chem. A* **121**, 3827-3850 (2017); DOI: 10.1021/acs.jpca.7b01186
- *A Vacuum Ultraviolet laser Pulsed Field Ionization-Photoion Study of Methane (CH₄): Determination of the Appearance Energy of Methylum From Methane with Unprecedented Precision and the Resulting Impact on the Bond Dissociation Energies of CH₄ and CH₄⁺*, Y.-C. Chang, B. Xiong, D. H. Bross, B. Ruscic, and C. Y. Ng, *Phys. Chem. Chem. Phys.* **19**, 9592-9605 (2017); DOI: 10.1039/c6cp08200a (part of 2017 PCCP Hot Articles collection)
- *Bond Dissociation Energies for Diatomic Molecules Containing 3d Transition Metals: Benchmark Scalar-Relativistic Coupled-Cluster Calculations for Twenty Molecules*, L. Cheng, J. Gauss, B. Ruscic, P. Armentrout, and J. Stanton, *J. Chem. Theory Comput.* **13**, 1044-1056 (2017); DOI: 10.1021/acs.jctc.6b00970
- *Active Thermochemical Tables (ATcT) Enthalpies of Formation Based on version 1.122b of the Thermochemical Network*, B. Ruscic and D. H. Bross, Argonne National Laboratory, Argonne, Ill. (2017); <https://atct.anl.gov/Thermochemical%20Data/version%201.122b/>
- *Active Thermochemical Tables (ATcT) Enthalpies of Formation Based on version 1.122 of the Thermochemical Network*, B. Ruscic and D. H. Bross, Argonne National Laboratory, Argonne, Ill. (2016), (including provenances, correlated species, and most influential determinations) <http://atct.anl.gov/Thermochemical%20Data/version%201.122/>
- *Extension of Active Thermochemical Tables (ATcT) Values ver. 1.118 with Provenances of the Enthalpies of Formation Based on Variance Decomposition Analysis and References*, B. Ruscic and D. H. Bross, Argonne National Laboratory, Argonne, Ill. (2016), <https://atct.anl.gov/Thermochemical%20Data/version%201.118/index.php>
- *Active Thermochemical Tables (ATcT) Enthalpies of Formation Based on version 1.118 of the Thermochemical Network (with a New Search Functionality Based on the ATcT Species Dictionary)*, B. Ruscic, Argonne National Laboratory, Argonne, Ill. (2016), <https://atct.anl.gov/Thermochemical%20Data/version%201.118/>

SPECTROSCOPIC INVESTIGATIONS OF MOLECULAR SYMMETRY BREAKDOWN

Trevor J. Sears

Department of Chemistry, Stony Brook University, Stony Brook, NY 11794-3400

trevor.sears@stonybrook.edu

Program Scope

This project aims to make precise measurements of the spectra of small molecules to address fundamental questions in chemical physics in the realm of nuclear spin symmetries and their breakdown in molecules, and parity non-conservation caused by the weak nuclear force. Nuclear spin symmetry is intimately connected to parity in symmetrical molecules and plays a central role in the physical and chemical properties of symmetric molecules, their collisional relaxation, and the establishment of thermodynamic equilibrium in an ensemble. Such effects are present in every molecular system or process, but their small size means they are often only directly observable under special conditions. However, their measurement is of fundamental, and often practical importance, and strongly relates to the themes of coherence in light and matter in the recent Basic Energy Sciences Advisory Committee (BESAC) report “Challenges at the Frontiers of Matter and Energy: Transformative Opportunities for Discovery Science”.

I. Recent Progress

A. Sub-Doppler Frequency Measurements and Pressure Effects

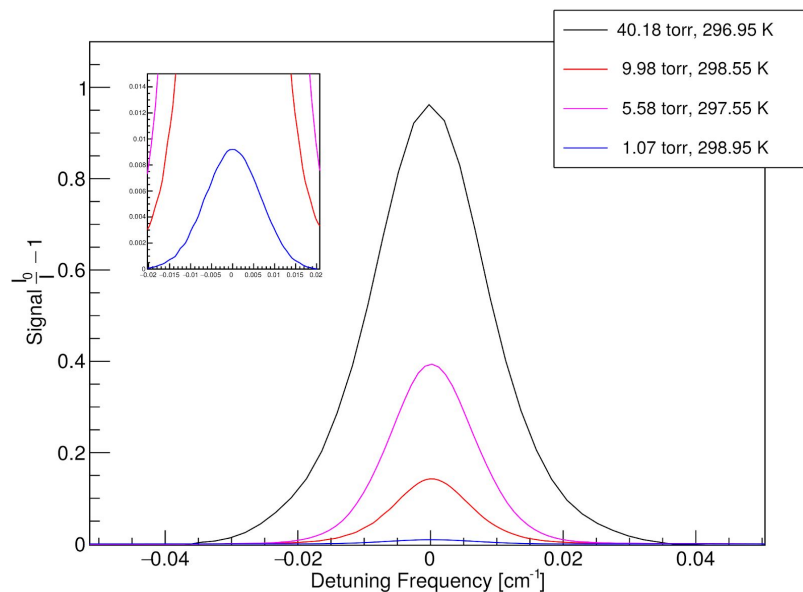
We have measured Doppler-free laser saturation dip absorption lines in the $\nu_1+\nu_3$ band of acetylene near 1.5 μm . The accuracy and precision of the measurements is typically better than 10 kHz. Measurements of the observed self-pressure-broadening coefficients for the sub-Doppler resonances showed that they are some 3.5 times larger than those derived from conventional pressure broadening of unsaturated Doppler broadened spectra. This is attributed to the contribution of velocity-changing collisions to the total dephasing rate in the low pressure sub-Doppler measurements. At higher pressures, when the homogeneous broadening becomes comparable to the typical Doppler shift per elastic collision, the velocity-changing collisions cease to contribute significantly to the incremental pressure broadening. We developed a time-dependent soft collision model to illustrate the transition between the low and high pressure regimes of sub-Doppler pressure broadening and this work was recently published.¹

B. Precision Line Shape Measurements

A recent report claimed [Iwakuni et al. *Phys. Rev. Letts.* **117**, 143902 (2016)] to have measured a large (10%) alternation in the magnitudes of self-pressure broadening coefficients between the ortho- and para- nuclear spin states (odd and even J values) of ground state acetylene. Outside of hydrogen, This would be the first clear confirmation of an effect originally considered by Anderson in 1949. Resonant rotational energy transfer between a pair of molecules separated by $\Delta J = \pm 2$ can have a significantly larger cross section than other inelastic interactions, and these can only occur in para-para or ortho-ortho collisions. Since the population statistics favor the ortho-spin states, the total pressure broadening can be larger for ortho- states. The reported effect was, however, large enough to make it surprising that it has apparently never previously been observed, but it may have been only just at the noise level of modern Fourier transform spectroscopy (FTS) studies. The original report was quickly followed by papers disputing the results on the basis of semi-empirical modeling [Lehmann, *J. Chem. Phys.* **146**, 094309 (2017)] and the approximate line shape model used in the analysis [Hartman and Tran, *Phys. Rev. Letts.* **119**, 069401 (2017)]. We are in the process of making new measurements of the disputed data using the comb-based spectrometer at Stony Brook. This instrument was previously used to make the most accurate

and precise measurements currently available on this band, but only ortho-transitions were recorded at that time.

Preliminary data has been recorded, but the frequency comb laser is presently under repair, so the new data does not have the ultimate precision and accuracy we would have liked. However, the data should easily be able to distinguish ortho-para differences of the magnitude apparent in the Iwakuni et al. report.



The figure shows some data for the R(8), a para- level, in the band in question. The pressure broadening is very obvious and a small pressure-dependent shift to negative frequency is just about discernable in this figure. The inset shows a magnification of the lowest pressure data trace. These data were recorded at temperatures near ambient, *i.e.* 296 K, and signal-to-noise ratios are considerably better than in the original Iwakuni et al. work. We are currently analysing the data by comparing results obtained using a

Voigt line profile model, as used in the earlier analysis, and a more accurate speed-dependent Voigt profile to address the issues raised in the Hartmann and Tran comment on the original work.

II. Future Work

A. Analysis of C₂H₂ Broadening Data

As described above, we have recorded precise line profile data for the transitions R(8) through R(16) in the $\nu_1 + \nu_3$ band of acetylene. These transitions showed the strongest ortho-para broadening differences in Iwakuni et al.'s original measurements. The data analysis is ongoing and requires careful comparison of the broadening coefficient obtained using the approximate (Voigt) and more accurate (speed-dependent Voigt) model line shape profiles. We expect to have a definitive result by the summer.

B. Nuclear Rotation-Vibration Splittings in CH₄

Despite decades of extensive studies, spectroscopic analysis of methane in the near-infrared region remains unsatisfactory due to the complexity of the molecular energy levels and the lack of full insight from the existing high resolution measurements. This issue is of great interest because of the quality and breadth of laboratory data required for accurate retrievals of methane in the Earth's atmosphere and interpretation of measurements of the atmosphere of the gas giants' planets, in particular Saturn's satellite, Titan.

In the 1.65 μm region, methane has a dense vibrational structure and the rotational levels of a spherical top contain multiple, nearly degenerate, sublevels of different symmetry. At the relevant upper state energies, precise calculation of the level splittings is not presently possible and many of the observed lines in the highest resolution Doppler-broadened laboratory spectra contain multiple unresolved nuclear spin-rotational components or even remain unassigned.

Assigned (rotational quantum number, J) rotational lines in the stronger sub-bands show partially resolved splittings at high rotational quantum number, due to nearly degenerate rotational levels of the same J , but different symmetry in the methane T_d symmetry group. Recent temperature-dependent spectroscopic measurements have resulted in the empirical assignment of the lower state energy levels of the stronger features but, even for these, the presence of multiple, unresolved and poorly known, contributions to the Doppler (and pressure) broadened profiles makes accurate modeling impossible. Quantum mechanical models of the rotation-vibration levels could be used to compute the level splittings, but they are still not sufficiently accurate to be of use for precise spectroscopic measurements. The splittings are not resolved in high resolution Doppler-limited spectra except at high- J and, again, models are insufficiently accurate to extrapolate to the lower J -values of interest. In addition, weaker, unresolved but accidentally overlapping lines, may be present, but given our current knowledge, we cannot be sure. Some sub-Doppler measurements of splittings have been reported by the Sasada group in Japan, but these are fragmentary and do not provide the desired absolute frequencies.

We propose to frequency measure these splittings for the low- J transitions in the strong Q-branches of the $1.65\ \mu\text{m}$ $\text{CH}_4\ 2\nu_3$ band using the comb-referenced sub-Doppler saturation dip technique we demonstrated in our recent work on NH_3 . [Twagirayezu et al. *J. Chem. Phys.* **145**, 144302 (2016)] The proposed work will provide accurate rest frequencies for features hidden under the Doppler profile in conventional spectra needed for accurate line shape models. It also lays the groundwork for higher resolution spectroscopic and dynamical measurements because the frequencies provide the information needed for experiments to produce and investigate non-equilibrium spin-state distributions. The targeted transitions in CH_4 have line strengths comparable to those for which extensive sub-Doppler measurements have been made in NH_3 , so that the existing spectrometer can be used with minimal upgrades. Future improvements to the spectrometer such as installing higher quality cavity mirrors to permit more sensitive detection, will be carried out in parallel with these proposed measurements.

III. Publications related to this project since 2018

- ¹. Frequency measurements and self-broadening of sub-Doppler transitions in the $\nu_1 + \nu_3$ band of acetylene, S. Twagirayezu, G. E. Hall and T. J. Sears, *J. Chem. Phys.*, **149**, 154308 (2018).

Theoretical Studies of Potential Energy Surfaces and Computational Methods

Ron Shepard

Chemical Sciences and Engineering Division,
Argonne National Laboratory, Lemont, IL 60439
[email: shepard@tcg.anl.gov]

Program Scope: This project involves the development, implementation, and application of theoretical methods for the calculation and characterization of potential energy surfaces (PES) involving molecular species that occur in combustion, atmospheric, and general gas-phase chemistry. An accurate and balanced treatment of reactants, intermediates, and products for both ground and excited electronic states is required. This difficult challenge is met with general multiconfiguration self-consistent field (MCSCF) and multireference configuration interaction (MRCI) methods [see *Chem. Rev.* **112**, 108 (2012)]. More recently, the *graphically contracted function* (GCF) method has been developed to address some of the practical limitations of the traditional MCSCF and MRCI approaches, including the number of active electrons that may be accommodated and the overall expense associated with the study of larger molecular systems [see *J. Chem. Phys.* **141**, 064105 (2014) and references therein]. These methods are developed and maintained within the COLUMBUS Program System [*WIREs Comput. Mol. Sci.* **1**, 191 (2011)].

Recent Progress: GCF METHOD: In the GCF method the wave function is written as a linear combination of GCFs, and each GCF in turn is formally equivalent to a linear combination of configuration state functions (CSFs) that comprise an underlying linear expansion space of dimension N_{CSF} . The CSF coefficients that define the GCFs are nonlinear functions of a smaller number of essential variables $N_{\phi} \ll N_{\text{CSF}}$, and the formulation results in computational effort that depends only on the nonlinear parameters, not on the potentially much larger linear dimension. The method scales much better with orbital basis function dimension and with the number of electrons than traditional high-level electronic structure methods. This nonlinear formulation has allowed, for example, expansions of $N_{\text{CSF}} > 10^{200}$ to be considered in the context of spin-density computation. The method is formulated in terms of spin eigenfunctions using the Graphical Unitary Group Approach (GUGA) of Shavitt, and consequently it does not suffer from spin contamination or spin instability; these are critical features in the study of radicals and excited states that occur in hydrocarbon combustion and atmospheric chemistry. GCF expansions with facet counts in the range $f_{\text{MAX}} \approx 4$ to 10 have been shown to approach the full-CI PES to within chemical accuracy of $\sim mE_h$ and to within $\sim \mu E_h$ error with $f_{\text{MAX}} \approx 50$. In the most recent formulations, called the multifacet generalization, an individual MFGCF is a matrix product state (MPS), and the wave function is a linear combination of these MPSs. No intrinsic restrictions are imposed on the orbital occupations, and in particular there are no artificial excitation-level or occupation restrictions with respect to a reference function or reference space; in this sense, the method is more correctly characterized as a multiconfigurational method rather than a multireference method. Because the wave function is a linear combination of GCF basis functions rather than a

This work was performed under the auspices of the Office of Basic Energy Sciences, Division of Chemical Sciences, Geosciences, and Biosciences, U.S. Department of Energy, under contract number DE-AC02-06CH11357.

single expansion term, this allows the method to be used for both ground and excited electronic states, the increased wave function flexibility leads to higher accuracy, and this expansion form facilitates the computation of transition moments, nonadiabatic coupling, and other properties that at present can only be computed reliably with multireference and multiconfigurational approaches. Our ongoing effort is focused on allowing different arc factors for facets with different irreducible representation labels. This generalization increases the wave function flexibility, and thereby lowers the computed state energies toward the full-CI limits, without a corresponding increase in computational effort.

ACME MCSCF: The conventional MCSCF method is limited to about $n=16$ to 18 active orbitals because the Hamiltonian diagonalization and reduced density matrix (RDM) computation effort increases dramatically with increasing active orbital dimension n (e.g. as n^{N_e} for full-CI type expansions with N_e electrons). We have formulated a new orbital optimization approach that eliminates this restriction. Within each iteration of the conventional MCSCF approach the symmetric eigenvalue equation, $\mathbf{H}\mathbf{V}=\mathbf{V}\mathbf{E}$, is solved in the configuration state function (CSF) basis of dimension N_{CSF} for the state of interest E_k , or in a state-averaged (SA) calculation, for the weighted sum of several N_{av} states of interest, $\bar{E} = \sum_k^{N_{\text{av}}} w_k E_k$. We consider the special case: $N_{\text{av}}=N_{\text{CSF}}$ and $w_k=1/N_{\text{CSF}} \forall k$. These conditions, combined with the trace identities, $\text{Tr}(\mathbf{E})=\text{Tr}(\mathbf{V}^T\mathbf{H}\mathbf{V})=\text{Tr}(\mathbf{H}\mathbf{V}\mathbf{V}^T)=\text{Tr}(\mathbf{H})$, result in

$$\bar{E} = \frac{1}{N_{\text{CSF}}} \text{Tr}(\mathbf{H}) = \frac{1}{N_{\text{CSF}}} \sum_k^{N_{\text{CSF}}} H_{kk} .$$

This SA energy does not depend on the wave function expansion coefficients V_{jk} and it can be computed using only the diagonal H_{kk} matrix elements. These H_{kk} elements depend only on the small subset of Hamiltonian integrals h_{pp} , g_{pppp} , g_{ppqq} , and g_{pqpp} , and require only $O(n^2)$ effort each to compute. This special case of state averaging is called the All Configuration Mean Energy (ACME) conditions with equal weights. In principle, this would allow \bar{E} to be computed with $O(N_{\text{CSF}}n^2)$ effort. The COLUMBUS MCSCF code is based on GUGA, in which the CSF expansion space is represented as walks within a Shavitt graph. A recursive procedure based on this graphical representation allows \bar{E} to be computed instead with only $O(\omega n^2)$ effort where ω is a factor that ranges from $O(N_e^0)$ up to $O(N_e^2)$, depending on the complexity of the Shavitt graph. The effort for this recursive procedure does not depend on N_{CSF} , and $\omega \ll N_{\text{CSF}}$. The ACME RDM can also be computed recursively and requires a comparable amount of effort. Given the RDM elements, the orbital optimization gradient and hessian can be constructed, and reliable second-order-convergent methods can be employed to optimize the orbitals. Due to the low-order effort scaling of the ACME algorithms, and to the elimination of the \mathbf{H} eigenvalue equation, essentially an unlimited number of active orbitals can be accommodated. There is no need to artificially limit the number of active orbitals or to artificially restrict valence orbitals to be doubly occupied as is typically required in traditional MCSCF implementations. The price for this flexibility is that the state-specific MCSCF wave functions and energies are not available during the optimization procedure and must be computed separately if desired.

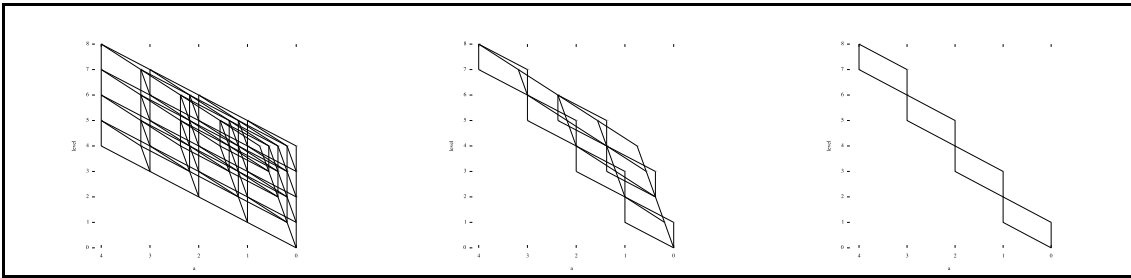


Fig. 1. Three examples of Shavitt graphs. All three graphs have the graph head (4,0,4) which corresponds to an 8-e, 8-orbital, singlet. The left figure is the full-CI expansion, the middle figure is the GVB-RCI expansion, and the right figure is the PPMC expansion.

Timings are given in Table 1 for sequences of calculations for the combined computation of the ACME \bar{E} and RDM arrays for three different wave function expansion forms: PPMC (Perfect Pairing MCSCF), GVB-RCI (Generalized Valence Bond Restricted CI), and full-CI. These timings are all for singlet wave functions with $n=N_e$ for the range $n=2$ to 256, and the corresponding CSF expansion dimensions are also included. The average nodes per level in the Shavitt graphs for these different expansion forms scale as $\omega \approx O(N_e^0)$, $\omega \approx O(N_e^1)$ and $\omega \approx O(N_e^2)$ respectively, predicting computational efforts that scale as $O(n^2)$, $O(n^3)$ and $O(n^4)$. Fig. 1 shows examples of the Shavitt graphs for these three types of expansions. Fig. 2 shows the actual timings along with these scaled curves for reference. It is seen that the actual timings approach the expected scaling behavior from above for increasing n and that the simple scaling models are accurate for $n \gtrsim 16$. The overhead associated with local memory allocations and table initializations, which is included in these timings, is dominant for the small n calculations and becomes insignificant for the larger cases. As seen in Table 1 and Fig. 2, the \bar{E} and RDM computation effort is quite reasonable even for the largest N_{CSF} expansions (up to $\sim 10^{150}$), demonstrating the dramatic difference in the efficient recursive ACME algorithm compared to the traditional MCSCF approach.

Table 1. Timings for combined \bar{E} and RDM computation[†].

$n=N_e$	$N_{\text{CSF}}^{(\text{PPMC})}$	t_{PPMC}	$N_{\text{CSF}}^{(\text{GVB-RCI})}$	$t_{\text{GVB-RCI}}$	$N_{\text{CSF}}^{(\text{Full-CI})}$	$t_{\text{full-CI}}$
2	2	4.0E-06	3	5.0E-06	3	5.0E-06
4	4	8.0E-06	10	1.3E-05	20	2.0E-05
8	16	2.2E-05	150	5.2E-05	1764	1.4E-04
16	256	6.3E-05	71398	2.7E-04	3.5E+007	1.4E-03
32	65536	2.3E-04	4.4E+10	1.8E-03	4.1E+016	1.8E-02
64	4.3E+09	7.7E-04	4.5E+22	1.3E-02	2.0E+035	2.9E-01
128	1.8E+19	3.0E-03	1.3E+47	9.4E-02	1.8E+073	4.4E+00
256	3.4E+38	1.2E-02	2.9E+96	8.2E-01	5.1E+149	7.3E+01

[†]) All times are in seconds for a single core of a 2.3 GHz Intel Core i7, a typical, low-power consumption, laptop CPU. All CSF expansions are for singlets with $n=N_e$.

Given the ability to optimize orbitals with the ACME conditions, subsequent state-specific high-level electronic structure calculations can be performed using these orbitals. Analytic geometry gradients can be computed for the high-level methods that use these orbitals. This analytic gradient procedure is based on the efficient and flexible

successive orbital transformation formulation that has been previously developed for MRCI wave functions. As in the MCSCF optimization step itself, the individual MCSCF state-specific wave functions and energies are not required or referenced; only the inexpensive ACME RDMs are required in this procedure. The successive orbital transformation formulation can also be applied to the efficient computation of nonadiabatic coupling between individual states computed with high-level electronic structure methods.

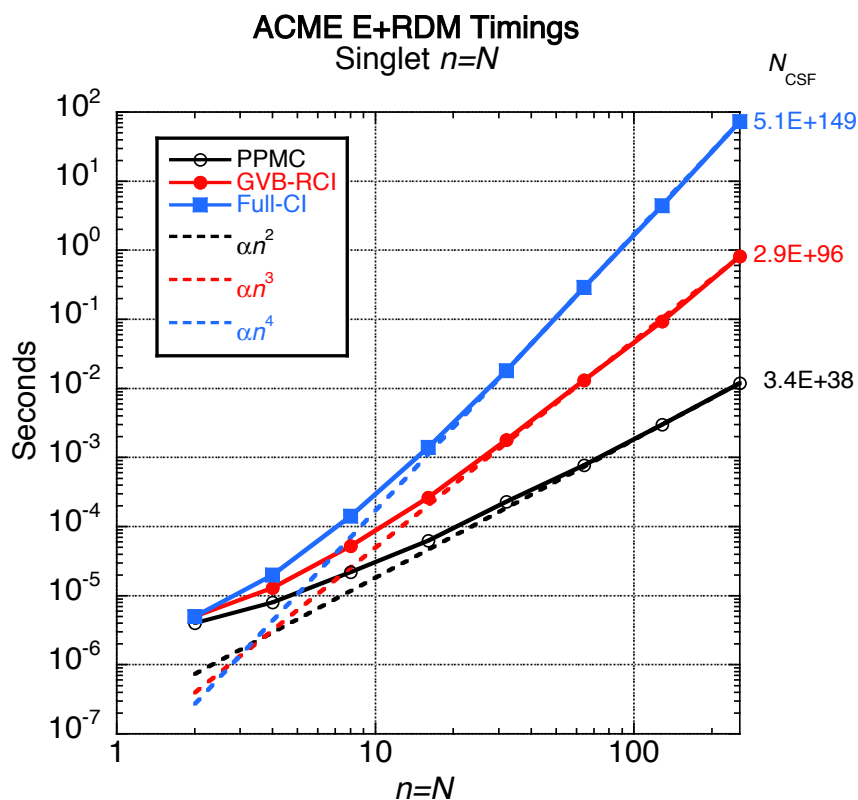


Fig. 2. Timings in seconds for the combined ACME \bar{E} and RDM computation for $n=N_e$ sequences of calculations for singlet PPMC, GVB-RCI, and full-CI expansions. Scaled curves αn^2 , αn^3 , and αn^4 are shown for reference.

Publications:

- “Shavitt Memorial Festschrift Collection,” *Theor. Chem. Acc.* (2016). ISSN: 2194-8666, ISSN 2194-8674 (electronic). Edited by R. Shepard, T. H. Dunning, Jr., and R. M. Pitzer.
- “Recent Developments with the Graphically Contracted Function Electronic Structure Method,” R. Shepard, Gergely Gidofalvi, and Scott R. Brozell, *8th Molecular Quantum Mechanics, Celebration of the Swedish School Abstracts*, 56 (2016).
- “Recent Developments with the Graphically Contracted Function Electronic Structure Method,” R. Shepard, Scott R. Brozell, and Gergely Gidofalvi, *ISTCP IX Abstracts* (2016).
- “Recent Developments with the Multifacet Graphically Contracted Function Electronic Structure Method,” R. Shepard, Scott Brozell, Gergely Gidofalvi, *Abstracts of Papers of the American Chemical Society* **253**, 212-COMP (2017).
- “On the All Configuration Mean Energy Condition,” 59th Sanibel Symposium in Honor of Klaus Ruedenberg Proceedings, (2019).
- “The All Configuration Mean Energy Multiconfiguration Self-Consistent-Field Method,” R. Shepard and S. R. Brozell, *Mol. Phys.* (submitted).

Mechanisms and Models for Simulating Gas Phase Chemical Reactivity

Raghu Sivaramakrishnan
Chemical Dynamics Group, Chemical Sciences & Engineering Division
Argonne National Laboratory, Lemont, IL 60439
raghu@anl.gov

I. Program Scope

Mechanisms describing the chemical reactivity of small gas phase species can be complex involving a myriad of unimolecular and bimolecular elementary steps. The primary scope of this program is to develop and validate detailed chemical kinetics mechanisms and models for use in predictive simulations of high temperature gas phase reactivity.

Kinetics modeling has been used predominantly as an engineering tool for making predictions for practical applications in combustion and chemical conversions. However, within the context of the chemical physics BES program we have also utilized the highly coupled nature of sequences of elementary reactions in our kinetics models along with associated theoretical and experimental efforts in our group to highlight a number of interesting problems pertinent to gas phase chemical reactivity. In such a context, modeling combustion chemistry provides access to a wide range of relevant physical (pressures, temperatures and gradients in these), chemical environments (small gas phase hydrocarbon species to particulate matter), internal energies, and timescales to allow us to highlight the role of quantum effects such as tunneling, anharmonic thermochemistry, and chemically activated molecules and nonthermal reactions among others.

II. Recent Progress

A. Path Analyses in Low-Temperature Propane Oxidation

Inspired by the modeling, experiment, and theoretical efforts to understand propane oxidation as part of the HPCC program we initiated path flux analyses on this chemical system using the “Sum over Histories Representation”^{1,2,3,4} in collaboration with M. J. Davis and Rex Skodje (Univ. of Colorado-Boulder). The SOHR method allows time-dependent kinetic observables to be computed using an expansion over global chemical pathways that follow chemical moieties as they move through a complex reaction network such as in propane oxidation.⁵ In particular, by decomposing the kinetics into individual chemical pathways with well-defined probabilities a quantitative mechanistic picture is obtained for the ignition process in propane-air mixtures at high pressures. Merchant et al.⁵ concluded the early stages of the ignition process in propane can be understood as a catalytic process with the OH-radical serving as the catalytic center. The present study using SOHR⁶ identified additional pathways apart from the primary cycles identified in ref. 5 for OH production. In particular, propylperoxy radical reactions were identified as sinks that impeded OH production from the primary pathways. The kinetics of these reactions are poorly characterized⁷ at conditions relevant to auto-ignition regimes and therefore experimental and theoretical studies may be warranted under such conditions. Theoretical efforts are in progress (see ab-initio chemical kinetics section) to improve our understanding of the reactions of peroxy radicals.

B. Chemistry for Engine Simulations

We continue our longstanding interactions with M. J. Davis and CFD modelers in the Energy Systems division (Sibendu Som, Gina Magnotti) at ANL in developing and interpreting the results from chemical kinetic mechanisms for large molecules and surrogates relevant to autoignition in compression-ignition engines. In particular, these efforts have been targeted towards understanding autoignition for a biodiesel surrogate model and utilizing global sensitivity analyses (GSA) tools to investigate the chemistry “in-situ” in a practical engine simulation. In recent years, the focus of our efforts was on calibration of a new GSA method⁸ that utilized small sample sizes (~ factor of 10 smaller than the prior version developed here) without sacrificing the accuracy in ordering the most sensitive reactions to

autoignition. This study provided the groundwork for performing GS with a limited number of simulations. This also led to the subsequent development of a sparse regression based GSA method that was successfully applied⁹ for chemical reaction selection in a realistic engine simulation.

C. High Accuracy Thermochemical Kinetics for $H + CH_3 (+M) \rightleftharpoons CH_4 (+M)$

Due to its paramount role as a chain-terminating process, the chemical kinetics of $H + CH_3 (+M) \rightleftharpoons CH_4 (+M)$ has received substantial attention¹⁰ from the atmospheric and combustion chemistry communities. With the exception of the inferred high-pressure limiting rate constants, $k_{rec,\infty}$, from a shock tube study¹¹ of $D + CH_3$, direct measurements of the title reaction in the recombination direction are limited to low temperatures¹² (<600 K). On the other hand, direct shock tube measurements¹³⁻¹⁵ of the rate constants in the dissociation direction, k_{diss} , span a higher temperature range 1500 - 4500 K, primarily due to the strong C-H bond in CH_4 . Reconciling the thermally disparate experimental database on k_{rec} and k_{diss} requires accurate equilibrium constants for the title reaction that span an extended range of temperatures.

In a CH_4 dissociation study, Sutherland et al.¹⁵ have utilized equilibrium constants (K_{eq}) calculated earlier by Ruscic¹⁶⁻¹⁸ to obtain Troe fits to the relevant experimental data¹²⁻¹⁵ on k_{rec} and k_{diss} . These K_{eq} values (300-4500 K) relied on thermochemical parameters for the CH_3 radical that were calculated using the usual rigid-rotor harmonic-oscillator (RRHO) approximation. Similarly, the IUPAC evaluation¹⁹ for the thermochemistry of CH_3 , which provides NASA polynomials that are widely used in combustion for simulations over extended T-ranges, also uses the same RRHO approximation. However, a theoretical study²⁰ of the CH_3 radical concluded that for this species the RRHO approximation is inadequate at high temperatures relevant to flame chemistry. In collaboration with Ruscic, accurate equilibrium constants were determined for the title reaction using the ATcT approach.²¹⁻²⁴ These accurate equilibrium constants were used along with results from a two-dimensional master equation approach²⁵ (in collaboration with Jasper and Klippenstein) and literature experiments on k_{rec} and k_{diss} to obtain an accurate representation for the kinetics of $H + CH_3 (+M) \rightleftharpoons CH_4 (+M)$. With experimental studies limited to rare gases (He, Ar, and Kr), theory also offers predictive results for bath gases (N_2 , H_2O , and CO_2) relevant to practical simulations. The impact of using an updated fit from this work for the title reaction is assessed through simulations of laminar flame speeds. Simulations of 1-10 atm CH_4 -air flames ($T_u = 298$ K) were performed using two popular combustion models, USC-Mech²⁶ and Aramco Mech.²⁷ Replacing $k(T,P)$ and CH_3 thermo with the present recommendations in either of these models^{26,27} leads to noticeable changes in flame speed predictions.

D. Siloxane Chemistry

As part of a DOE funded project, Tranter and Wooldridge (Univ. of Michigan) are pursuing experimental studies relevant to siloxane oxidation and combustion. Preliminary measurements²⁸ in a Rapid Compression Machine (RCM) indicated that doping small quantities of hexamethyldisiloxane (HMDSO) and trimethylsilanol (TMSO) accelerated ignition in syngas-air mixtures. With a view to understanding the chemistry responsible for ignition enhancement we have initiated theoretical studies to determine thermochemistry for the various siloxane species as well as characterize the PES's for HMDSO decomposition and oxidation ($R + O_2$ and other reactions). Two molecular channels are active and have energies below the lowest energetically accessible bond fission channel (CH_3 loss) in the HMDSO decomposition PES. The two molecular processes have barriers above 75 kcal/mol effectively ruling out significant decomposition at temperatures relevant to the syngas autoignition studies. However, it is interesting to note that the energetics for these processes are similar to that observed in disilane.²⁹ The lowest energy saddle point for dissociation to $(CH_3)_3SiOH + (CH_3)_2Si=CH_2$ is lower in energy than the separated products calling for the application of a two transition state model for the kinetics of this lowest energy process. Ignition simulations³⁰ indicate the potential role for $(CH_3)_3SiOSi(CH_3)_2CH_2 + O_2$ and subsequent oxidation reactions. Preliminary theoretical studies have therefore been initiated to explore the $(CH_3)_3SiOSi(CH_3)_2CH_2O_2$ potential energy surface. Ultimately, the kinetics for these channels will be calculated to aid in interpreting and modeling the siloxane ignition studies.

E. Radical-Radical Reactions

In prior studies³¹ we have highlighted the role of chemically activated adducts in radical-radical reactions and emphasized the role of unaccounted for pathways that can be accessed through such energized adducts to explain the evolution of species in flames. Most detailed chemical kinetics models often consider only the recombination process (and often at the high pressure limit) in a radical-radical reaction for C₄ and larger hydrocarbons. For H + alkyl and CH₃ + alkyl radical reactions, prior theoretical studies^{32,33} have determined high-pressure limiting rate constants for the recombination processes in selected straight and branched chain alkyl radicals. However, the presumption that recombination will be the dominant process may not hold good since steric effects may dictate large contributions from disproportionation processes. Additionally, at elevated temperatures there is an increased likelihood to access higher energy channels. Tranter has initiated experimental efforts to determine rate constants for such self-reactions of all four butyl radical isomers (n, sec, iso, and tert). In collaboration with theoretical predictions from Jasper, we are in the process of simulating these experiments to determine the role of addition vs disproportionation in these bimolecular processes. In the experimental conditions accessed (700-1300K) by Tranter, these alkyl radicals also dissociate predominantly^{34,35,36} via,



and lead to reactive H, CH₃, and C₂H₅ radicals in each of these radical systems. Proper interpretation of the experiments also requires consideration of reactions of these reactive atoms/radicals with the parent butyl radicals, i. e. H + tert-C₄H₉, CH₃ + iso-C₄H₉/sec-C₄H₉ and C₂H₅ + n-C₄H₉. Again, as with the self-reactions of butyl radicals, addition and disproportionation processes occur in these reaction systems. Additionally, energetically accessible addition-elimination radical products can also be accessed in these reactions. While detailed kinetics models consider recombination to be the dominant channel²⁶ (or the only channel²⁷) for these reactions, our preliminary results indicate that even for the larger C₂H₅ + n-C₄H₉ system at T > 1000 K and P = 1 bar there is significant contribution (~20%) to addition-elimination leading to n-C₃H₇ + n-C₃H₇. At higher temperatures and lower pressures and for the other three smaller C₅ and C₄ radical systems, recombinations are even less important. Another area of interest in such radical-radical reactions is the role of the roaming transition state mediating direct abstraction such that this may be the dominant kinetic process at low temperatures and pressures. In collaboration with Klippenstein we plan on initiating theoretical and modeling studies to characterize this in the C₂H₅ + C₂H₅ system.

III. Acknowledgements

This work was supported by the U.S. Department of Energy, Office of Science, Office of Basic Energy Sciences, Division of Chemical Sciences, Geosciences, and Biosciences under Contract No. DE-AC02-06CH11357.

IV. References

1. S. R. Bai, D. Y. Zhou, M. J. Davis, R. T. Skodje, *J. Phys. Chem. Lett.* 6, 183 (2015).
2. S. R. Bai, M. J. Davis, R. T. Skodje, *J. Phys. Chem. A* 119, 11039 (2015).
3. S. R. Bai, R. T. Skodje, *Int. Rev. Phys. Chem.* 35, 539 (2016).
4. S. R. Bai, R. T. Skodje, *J. Phys. Chem. Lett.* 8, 3826 (2017).
5. S. S. Merchant, C. F. Goldsmith, A. G. Vandeputte, M. P. Burke, S. J. Klippenstein, W. H. Green, *Combust. Flame* 162, 3658 (2015).
6. S. Bai, M. J. Davis, R. Sivaramakrishnan, R. T. Skodje, *Comb. and Flame* 202, 154 (2019).
7. R. Atkinson, D. L. Baulch, R. A. Cox, J. N. Crowley, R. F. Hampson, R. G. Hynes, M. E. Jenkin, M. J. Rossi and J. Troe, *Atmos. Chem. Phys.* 6, 3625 (2006) and references within.
8. M. J. Davis, W. Liu, R. Sivaramakrishnan, *J. Phys. Chem. A* 121, 553 (2017).
9. G. Magnotti, Z. Wang, W. Liu, R. Sivaramakrishnan, S. Som, M. J. Davis, *J. Phys. Chem. A* 122, 7227 (2018).
10. D.L. Baulch, C.T. Bowman, C.J. Cobos, R.A. Cox, Th. Just, J.A. Kerr, M.J. Pilling, D. Stocker, J. Troe, W. Tsang, R.W. Walker, J. Warnatz, *J. Phys. Chem. Ref. Data* 34 (2005) 757-1397.
11. M.-C. Su, J.V. Michael, *Proc. Combust. Inst.* 29 (2002) 1219-1227

12. M. Brouard, M.T. Macpherson, M.J. Pilling, *J. Phys. Chem.* 93 (1989) 4047.
13. J.H. Kiefer, S.S. Kumaran, *J. Phys. Chem.* 97 (1993) 414-420.
14. (a) D.F. Davidson, M.D. Di Rosa, A.Y. Chang, R.K. Hanson, C.T. Bowman, *Symp. Int. on Combust.* 24 (1992) 589-596. (b) D.F. Davidson, R.K. Hanson, C.T. Bowman, *Int. J. Chem. Kin.* 27 (1995) 305-308. (c) S.K. Wang, D.F. Davidson, R.K. Hanson, *J. Phys. Chem. A* 120 (2016) 5427-5434.
15. J.W. Sutherland, M.-C. Su, J.V. Michael, *Int. J. Chem. Kin.* 33 (2001) 669-684.
16. B. Ruscic Private communication (Sept. 2000) to the authors of Ref. 15.
17. (a) B. Ruscic, M. Litorja, R.L. Asher, *J. Phys. Chem. A* 103 (1999) 8625 - 8633 (b) G. Herzberg, *J. Mol. Spectrosc.* 33 (1970) 147-168.
18. M.W. Chase, Jr., C.A. Davies, J.R. Downey, Jr., D.J. Frurip, R.A. McDonald, A.N. Syverud, *J. Phys. Chem. Ref. Data* 14 (1985) (Suppl. 1) 1-926.
19. B. Ruscic, J.E. Boggs, A. Burcat, A.G. Csaszar, J. Demaison, R. Janoschek, J.M.L. Martin, M.L. Morton, M.J. Rossi, J.F. Stanton, P.G. Szalay, P.R. Westmoreland, F. Zabel, T. Berces, *J. Phys. Chem. Ref. Data* 34 (2005) 573.
20. D.M. Medvedev, L.B. Harding, S.K. Gray, *Mol. Phys.* 104 (2006) 104, 73.
21. B. Ruscic, R.E. Pinzon, M.L. Morton, G. von Laszewski, S. Bittner, S.G. Nijssure, K.A. Amin, M. Minkoff, A.F. Wagner, *J. Phys. Chem. A* 108 (2004) 9979-9997.
22. B. Ruscic, R.E. Pinzon, G. von Laszewski, D. Kodeboyina, A. Burcat, D. Leahy, D. Montoya, A.F. Wagner, *J. Phys. Conf. Ser.* 16 (2005) 561-570.
23. B. Ruscic, R.E. Pinzon, M.L. Morton, N.K. Srinivasan, M.-C. Su, J.W. Sutherland, J.V. Michael, *J. Phys. Chem. A* 110 (2006) 110, 6592-6600.
24. B. Ruscic, D. Feller, K.A. Peterson, *Theor. Chem. Acc.* 133 (2014) 1415.
25. A.W. Jasper, K.M. Pelzer, J.A. Miller, E. Kamarchik, L.B. Harding, S.J. Klippenstein, *Science* 346 (2014) 1212.
26. H. Wang, X. You, A.V. Joshi, S.G. Davis, A. Laskin, F. Egolfopoulos, C.K. Law, USC Mech Version II. High-Temperature Combustion Reaction Model of H₂/CO/C₁-C₄ Compounds. http://ignis.usc.edu/USC_Mech_11.htm
27. W.K. Metcalfe, S.M. Burke, S.S. Ahmed, H.J. Curran, *Int. J. Chem. Kin.* 45 (2013) 638-675.
28. R. A. Schwind, M. S. Wooldridge, R. S. Tranter, Spring Technical Meeting of the Central States Section of the Combustion Institute, March 2018.
29. K. Matsumoto, S. J. Klippenstein, K. Tonokura, M. Koshi, *J. Phys. Chem. A* 109 (2005) 4911-4920.
30. R. A. Schwind, M. S. Wooldridge, R. Sivaramakrishnan, Paper 2A06, 11th US National Combustion Meeting, Pasadena, CA, March 2019.
31. N. J. Labbe, R. Sivaramakrishnan, S. J. Klippenstein, *Proc. Combust. Inst.* 35, 447 (2015).
32. L. B. Harding, Y. Georgievskii, S. J. Klippenstein, *J. Phys. Chem. A* 109, 4646 (2005).
33. S. J. Klippenstein, Y. Georgievskii, L. B. Harding, *Phys. Chem. Chem. Phys.* 8, 1133 (2006).
34. V. D. Knyazev, I. A. Dubinsky, I. R. Slagle, D. Gutman, *J. Phys. Chem.* 98, 5279 (1994).
35. V. D. Knyazev, I. A. Dubinsky, I. R. Slagle, D. Gutman, *J. Phys. Chem.* 98, 11099 (1994).
36. V. D. Knyazev, I. R. Slagle, *J. Phys. Chem.* 100, 5318 (1996).

V. Journal articles supported by this project 2017-2019

1. M. J. Davis, W. Liu, R. Sivaramakrishnan, "Global Sensitivity Analysis with Small Sample Sizes: Ordinary Least Squares Approach", *J. Phys. Chem. A* **121** (2017) 553-570.
2. P. J. Weddle, C. Karakaya, H. Zhu, R. Sivaramakrishnan, K. Prozument, R. J. Kee, "Boundary-layer Model to Predict Chemically Reacting Flow within Heated, High-Speed, Micro-tubular Reactors", *Int. J. Chem. Kin.* **50** (2018) 473-480.
3. G. Magnotti, Z. Wang, W. Liu, R. Sivaramakrishnan, S. Som, M. J. Davis, "Sparsity Facilitates Chemical-Reaction Selection for Engine Simulations", *J. Phys. Chem. A* **122** (2018) 7227-7237.
4. S. Bai, M. J. Davis, R. Sivaramakrishnan, R. T. Skodje, "A Chemical Pathway Perspective on the Kinetics of Low-Temperature Ignition of Propane", *Comb. and Flame* 202 (2019) 154-178.
5. N. J. Labbe, A. W. Jasper, S. J. Klippenstein, J. A. Miller, R. Sivaramakrishnan, B. Ruscic, "From Anharmonic Partition Functions to Flame Chemistry: High Accuracy Thermochemical Kinetics for H + CH₃ (+M) ⇌ CH₄ (+M)", In Preparation, *J. Phys. Chem. A* (2019).
6. J. B. Randazzo, A. W. Jasper, R. Sivaramakrishnan, R. S. Tranter, "An Experimental and Theoretical Study of the High Temperature Reactions of the Four Butyl Radical Isomers", In Preparation, *Phys. Chem. Chem. Phys.* (2019).

Quantum Chemistry of Radicals and Reactive Intermediates

John F. Stanton
Quantum Theory Project
Departments of Chemistry and Physics
University of Florida
Gainesville, FL 32611
johnstanton@ufl.edu

Scope of Research

My research group works in the area of theoretical chemical physics, especially on the properties and chemistry of organic radicals and other reactive intermediates. This research follows a number of paths, including first-principles calculation of bond energies and other thermochemical information (as well as development of methodology needed for such calculations), methods for the simulation and analysis of molecular spectra (especially those relevant to experiments that can be used to glean thermochemical information), the development of *ab initio* quantum chemical methods needed for the accurate treatment of fundamental aspects of electronic structure and potential energy surfaces, and computational kinetics including semiclassical transition state theory and master equation modeling of chemical reactions.

Summary of Selected Recent Accomplishments

- Our work on fourth-order vibrational perturbation theory (VPT4), published early during the reporting period, has continued. As part of our initial application, analytic differentiation of fitted potential energy surfaces gave the required anharmonic constants (cubic through sextic in order) to machine precision, which enabled a fair comparison of the variational and VPT4 energies with corresponding VPT2 results from which VPT4 tends not to differ by much. This is important, because the principal finding of our VPT4 studies is that VPT4 is a decided improvement upon VPT2 when the latter is accurate, but less so in the majority of cases¹ when VPT2 differs substantially from accurate variational calculations. Hence, most of the important comparisons are between level energies that differ by 1 cm⁻¹ or less. In any event, this technology has enabled an ongoing study of the well-documented and investigated reaction whereby formaldehyde dissociates to molecular hydrogen and CO through a tight transition state. In particular, this study is using the VPT4-variant of semiclassical transition state theory (VPT4-SCTST) to compute state dependent rates, which will be compared to those calculated previously for this system, as well as values that come from VPT2-SCTST. An additional interest here are the Siegert eigenvalues associated with the transition state, the importance of which was first identified by Siedeman and Miller² many years ago. Together with an established collaborator (P.B. Changala at Boulder), we will also carry out fully variational (using complex scaling) calculations for the Siegert eigenvalues. The results of this work are just beginning to be generated, and will be presented in next year's report.

¹An exception is when there is a weak effect of Darling-Dennison resonance, in which VPT4 is substantially better than VPT2.

²T. Seideman and W.H. Miller *J. Chem. Phys.* 95, 1768 (1981).

- Together with the Continetti group, we have made an important discovery. At last year’s meeting in Gaithersburg, R.E. Continetti and I had extensive discussions about a reported observation of the OCCO molecule by others, which was under further study in the UCSD laboratory, where potential fragmentation channels were under investigation. OCCO, formally a dimer of the most stable diatomic molecule, had presumably been generated via photodetachment of its anion, the latter being produced by passing glyoxal through a discharge. After a great deal of thinking, and the screening of many alternative candidates by quantum chemical calculation and subsequent simulations of photodetachment spectra, it was realized that the carrier of the spectrum was not OCCO, but rather the oxyallyl radical. The laboratory study in the Continetti group was able to generate the same reported spectrum, and a combination of theory and experiment conclusively showed it to be due to the (previously reported) oxyallyl molecule. Hence, the rather long and somewhat celebrated search for OCCO continues.

- In collaboration with the Zwier group, we have worked to analyze the structure and microwave spectrum of the 2-furanyloxy radical, which was studied at Purdue by chirped-pulse microwave (CP-MW) spectroscopy and investigated here with high-level coupled-cluster calculations. This paper served to demonstrate the already established power of CP-MW spectroscopy for the analysis of reactions (in this case, pyrolysis of a second-generation biofuel, 2-methoxyfuran), and used a combination of high-level quantum chemistry and the very high-precision nature of rotational spectroscopy to analyze the distribution of unpaired electron spin in the molecule.

- In collaboration with the Kaiser group and collaborators elsewhere, we have worked on the thermodynamics and kinetics associated with the observation of a doubly-bridged GeSiH₂ molecule, which is apparently generated in a reaction between atomic germanium and silane (SiH₄) whereby the germanium inserts into an Si-H bond followed by intersystem crossing and subsequent elimination of molecular hydrogen. High-accuracy mHEAT calculations (see below) were essential to unravel the nature of this reaction, which provides insight into an area of chemistry that is clearly of potential technological importance.

- In addition, with Ruscic, we have been working on several projects associated with the Active Thermochemical Tables (ATcT) paradigm that has had a major impact on the quality and precision of thermochemical data. Among these is a study of the prototype isomerization between methyl cyanide (CH₃CN) and isocyanide (CH₃NC), which has been an important benchmark in chemical kinetics for many years. In this work, carried out with my excellent kineticist assistant, T. Lam Nguyen (as well as the Ruscic group), this isomerization reaction was considered over a large range of temperature (400-1000 K) and pressures (10 mTorr to 100 Ktorr), using high-level quantum chemistry, in conjunction with VPT2-based SCTST and a provisional two-dimensional master equation approach. It was found that this – wholly statistical – approach was able to satisfactorily reproduce the experimental values (within about 10% at all temperatures, including in the fall-off region). This is a fairly significant finding, as the adequacy of statistical kinetic models for this benchmark isomerization reaction had previously been questioned.

- Driven largely by our work in chemical kinetics and also by our role in a Task Force associated with Ruscic’s thermochemical tables, we have developed, documented and benchmarked a new model thermochemistry. For several years, our group has used the so-called HEAT family of methods, which were originally established fifteen years ago³. While extremely accurate (*ca.* 1 kJ (2 σ) accuracy for bond energies and enthalpies of formation for small compounds), HEAT remains inapplicable to “large” molecules that lack high symmetry. That is, while the method has been used for benzene and other similarly sized – but symmetric – species, the bulk of our kinetics applications and much of the new work driven by the ATcT effort demand a more computationally

³A. Tajti *et al.* *J. Chem. Phys.* 121, 11599 (2014).

feasible approach. A paper documenting our efforts to establish a workable strategy and the eventual benchmarking of the successful mHEAT+ approach has recently been accepted⁴. Frankly, the PI finds it quite surprising that the accuracy of the new method is not substantially lower than that of HEAT itself, and he is optimistic that the scope of applications amenable to “high-accuracy” theoretical thermochemistry applications will widen considerably. This bodes well for the important ATcT project of Ruscic, which is the decided gold standard for modern thermochemistry.

• Additional information about our DOE-supported research can be found in the publications listed at the end of this document.

Students and Postdoctoral Supported:

T.L. Nguyen (postdoc, Florida)

C.A. Lopez (student, Austin)

J.T. Thorpe (student, Florida)

M.B. Bentley (student, Florida)

References from 3/2018-3/2019 acknowledging DE-FG02-07ER15884

T.L. Nguyen and J.F. Stanton Accurate Rate Coefficients for $H + NH_3 \rightarrow H + NH_2$ from High-Level Theoretical Calculations, *Int. J. Chem. Kin.*, 51, 321 (2019).

W.J. Morgan, D.A. Matthews, M. Ringholm, J. Agarwal, J.Z. Gong, K. Ruud, W.D. Allen, J.F. Stanton and H.F. Schaefer Geometrical Derivatives at the Complete Basis-Set Limit: Application to the Equilibrium Structure and Molecular Force Field of Formaldehyde *J. Comp. Theo. Chem.* 14, 1333 (2018).

A.M. Thomas, B.B. Dangi, T. Yang, G. Tarczay, R.I. Kaiser, A.H.H.Chang, T.L. Nguyen and J.F. Stanton Synthesis of the Germaniumsilylene Butterfly Molecule ($Ge(H_2)Si$), *J. Phys. Chem. Lett.*, 10, 1264 (2019).

T.L. Nguyen and J.F. Stanton Three-Dimensional Master Equation (3DME) Approach, *J. Phys. Chem. A* 122, 7757 (2018).

C. Abeysekera, A. Hernandez-Castillo, J.F. Stanton and T.S. Zwier Broadband Microwave Spectroscopy of 2-Furanyloxy Radical: Primary Photolysis Product of 2-Methoxyfuran *J. Phys. Chem. A* 122, 6879 (2018).

K.G. Lunny, Y. Benitez, Y. Albeck, D. Strasser, J.F. Stanton and R.E. Continetti Spectroscopy of Ethylenedione and Ethynediolide: A Reinvestigation, *Angew Chim. Int. Ed.* 57, 5394 (2018).

J.Z. Gong, D.A. Matthews and J.F. Stanton Fourth-Order Perturbation Theory with the Watson Hamiltonian: Report of Working Equations and Some Preliminary Results, *J. Chem. Phys.* 149, 114102 (2018).

T.L. Nguyen, J.H. Thorpe and J.F. Stanton High-Level Theoretical Study of the Acetonitrile-Methyl Isocyanate Isomerization *J. Phys. Chem. Lett.* 9, 2532 (2018).

⁴J.T. Thorpe, C.A. Lopez, T.L. Nguyen, J.H. Baraban, D.H. Bross and B. Ruscic *J. Chem. Phys.*, in press.

Universal and State-Resolved Imaging Studies of Chemical Dynamics

Arthur G. Suits

Department of Chemistry, University of Missouri, Columbia MO 65211
suitsa@missouri.edu

I. Program Scope

The focus of this program is on combining universal ion imaging probes providing global insight with high-resolution state-resolved probes providing quantum mechanical detail, to develop a molecular-level understanding of chemical phenomena. Particular emphasis is placed upon elementary reactions involving transient species and in revealing new aspects of reaction mechanisms and the dynamical behavior of molecules. Much of the current effort here is in generalizing (or unlearning!) the lessons from simple systems as we investigate the behavior of larger polyatomic molecules. This research is conducted using state-of-the-art molecular beam machines, photodissociation, reactive scattering, and vacuum ultraviolet lasers in conjunction with ion imaging and chirped-pulse microwave techniques. A major focus of our effort remains crossed-beam reactive scattering of polyatomic molecules, with new directions introduced below.

II. Recent Progress

Roaming mediated dynamics in bimolecular reactions

Our DOE-supported work first revealed the roaming mechanism in formaldehyde photodissociation fifteen years ago, and the insights derived from those advances continue to shape our perspective. In particular, we now find related behavior in bimolecular processes that prompt us to generalize our understanding of what we mean by roaming and roaming-mediated dynamics. We noted some years ago that isomerization of nitro-compounds to nitrites can proceed by a roaming-mediated path that accounts for the efficiency of that process. We first encountered bimolecular roaming dynamics in reactive scattering of Cl atom with alkenes in 2014, in collaboration with Alex Mebel in this program. In that case, electrophilic addition to the π system forms a strongly bound adduct, but to eliminate HCl the system must redissociate in a roaming-like event to access the abstraction geometry. Recently, we have been studying the reaction of ground state oxygen atoms with dimethylamine and trimethylamine in crossed beams as introduced in last year's abstract. Since then, we have collaborated with theorist Spridoula Matsika at Temple, which allowed us to provide a quantitative basis for our speculations as described in the following.

We used crossed-beam DC slice imaging with an intense O (3P) radical beam and 157 nm VUV probe. We studied reaction with dimethylamine (DMA) and trimethylamine (TMA), detecting the aminoalkyl radical product with single photon ionization. We characterized the translational energy release and angular distributions of the reactions using crossed beam scattering combined with universal DC slice imaging and found both reactions proceeded via a long-lived intermediate even at the highest collision energy studied, over 8 kcal/mol. *Ab initio* calculations on the energies and structures along the reaction pathways were also performed to gain insight to the underlying dynamics.

A careful search along the triplet and singlet potential energy surfaces (PESs) was performed by *ab initio* calculations at the CBS-QB3 level of theory. For the triplet PESs of the O (3P) + TMA

reaction, we could not locate any transition state (TS) for the direct H abstraction pathway to generate OH and $(\text{CH}_3)_2\text{NCH}_2$ products that we probed experimentally, suggesting it is barrierless. Interestingly, we found a roaming-type TS that has one low imaginary frequency (200 cm^{-1}) indicating a flat PES in this region, and two very low bound frequencies (40 and 50 cm^{-1}) corresponding to motions of the O atom relative to the TMA fragment originating in a shallow entrance well. However, based on the fact of the observed long-lived complex formation and relatively high collision energy $E_{\text{coll}} = 8.0\text{ kcal mol}^{-1}$ in the experiment, this shallow well is not likely a key aspect of the dynamics. We then searched through the singlet PESs since the coupling between singlet and triplet PESs inducing ISC is ubiquitous in chemistry and it is widely observed in O (^3P) reactions with unsaturated hydrocarbons such as C_2H_4 and CH_2CCH_2 . We found one transition state (TS) separating two very deep complex wells ($\text{ON}(\text{CH}_3)_3$ and $(\text{CH}_3)_2\text{NCH}_2\text{OH}$) on the reaction pathway to form the probed products. However, this TS has a very high barrier energy, 45 kcal mol^{-1} above the O(^3P) + TMA reactant asymptotic limit, essentially representing re-dissociation to O(^1D) from the complex. We concluded that the only plausible pathway for the reaction is that the O (^3P) radical attacks TMA to initiate direct H abstraction from the methyl group. Then, due to the long-range dipole-dipole interaction and the high dimensionality of the system, OH and $(\text{CH}_3)_2\text{NCH}_2$ radicals do not part immediately but undergo multiple collisions permitting ISC.

To confirm this, we first performed a direct dynamics trajectory on the triplet surface using Born-Oppenheimer Molecular Dynamics starting from a submerged TS that appeared at low levels of theory for the abstraction. That trajectory showed two things: the dynamics were direct, resulting in a rebound trajectory in less than a picosecond, yet the interaction between the incipient radical fragments was protracted in the long-range region as implied by the dipole-dipole interaction. The reaction was over in half a picosecond, but that still provided ample time for interaction between the two radicals. We then turned to Spiridoula Matsika who performed multireference (MCQDPT2) calculations on a number of points for the six lowest surfaces (S_0 - S_2 and T_1 - T_3). She found that four of these surfaces are nearly degenerate in the region of the triplet minimum in the exit channel. Furthermore, the spin-orbit coupling there, determined by CASSCF calculations, was large ($\sim 60\text{ cm}^{-1}$) for both S_0 - T_2 and S_1 - T_1 . Finally, the coupling of both of these pairs of surfaces involved a simultaneous change in the electron angular momentum and spin on the OH radical, satisfying the El-Sayed criteria for ultrafast ISC. Our view of this process then is that direct abstraction takes place on the triplet surface, with some extended interaction between the radical pair owing to the dipole-dipole interaction and the relatively high density of states, allowing time and circumstances to permit efficient ISC to a very strongly bound hydroxylamine intermediate. The results were published in *Nature Chem* and featured in *Physics Today*.

O (^3P) + alcohols

We have concluded and published our crossed-beam study of O (^3P) reaction with propanol isomers under single collision conditions with well-defined collision energies of 8 and 10 kcal mol $^{-1}$. The hydroxypropyl radical products, generated from the α -H and β -H abstraction for 1-propanol and α -H abstraction for 2-propanol, were detected with our universal VUV (157 nm) soft ionization probe with velocity map imaging technique. Backward-sideways scattering but more favorable backward scattering was observed for both propanol isomer reactions under two different collision energy in the experiment. Low average translational energy release was obtained, accounting for 20%-30% of the total available energy, which indicates that a large amount of energy is released as the internal excitation of the products. This indicates high internal

Progress in Multi-mass and time resolved imaging

Over the past year, we have begun development of a new experimental apparatus to perform time-resolved photofragment imaging. The experiment is housed in a new temperature-controlled laboratory. This houses the principal tool for our time-resolved experiments, a KMLabs Wyvern 1000 femtosecond laser system. Development of this experiment has proceeded on three main fronts, first was developing the tools to characterize and control our pump and probe laser pulses, second was to develop a new apparatus alongside our standard suite of tools (DC Slice imaging, mass spectroscopy), and thirdly was to implement multi-mass imaging, based on the method of Wen Li and co-workers. To-date we have completed the first two of these objectives and we now work to incorporate the multimass and coincidence detection approach of Li and coworkers.

IV. DOE Publications 2016-present

Shi, Y. Kamasah, A., Suits, A. G., “H Abstraction Channels in the Crossed-Beam Reaction of F + 1-Propanol, 1-Butene and 1-Hexene by DC Slice Imaging” *J. Phys. Chem. A*, 120.45 (2016): 8933-8940. DOI: 10.1021/acs.jpca.6b08408.

A. Kamasah, H. Li, J. Onvlee, A. van der Avoird, D. H. Parker, and A. G. Suits, “Imaging the inelastic scattering of vibrationally excited NO(v=1) with Ar,” *Chem. Phys. Lett.* (2018) **692**, 124-128. DOI: 10.1016/j.cplett.2017.12.016

A. G. Suits, “Invited Review Article: Photofragment Imaging,” (2018) 89, 111101 DOI: [10.1063/1.5045325](https://doi.org/10.1063/1.5045325)

H. Li, A. Kamasah, S. Matsika and A. G. Suits, “Intersystem Crossing in the Exit Channel,” *Nature Chem* (2018) DOI:10.1038/s41557-018-0186-5

H. Li, A. Kamasah, and A. G. Suits, “Imaging H abstraction dynamics in crossed molecular beams: O(³P) + propanol isomers,” *Phys Chem Chem Phys*, (2018) DOI:10.1039/C8CP06351F.

Multiscale Interaction of Turbulence, Temperature, and Soot Formation: Measurements for Critical Assessments of Chemical Kinetics and Mechanisms

Jeffrey A. Sutton
Department of Mechanical and Aerospace Engineering
Ohio State University
Columbus, OH 43210
sutton.235@osu.edu

Project Scope

This program targets an improved understanding of how turbulence affects soot formation chemistry (directly and indirectly) with a particular focus on detailing the multiscale coupling between flow turbulence, mixing, thermal transport, and soot formation kinetics in gas-phase reacting systems. There is ample evidence that soot formation and growth is strongly affected by turbulence. This is due to the fact that soot formation chemistry is characterized by slow time scales and thus surrounding fluid mechanic and mixing time scales not only influence the kinetic processes, but may dictate them. In this manner, the assessment of soot formation and the resulting chemical kinetic mechanisms for application under turbulent conditions must be benchmarked against measurements in turbulent reacting flows. This project targets simultaneous, quantitative multi-dimensional velocity, soot volume fraction, and gas-phase temperature imaging in turbulent non-premixed sooting flames to elucidate the relative effects of fluid kinematics, mixing, thermal processes, and turbulence/scalar time/length scales on soot formation chemistry and topology.

The local gas-phase temperature field is critically important to further understand soot formation under turbulent conditions because of its direct linkage between turbulence (i.e., thermal and molecular mixing) and chemical kinetics (i.e., temperature-dependent reaction rates). In this program, a new implementation of filtered Rayleigh scattering (FRS) is applied for quantitative 2D temperature measurements in turbulent sooting non-premixed flames. The combined velocity (via PIV), soot volume fraction (via LII), and gas-phase temperature imaging will provide a previously unavailable database concerning turbulence-temperature-soot interaction. From these measurements, novel multi-parameter statistics will be derived that detail the coupling and importance of various kinematic and thermal parameters. This analysis is necessary for understanding relevant formation pathways, transport mechanisms, and developing soot mechanisms to be applied under turbulent conditions.

Recent Progress

Development of Simultaneous Velocity and Temperature Imaging in Non-Sooting Flames

While the implementation of laser-induced incandescence (LII) and particle imaging velocimetry (PIV) is difficult in sooting environments, the methods have been successfully applied [e.g., 1-4] and thus represent known measurement strategies under sooting conditions. The primary diagnostic challenge lies in developing and applying a robust and accurate temperature imaging methodology that can be applied in sooting turbulent non-premixed flames and simultaneously with LII and PIV. Of the numerous laser-based thermometry approaches that exist, few are applicable in the presence of soot or PIV tracer particles due to the scattering/interference from the particles. In the current program, the targeted method for temperature measurements is filtered

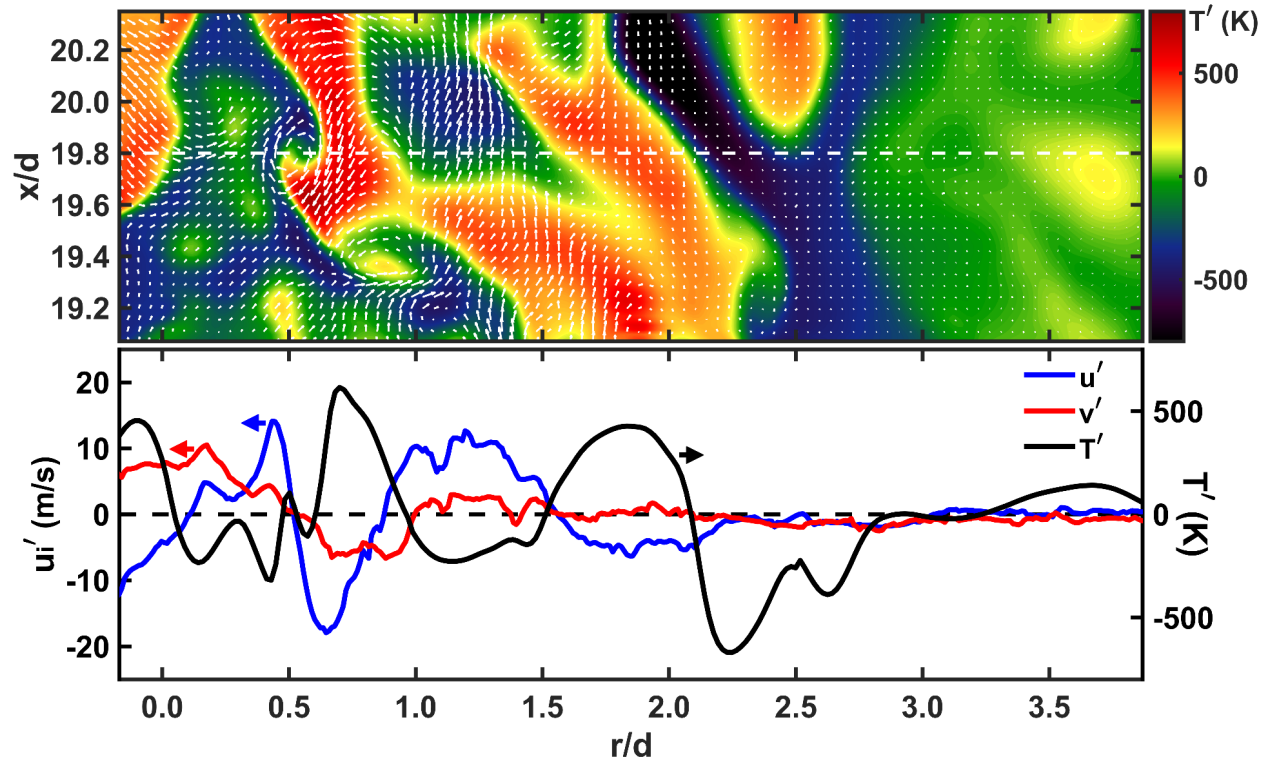


Figure 1: (Top) Sample simultaneous single-shot measurement of temperature (shown as a colormap) and velocity fluctuations (shown as vectors). (Bottom) Corresponding radial profiles extracted from $x/d = 19.8$ of temperature fluctuations (black), axial velocity fluctuations (blue), and radial velocity fluctuation (red). Measurements are from a $Re = 20,000$ CH₄/H₂/Ar flame

Rayleigh scattering (FRS). FRS is a variant of the traditional laser Rayleigh scattering (LRS) technique which uses the combination of a spectrally narrow laser and an atomic or molecular filter (cell filled with an absorbing species such as molecular iodine, I₂) placed in front of the detector [5]. This combination rejects interference that is spectrally identical to the incident laser light (i.e., scattered light from particles), while collecting gas-phase information. In this program we have developed particular fuel combinations for both non-sooting and sooting flames such that the measured FRS signal is a known function of temperature. This allows quantitative single-shot temperature measurements using only an FRS measurement.

In the first six months of the program, we have developed our temperature measurement methodology in non-sooting flames (but in the presence of PIV tracer particles) to satisfy three goals: (i) demonstrate accurate temperature measurements in particle-laden flames, (ii) demonstrate accurate simultaneous temperature and velocity measurements, and (iii) develop a series of non-sooting flames that can be directly compared to the targeted sooting flames to examine the effects of soot on flow turbulence and mixing. Figure 1 shows an example of joint temperature and velocity imaging extracted from a simultaneous FRS and stereo PIV measurement. Beneath the image are sample radial profiles of temperature (T') and velocity (u' and v') fluctuations extracted from the image. The temperature fluctuation field is shown as a false colormap and the velocity fluctuations are shown as white vectors overlaid on the colormap. As noted from Fig. 1, the FRS temperature images are of high quality and exhibit high SNR, where

the SNR is defined as the ratio of the mean value to the standard deviation within a uniform region. In the coflow region of these temperature measurements ($T \approx 300\text{K}$) the SNR is 69. Our previous work has shown that FRS exhibits a favorable temperature-dependence; that is, the SNR actually increases with temperature [6]. For example, it is estimated that the SNR is 76 at 1500 K. The high SNR and spatial resolution of the temperature imaging permits measurements into the dissipative range which is critical for monitoring the small-scale dissipation processes that have been shown to impact soot formation [7]. This data represents the first measurements of the simultaneous 2D temperature and velocity fields in turbulent non-premixed flames. The joint velocity and temperature measurements have been used to calculate axial and radial scalar (heat) flux and examine whether counter-gradient diffusion exists and to examine the role of vorticity and fluid dynamic strain rate on thermal dissipation formation and structure.

Additional Progress

As described earlier, particle image velocimetry (PIV) is a critical part of the measurement program to understand how the various flow kinematic properties affect soot formation, growth, and transport. PIV in sooting flames is difficult due to the interference from the intense flame luminosity, which is primarily from the radiating soot. PIV image pairs typically are captured using an interline frame transfer camera, which allows the acquisition of two frames in quick succession. The first frame has an exposure time on the order of microseconds, while the second frame has an exposure time equal to the readout time of the first image which is on the order of 100 ms. Previous work [i.e., 2] has shown that the second PIV frames are affected significantly by luminosity and at times are unusable or lead to inaccurate velocity measurements at best. In the current program, we take an alternative approach for eliminating flame (soot) luminosity. We have designed and fabricated a dual-sensor PIV camera system that uses two ultra-high-resolution sCMOS cameras, each with a resolution of 2560×2160 pixels. A 3D rendering of the system is shown in Fig. 2. The two camera sensors are coupled to a single lens through a 50/50 beamsplitter and sub-micron-level adjustment. In this manner, each camera sensor is responsible for one of the particle image pairs and thus, a short, microsecond-level shutter time is available for each PIV image and luminosity effects are minimized for each frame.

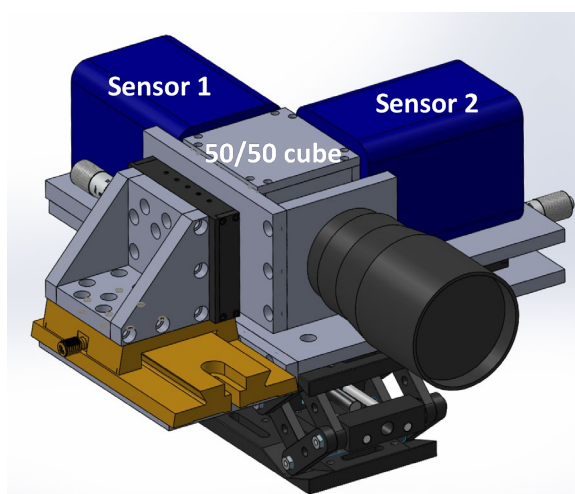


Figure 2: 3D rendering of dual-sensor PIV camera for velocity measurements in highly luminous sooting flames

We also have been working to further refine our in-house Rayleigh Brillouin scattering (RBS) spectroscopic model to include sooting fuels such as acetylene and ethylene. Accurate interpretation of the measured FRS signal requires accurate modeling of the RBS spectral lineshape of the hydrocarbon fuels. Previously, we have shown that the modeling for CH_4 , H_2 , Ar , O_2 , N_2 , H_2O , CO , and CO_2 is quite accurate [8]. In this program we will add C_2H_2 and C_2H_4 to our existing codes and verify the model results (spectral lineshapes) through high-resolution spectroscopic measurements of RBS emission from the selected species. To date, we have added the species to our modeling library including known transport properties, set up the requisite

experiment and performed preliminary measurements in species such as N₂ and air to assess the accuracy of our measurement system.

Future Plans

Near-term work includes the development and application of FRS for quantitative temperature measurements in turbulent sooting flames. After successful implementation, the first joint FRS-PIV-LII studies will begin. A series of turbulent sooting and non-sooting flames have been developed for study that span a broad range of Reynolds and Damköhler numbers. A key focus of the initial sets of experiments is to characterize accuracy and precision of all measurements independently and then together to examine “crosstalk” effects.

With the simultaneous temperature-velocity-soot volume fraction database, longer-term work includes a detailed statistical characterization of the flames including statistical moments, integral scales, and joint statistics. A significant utility of the simultaneous LII-PIV-FRS imaging lies in the ability to formulate a set of joint statistics (including bivariate correlations, joint PDFs, conditional statistics, and multi-variate correlations) between multiple parameters with a particular focus on examining the relative roles of turbulent and thermal transport on soot formation. Finally, an investigation of the relative roles of flow kinematics and thermal variations on soot topology will be investigated.

References

- [1] Narayanaswamy, V., Clemens, N.T., *Combust. Flame*, 2013, 34, 1455-1463.
- [2] Köhler, M., Geigle, K.P., Meier, W., Crosland, B.M., Thomson, K.A., Smallwood, G.J., *Appl. Phys. B*, 2011, 104, 409-425.
- [3] Park, O., Burns, R.A., Buxton, O.R.H., Clemens, N.T., *Proc. Combust. Inst.*, 2017, 36, 899-907
- [4] Köhler, M., Boxx, I., Geigle, Meier, W., *Appl. Phys. B*, 2011, 103, 271.
- [5] Forkey, J.N., Finkelstein, N.D., Lempert, W.R., Miles, R.B., *AIAA J.* 1996, 34(3) 442.
- [6] McManus, T.A., Sutton, J.A., *Appl. Opt.*, 2019, 57(11), 2936-2947.
- [7] Attili A., Bisetti F., Mueller M.E., Pitsch H., *Combust. Flame*, 2014, 161(7):1849-65.
- [8] McManus, T.A., Trueba-Monje, I., Sutton, J.A., *Appl. Phys. B*, 2019, 125-13

Publications Supported by this DOE Project (2016 – present)

This program is a new start that began in August 2018.

Elementary Reactions of PAH Formation

Robert S. Tranter

Chemical Sciences and Engineering Division, Argonne National Laboratory

Lemont, IL-60439

tranter@anl.gov

I. Program Scope

This program is focused on the experimental determination of kinetic and mechanistic parameters of elementary reactions, in particular those involved in the formation and destruction of the building blocks for aromatic species. The program also encompasses dissociation of novel fuels such as ethers and cyclic species and their dissociation products that are representative of intermediates in combustion mechanisms. Thermal sources of radicals are investigated and characterized for use in more complex reaction systems where secondary chemistry can be significant. Recently, the scope has been increased to include thermally initiated roaming reactions. The approach involves a diaphragmless shock tube (DFST) equipped with laser schlieren densitometry (LS) and a time-of-flight mass spectrometer (TOF-MS). The combination of these techniques accesses a wide range of reaction temperatures and pressures. Finally, X-ray diagnostics are exploited to study flows in hostile environments to obtain a better understanding of how to accurately interpret information from some common experimental devices.

II. Recent Progress

A. Cyclic species: Decomposition of cycloalkanes

Cyclic hydrocarbons are important in a broad range of high temperature chemical systems. They form a significant fraction of energy sources such as aviation fuels, diesel and kerosene, and heterocyclic species are potential biofuels and intermediates in combustion and pyrolysis. However, even apparently simple molecules such as cycloalkanes present significant challenges to accurate determination of the thermal decomposition mechanism and measurements of rate coefficients. Thus a study of the decomposition of several cycloalkanes and heterocyclic species has been undertaken to determine reaction mechanisms and obtain rate coefficients for key steps. With respect to cycloalkanes, the studies include cyclopentane and cycloheptane to examine the effect of altering the ring size relative to cyclohexane.

#	Rxn
1	c-alkane = [biradical] = 1-alkene
2	1-alkene = allyl + n-alkyl
3	allyl = allene + H
4	n-alkyl = alkene + H/CH ₃ /alkyl
5	c-alkane + H/CH ₃ = c-alkyl + H ₂ /CH ₄

Table 1: Generic reaction mechanism for the initial steps in the high temperature dissociation of cyclopentane and cyclohexane.

Pyrolysis and oxidation of cyclohexane has been extensively studied by other groups. Of particular relevance to the current work is an experimental and theoretical investigation by Kiefer et al. [1] that used the shock tube/laser schlieren densitometry method; similar to that employed here. However, for other cycloalkanes the literature is limited, particularly at high temperatures, with a primary source being a theoretical study by Sirjean et al. [2] who studied dissociation of several cycloalkanes from cyclopropane to cyclohexane. We have previously studied the dissociation of cyclopentane [3] and obtained good agreement with the calculated high pressure limit rate expression from Sirjean et al. The LS experiments spanned 35-300 Torr and resolved the high temperature pressure dependent falloff which was reproduced by RRKM calculations. The unimolecular rate coefficients for dissociation of cyclopentane were about a factor of five lower than those obtained for cyclohexane by Kiefer et al. The generic reaction mechanism shown in Table 1, with sub-models for radical species, adequately describes the initial steps for pyrolysis of cyclopentane and cyclohexane. It is not clear if this mechanism is applicable to cycloalkanes larger than cyclohexane. Furthermore, it is also not clear if the rate of dissociation of cycloalkanes larger than cyclohexane will be lower than that for cyclohexane. The literature on the dissociation of cycloalkanes with more than 6 carbon atoms is sparse and mainly consists of estimates of bond dissociation energies by Seubold et al. [4]. To

address this a LS study of cycloheptane pyrolysis has been conducted ($P_2 = 30\text{-}240$ Torr; $T_2 = 1600 - 2000$ K; 0.5-2% cycloheptane/Kr).

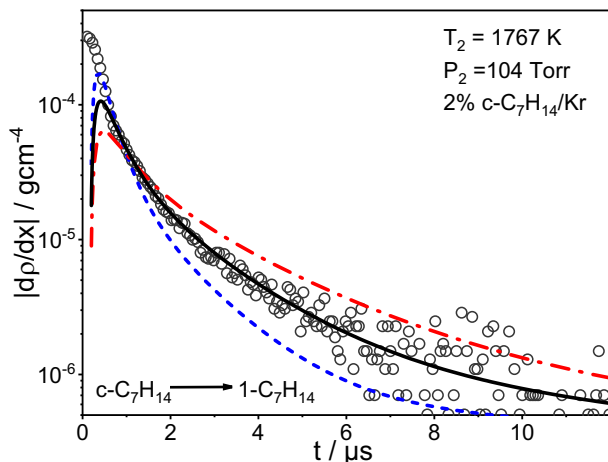


Figure 1: Example semi-log density gradient plot for dissociation of cycloheptane. Symbols represent experimental data. Solid lines are simulation results. Dashed and dash-dot lines indicate the sensitivity of the simulation to changes in $k_{(c-C_7H_{14} \rightarrow 1C_7H_{14})}$ by a factor of two.

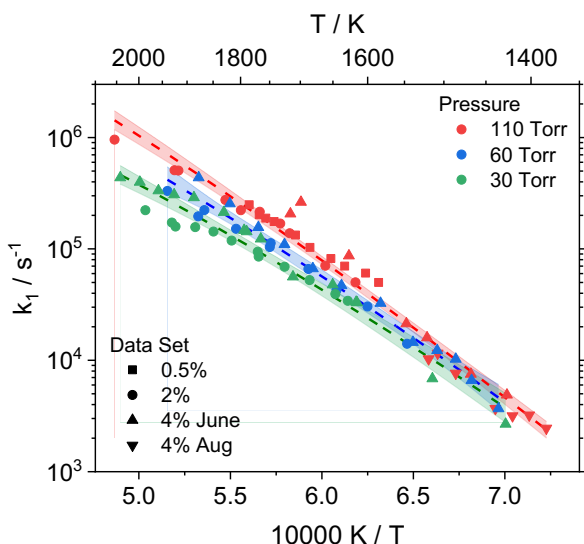


Figure 2: Rate coefficients for the initial dissociation of cycloheptane to 1-heptene. Lines are least squares fits to the experimental data.

An example LS experiment is shown in Fig. 1 along with the results of simulations using a model based on Table 1. LS experiments are sensitive to both rate of reaction and enthalpy of reaction. Dissociation of cycloheptane is only mildly endothermic (~ 12.6 kcal/mol) and creates only a weak LS signal. However, dissociation of 1-heptene, product of reaction 1, is strongly endothermic (74.9 kcal/mol) and as it is produced and dissociates, reaction 2, causing the initial rise in the simulation results. The simulations are sensitive to the rate of reaction 1, Fig. 1, but not reaction 2. This seems somewhat counterintuitive due to the relative magnitudes of their reaction enthalpies. However, reaction 1 is the rate determining step for production of 1-heptene and at temperatures where dissociation of cycloheptane can be observed k_2 is already large ($> 10^6$ s $^{-1}$). Thus, the simulations are insensitive to even quite large changes in k_2 . As noted above, the secondary chemistry is largely dominated by the products of 1-heptene dissociation and to produce an accurate model, LS experiments on 1-heptene have also been conducted. 1-heptene dissociates to allyl and *n*-butyl radicals. Both these radicals have been studied by LS. Simulations of the complete set of cycloheptane experiments confirm that the generic mechanism, Table 1, applies to dissociation of cycloheptane. The rate coefficients obtained for reaction 1 are shown in Fig. 2. They display a pressure dependence and magnitude similar to those for cyclopentane dissociation, which is consistent with the trend in bond energies estimated by Seubold et al. In ongoing work, a RRKM model for cycloheptane is being developed to allow extrapolation to other pressures. Additionally, the reactions of H-atoms with cycloheptane (and cyclopentane) are important and the focus of ongoing work, as is the refinement of the lower temperature studies of 1-heptene dissociation.

B. Alkyl radicals: low temperature creation, self-reaction and dissociation

Alkyl nitrites have proved to be a simple and clean source for thermally generating alkyl radicals in DFST/LS experiments over the important temperature range of 700 – 1000 K. These studies have allowed recombination/disproportionation reactions of alkyl radicals to be studied as well as dissociation of the radicals and the reaction of the alkyl radicals with their dissociation products. Table 2 shows a generic

#	Rxn	$\Delta H_{r,298K}$
1	$R-CH_2-O-NO = R-CH_2-O + NO$	41.9 ± 0.6
2	$R-CH_2O = R + CH_2O$	11.3 ± 0.3
3	$R = R' + \text{alkene}$	23.3
4	$R = H + \text{alkene}$	34.4 ± 1.7
5	$R + R = RR$	-86.8 ± 1.6
6	$R + R = R-H + RH$	-66.0 ± 2.7
7	$R + H = RH$	-100.0 ± 1.3
8	$R + H = R-H + H_2$	-69.9 ± 1.7
9	$R + R' = RR'$	-89.3
10	$CH_3 + CH_3 = C_2H_6$	-90.0

Table 2: Generic mechanism for decomposition of alkyl nitrites. $R' = CH_3$ or larger alkyl radical. $\Delta H_{r,298K}$ are averaged from $R = C_2H_5$, $n-C_3H_7$ and $i-C_3H_7$.

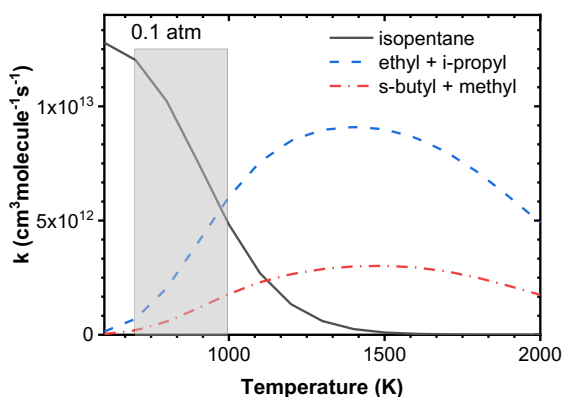


Figure 3. Comparison of addition and addition/elimination reactions for $CH_3 + iso\text{-butyl}$. The shaded box represents the range of the LS experiments.

contributions to the observed LS signals, making constructing a chemical model to simulate the LS profiles challenging. However, a combination of literature data (mainly from photolysis/PIMS experiments by Knyazev and Slagle) and calculations of specific rate coefficients by Jasper and Sivaramakrishnan sufficiently constrain the models. At the current T_2 and P_2 addition of H and CH_3 to the butyl radicals can result not only in addition products but addition/elimination channels also become accessible. Calculations by Jasper and Sivaramakrishnan show that the addition/elimination paths are most significant at low pressures and high temperatures and that they cannot be neglected over the range of the LS experiments. For example, the addition/elimination reactions of $CH_3 + iso\text{-butyl}$ are shown in Fig. 3. Over the pressure range 0.01 – 10atm there are three possible channels. Two of these are effectively reactions catalyzed by methyl radical and result in open shell products; ethyl + *i*-propyl radicals or *s*-butyl + CH_3 radicals. The third channel forms the closed shell addition product, *iso*-pentane. The open shell products are much more reactive than *iso*-pentane and will result in different secondary reactions. Furthermore, the enthalpies of reactions of the addition/elimination channels are around 90 kcal/mol less exothermic than the addition channel which has a significant effect on the LS profiles. As illustrated in Fig. 3 over the temperature range

mechanism for dissociation of alkyl nitrites and the reactions of the alkyl radicals produced. An earlier version of this mechanism was created for alkyl radicals up to C3 and this has now been extended to larger radicals by replacing CH_3 in reactions 3 and 9 with R' . Prior combined experimental and theoretical studies focused on C2 and C3 alkyl radicals with Goldsmith and a resonantly stabilized radical (2-methylallyl) with Jasper. Recently, with Jasper and Sivaramakrishnan, the C4 alkyl radicals (*n*-butyl, *sec*-butyl, *iso*-butyl and *tert*-butyl) have been studied.

As indicated in Table 2, alkyl nitrites dissociate by loss of NO to generate an alkoxy radical. Under the conditions of these experiments the alkoxy radical dissociates effectively immediately by elimination of H_2CO yielding a radical with one less carbon atom than the nitrite. At the lower temperatures of these studies the alkyl radicals are thermally stable and reaction 5, recombination, and reaction 6, disproportionation, dominate the secondary chemistry. For *n*-alkyl radicals $k_6/k_5 = 0.05-0.1$. As the degree of branching increases the disproportionation channel becomes increasingly dominant and for *tert*-butyl is heavily favored over reaction 5 ($k_6/k_5 \sim 2$). [5] As the reaction temperature is increased the alkyl radicals begin to dissociate. The *iso*-butyl and *sec*-butyl radicals eliminate CH_3 to form propene by reaction 3, *tert*-butyl loses a H-atom to give *i*-butene (reaction 4) and *n*-butyl dissociates ethene and ethyl radical. Above about 850 K the ethyl radical also dissociates to ethene + H, further complicating the secondary chemistry of *n*-butyl. Once R' is formed in sufficient quantities then reactions between R and R' also occur. The secondary reactions are all strongly exothermic and make significant

of the LS experiments formation of *iso*-pentane dominates at low temperatures but only accounts for about 47% of the products at 1000 K.

The nitrites provide not only convenient sources for studying self-reaction of radicals but also a well characterized source of radicals for reaction with other species. Furthermore, they can also be used as relatively clean sources for crating initial bursts of H atoms and CH₃ radicals at modest temperatures. Currently, this ability is being exploited to study H + 1,3-pentadiene over the range 1050-1350 K. At these temperature 1,3-pentadiene is stable in LS experiments but the temperature range is largely inaccessible to LS experiments with the traditional source of H-atoms, ethyl iodide.

C. Future work

The DFST/TOF-MS/LS studies of aromatics and resonantly stabilized radicals are being expanded to include reactions between radicals and oxygen molecules. Organonitrites will be exploited as sources of a broad range of radicals including unsaturated ones, resonantly stabilized and aromatic radicals. These will allow key processes in formation of polyaromatic hydrocarbons to be tested and characterized. These experiments will be supplemented with photoionization mass spectrometry experiments in the miniature high repetition rate shock tube, discussed elsewhere. It is anticipated that Michael's high purity shock tube will be converted to a DFST and optical diagnostics will be implemented to complement the DFST/TOF-MS/LS experiments.

III. References

- 1) Kiefer J. H., Gupte K.S., Harding L.B., Klippenstein S.J., J. Phys. Chem. A., **2009**, 113 13570–13583.
- 2) Sirjean B., Glaude P. A., Ruiz-Lopez M. F., Fournet R., J. Phys. Chem. A **2006**, 110, 12693-12704.
- 3) Randazzo J. B., Annesley C. J., Bell K., and Tranter R. S. 'A Shock Tube Laser Schlieren Study of Cyclopentane Pyrolysis' Proc. Combust. Inst. **2017**, 36, 273-280.
- 4) Seubold F. H., J. Chem. Phys., 1954, 22, 945-946.
- 5) Gibian M. J., Corley R. C., Chem. Rev., **1973**, 73, 441–464

IV. Publications and submitted journal articles supported by this project 2017-2019

- 1) Fuller M. E., Skowron M., Tranter R. S. and Goldsmith C. F. 'A modular, multi diagnostic, automated shock tube for gas-phase chemistry' Rev. Sci. Instrum. **2019** (submitted).
- 2) Randazzo J. B., Fuller M. E., Goldsmith C. F. and Tranter R. S. 'Thermal Dissociation Of Alkyl Nitrites And Recombination Of Alkyl Radicals' Proc. Combust. Inst. **2019**, 37,703-710.
- 3) Hansen N., Tranter R. S., Randazzo J. B., Lockhart J. P. A., and Kastengren A. L. 'Investigation of Sampling-Probe Distorted Temperature Fields with X-Ray Fluorescence Spectroscopy' Proc. Combust. Inst. **2019**, 37, 1401-1408.
- 4) Tranter R. S., Randazzo J. B., Lockhart J. P. A., Chen X. and Goldsmith C. F. 'High Temperature Pyrolysis of 2-Methyl Furan' Phys. Chem. Chem. Phys. **2018**, 20, 10826 – 10837.
- 5) Lockhart J. P. A., Goldsmith C. F., Randazzo J. B., Ruscic B. and Tranter R. S. 'An Experimental and Theoretical Study of the Thermal Decomposition of C₄H₆ Isomers' J. Phys. Chem. A, **2017**, 121, 3827-3850.
- 6) Hansen N., Tranter R.S., Moshhammer K., Randazzo J.B., Lockhart J.P.A., Fugazzi P. G., Tao T., and Kastengren A.L. '2D-Imaging of Sampling-Probe Perturbations in Laminar Premixed Flames Using Kr X-Ray Fluorescence' Combust. Flame, **2017**, 181, 214-224.
- 7) Tranter R. S., Jasper A. W., Randazzo J. B., Lockhart J. P. A., and Porterfield J. P. 'Recombination and Dissociation of 2-Methyl Allyl Radicals: Experiment and Theory' Proc. Combust. Inst. **2017**, 36, 211-218.
- 8) Randazzo J. B., Annesley C. J., Bell K., and Tranter R. S. 'A Shock Tube Laser Schlieren Study of Cyclopentane Pyrolysis' Proc. Combust. Inst. **2017**, 36, 273-280.
- 9) Tranter R. S., Kastengren A. L., Porterfield J. P., Randazzo J. B., Lockhart J. P. A., Baraban J. H., and Ellison G. B. 'Measuring Flow Profiles in Heated Miniature Reactors With X-ray Fluorescence Spectroscopy' Proc. Combust. Inst. **2017**, 36, 4603-4610.

Nonadiabatic Photochemistry

Donald Truhlar,¹ David R. Yarkony,² and Hua Guo³

¹Department of Chemistry, University of Minnesota, Minneapolis, Minnesota 55455

²Department of Chemistry, Johns Hopkins University, Baltimore, Maryland 21218

³Department of Chemistry and Chemical Biology, University of New Mexico, Albuquerque, 87131

Program Scope

This project involves the development and application of methods for treating electronically nonadiabatic processes with the emphasis on photochemical dynamics studied on accurate coupled potential energy surfaces generated by quantum mechanical electronic structure theory.

Recent Progress

Donald G. Truhlar: The electronic spectrum of thiophenol was simulated by a normal-mode sampling approach combined with TDDFT in the Tamm-Dancoff approximation (TDA). The vertical excitation energies were compared with electronic structure calculations by completely renormalized equation-of-motion coupled cluster theory with single and double excitations and noniterative inclusion of connected triples (CR-EOM-CCSD(T)) and by multi-reference perturbation theory. The spectrum was computed both with and without solvation effects, and these spectra are compared to each other and to experiment. Using multireference-perturbation-theory adiabatic wave functions and model-space diabaticization by the fourfold way, diabatic potential energy surfaces of the lowest three singlet states ($^1\pi\pi$, $^1\pi\pi^*$, and $^1n_\pi\sigma^*$) were constructed along the S-H stretching coordinate, the C-C-S-H torsion coordinate, and the ν_{16a} and ν_{16b} normal coordinates. The first two of these two are primary coordinates for the photodissociation, and the diabatic crossing seams of the three states were calculated and plotted as functions of the two coordinates. The other two coordinates are out-of-plane ring distortion modes studied to assess the extent of their role in coupling the states near the first conical intersection, and the ν_{16a} mode was shown to be an important coupling mode there. The current study is the first step toward a detailed mechanistic analysis of the photoinduced S-H fission process of thiophenol, a test system to understand $^1n_\pi\sigma^*$ -mediated reactions, at the same time already providing a better understanding of the thiophenol electronic excitations by clarifying the assignment of the experimental results.

It is well known that classical trajectories, even if they are initiated with zero point energy (ZPE) in each mode (trajectories initiated this way are commonly called quasiclassical trajectories) do not maintain ZPE in the final states. The energy of high-frequency modes will typically leak into low-frequency modes or relative translation of subsystems during the time evolution. This can lead to severe problems such as unphysical dissociation of a molecule, production of energetically disallowed reaction products, and unphysical product energy distributions. Here a new molecular dynamics method called extended Hamiltonian molecular dynamics (EHMD) is developed to improve the ZPE problem in classical molecular dynamics. In EHMD, two images of a trajectory are connected by one or more springs. The EHMD method is tested with the Henon-Heiles Hamiltonian in reduced and real units and with a Hamiltonian with quartic anharmonicity in real units, and the method is found to improve zero-point maintenance as intended.

We will soon publish a paper on the calculation and fitting externally correlated coupled potential energy surfaces and surface couplings for the electronically inelastic reaction $\text{OH}^* + \text{H}_2 \rightarrow \text{H}_2\text{O} + \text{H}$, where * denotes electronic excitation. We used the orbital-based fourfold way for diabaticization of adiabatic surfaces computed by XMS-CASPT2.

David R. Yarkony: Our algorithm for diabaticizing electronic structure developed previously is unique in two

respects. It simultaneously fits and diabaticizes the *ab initio* adiabatic electronic structure data and uses derivative couplings to define the diabatic representation. This is accomplished by fitting *ab initio* data, energies, energy gradients, and energy difference scaled derivative couplings to construct quasi-diabatic Hamiltonians (\mathbf{H}^d). Since the *ab initio* data are obtained from multireference (single and double excitation) configuration interaction (MRCISD) wave functions the local topology of a conical intersections is correctly described. Owing to the importance of CIs in nonadiabatic dynamics our algorithm takes special care to accurately represent the CI seam, using a partially diagonalized representation. The original algorithm, known as SURFGEN, uses a flexible functional form to construct \mathbf{H}^d . The use of fit representations, to be distinguished from on the fly methods, enables us to address computational problems that require high accuracy, quantum nuclear dynamics and or long propagation times.

The algorithmic part of our DoE sponsored research has as its goal, in collaboration with Guo, the incorporation Neural Networks (NN) into SURFGEN. SURGEN has the advantage that the symmetry-adapted functions used to construct the quasi diabatic representation \mathbf{H}^d can be tailored to the problem at hand. While this is advantageous in controlling the size of the expansion, the choice of additional functions is often not obvious and the construction of an improved expansion can be tedious. In addition, the incorporation of complete nuclear permutation inversion (CNPI) symmetry can be challenging owing to the general product form allowed by SURFGEN.

We completed the determination of accurate (based exclusively on MRCISD wave functions) coupled diabatic potential energy surfaces for the photodissociation reactions



These accurate surfaces have been used by Guo in full and reduced dimensional quantum nuclear dynamics, described in previous and current reports, to address both practical and conceptual issues, the geometric phase and vector potential, in nonadiabatic quantum chemistry.

Hua Guo: In collaboration with Yarkony, we have devoted much effort to advancing neural network (NN) representations of quasi-diabatic potential energy matrix (PEM). One such approach is to use different NNs for the elements of the PEM, after diabaticization has already been done. A key issue is the implementation of the permutation symmetry for identical nuclei in the molecular system. The permutation symmetry of individual elements of the PEM is dependent on the system and electronic states involved. For the dissociation of water and ammonia, for example, we have introduced symmetry adaptation based on the permutation invariant polynomial-neural network (PIP-NN) approach. When a PEM element is symmetric under exchange of identical atoms, the PIPs can be directly used as the input of the NN. When a PEM element is antisymmetric, such as those in the off-diagonal position in the NH_3 system, its symmetry adaption can also be based on PIPs, but with an additional multiplicative factor that enforces the antisymmetry. This approach has been demonstrated to be quite accurate. Another approach is based on the simultaneous diabaticization-fitting method, which is described above.

We continue to investigate nonadiabatic dynamics in photochemical systems using quantum dynamical methods. One such example is the predissociation of HCO, which has been extensively investigated before. A better resolved experimental study by Zhang (UC Riverside) has recently been carried out, which showed strong oscillations in the CO rotational state distribution. Using the latest diabatic PEM developed by Dawes (Missouri U Sci. and Tech), we have collaborated with Xie (Nanjing U) to provide a quantum mechanical characterization of the predissociation dynamics. Our investigation revealed that the oscillation in the CO product rotational state distribution can be attributed to interference between different dissociation pathways on the ground electronic state potential, facilitated by the isomerization barrier. This system can be likened to Young's double slit experiment, but with a molecular twist. Another example is the

photodissociation of hydroxymethyl in the $3p_x$ Rydberg state. Using the diabatic PEM developed by Yarkony, we determined its absorption spectrum with quantum dynamical calculations in all nine degrees of freedom. The agreement with experimental measurement of Riesler (USC) was excellent, which helped to confirm the assignments of the vibronic features and their lifetimes. We have written two reviews on our recent work with Yarkony.

Future Plans

Donald G. Truhlar: We will also finish a set of diabatic potential energy surfaces for electronically nonadiabatic photodissociation of methylamine, for which we are using orbital-free DQ diabatization. The fitting is based on extending the anchor points reactive potential method to include more primary coordinates and reactive molecular mechanics. We will complete the fitting of the surfaces and couplings, and we will perform semiclassical dynamics simulations of the electronically nonadiabatic processes by the CSDM method. These calculations will include electronically adiabatic and electronically nonadiabatic tunneling by our recently developed army ants tunneling approximation. We will also provide these surfaces and couplings to Hua Guo for quantum mechanical wave packet calculations. We will compare semiclassical dynamics calculations on the OH_3 system to quantum wave packet calculations of Guo. We are working on new orbital-free diabatization schemes that use the nonadiabatic coupling vectors as input. We also propose to further develop the dual-functional Tamm-Dancoff approximation.

David R. Yarkony: In the coming performance period we, working with Guo, will continue to develop our neural network version of SURFGEN, incorporating parallel computing techniques to reduce the time to solution while increasing the size of the systems that are tractable.

We will compare our coupled diabatic PESs for OH_3 and CH_3NH_2 (currently being tested by Guo) with those produced by Truhlar's group. We will work with Guo to study the quantum dynamics of methylamine photodissociation and of $\text{OH(A)}+\text{H}_2$ collisional quenching.

Hua Guo: We plan to devote our future effort in the next year to the elucidation of the $\text{H}_2 + \text{OH(A)}$ reaction, which can lead to the non-reactive $\text{H}_2 + \text{OH(X)}$ channel (quenching of OH(A)) and the reactive $\text{H} + \text{H}_2\text{O}$ channel, using both the PEMs recently developed by Truhlar and Yarkony.

Another system we plan to work on is the photodissociation of methylamine (CH_3NH_2), for which PEMs are being developed by Truhlar and Yarkony. This molecule bears some similarity with the more extensively investigated NH_3 system. The initial step is to determine the absorption spectrum for CH_3NH_2 and its deuterated isotopomers. This will be followed by quantum dynamics of the dissociation.

Selected recent publications acknowledging this grant¹⁻²⁶

1. Hu, S.-X.; Li, W.-L.; Lu, J.-B.; Bao, J. L.; Yu, H. S.; Truhlar, D. G.; Gibson, J. K.; Marçalo, J.; Zhou, M.; Riedel, S., et al. On the Upper Limits of Oxidation States in Chemistry, *Angew. Chem. Int. Ed.* **2018**, *57*, 3242-3245.
2. Gao, L. G.; Zheng, J.; Fernández-Ramos, A.; Truhlar, D. G.; Xu, X. Kinetics of the methanol reaction with OH at interstellar, atmospheric, and combustion temperatures, *J. Am. Chem. Soc.* **2018**, *140*, 2906-2918.
3. Shu, Y.; Truhlar, D. G. Improved potential energy surfaces of thioanisole and the effect of upper surface variations on the product distribution upon photodissociation, *Chem. Phys.* **2018**, *in press*.
4. Xing, L.; Bao, J. L.; Wang, Z.; Wang, X.; Truhlar, D. G. Hydrogen shift isomerizations in the kinetics of the second oxidation mechanism of alkane combustion. Reactions of the hydroperoxypentylperoxy OOQOOH radical, *Combust. Flame* **2018**, *197*, 88-101.
5. Zhang, L.; Truhlar, D. G.; Sun, S. Electronic spectrum and characterization of diabatic potential energy surfaces for thiophenol, *Phys. Chem. Chem. Phys.* **2018**, *20*, 28144-28154.

6. Shu, Y.; Dong, S. S.; Parker, K. A.; Bao, J. L.; Zhang, L.; Truhlar, D. G. Extended Hamiltonian molecular dynamics: semiclassical trajectories with improved maintenance of zero point energy, *Phys. Chem. Chem. Phys.* **2018**, *20*, 30209-30218.
7. Xing, L.; Bao, J. L.; Wang, Z.; Wang, X.; Truhlar, D. G. Relative rates of hydrogen shift isomerizations depend strongly on multiple-structure anharmonicity, *J. Am. Chem. Soc.* **2018**, *140*, 17556-17570.
8. Bao, J. L.; Truhlar, D. G. Effect of energy dependence of the density of states on pressure-dependent rate constants, *Phys. Chem. Chem. Phys.* **2018**, *20*, 30475-30479.
9. Long, B.; Bao, J. L.; Truhlar, D. G. Kinetics of the strongly correlated CH₃O + O₂ reaction: The importance of quadruple excitations in atmospheric and combustion chemistry, *J. Am. Chem. Soc.* **2019**, *141*, 611-617.
10. Zhang, R. M.; Truhlar, D. G.; Xu, X. Kinetics of the toluene reaction with OH radical, *Research in press*.
11. Shu, Y.; Kryven, J.; Oliveira-Filho, A. G. S. d.; Mielke, S. L.; Song, G.-L.; Li, S. L.; Meana-Pañeda, R.; Fu, B.; Bowman, J. M.; Truhlar, D. G. Direct diabaticization and analytic representation of coupled potential energy surfaces and couplings for the reactive quenching of the excited ²Σ⁺ state of OH by molecular hydrogen, *J. Chem. Phys.* **submitted**.
12. Caracciolo, A.; Lu, D.; Balucani, N.; Vanuzzo, G.; Stranges, D.; Wang, X.; Li, J.; Guo, H.; Casavecchia, P. Combined experimental–theoretical study of the OH + CO → H + CO₂ reaction dynamics, *J. Phys. Chem. Lett.* **2018**, *9*, 1229-1236.
13. Li, J.; Guo, H. Thermal rate coefficients and kinetic isotope effects for the reaction OH + CH₄ → H₂O + CH₃ on an ab initio-based potential energy surface, *J. Phys. Chem. A* **2018**, *122*, 2645-2652.
14. Liu, X.; Xie, C.; Guo, H. A new potential energy surface and state-to-state quantum dynamics of the Li + HF → H + LiF reaction, *Chem. Phys.* **2018**, *509*, 66-71.
15. Zhao, B.; Manthe, U.; Guo, H. Fermi resonance controlled product branching in the H + HOD reaction, *Phys. Chem. Chem. Phys.* **2018**, *20*, 17029-17037.
16. Ndengué, S.; Dawes, R.; Gatti, F.; Guo, H. Influence of Renner–Teller coupling between electronic states on H + CO inelastic scattering, *J. Phys. Chem. A* **2018**, *122*, 6381-6390.
17. Xie, C.; Zhu, X.; Yarkony, D. R.; Guo, H. Permutation invariant polynomial neural network approach to fitting potential energy surfaces. IV. Coupled diabatic potential energy matrices, *J. Chem. Phys.* **2018**, *149*, 144107.
18. Han, S.; Xie, D.; Guo, H. Modified Gaussian wave packet method for calculating initial state wave functions in photodissociation, *J. Chem. Theo. Comput.* **2018**, *14*, 5527-5534.
19. Xie, C.; Liu, X.; Guo, H. State-to-state quantum dynamics of the H + LiF → Li + HF reaction on an accurate ab initio potential energy surface, *Chem. Phys.* **2018**, *515*, 427-433.
20. Han, S.; Zheng, X.; Ndengué, S.; Song, Y.; Dawes, R.; Xie, D.; Zhang, J.; Guo, H. Dynamical interference in the vibronic bond breaking reaction of HCO, *Sci. Adv.* **2019**, *5*, eaau0582.
21. Zuo, J.; Chen, Q.; Hu, X.; Guo, H.; Xie, D. Dissection of the multichannel reaction of acetylene with atomic oxygen: from the global potential energy surface to rate coefficients and branching dynamics, *Phys. Chem. Chem. Phys.* **2019**, *21*, 1408-1416.
22. Xie, C.; Malbon, C. L.; Guo, H.; Yarkony, D. R. Up to a sign. The insidious effects of energetically inaccessible conical intersections on unimolecular reactions, *Acc. Chem. Res.* **2019**, *52*, 501-509.
23. Yarkony, D. R.; Xie, C.; Zhu, X.; Wang, Y.; Malbon, C. L.; Guo, H. Diabatic and adiabatic representations: Electronic structure caveats, *Comput. Theo. Chem.* **2019**, *1152*, 41-52.
24. Lu, D.-d.; Xie, C.-j.; Li, J.; Guo, H. Rate coefficients and branching ratio for multi-channel hydrogen abstractions from CH₃OH by F, *Chin. J. Chem. Phys.* **2019**, *32*, 84-88.
25. Xie, C.; Malbon, C. L.; Xie, D.; Yarkony, D. R.; Guo, H. Nonadiabatic dynamics in photodissociation of hydroxymethyl in the 3²A(3p_x) Rydberg state: A nine-dimensional quantum study, *J. Phys. Chem. A* **2019**, *123*, 1937-1944.
26. Guan, Y.; Zhang, D. H.; Guo, H.; Yarkony, D. R. Representation of coupled adiabatic potential energy surfaces using neural network based quasi-diabatic Hamiltonians: 1,2 ²A' states of LiFH, *Phys. Chem. Chem. Phys.* **2019**, *in press*.

Probing Nonvalence Excited States of Anions Using Photodetachment and Photoelectron Spectroscopy

Lai-Sheng Wang

Department of Chemistry, Brown University, Providence, RI 02912

Email: lai-sheng_wang@brown.edu

Program Scope

This program is aimed at providing energetic, electronic, and vibrational information about radical species important in combustion using novel anion spectroscopic techniques. Negative ions do not possess Rydberg states, but highly diffuse nonvalenced excited states can exist for anions as a result of long-range forces between an electron and a molecule, including charge-dipole, charge-quadrupole, or charge and induced-dipole interactions. A major goal of this project is to probe this class of anionic excited states that exist in polycyclic aromatic hydrocarbon (PAH) molecules or functionalized PAH molecules. The weakly-bound nature of these nonvalence excited states implies that vibrational excitation in the neutral core can induce autodetachment via vibronic coupling. We have developed a high-resolution electro-spray photoelectron imaging apparatus equipped with a cryogenically-controlled ion trap, which is ideal to probe this class of nonvalence anionic excited states. Photodetachment spectroscopy is used to search for the nonvalence excited states of cold anions via resonant two-photon detachment or vibrational autodetachment. The autodetachment process is investigated by resonantly-enhanced photoelectron spectroscopy. The combination of photodetachment spectroscopy and resonant photoelectron spectroscopy can probe the dynamics of the vibronic interactions leading to autodetachment, as well as detailed energetic, electronic, and vibrational information about the underlying neutral radicals. Three types of anionic species are investigated: 1) O-containing PAH anions with dipole-bound excited states; 2) O- and/or N-functionalized PAH anions with quadrupole-bound excited states; and 3) PAH and fullerene anions with polarization-bound excited states.

Recent Progress

Probing the Interactions between the Encapsulated Water Molecule and the Fullerene Cages in $H_2O@C_{60}^-$ and $H_2O@C_{59}N^-$. A high-resolution photoelectron imaging study was carried out on cryogenically-cooled $H_2O@C_{60}^-$ and $H_2O@C_{59}N^-$ endohedral fullerene anions (Fig. 1). The electron affinity (EA) of $H_2O@C_{60}$ was measured to be 2.6923 ± 0.0008 eV, which was 0.0088 eV higher than the EA of C_{60} , while the EA of $H_2O@C_{59}N$ was measured to be $3.0058 \text{ eV} \pm 0.0007$ eV, which was 0.0092 eV lower than the EA of $C_{59}N$. The opposite shifts were found to be due to the different electrostatic interactions between the encapsulated water molecule and the fullerene cages in the two systems. There was a net Coulombic attraction between the guest and host in

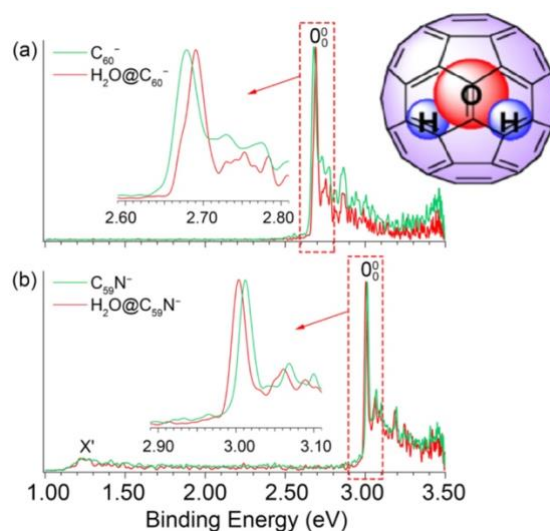


Fig. 1 Comparisons of the photoelectron spectra of (a) C_{60}^- and $H_2O@C_{60}^-$, (b) $C_{59}N^-$ and $H_2O@C_{59}N^-$.

$\text{H}_2\text{O}@C_{60}^-$, but a repulsive interaction in $\text{H}_2\text{O}@C_{59}\text{N}^-$. Low-frequency features were also observed in the photoelectron spectra which were tentatively attributed to the hindered rotational excitations of the encapsulated H_2O molecule, providing further insights into the guest-host interactions in $\text{H}_2\text{O}@C_{60}^-$ and $\text{H}_2\text{O}@C_{59}\text{N}^-$.

Dipole-Bound Excited States and Resonant Photoelectron Imaging of Phenoxide and Thiophenoxide Anions. Cryogenically-cooled phenoxide ($\text{C}_6\text{H}_5\text{O}^-$) and thiophenoxide ($\text{C}_6\text{H}_5\text{S}^-$) anions were investigated using photodetachment spectroscopy and resonant photoelectron-imaging. A dipole-bound excited state was known for $\text{C}_6\text{H}_5\text{O}^-$ at 97 cm^{-1} below the detachment threshold in a previous study, which yielded eight resonant photoelectron spectra via excitations to eight vibrational levels of the dipole-bound state (DBS) followed by autodetachment. In this study, a complete photodetachment spectrum of $\text{C}_6\text{H}_5\text{O}^-$ covering a spectral range $2,600\text{ cm}^{-1}$ above the detachment threshold and revealing nine additional vibrational resonances of the DBS (Fig. 2). A dipole-bound excited state was also observed for $\text{C}_6\text{H}_5\text{S}^-$, 39 cm^{-1} below its detachment threshold of $18,982\text{ cm}^{-1}$. Photodetachment spectroscopy covering a spectral range $1,500\text{ cm}^{-1}$ above threshold revealed twelve vibrational resonances for the DBS of $\text{C}_6\text{H}_5\text{S}^-$. By tuning the detachment laser to the vibrational resonances in the DBS of $\text{C}_6\text{H}_5\text{O}^-$ and $\text{C}_6\text{H}_5\text{S}^-$, highly non-Franck-Condon resonant photoelectron spectra were obtained, as a result of mode-selectivity and the $\Delta v = -1$ propensity rule for vibrational autodetachment. Five new fundamental vibrational frequencies were obtained for the ground state of the $\text{C}_6\text{H}_5\text{O}$ (X^2B_1) radical. Intramolecular inelastic scattering was observed in some of the resonant photoelectron spectra, leading to the excitation of the Franck-Condon-inactive lowest-frequency bending mode (ν_{20}) of $\text{C}_6\text{H}_5\text{O}$. The first excited state of $\text{C}_6\text{H}_5\text{O}$ (A^2B_2) was observed to be 0.953 eV above the ground state. Twelve resonant photoelectron spectra were obtained for $\text{C}_6\text{H}_5\text{S}^-$, allowing the

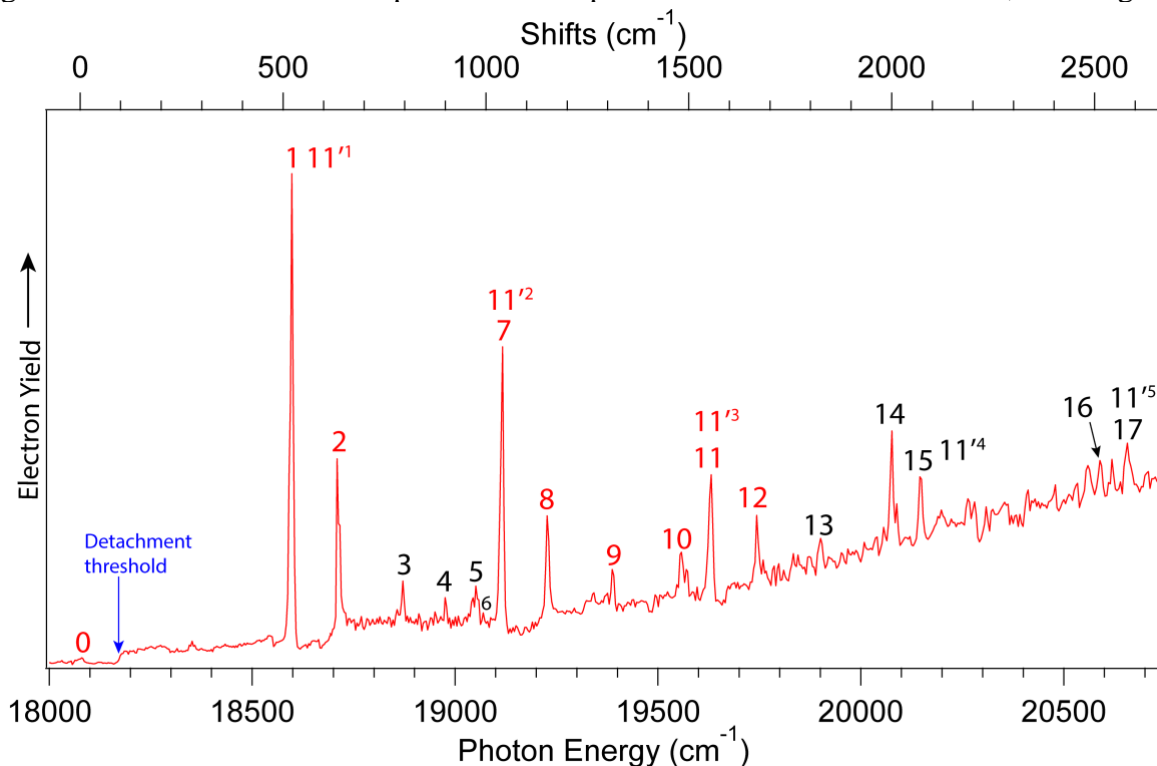


Fig. 2 Photodetachment spectrum of $\text{C}_6\text{H}_5\text{O}^-$ by measuring the total electron yield as a function of photon energy across the detachment threshold. Seventeen vibrational resonances were observed above the detachment threshold.

measurements of seven fundamental vibrational frequencies of the C_6H_5S radical, whereas the non-resonant photoelectron spectrum only exhibited a single Franck-Condon active mode. This study again demonstrated that the combination of photodetachment spectroscopy and resonant photoelectron spectroscopy is a powerful technique to obtain vibrational information about polar radical species.

Tautomer-Specific Resonant Photoelectron Imaging of Deprotonated Cytosine Anions.

We have found that conformer-specific resonant photoelectron spectra could be obtained via autodetachment from dipole-bound excited states of molecular anions. Tautomers of the nucleobases play fundamental roles in spontaneous mutations of DNA. Tautomers of neutral nucleobases have been studied in the gas phase, but much less is known about their charged species. We have observed three tautomers of deprotonated cytosine anions, [*trans*-keto-amino-N3H-H_{8b}] (**tKAN3H8b**⁻), [*cis*-keto-amino-N3H-H_{8a}] (**cKAN3H8a**⁻), and [keto-amino-H] (**KAN1**⁻), produced by electrospray ionization from a cytosine solution. These anions were investigated using high-resolution photoelectron and photodetachment spectroscopy, and resonant photoelectron imaging via excited dipole-bound states (DBSs). The ground vibrational levels of the DBSs of **cKAN3H8a**⁻ and **tKAN3H8b**⁻ were observed below the corresponding detachment threshold by 325 and 577 cm^{-1} , respectively. The **KAN1**⁻ anion, being higher in energy, was tentatively observed in the photodetachment spectrum due to its weak intensity. Resonant

photoelectron imaging via autodetachment from the vibrational levels of the DBSs allowed tautomer-specific resonant photoelectron spectroscopy to be conducted for **cKAN3H8a**⁻ and **tKAN3H8b**⁻ (Fig. 3). Accurate electronic and vibrational information was obtained for the **cKAN3H8a** and **tKAN3H8b** radicals, and their electron affinities were measured to be 3.0471(5) and 3.0870(5) eV, respectively. The three observed anions could all be derived from deprotonation of the keto-amino-N3H tautomer, but could also be from the canonical keto-amino-N1H cytosine and the rare *trans*- and *cis*-keto-imino tautomers. This study suggests a new method to study tautomers of nucleobases using electrospray and anion spectroscopy.

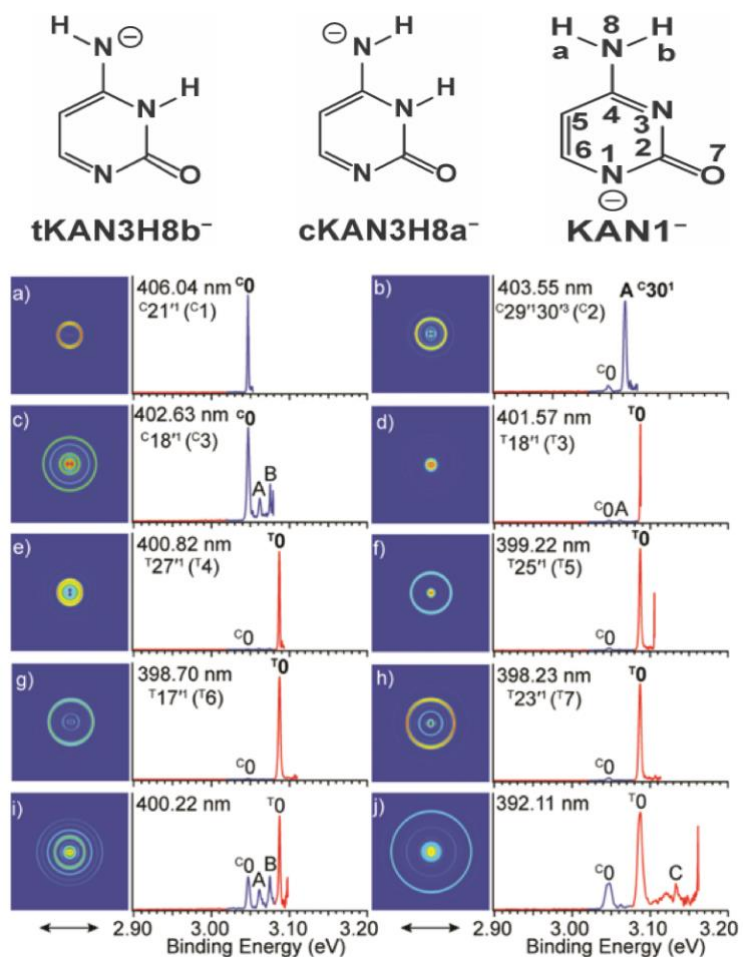


Fig. 3 Tautomer-specific resonant photoelectron images and spectra, (a) to (h), compared to two non-resonant spectra at (i) 400.22 nm and (j) 392.11 nm. (a)-(c) correspond to autodetachment from fundamental vibrational levels of the DBS of **cKAN3H8a**⁻, while d)-h) are from the DBS of **tKAN3H8b**⁻.

Future Plans

Experiments on dipole-bound excited states will be continued. Specifically, a series of halogen-substituted $p\text{-XC}_6\text{H}_4\text{O}^-$ ($X = \text{F-I}$) phenoxide anions will be investigated. The dipole moments of the $p\text{-XC}_6\text{H}_4\text{O}$ radicals decrease from $X = \text{I}$ to F , which will allow us to investigate the relationship between dipole moment and the binding energies of the dipole-bound states and the minimum dipole moment that is needed to support a dipole-bound state in a series of similar molecules. We will also investigate more complex O-containing polycyclic aromatic systems, such as the biphenol oxide anions and phenoxide with complex substituents.

Work supported by the BES-GPCP program (2018- present)

1. G. Z. Zhu, Y. Liu, Y. Hashikawa, Q. F. Zhang, Y. Murata, and L. S. Wang. Probing the Interaction between the Encapsulated Water Molecule and the Fullerene Cages in $\text{H}_2\text{O}@C_{60}^-$ and $\text{H}_2\text{O}@C_{59}\text{N}^-$. *Chem. Sci.* **9**, 5666-5671 (2018). (DOI: 10.1039/C8SC01031E)
2. G. Z. Zhu, C. H. Qian, and L. S. Wang. Dipole-Bound Excited States and Resonant Photoelectron Imaging of Phenoxide and Thiophenoxide Anions. *J. Chem. Phys.* **149**, 164301 (2018). (DOI: 10.1063/1.5049715)
3. G. Z. Zhu, C. H. Qian, and L. S. Wang. Tautomer-Specific Resonant Photoelectron Imaging of Deprotonated Cytosine Anions. *Angew. Chem. Int. Ed.* (2019). DOI: 10.1002/anie.201903444.

Fundamental chemical kinetics of siloxane and silicon compounds

DOE BES Grant #18SC503179

Margaret S. Wooldridge (PI)

University of Michigan, Department of Mechanical Engineering, 2350 Hayward St., Ann Arbor, MI, 48109-2125, mswool@umich.edu

Andrew B. Mansfield

Eastern Michigan University Mechanical, Engineering, College of Technology, Ypsilanti, MI, 48197, amansfi3@emich.edu,

Robert S. Tranter

Chemical Sciences and Engineering Division, Argonne National Laboratory, Argonne, IL, 60439, tranter@anl.gov

Program Scope

Siloxanes and other silicon compounds play significant roles as impurities in land-fill gas and as primary feedstock materials for high-value and large-volume products, yet the fundamental reaction chemistry of gas-phase silicon compounds remains largely unexplored. The proposed work integrates two complementary experimental efforts to significantly advance the science of gas-phase silicon reaction chemistry. The primary research focus is on the elementary thermal reactions of siloxanes and their decomposition products with a progression in the chemical structure of the compounds studied to elucidate the effects of bond structure. An additional area of interest is the interaction of gas-phase species with silica nanoparticles that are formed naturally as products of the thermal reactions of siloxanes and during oxidation.

Methodology

Experiments will be conducted using the University of Michigan (UM) rapid compression facility (RCF) and the shock tube facility (STF) at the Argonne National Laboratory (ANL). The combination of experimental approaches will allow a broad and complementary range of state conditions to be studied with temperatures in the range of 700-2000 K and pressures of 0.1-50 bar. With the RCF studies, rapid gas-sampling coupled with gas-chromatography and mass spectrometry will be applied to measure stable intermediates and products allowing reaction pathways to be identified and limiting elementary rate coefficients to be determined. Narrow-line laser absorption measurements will be used to measure the formation of the OH radical in the RCF systems as well as to measure the interaction of OH with silicon nanoparticles. Elementary rate coefficients and mechanisms of the thermal decomposition reactions will be determined in studies at ANL with a combination of optical measurements and online mass spectrometry. In addition, the portable ANL mini-STF will be used at the UM to conduct simultaneous laser absorption and time-of-flight mass spectrometry measurements. Together the UM and ANL data sets will be the foundation for accurate models of gas-phase silicon chemistry over a wide range of conditions that is relevant for improving the synthesis of high-cost and high volume materials and for improving energy conversion, durability and control in systems that are challenged by silicon impurities. These would be the first measurements to systematically address such a large spectrum of fundamental gas-phase silicon chemistry and consideration of particle formation kinetics. Successful outcomes will include multiple categories of pioneering data, and directly address the two DOE BES Grand Challenges of *Synthesizing new forms of matter with tailored properties* and *Understanding and controlling material properties emerging from complex atomic and electronic interactions*.

Recent Progress

The impact of two organic silicon species with different but related chemical structures (see **Figure 1**), trimethylsilanol (TMSO) and hexamethyldisiloxane (HMDSO), on syngas auto-ignition behavior was investigated in the first part of this project using physical and computational experiments. The UM RCF was used to create temperatures of 1010 – 1070 K and pressures of 8 to 10.3 atm for auto-ignition experiments. Experiments with trace concentrations of TMSO (100 ppm, mole basis) or HMDSO (100 ppm) were added to a surrogate syngas blend (CO and H₂, with a molar ratio of 2.34:1, air levels of dilution, with molar equivalence ratios of $\phi = 0.1$).

The measured ignition delay times (presented in **Figure 2**) showed both siloxane species promote ignition behavior with TMSO yielding faster ignition delay times by approximately 37% and HMDSO yielding faster times by approximately 50% compared with the reference syngas mixture which contained no siloxanes. A computational study was conducted to interpret the results of the ignition experiments. Because detailed chemistry does not exist for these organo-silicon compounds, the effects of the addition of CH₃, H, and OH radicals to H₂ and CO mixtures were explored to simulate the potential rapid decomposition of the siloxanes in the H₂ and CO system. Addition of the radicals decreased the predicted ignition delay times when compared with the H₂ and CO mixture simulations without the radical species, but the simulations did not fully capture the behavior observed in the experiments, indicating the siloxane chemistry is more complex than providing a rapid source of radicals.

Future Plans

Current and future work includes additional STF and RCF studies of HMDSO, TMSO and ring siloxane compounds. Initial STF studies have been completed at ANL and using the advanced light source at Lawrence Berkeley National Laboratory. A second ALS session is planned for summer 2019. We are also partnering with Dr. Raghu Sivaramakrishnan (ANL) to develop siloxane thermochemistry which will allow further insights into the elementary reactions controlling siloxane combustion.

DOE publications supported by this project

Schwind, R. A., Wooldridge, M. S., Sivaramakrishnan, R., (2019) "Understanding Siloxane Combustion Chemistry: Computational and Experimental Studies of Hexamethyldisiloxane (HMDSO)," 11th National Meeting of the U.S. Sections of the Combustion Institute, Paper No. 1A18, Pasadena, CA.

Schwind, R. A., Wooldridge, M. S., "Effects of Organic Silicon Compounds on Syngas Auto-ignition Behavior," in preparation for submission to *Combustion and Flame* May 2019.

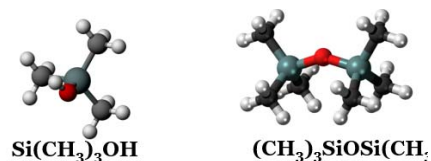


Figure 1. Molecular structures of the siloxanes trimethylsilanol (TMSO, left) and hexamethyldisiloxane (HMDSO, right).

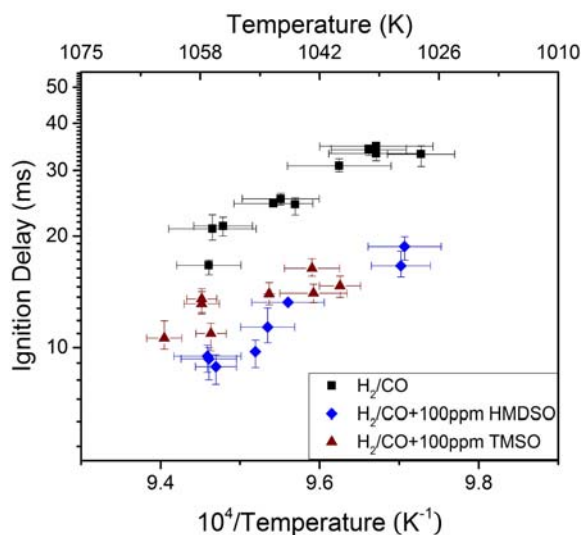


Figure 2. Experimental RCF results for ignition delay times for $P = 8.7\text{-}10.25$ atm. The error bars represent the uncertainties in the ignition delay time measurements and the assigned temperatures. Schwind and Wooldridge (2019).

Isomer-specific spectroscopy of aromatics and their resonance-stabilized radical intermediates

Timothy S. Zwier

Department of Chemistry, Purdue University, West Lafayette, IN 47907-2084
zwier@purdue.edu

Program Definition and Scope

There are many circumstances in which complex gas-phase reaction mixtures must be interrogated and understood, including combustion, plasmas, atmospheres, molecular clouds, and more. Spectroscopic tools need to be developed to selectively detect and characterize the widening array of precursors and the reactive intermediates they generate, often under extreme conditions of temperature, pressure, or . Future progress in these field requires development of detection schemes that are isomer-specific and even conformation-specific. This research program uses an array of laser-based and broadband microwave methods to carry out conformation-specific spectroscopy on key components and reactive intermediates formed by photolysis, pyrolysis, combustion, or electron-driven chemistry.

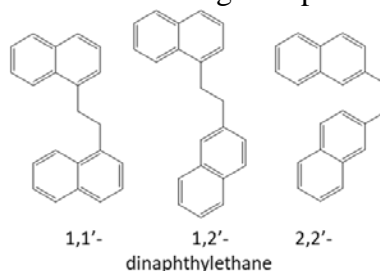
Recent Progress

A. Chemically linked diaromatics

We are studying the conformation-specific spectroscopy of a series of synthesized diaryl compounds involving a series of prototypical PAHs linked by short alkyl chains. Current models of soot formation require dimerization of PAHs as small as pyrene to account for the observed soot particle size distribution. However, the work of Sabbah *et al.*[JPCL **1**, 2962(2010)] has shown that physical dimerization of pyrene will be insignificant at flame temperatures, calling basic tenets of the model into question. It has been suggested that short chemical linkages are responsible for dimerization of smaller PAHs at flame temperatures. This hypothesis is being tested by determining the conformational preferences of the series of diarylalkanes linked at unique sites on the PAHs. By combining the single-conformation spectroscopic data with theoretical modeling, we can test how the relative energies and temperature-dependent populations of extended and π -stacked conformers vary with chemical linker, PAH size and shape, and substitution site.

Equally important, these flexible diaryls have two UV chromophores whose excitonic coupling depends on the nature and conformation of the alkyl chain. We hope to study the conformation-specific, state-selected vibronic coupling present in these challenging circumstances where the two chromophores are identical or nearly identical, making the vibronic levels of the first two excited states intermingled with one another. The process of vibronic mixing is important in a wide-array of circumstances of interest to DOE.

We currently have a complete data set on the first set of molecules in this series: 1,1'-, 2,2'-, and 1,2'-dinaphthylethane, with structures shown below. We are working with Ned Sibert to understand the alkyl CH stretch spectra and Lyudmila Slipchenko's groups to model the vibronic coupling in the flexible bichromophore.



B. Mass-correlated broadband microwave spectra of intermediates formed in flash pyrolysis (ref. 9, 10, 11, 13)

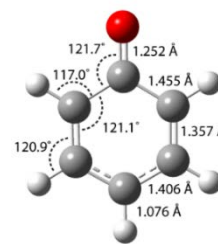
We are now regularly using a multiplexed detection scheme for characterizing complex gas mixtures that combines chirped-pulse Fourier Transform microwave detection (CP-FTMW), with

VUV photoionization time-of-flight mass spectrometry. Using 118 nm light to carry out VUV photoionization, we can record mass spectra that reflect the composition of the mixture of interest with little molecular fragmentation, whether it's the effluent from a flash pyrolysis source, a discharge, or a photochemical mixture. We have focused particularly to date on recording TOFMS as a function of pyrolysis source temperature, looking for correlations between the masses appearing in the mass spectrum and rotational transitions in the microwave. Since we view this combination as a powerful tool for characterizing complex gas mixtures, we have described the instrument and its capabilities in detail in a Rev. Sci. Instr. article (ref. 9).

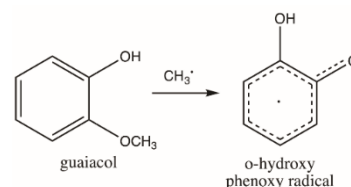
During the past year, we have published our broadband microwave study of the 2-furanyloxy radical formed by pyrolysis of 2-methoxyfuran, a second generation biofuel (ref. 10). Using Chirped-Pulse Fourier Transform microwave (CP-FTMW) methods, combined with strong-field coherence breaking, a set of transitions due to the radical were identified and assigned. The experimental rotational constants, centrifugal distortion constants, and spin-rotation coupling constants were determined for the radical and compared with *ab initio* predictions at the CCSD(T) level of theory, calculated by John Stanton. Atomic spin densities confirm that the 2-furanyloxy radical is best viewed as a carbon-centered allylic lactone radical, with 80% of the spin density on the two allylic carbons, and 20% on the pendant O(6) atom.



Phenoxy radical ($\text{C}_6\text{H}_5\text{O}$) is resonantly stabilized due to hyperconjugation of the oxyl radical moiety with the aromatic ring. Given the importance of the radical in combustion and atmospheric chemistry, several previous spectroscopic studies have been carried out, but no rotationally resolved data were available for structural characterization. We have used a combination of broadband microwave spectroscopy and VUV photoionization TOFMS to record rotational spectra of phenoxy, its per-deuterated isotopomers and the full set of singly ^{13}C substituted analogs in natural abundance. Rotational parameters associated with the fits to the full set of isotopomers were used by our collaborator, John Stanton, to produce a highly-accurate r_0 structure for the phenoxy radical. High-level *ab initio* calculations carried out by Stanton also accurately reproduce the rotational constants and spin-rotation parameters. The structure of phenoxy radical is distinctly quinoidal, with delocalization of the unpaired electron spin density on the oxygen and phenyl ring. The fitted Fermi contact terms for the ^{13}C atoms reflect a weighting of resonance structures that is 27% on the O-atom, 21.5% on each of the two ortho C's, and 30% on the para C, providing a quantitative measure of its sites for subsequent reactions that will control its abundances in combustion and atmospheric environments.



The initial step in the pyrolysis of guaiacol is formation of the resonance-stabilized *ortho*-hydroxy phenoxy radical by methyl loss. We have obtained broadband rotational spectra over the 8-18 GHz region, and assigned 40 transitions due to the radical. The fit included three rotational, five spin-rotational coupling constants, a set of hyperfine constants (T_{aa} , T_{bb} - T_{cc} , T_{ab}) and the Fermi contact



hyperfine constant associated with the hydrogen at the position *para* to the oxy radical. The large value of this Fermi contact term (-29.5 MHz) is consistent with the fact that the carbon atom to which it is bonded carries the largest atomic spin density (+0.342), acting as a reporter for nearby unpaired spin density.

C. Broadband Microwave Spectra of Model Components of Lignin

We have recorded broadband chirped-pulse microwave spectra over the 2-18 GHz frequency range for a series of four model aromatic components of lignin; namely, guaiacol (*ortho*-methoxy phenol), syringol (2,6-dimethoxy phenol), 4-methyl guaiacol, and 4-vinyl guaiacol, under jet-cooled conditions in the gas phase. In guaiacol, spectral fits of the singly ^{13}C isotopologues enabled determination of the phenyl ring C-atom positions. Distortions of the phenyl ring lengthen the C(1)-C(6) bond between the two substituted C-atoms, leading to clear bond alternation that reflects an increase in the phenyl ring resonance structure with double bonds at C(1)-C(2), C(3)-C(4) and C(5)-C(6). Syringol, with its' symmetric methoxy substituents, possesses a microwave spectrum with tunneling doublets in the a-type transitions associated with H-atom tunneling. These splittings were fit to determine a barrier to hindered rotation of the OH group of 1960 cm^{-1} , a value nearly 50% greater than that in phenol, due to the presence of the intramolecular $\text{OH}\cdots\text{OCH}_3$ H-bonds at the two equivalent planar geometries. In 4-methyl guaiacol, methyl rotor splittings are used to refine an earlier measurement of the three-fold barrier $V_3 = 63\text{ cm}^{-1}$.

D. Molecular rotational states as a Platform for Studying Quantum Coherences (ref. 12)

In the weak-field limit in which microwave spectroscopy is typically carried out, application of a single-frequency pulse that is resonant with a molecular transition will create a coherence between the pair of states involved in the rotational transition, producing a free-induction decay (FID) that, after Fourier transform, produces a molecular signal at that same resonance frequency. With the advent of chirped-pulse Fourier transform microwave methods (CP-FTMW), the high-powered amplifiers needed to produce broadband microwave spectra also open up other experiments that probe the molecular response in the high-field regime.

We are exploring the effects of resonant frequency pulses interrogating jet-cooled molecules under conditions of sufficient power to Rabi oscillate the two-state system through many Rabi cycles. In this high-power regime, the Fourier-transformed FID shows coherent signal not only at the applied resonant frequency but at a series of molecular rotational transitions initially connected to the original one by sharing an upper or lower level with it. As the duration of the single-frequency excitation is increased, the number of observed off-resonant, but dipole-allowed, molecular coherences grow. The phenomenon is quite general, having been demonstrated in *Z*-phenylvinyl nitrile (*Z*-PVN), *E*-PVN, benzonitrile, guaiacol, and 4-pentynenitrile. Even in molecular samples containing more than one independent species, only transitions due to the single component responsible for the original resonant transition are present. In collaboration with F. Robicheaux (Purdue), we have developed a time-dependent quantum model of the molecular/photon system and use it in conjunction with experiment to test possible sources of the phenomenon. To date, we do not have a robust physical model for this phenomenon.

Future Work

- (1) Single-conformation spectroscopy of 9-ethyl anthracene, 9,9'-dianthracylethane, and 1,2-dianthracylethane.
- (2) Pyrolysis of a series of methoxy pyridines using mass-correlated, broadband microwave spectroscopy.
- (3) Incorporation and initial testing of CP-FTMW/ VUV TOFMS as a tool for characterizing highly oxygenated intermediates from a stirred flow reactor, in collaboration with Nils Hansen.
- (4) Characterization of the broadband microwave spectra of molecules containing multiple tunneling pathways, seeking to understand and manipulate rotational coherences between states in the tunneling manifold.

Publications acknowledging DOE support, 2016-present

1. Daniel P. Tabor, Daniel M. Hewett, Sebastian Bocklitz, Joseph A. Korn, Anthony J. Tomaine, Arun K. Ghosh, Timothy S. Zwier, and Edwin L. Sibert III, "Anharmonic modeling of the conformation-specific IR spectra of ethyl, n-propyl, and n-butylbenzene", *J. Chem. Phys.* **144**, 224310 (2016).
2. Nathanael M. Kidwell, Deepali N. Mehta-Hurt, Joseph A. Korn, and Timothy S. Zwier, "Infrared and Electronic Spectroscopy of Jet-cooled 5-methyl-2-furanylmethyl Radical derived from the Biofuel 2,5-Dimethylfuran", *J. Phys. Chem. A* **120**, 6434-43 (2016).
3. A.O. Hernandez, Chamara Abeysekera, Brian M. Hays, and Timothy S. Zwier, "Broadband Multi-resonant Strong Field Coherence Breaking as a Tool for Single Isomer Microwave Spectroscopy", *J. Chem. Phys.* **145**, 114203 (2016).
4. Joseph A. Korn, Khadija Jawad, Daniel P. Tabor, Edwin L. Sibert III, and Timothy S. Zwier, "Conformation-specific Spectroscopy of Alkylbenzyl Radicals: α -ethylbenzyl and α -propylbenzyl radicals", *J. Chem. Phys.* **145**, 124314 (2016).
5. Alicia O. Hernandez-Castillo, Chamara Abeysekera, Brian M. Hays, Isabelle Kleiner, Ha Vinh Lam Nguyen, and Timothy S. Zwier, "Conformational Preferences and Internal Rotation of Methyl Butyrate by Microwave Spectroscopy", *J. Mol. Spec.* **337**, 51-58 (2017).
6. Daniel M. Hewett, Sebastian Bocklitz, Daniel P. Tabor, Edwin L. Sibert III, Martin Suhm, and Timothy S. Zwier, "Identifying the First Folded Alkylbenzene via Ultraviolet, Infrared, and Raman Spectroscopy of Pentylbenzene through Decylbenzene", *Chem. Sci.* **8**, 5305-18 (2017).
7. Daniel M. Hewett, Daniel P. Tabor, Joshua L. Fischer, Edwin L. Sibert III, and Timothy S. Zwier, "Infrared-Enhanced Fluorescence-Gain Spectroscopy: Conformation-Specific Excited-State Infrared Spectra of Alkylbenzenes", *J. Phys. Chem. Lett.* **8**, 5296-5300 (2017).
8. Piyush Mishra, Daniel M. Hewett, and Timothy S. Zwier, "Conformational Explosion: Understanding the complexity of short chain para-dialkylbenzene potential energy surfaces", *J. Chem. Phys.* **148**, 184304 (2018).
9. Sean M. Fritz, Brian M. Hays, Alicia O. Hernandez-Castillo, Chamara Abeysekera, and Timothy S. Zwier, "Multiplexed Characterization of Complex Gas Phase Mixtures combining Chirped-Pulse Fourier Transform Microwave Spectroscopy and VUV photoionization Time-of-Flight Mass Spectrometry", *Rev. Sci. Instr.* **89**, 093101 (2018).
10. Chamara Abeysekera, A.O. Hernandez-Castillo, John F. Stanton, and Timothy S. Zwier, Broadband Microwave Spectroscopy of 2-Furanyloxy Radical: Primary Pyrolysis Product of 2-Methoxyfuran, *J. Phys. Chem. A* **122**, 6879-85 (2018).
11. A.O. Hernandez-Castillo, Chamara Abeysekera, John F. Stanton, and Timothy S. Zwier, "Structural Characterization of the Phenoxy Radical with Mass-Correlated Broadband Microwave Spectroscopy", (submitted).
12. A.O. Hernandez-Castillo, Chamara Abeysekera, F. Robicheaux, and Timothy S. Zwier, "Propagating Molecular Rotational Coherences through Single-Frequency Pulses in the Strong Field Regime", (submitted).
13. A.O. Hernández-Castillo, Sean M. Fritz, John F. Stanton, and Timothy S. Zwier. "Mass-Correlated Broadband Microwave Spectroscopy of *ortho*-hydroxy phenoxy Radical: Primary Product of Guaiacol Pyrolysis", (in preparation).
14. A.O. Hernández-Castillo, Sean Fritz, Iciar Uriarte, Emilio Cocinero, and Timothy S. Zwier. "Spectroscopic Characterization of Model Aromatic Substituents of Lignin by Broadband Chirped-Pulse Microwave Spectroscopy", (in preparation).

Participant List

39th Annual Gas Phase Chemical Physics Research Meeting Participant List

Last Name	First Name	Organization	Email_Address
Ahmed	Musahid	Lawrence Berkeley National Laboratory	mahmed@lbl.gov
Allendorf	Sarah	Sandia National Lab	swallen@sandia.gov
Anderson	Scott	University of Utah	anderson@chem.utah.edu
Bellan	Josette	California Institute of Technology	Josette.Bellan@jpl.nasa.gov
Bowen	Kit	Johns Hopkins University	kbowen@jhu.edu
Burke	Michael	Columbia University	mpburke@columbia.edu
Chandler	David	Sandia National Laboratories	chand@sandia.gov
Chen	Jacqueline	Sandia National Laboratories	jhchen@sandia.gov
Continetti	Robert	UC San Diego	rcontinetti@ucsd.edu
Davis	Michael	Argonne National Laboratory	davis@tcg.anl.gov
Davis	Floyd	Cornell University	hfd1@cornell.edu
Dawes	Richard	Missouri University of Science and Technology	dawesr@mst.edu
Douberly	Gary	University of Georgia	douberly@uga.edu
Duncan	Michael	University of Georgia	maduncan@uga.edu
Ellison	G. Barney	University of Colorado Boulder	barney@jila.colorado.edu
Field	Robert	MIT	rwfield@mit.edu
Frank	Jonathan	Sandia National Laboratories	jhfrank@sandia.gov
Goldsmith	Claude Franklin	Brown University	franklin_goldsmith@brown.edu
Green	William	MIT	whgreen@mit.edu
Hansen	Nils	Sandia National Laboratories	nhansen@sandia.gov
Hwang	Robert	Sandia National Laboratories	gdecast@sandia.gov
Jasper	Ahren	Argonne National Laboratory	ajasper@anl.gov
Jenks	Cynthia	Argonne National Laboratory	cjenks@anl.gov
Kaiser	Ralf	University of Hawaii at Manoa	ralfk@hawaii.edu
Kliewer	Christopher	Sandia National Laboratories	cjkliew@sandia.gov
Klippenstein	Stephen	Argonne National Laboratory	sjk@anl.gov
Labbe	Nicole	University of Colorado Boulder	Nicole.labbe@colorado.edu
Leone	Stephen	LBNL and University of California Berkeley	srl@berkeley.edu

Lester	Marsha	University of Pennsylvania	milester@sas.upenn.edu
Lucht	Robert	Purdue University	lucht@purdue.edu
McCunn-Jordan	Laura	Marshall University	mccunn@marshall.edu
Michelsen	Hope	Sandia National Labs	hamiche@sandia.gov
Najm	Habib	Sandia National Laboratories	hnnajm@sandia.gov
Nesbitt	David	JILA/University of Colorado	djn@jila.colorado.edu
Neumark	Daniel	University of California, Berkeley	dneumark@berkeley.edu
Neuscamman	Eric	University of California, Berkeley	eric.neuscamman@gmail.com
Osborn	David	Sandia National Laboratories	dlosbor@sandia.gov
Pepiot	Perrine	Cornell University	pp427@cornell.edu
Pitz	William	LLNL	PITZ1@LLNL.GOV
Pratt	Stephen	Argonne National Laboratory	stpratt@anl.gov
Prendergast	David	Lawrence Berkeley National Laboratory	dgprendergast@lbl.gov
Prozument	Kirill	Argonne National Laboratory	prozument@anl.gov
Ramasesha	Krupa	Sandia National Laboratories	kramase@sandia.gov
Reisler	Hanna	University of Southern California	reisler@usc.edu
Ruscic	Branko	Argonne National Laboratory	ruscic@anl.gov
Sears	Trevor	Stony Brook University	trevor.sears@stonybrook.edu
Shaddix	Christopher	Sandia National Laboratories	crshadd@sandia.gov
Shepard	Ron	Argonne National Laboratory	shepard@tcg.anl.gov
Sheps	Leonid	Sandia National Laboratories	lsheps@sandia.gov
Sisk	Wade	DOE/BES	Wade.Sisk@science.doe.gov
Sivaramakrishnan	Raghu	Argonne National Laboratory	raghu@anl.gov
Stanton	John	University of Florida	johnstanton@ufl.edu
Suits	Arthur	University of Missouri-Columbia	suitsa@missouri.edu
Sutton	Jeffrey	Ohio State University	sutton.235@osu.edu
Taatjes	Craig	Sandia National Laboratories	cataatj@sandia.gov
Tranter	Robert	Argonne National Laboratory	tranter@anl.gov
Wang	Lai-Sheng	Brown University	lai-sheng_wang@brown.edu
Wasielewski	Michael	Northwestern University	m-wasielewski@northwestern.edu
Wilson	Kevin	Lawrence Berkeley National Laboratory	krwilson@lbl.gov
Wooldridge	Margaret	University of Michigan	mswool@umich.edu
Yarkony	David	Johns Hopkins University	yarkony@jhu.edu
Zádor	Judit	Sandia National Laboratories	jzador@sandia.gov
Zwier	Timothy	Purdue University	zwier@purdue.edu